Identification of compensatory mechanisms and disease pathways in mitochondrial disease and synucleinopathy

Kumulative Dissertation
zur Erlangung des Doktorgrades (Dr. rer. nat.)
der
Mathematisch-Naturwissenschaftlichen Fakultät
der
Rheinischen Friedrich-Wilhelms-Universität Bonn

vorgelegt von

Joshua Jackson
aus Stourbridge, Vereinigtes Königreich von Großbritannien und Nordirland

Bonn, 2025

Angefertigt mit Genehmigung
der
Mathematisch-Naturwissenschaftlichen Fakultät
der
Rheinischen Friedrich-Wilhelms-Universität Bonn

Gutachter/Betreuer: Prof. Dr. Dr. Pierluigi Nicotera
Gutachter: Prof. Dr. Joachim Schultze

Tag der Promotion: 13.05.2025
Erscheinungsjahr: 2025

Abstract

Mitochondria play vital roles in a variety of processes such as cellular metabolism, intracellular signalling and cell death. Defects in mitochondria can lead to inherited metabolic disorders and neurodegenerative diseases. There is often a poor genotype-to-phenotype correlation in mitochondrial diseases, with distinct mutations that lead to a wide variety of clinical manifestations, age of onset and disease severity. This heterogeneity of symptoms, in combination with a relatively low frequency in the population, makes the development of novel treatments particularly challenging.

In invertebrates and some mouse models of mitochondrial diseases, inhibition of the mitochondrial oxidative phosphorylation (OXPHOS) can lead to a paradoxical lifespan extension through the engagement of compensatory mechanisms. As an explanation of this phenomena, the “mitochondrial threshold effect theory” states that mitochondrial dysfunction below a certain threshold promotes stress resilience and metabolic rewiring, leading to enhanced longevity. However, if damage exceeds a certain threshold, animals develop disease. In a human context, a better understanding of the “mitochondrial threshold effect” may explain some of the molecular signatures and variable disease traits observed in patients.

We sought to explore the compensatory mechanisms that organisms activate in response to the inhibition of OXPHOS using *Caenorhabditis elegans* as a genetically tractable model, in combination with mouse and human cells. Our goals were to investigate the underlying molecular mechanisms that contribute to mitochondrial dysfunction and neurodegenerative processes.

By performing a cross-species analysis, we identified VPS-39/VPS39 and SPL-1/SGPL1 to be part of the molecular mechanisms that compensate for mitochondrial dysfunction. In the context of neurodegenerative processes, we found that the actin nucleation promoting factor WSP-1/N-WASP is a disease modifier that contributes to mitochondrial dysfunction and proteotoxicity. Together, these results build on our growing understanding of the mechanisms that counteract mitochondrial dysfunction and pathogenic processes.

Publications

This cumulative thesis is comprised of the following peer-reviewed publications:

Jackson J, Wischhof L, Scifo E, Pellizzer A, Wang Y, Piazzesi A, Gentile D, Siddig S, Stork M, Hopkins CE *et al* (2022) SGPL1 stimulates VPS39 recruitment to the mitochondria in MICU1 deficient cells. *Mol Metab* 61: 101503. https://doi.org/10.1016/j.molmet.2022.101503

Jackson J, Hoffmann C, Scifo E, Wang H, Wischhof L, Piazzesi A, Mondal M, Shields H, Zhou X, Mondin M *et al* (2024) Actin-nucleation promoting factor N-WASP influences alpha-synuclein condensates and pathology. *Cell Death Dis* 15: 304. https://doi.org/10.1038/s41419-024-06686-7

I contributed to the following peer-reviewed articles, however I do not discuss them in my dissertation:

Matveeva A, Watters O, Rukhadze A, Khemka N, Gentile D, Perez IF, Llorente-Folch I, Farrell C, Lo Cacciato E, Jackson J *et al* (2024) Integrated analysis of transcriptomic and proteomic alterations in mouse models of ALS/FTD identify early metabolic adaptions with similarities to mitochondrial dysfunction disorders. *Amyotroph Lateral Scler Frontotemporal Degener* 25: 135-149

Piazzesi A, Wang Y, Jackson J, Wischhof L, Zeisler-Diehl V, Scifo E, Oganezova I, Hoffmann T, Gomez Martin P, Bertan F *et al* (2022) CEST-2.2 overexpression alters lipid metabolism and extends longevity of mitochondrial mutants. *EMBO Rep*: e52606

Bertan F, Wischhof L, Scifo E, Guranda M, Jackson J, Marsal-Cots A, Piazzesi A, Stork M, Peitz M, Prehn JHM *et al* (2021) Comparative analysis of CI- and CIV-containing respiratory supercomplexes at single-cell resolution. *Cell Rep Methods* 1: 100002

Table of contents

List of abbreviations

α-Syn	Alpha synuclein
Aß	Amyloid ß
AD	Alzheimer's disease
ADP	Adenosine diphosphate
APP	Amyloid precursor protein
ATP	Adenosine triphosphate
CMT	Charcot-Marie-Tooth
DNA	Deoxyribonucleic acid
CI	Complex I, NADH:ubiquinone oxidoreductase
CII	Complex II, succinate dehydrogenase
CIII	Complex III, cytochrome bc_1 oxidoreductase
CIV	Complex IV, cytochrome c oxidase
CV	Complex V, ATP synthase
ETC	Electron transport chain
EMRE	Essential MCU regulator
ER UPR	Endoplasmic reticulum unfolded protein response
IBM	Inner boundary membrane
IDR	Intrinsically disordered regions
IMM	Inner mitochondrial membrane
KO	Knock-out
LLPS	Liquid-liquid phase separation
MAMs	Mitochondria associated membranes
MELAS	Myopathy, Encepalopathy, Lactic Acidosis, and Stroke-like symptoms
MERRF	Myoclonic epilepsy with ragged-red fibers
MCU	Mitochondrial Calcium Uniporter
MICOS	Mitochondrial contact site and cristae organising system
MICU	Mitochondrial calcium uptake protein
mPTP	Mitochondrial permeability transition pore
MPP+	1-methyl-4-phenylpyridinium
MPPP	Desmethylprodine or 1-methyl-4-phenyl-4-propionoxypiperidine
MPTP	1-methyl-4-phenyl-1,2,3,6-tetrahydropyridine

mtDNA	Mitochondrial DNA
mtUPR	Mitochondrial unfolded protein response
N-WASP	Neural Wiskott-Aldrich syndrome protein
NAD+	Nicotinamide adenine dinucleotide, oxidised
NADH	Nicotinamide adenine dinucleotide, reduced
NCLX	Mitochondrial Sodium Calcium exchanger
OMM	Outer mitochondrial membrane
OXPHOS	Oxidative Phosphorylation
PD	Parkinson's disease
PFFs	Preformed fibrils
PRMs	Proline-rich motifs
SAM	Sorting and assembly machinery
TIM	Translocase of the inner membrane
TOM	Translocase of the outer membrane
RNA	Ribonucleic acid
RNAi	RNA interference
ROS	Reactive Oxygen Species
TCA cycle	Tricarboxylic acid cycle (also known as the citric acid or Krebs cycle)
VDAC	Voltage-dependent anion channel

List of figures

Introduction

Mitochondria in the healthy cell

Mitochondria control cellular metabolism

Mitochondria are double membrane bound organelles essential for cellular metabolism. Derived from ancient symbiosis of α-proteobacteria, they have become central to the generation of ATP through the process of oxidative phosphorylation (OXPHOS). In addition to OXPHOS, mitochondria are a crucial hub for lipid, nucleotide, amino acid anabolism and catabolism. Furthermore, mitochondria play vital roles in innate immunity, response to cellular stress, heme synthesis, Fe-S cluster biosynthesis, cellular differentiation, growth, repair, epigenetic remodelling, calcium signalling, etc. (Figure 1A-B) (Gray, 2012; Spinelli & Haigis, 2018; Monzel *et al*, 2023; Suomalainen & Nunnari, 2024).

Mitochondria are subdivided into different compartments that are individually optimised for specific functions. The different components of the mitochondria are the outer mitochondrial membrane (OMM), the intermembrane space (IMS), the inner mitochondrial membrane (IMM) and the matrix. These components can be further divided, for example, the IMM forms invaginated structures called cristae, which house OXPHOS components. The cristae membrane is separated from the inner boundary membrane by the cristae junction (Figure 1C) (Protasoni & Zeviani, 2021; Suomalainen & Nunnari, 2024).

Due to their bacterial origin, mitochondria have their own genome. The mitochondrial DNA (mtDNA) is found within the mitochondrial matrix and is 16.5 kilobases long and encodes 37 genes. These genes encode 13 OXPHOS complex subunits, 22 mitochondrial tRNAs, and 2 ribosomal RNAs. During eukaryotic evolution, most of the mitochondrial genes have been lost to the nuclear genome, which encodes over 99% of the mitochondrial proteome. In order for mitochondria to function effectively, they require a complex set molecular factors to coordinate the synthesis and transport of proteins from both sets of genomes to their correct mitochondrial compartments (Anderson *et al*, 1981; Pagliarini *et al*, 2008; Gray, 2012; Calvo *et al*, 2016; Rath *et al*, 2021).

Mitochondria are central to cellular function due to their role in ATP generation through the process of OXPHOS. Briefly, the electron donors NADH or $FADH_2$ are generated through the processes of glycolysis, fatty acid oxidation, or the tricarboxylic acid (TCA) cycle. NADH and $FADH_2$ are then oxidised by NADH:ubiquinone oxidoreductase (CI) or succinate dehydrogenase (CII), respectively. Electrons from this oxidation are subsequently passed along to cytochrome bc_1 oxidoreductase (CIII) and cytochrome c oxidase (CIV) by the electron carriers ubiquinone and cytochrome c. In parallel to electron transfer, CI, CIII and CIV pump protons into the IMS and create an electrochemical gradient. Once the electrons reach complex IV, they are used to reduce molecular oxygen to H_2O. Finally, the proton gradient that is established by the electron transport chain (ETC) is utilised by the ATP synthase (CV), to generate ATP from ADP and inorganic phosphate (Figure 1A). The respiratory complexes of the OXPHOS system are known to form a variety of higher order supercomplexes (e.g. $CICIII_2CIV$), which are thought to increase complex stability, enhance their efficiency, and reduce reactive oxygen species (ROS) production (Enriquez, 2016; Letts & Sazanov, 2017; Vercellino & Sazanov, 2022).

Calcium signalling and mitochondria

Calcium (Ca^{2+}) is an essential second messenger for numerous cellular signalling processes. Ca^{2+} signalling plays an important role in all biological processes, including fertilisation, embryo patterning, differentiation, cellular proliferation, and apoptosis. A variety of extracellular and intracellular stimuli can trigger rapid changes in cytosolic Ca^{2+} concentration from the basal concentration of around 100nM up to levels of around 1µM (Berridge *et al*, 2000; Bootman & Bultynck, 2020).

Increased cytosolic Ca^{2+} concentration can occur through influx from the extracellular space or from its release from intracellular stores. While the global Ca^{2+} concentration can increase upon stimulation, Ca^{2+} microdomains can also form at the organelle contact sites, with local concentrations reaching an excess of 100µM. The impact of Ca^{2+} on intracellular pathways depends on the cell type and the spatiotemporal pattern of Ca^{2+} increase. Following stimulation, free Ca^{2+} is rapidly buffered by Ca^{2+} binding proteins (e.g. parvalbumin, calmodulin, troponin C, etc.) and

through transient sequestration by mitochondria (Berridge *et al.*, 2000; Clapham, 2007; Chandran *et al*, 2019; Bootman & Bultynck, 2020).

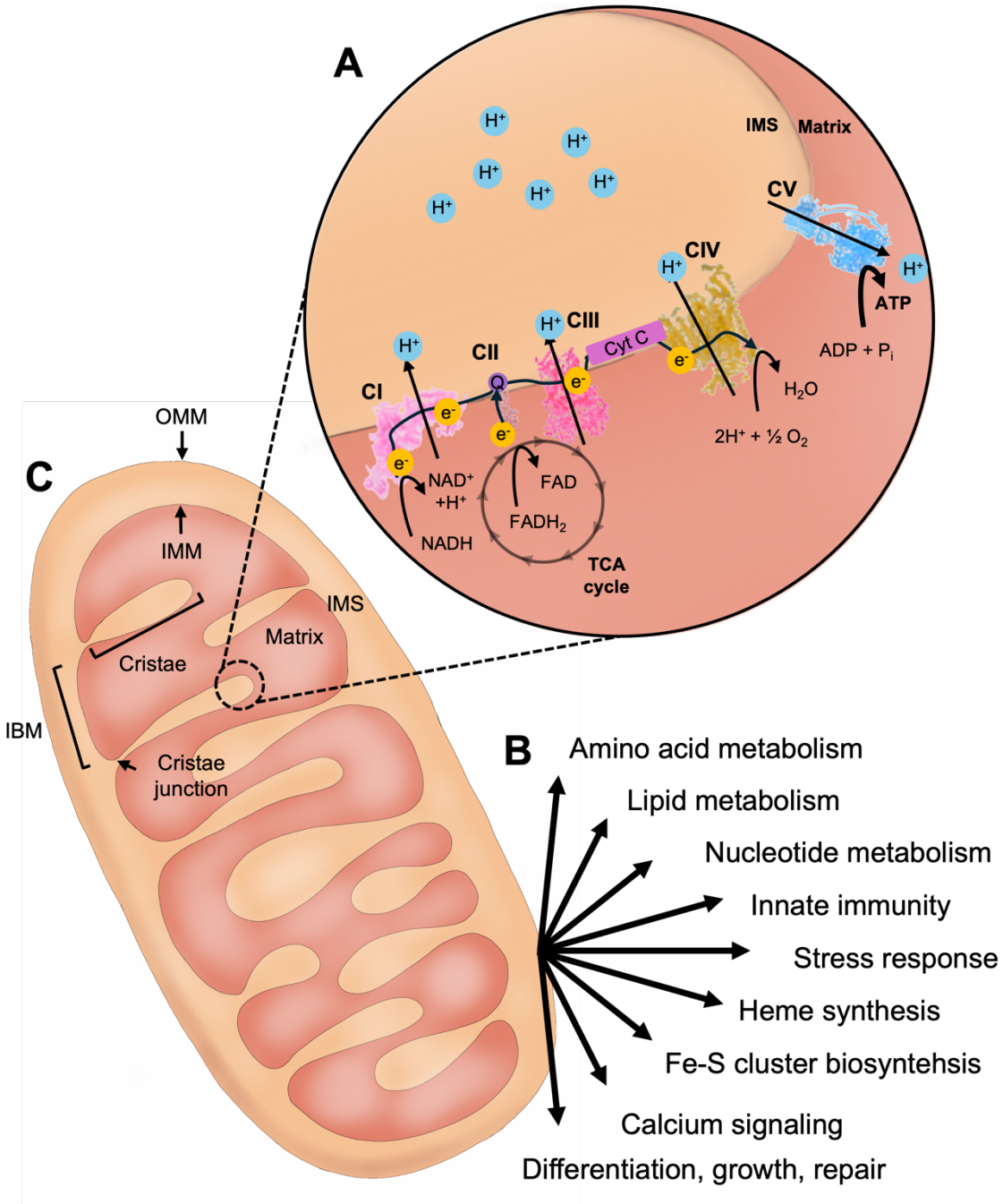

Figure 1. Morphology and functions of mitochondria.
(A) Overview of the OXPHOS pathway. (B) Pathways which mitochondria are involved with. (C) Mitochondrial structure and internal organisation.

It is known that mitochondria can shape Ca^{2+} homeostasis and signalling. The main gateways for Ca^{2+} to enter the mitochondrial matrix are the Voltage-Dependent Anion Channel (VDAC) and Mitochondrial Calcium Uniporter (MCU) channels, which are located in the outer and inner mitochondrial membranes, respectively. Passage of Ca^{2+} across the VDAC is largely passive, whereas the influx in the matrix is primarily regulated by the MCU complex. Ca^{2+} efflux depends on several components, including the NCLX exchanger (Palty *et al*, 2010). The MCU complex in the IMM is often found in proximity to the VDAC in the OMM. VDAC1 is part of a complex that forms the ER-mitochondrial contacts, alongside IP3R, GRP75, DJ-1, and a variety of other proteins. The proximity of mitochondria to the ER facilitates the rapid transfer of Ca^{2+} between organelles (Figure 2A) (Szabadkai *et al*, 2006; Xu *et al*, 2018; Carreras-Sureda *et al*, 2019; Liu *et al*, 2019; Feno *et al*, 2021).

Ca^{2+} influx into the mitochondria has been shown to influence bioenergetics. Physically trapping IP_3R in ER-mitochondria contacts has been shown to result in increased production of NADH upon stimulation of Ca^{2+} release from the ER, possibly through the modulation of Ca^{2+}-sensitive matrix dehydrogenases (Katona *et al*, 2022). Additionally, kinetic and force-flow analysis has revealed that increased Ca^{2+} concentration can increase the activity of CI, CIII, and CIV. This increase in ETC activity results in increased membrane potential and enhanced ATP production via CV (Territo *et al*, 2000; Glancy *et al*, 2013).

Beyond its influence on ATP production, mitochondrial Ca^{2+} also plays an important role in some forms of cell death, particularly those that involve mitochondrial permeability transition pore (mPTP) opening. While the identity of the mPTP is still debated, evidence points to F_1F_0-ATPase as a promising candidate. Excess matrix Ca^{2+} has been demonstrated to result in mPTP opening, via a Ca^{2+}-induced conformational change in F_1F_0-ATPase. Persistent opening of mPTP leads to mitochondrial swelling and subsequent release of pro-apoptotic molecules that trigger cell death (Baumgartner *et al*, 2009; Giorgi *et al*, 2012; Hwang *et al*, 2014; Bonora *et al*, 2017; Bonora *et al*, 2022; Bernardi *et al*, 2023).

Regulation of mitochondrial calcium influx

Since mitochondrial Ca^{2+} levels have an influence on ATP production and the induction of some forms of cell death, appropriate control of mitochondrial Ca^{2+} influx and efflux is vital.

The Voltage-Dependent Anion Channel (VDAC) is a major route of metabolites across the mitochondrial outer membrane, and comes in three isoforms, VDAC1, VDAC2 and VDAC3 (Blachly-Dyson *et al*, 1993; Blachly-Dyson *et al*, 1994; Sampson *et al*, 1996). VDACs are key players in mitochondrial Ca^{2+} signalling, especially at the mitochondria associated membranes (MAMs) (Szabadkai *et al.*, 2006; Xu *et al.*, 2018; Liu *et al.*, 2019). VDACs can interact with partners on the membranes of adjacent organelles and form multiprotein complexes that facilitate rapid exchange of Ca^{2+} in specific membrane domains. In this regard, mitochondria can interact with lysosomes (via VDAC1-TRPML1) (Peng *et al*, 2020), the endoplasmic reticulum (via VDAC1/2-DJ-1-GRP75-IP3R) (Szabadkai *et al.*, 2006; Liu *et al.*, 2019), and the sarcoplasmic reticulum (via VDAC2-RyR2) (Min *et al*, 2012). Consistent with the pathophysiological importance of VDACs, VDAC2 knockout mice are embryonically lethal (Cheng *et al*, 2003), whereas VDAC1/VDAC3 single- and double-knockout animals are viable but display impaired energy production (Baines *et al*, 2007; Anflous-Pharayra *et al*, 2011).

While the impairment caused by VDAC knockout can be partly attributed to altered mitochondrial Ca^{2+} signalling, it may also be due to disruption of the transport of other metabolites and ions into the mitochondria. VDACs can interact with a large variety of proteins, which likely allows regulation of channel conductivity by multiple pathways. Proteins that interact with VDAC include α-Syn, Aβ, phosphorylated tau, and SOD1, which are all involved in neurological disease. α-Syn, in particular, has been shown to be able to translocate into the mitochondria via VDACs, and may even play a physiological role in tuning the transport of Ca^{2+} through its pore (Manczak & Reddy, 2012; Rostovtseva *et al*, 2015; Magri *et al*, 2016).

Ca^{2+} transport across the IMM is controlled by the highly selective, rubidium red sensitive Mitochondrial Calcium Uniporter (MCU) (Kirichok *et al*, 2004; De Stefani *et al*, 2011). Uptake of Ca^{2+} via the MCU complex follows a sigmoidal response that is dependent not only on cytosolic Ca^{2+} concentration, but also on the concentration within the mitochondrial matrix (Csordas *et al*, 2013; Vais *et al*, 2016).

The core of the MCU complex consists of at least three evolutionarily conserved subunits: the pore-forming subunits MCU and MCUb, and the regulatory subunits MICU1 and EMRE. MCU and MICU1 homologs are found in most eukaryotic lineages and are strongly co-expressed in mammals (Baughman *et al*, 2011; De Stefani *et al.*, 2011; Bick *et al*, 2012; Raffaello *et al*, 2013; Sancak *et al*, 2013). The components of the MCU channel form multimeric complexes to regulate Ca^{2+} uptake (Figure 2B). The interaction between EMRE and MCU is thought to facilitate the formation of dimers of the MCU complex. These dimers form a V-shape conformation that forms preferentially in curved membranes (Wang *et al*, 2019).

While the electrophysiological properties of the MCU complex have been known since the 1960s, the genetic nature of MCU was discovered only in 2011, through *in silico* analysis of its tissue expression pattern and its co-occurrence with the first identified MCU complex component, MICU1 (Baughman *et al.*, 2011; De Stefani *et al.*, 2011). The MCU protein is a 40 kDa protein, and consists of two coiled-coil domains, two transmembrane domains, and a loop domain. The majority of the protein is found to protrude into the mitochondrial matrix, while the loop domain projects into the intermembrane space, and is essential for Ca^{2+} uptake. MCU oligomers assemble to form the channel pore of the uniporter complex (Baughman *et al.*, 2011; De Stefani *et al.*, 2011).

MCU$^{-/-}$ mice are viable and have no major alterations in basal metabolism but lack the ability to rapidly uptake Ca^{2+} into the mitochondria and display reduced ability to perform strenuous activity. Cells derived from these mice do not show Ca^{2+}-induced permeability transition pore opening but can still undergo apoptosis (Pan *et al*, 2013). *MCU (null)* mutations in *Drosophila* similarly lead to the loss of rapid Ca^{2+} uptake. Contrary to mice, MCU defects in *Drosophila* inhibit mitochondrial respiration and negatively affect lifespan (Tufi *et al*, 2019).

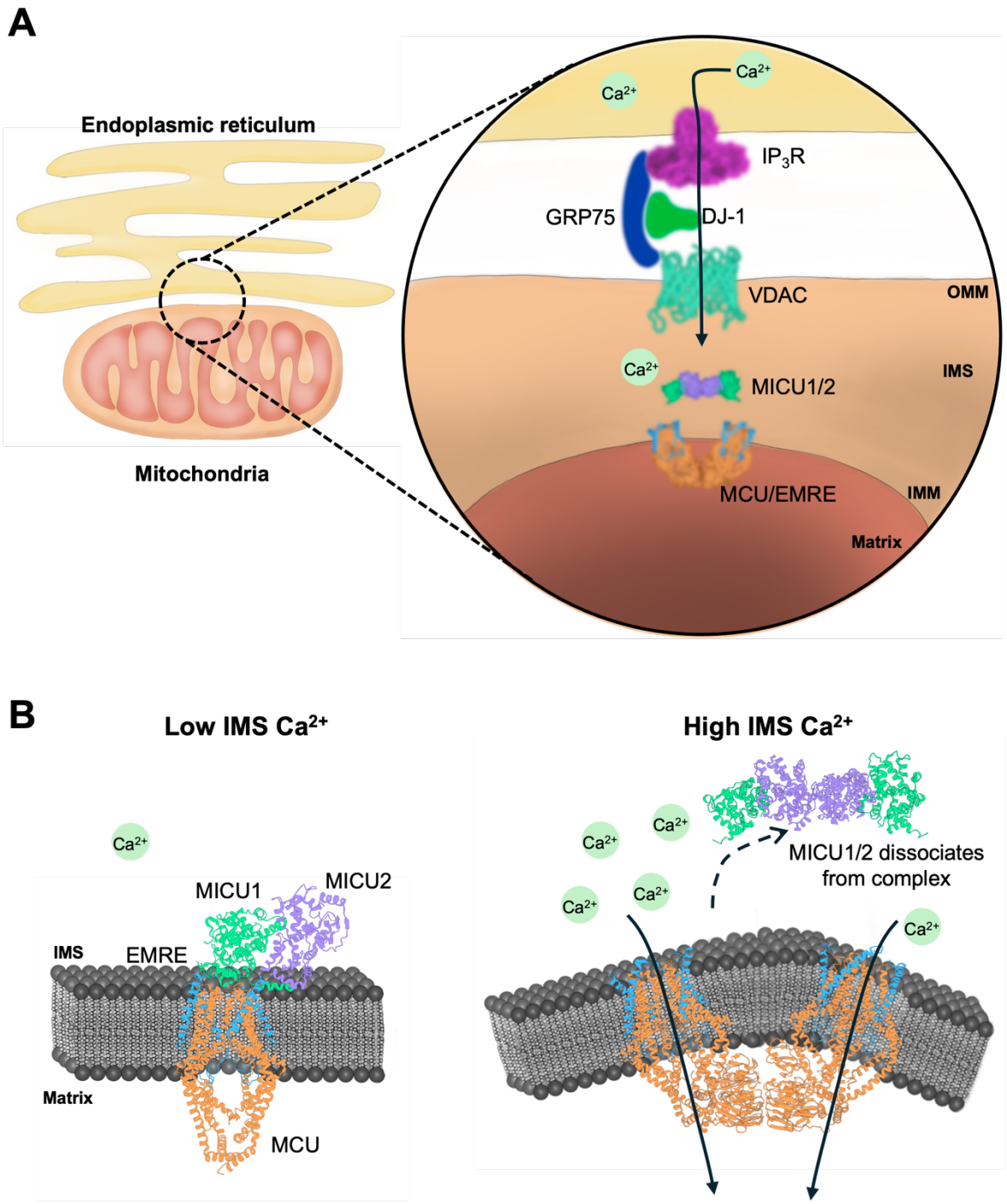

Figure 2. Calcium entry into the mitochondria.
(A) The MCU complex is often found in proximity to mitochondria-endoplasmic reticulum contact sites. Ca^{2+} can be rapidly transferred from the ER to mitochondria as part of Ca^{2+} signalling. (B) Increased Ca^{2+} concentration in the intermembrane space leads to a rearrangement of the MCU comlplex, with MICU1/MICU2 dimers dissociating from the complex to allow Ca^{2+} entry into the mitochondrial matrix.

MCUb shares around 50% homology with the MCU protein and contains the same domain structure. MCUb is conserved in vertebrates but is absent in most other species where MCU is present. MCU and MCUb can form hetero-tetramers, however, incorporation of MCUb in the channel leads to a decreased transfer of Ca^{2+} through the channel. This is likely due to a E256V substitution in the short loop region. The ratio between MCU and MCUb seems to be tissue specific, and possibly sets the capacity of mitochondrial Ca^{2+} uptake (Raffaello *et al.*, 2013; De Stefani *et al*, 2016).

Essential MCU Regulator (EMRE) is a 10kDa protein that spans the inner mitochondrial membrane and contains a highly conserved C-terminus, which projects into the matrix. The exact role of EMRE within the MCU complex is not fully understood, but some studies show that its downregulation prevents Ca^{2+} uptake. Furthermore, EMRE is necessary for the interaction of MCU and MICU1 (Sancak *et al.*, 2013; Vais *et al.*, 2016; Liu *et al*, 2020). However, the importance of EMRE is likely species specific, as it seems to be essential for the assembly of the mammalian MCU complex, but not in fungi (Kovacs-Bogdan *et al*, 2014). Substitution of amino acids in the C-terminus of EMRE leads to loss of inhibition of the MCU channel opening upon high matrix Ca^{2+} concentration, suggesting that it acts as a sensor (Vais *et al.*, 2016). Loss of EMRE function in *Drosophila* leads to a loss of rapid mitochondrial Ca^{2+} uptake, a reduction in lifespan, and a mild impairment in respiration (Tufi *et al.*, 2019).

MICU1 was the first component of the MCU complex to be discovered and is part of the MICU family of regulators of Ca^{2+} uptake by the MCU channel. MICU family members reside in the intermembrane space, and they are responsible for the sigmoidal response of the MCU complex to cytoplasmic Ca^{2+} concentrations. MICU1 silencing in cells results in mitochondrial Ca^{2+} overload, suggesting that the MICU family are gatekeepers of the MCU complex (Perocchi *et al*, 2010; Mallilankaraman *et al*, 2012b; Csordas *et al.*, 2013). MICU1 multimers interact with the MCU complex under low Ca^{2+} concentrations and dissociate from the uniporter in the response to Ca^{2+}, in a membrane potential independent manner (Waldeck-Weiermair *et al*, 2015).

Homozygous MICU1 knockout mice are not viable and die shortly after birth with no obvious phenotypic defects. A few escaper animals survive past 1 week of age but display reduced strength and cerebellar defects. The addition of an EMRE1

heterozygous loss of function mutation improves the health of MICU1 null mice (Antony *et al*, 2016; Liu *et al*, 2016). Skeletal muscle-specific MICU1 knockout results in muscle weakness and atrophy, and decreased ability to repair sarcolemmal damage (Debattisti *et al*, 2019). Liver-specific MICU1 knockdown in mice leads to mitochondrial Ca^{2+} overload, which impairs tissue regeneration following injury, due to a sustained inflammatory response and mPTP-dependent necrosis (Antony *et al.*, 2016). *Drosophila* harbouring a homozygous *MICU1* loss of function mutation do not develop further than the third instar stage, and genetic inhibition of the *MCU* does not rescue this defect. MICU1 deficient larvae display impaired ATP production and reduced abundance of mitochondria within the cells (Tufi *et al.*, 2019). Fibroblasts taken from patients with *MICU1* mutations have been reported to display altered mitochondrial Ca^{2+} uptake. Some evidence suggests an increased uptake in response to ER Ca^{2+} release and a higher rate of uptake in basal conditions. Contrasting evidence shows a counterintuitive reduction in Ca^{2+} uptake, which may be due to a basal increase in matrix Ca^{2+}, which decreases the ability for further uptake (Logan *et al*, 2014; Lewis-Smith *et al*, 2016). Furthermore, there is an association between increased fragmentation of the mitochondrial network and higher Ca^{2+} levels in the matrix (Logan *et al.*, 2014).

MICU2 forms a heterodimer with MICU1. MICU2 relies on the presence of MICU1 for its function, since the downregulation of MICU1 also decreases MICU2 protein levels. Knockout of either MICU1 or MICU2 reduces the threshold at which Ca^{2+} enters the mitochondria. However, their functions are non-redundant, since overexpression of MICU2 in MICU1 KO cells (or *vice versa*) are unable to rescue Ca^{2+} uptake dysregulation (Plovanich *et al*, 2013; Kamer & Mootha, 2014; Patron *et al*, 2014). Dimerisation of MICU1 and MICU2 relies on the activity of Mia40/CHCHD4, which oxidises MICU1 and promotes the formation of a disulphide bond following the import of MICU1 into the IMS and its subsequent interaction with MCU (Petrungaro *et al*, 2015). Patient-derived *MICU2* mutant cells display disrupted Ca^{2+} homeostasis, which may explain neurodegeneration as observed in affected patient carriers (Shamseldin *et al*, 2017).

MICU3 is a tissue-specific member of the MICU family and is highly expressed in the nervous system (Plovanich *et al.*, 2013). Although its function is poorly understood, new evidence in *Drosophila* shows that *MICU3* loss of function

leads to reduced lifespan and neuron-dependent climbing, but no obvious alteration in respiration (Tufi *et al.*, 2019).

In addition to its role in the MCU complex, MICU1 has also been shown to be a critical component of the cristae junctions and interacts with the MICOS complex subunits MIC60 and CHCHD2. MICU1 localises to the inner boundary membrane (IBM) during resting and stimulated conditions, while MCU is evenly distributed across the entire IMM. Upon Ca^{2+} stimulation, MICU1 oligomers separate into dimers and temporarily open the cristae junction, allowing Ca^{2+} to enter the cristae and flow unrestricted into the matrix via constitutively active MCU channels. The dimerised MICU1 then traps MCU in the IBM and ensures continued uptake of Ca^{2+} into the matrix after the cristae junction has closed. Knockdown of MICU1 leads to a widening of the cristae junction, a decrease in membrane potential, and redistribution of cytochrome C from the cristae to the IMS. The redistribution of cytochrome C primes the cells and makes them more sensitive to apoptotic stimuli (Gottschalk *et al*, 2019; Gottschalk *et al*, 2022; Tomar *et al*, 2023).

Two further regulatory subunits of the MCU complex exist – MCUR1 and SLC25A23. Both were identified in an RNAi screen of mitochondrial membrane proteins that influence Ca2+ uptake. Knockdown of either subunit impairs mitochondrial Ca^{2+} uptake (Mallilankaraman *et al*, 2012a; Hoffman *et al*, 2014; Paupe *et al*, 2015).

Efflux of Ca2+ from the mitochondria is thought to be largely controlled by the mitochondrial NCLX (Palty *et al.*, 2010). Tamoxifen-induced, cardiac-specific knockout of NCLX in mice results in death of most of the animals within two weeks of induction. The ensuing Ca^{2+} overload in NCLX-knockout cardiac cells results in mPTP opening and cell death (Luongo *et al*, 2017). The IMM protein TMEM65 also plays an essential role in the regulation of NCLX, and deletion leads to Ca^{2+} overload and excessive mPTP opening (Garbincius *et al*, 2023; Vetralla *et al*, 2023). In conditions of high membrane potential, the H^{+}/ Ca^{2+} exchanger, TMIMB5, plays a greater role than NCLX in the efflux of Ca^{2+} (Austin *et al*, 2022; Patron *et al*, 2022).

Together, it is clear that appropriate homeostasis of Ca^{2+} within the mitochondria is essential for cellular health, and that breakdown of this homeostasis could lead to reduced ATP production and cell death. Thus, dysregulation of mitochondrial Ca^{2+} may play an important role in disease.

The spectrum of mitochondrial disease

Clinical variation in mitochondrial syndromes and disease

Considering the vital role of mitochondria in many cellular processes, it is unsurprising that patient mutations in over 350 genes have currently been linked with mitochondrial syndromes and disease (Ng *et al*, 2021a). The clinical outcomes of these mutations can vary greatly between individuals, in the age of onset, the tissues involved, and disease severity (Blok *et al*, 2009; Mancuso *et al*, 2013; Sommerville *et al*, 2017; Pickett *et al*, 2018; Sofou *et al*, 2018). Disease-causing mutations are typically found in genes encoding the ETC subunits, OXPHOS assembly factors, or in factors associated with mtDNA maintenance. Mutations have also been observed in components of the mitochondrial protein quality control system, protein import systems, and in metabolite transporters (Frazier *et al*, 2019).

Mitochondrial disease commonly results in myopathy and/or neuropathy due to the high energy demands of the brain, muscle, heart, retina and cochlea (Mink *et al*, 1981). However, there can also be additional involvement of the liver, kidneys, and other tissues (Figure 3) (Ng & McFarland, 2023).

An example of the clinical variation of mitochondrial disease comes from patients with mutations in the *AIFM1* gene, which encodes for apoptosis-inducing factor (AIF). AIF resides in the IMS, where it regulates oxidative folding of imported polypeptides alongside CHCHD4. Multiple patient mutations in *AIFM1* have been identified, which lead to variable symptoms including ataxia, hearing loss, neuropathy, myoclonus, encephalomyopathy, Charcot-Marie-Tooth disease, etc. Symptoms typically present during infancy, however there are some cases with a later age of onset, for example a patient with a 1357G>C mutation that developed symptoms of sensory neuropathy and hearing loss in their 30s (Bano & Prehn, 2018; Kawarai *et al*, 2020; Wischhof *et al*, 2022).

Another example of patient variation comes from loss-of-function mutations in the nuclear genome-encoded MICU1, which can result in a broad range of symptoms that present at an early age. These symptoms may include proximal myopathy, learning difficulties, extrapyramidal movement disorder, ataxia, reduced attention and sleep disorders, fatigue and lethargy, nystagmus, bilateral optic atrophy, hypotonia, global muscle weakness, microcephaly, ophthalmoplegia, ptosis,

and axonal peripheral neuropathy (Logan *et al.*, 2014; Wilton *et al*, 2020; Kohlschmidt *et al*, 2021; Tomar *et al.*, 2023). A variety of loss-of-function mutations

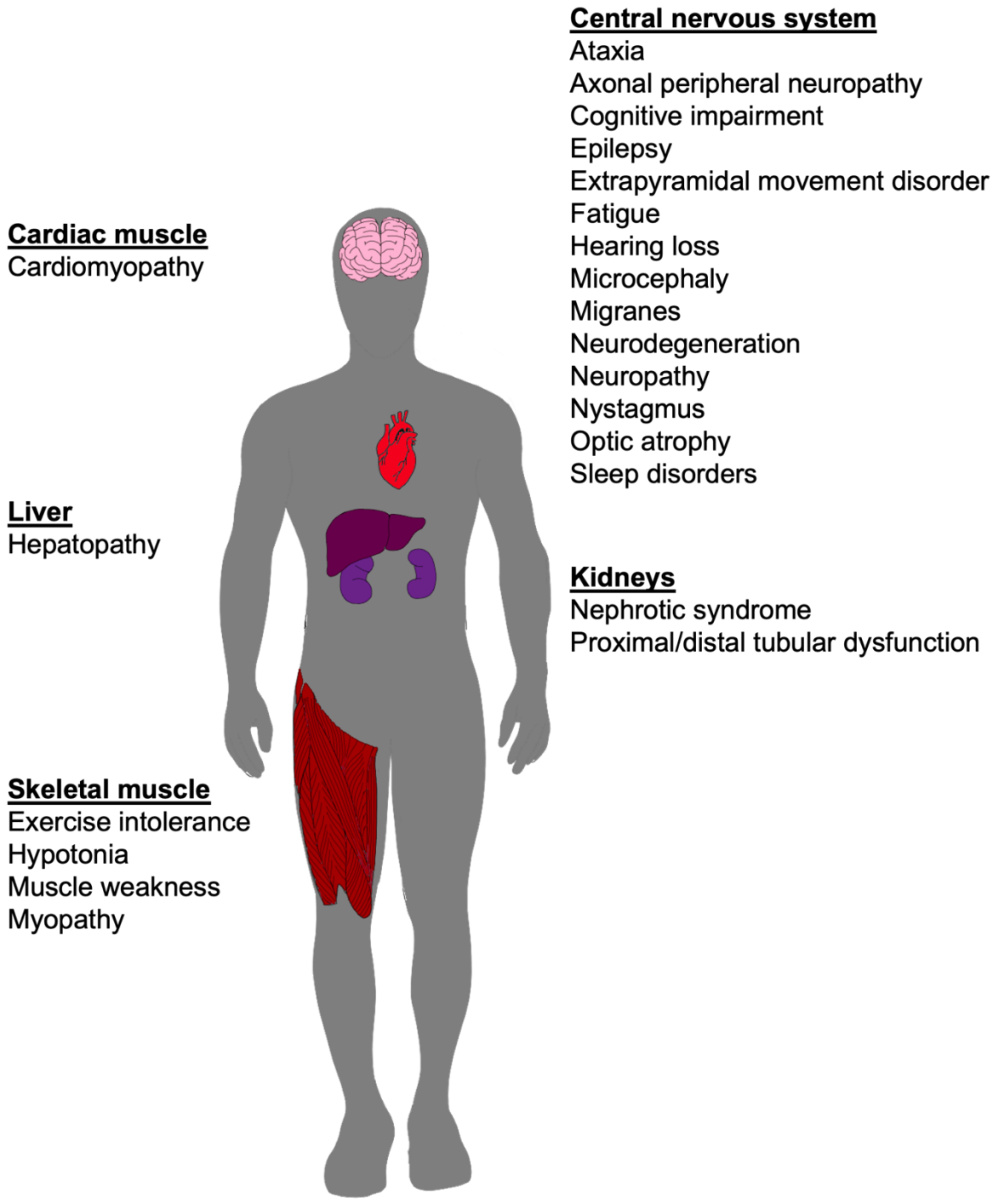

Figure 3. Symptoms of mitochondrial disease.
Mitochondrial disease results in a large variation in symptoms, of which most affect tissues of high energy demand, such as the brain and muscle.

have been identified to date, including nonsense mutations resulting in premature stop codons (p.(Arg18*) and p.(Arg185*)), deletions in the in exons 1 and 2, and mutations in intronic splice donor/acceptor sites (c.741+1G>A and c.1078–1G>C) (Logan *et al.*, 2014; Lewis-Smith *et al.*, 2016; Kohlschmidt *et al.*, 2021). Electron micrographs of muscle biopsies show enlarged mitochondria with electron dense inclusions in the matrix, and disorganized cristae, which is consistent with the function of MICU1 in the MICOS complex (Kohlschmidt *et al.*, 2021; Tomar *et al.*, 2023).

As demonstrated above, mutations in the mitochondrial and nuclear genome can both result in disease that is highly variable. Currently, a sufficient understanding of the mechanisms that underlie this heterogeneity in mitochondrial disease is lacking.

Challenges in diagnosis and treatment of mitochondrial disease

Diagnosis of mitochondrial disease can be challenging, due to the heterogeneity of symptoms and age of onset. Histopathological analyses were based on well-established tissue staining techniques, such as the Gomori trichrome and COX staining of muscle biopsies. The presence of “ragged red fibers” or fibers lacking COX staining could be used to diagnose mitochondrial disease affecting the skeletal muscle (Gomori, 1950; DiMauro *et al*, 1980; Byrne *et al*, 1985; Nakano *et al*, 1987). Recently, progress has been made to develop less invasive methods of diagnosis. Examples include the assessment of expression of biomarkers such as FGF21, GDF15, circulating blood mtDNA, circulating serum neurofilament light chain, etc. (Tyynismaa *et al*, 2010; Kalko *et al*, 2014; Lin *et al*, 2020; Maresca *et al*, 2020; Varhaug *et al*, 2021). Since around 2/3 of adult-onset mitochondrial disease is caused by mtDNA mutations, screening of common mtDNA variants or amplification and sequencing of the whole mitochondrial genome can be beneficial, following the diagnosis of mitochondrial disease. If this fails to identify a genetic cause, then whole genome or whole exome sequencing may be carried out (Ng *et al.*, 2021a).

Mitochondrial diseases are often diagnosed as syndromes, which are named by their clinical features rather than the genetic cause. An example of this is Myopathy, Encepalopathy, Lactic Acidosis, and Stroke-like symptoms (MELAS). The majority of MELAS cases are caused by a mutation in MT-TL1 (m.3243A>G), while

the remaining cases are caused by other mtDNA variations, or mutations in the nuclear gene *POLG* (Pavlakis *et al*, 1984; Goto *et al*, 1990; Ng *et al*, 2021b).

Many mitochondrial diseases manifest in childhood. One of the most common childhood mitochondrial diseases is Leigh Syndrome. Mutations in over 75 genes across both the mitochondrial and genomic DNA can lead to Leigh Syndrome. As one of the most clinically heterogeneous syndromes, Leigh syndrome is defined by an early onset around 2 years of age, and neurological symptoms such as developmental delay, hypotonia, dystonia, ataxia, nystagmus and optic atrophy. Additional tissues that are affected include cardiac, hepatic, gastrointestinal, and renal systems. Premature death of the patients typically occurs by 3 years of age (Leigh, 1951; Rahman *et al*, 1996; Lake *et al*, 2016; Bakare *et al*, 2021). Additional examples of childhood onset mitochondrial disease include: Learns-Sayre syndrome, Pearson syndrome, Alpers-Huttenlocher syndrome, and Barth syndrome (Ng & McFarland, 2023).

As mitochondrial diseases are relatively rare, clinically heterogeneous and have a poor genotype-to-phenotype correlation, the development of novel therapeutic strategies remain difficult. Therefore, current options are limited, and include combinations of exercise and dietary supplements (Parikh *et al*, 2017; Hirano *et al*, 2018). Because of the complexity of mitochondrial diseases, one treatment will likely not benefit all patients, and may even be detrimental to others. For example, valproate has been shown as an effective treatment for patients with myoclonic epilepsy, however if the patient has a mutation in *POLG*, this can result in liver failure (Hynynen *et al*, 2014; Kang *et al*, 2024).

In order to develop new treatments, an improved understanding of the molecular mechanisms that underlie mitochondrial disease is necessary. These mechanisms can be investigated in animal models of mitochondrial disease.

Mitochondrial disease modelling

Animal models have been crucial in furthering our understanding of the molecular mechanisms underlying human disease. Knockout mouse models of genes (e.g., *Surf1, Ndufs4, Tfam,* and *Sod2)* or models with patient gene mutations such as the *Twinkle* deletor animals, recapitulate many pathological signatures of

human mitochondrial disease (Li *et al*, 1995; Larsson *et al*, 1998; Wang *et al*, 1999; Tyynismaa *et al*, 2005; Dell'agnello *et al*, 2007; Kruse *et al*, 2008).

As an example of a mouse model of mitochondria disease, *Ndufs4* knockout impairs CI activity and promote Leigh syndrome-like symptoms, including ataxia, blindness, reduced rate of growth, and premature death. Interestingly, brain-specific *Ndufs4* KO causes neurodegeneration as in full KO animals. The increased impact of the *Ndufs4* KO on the nervous system mimics the primarily neurological nature of Leigh syndrome (Rahman *et al.*, 1996; Kruse *et al.*, 2008; Quintana *et al*, 2010).

Mouse models also exist that aim to model human disease associated with *AIFM1* mutations. For example, an *Aifm1(R200del)* knock-in mouse line was generated to attempt to model patient disease associated with *AIFM1(R201del)* mutations. Patients with this mutation develop severe encephalomyopathy, while the mouse model develops early-onset myopathy and late-onset peripheral neuropathy, with no obvious brain defects (Ghezzi *et al*, 2010; Wischhof *et al*, 2018). Another mouse model to investigate *Aifm1* deficiency is the hypomorphic harlequin model. Harlequin mice develop severe ataxia and cerebellar degeneration, with variable levels of myopathy (Klein *et al*, 2002). While both the harlequin and the *Aifm1(R200del)* knock-in models have reduced levels of AIF expression and CI impairment, each model has a different pathological manifestation (Wischhof *et al.*, 2018).

While some mouse models of mitochondrial disease can recapitulate many aspects of human disease, others have less overlap with human phenotypes. In humans, *MICU1* loss of function mutations or deletions lead to a wide spectrum of phenotypes. Some patients have relatively mild symptoms such as fatigue or episodes of muscle weakness, while others develop more severe symptoms including myopathy with extrapyramidal signs, ataxia, or optic atrophy (Logan *et al.*, 2014; Lewis-Smith *et al.*, 2016; Musa *et al*, 2019; Bitarafan *et al*, 2021; Kohlschmidt *et al.*, 2021; Sharova *et al*, 2022). *Micu1* knockout in mice leads to the death of most animals within the first week of life. The few animals that survive longer do show signs of developmental delay, ataxia, and impaired muscle function, similar to some patients with *MICU1* mutations (Antony *et al.*, 2016; Liu *et al.*, 2016). The relative severity in this mouse model is likely due to a full loss of MICU1 activity, while human patients have mutations that still retain some function.

While animal and cellular models of mitochondrial disease recapitulate certain aspects of human disease pathology, they do not address the problem of heterogeneity in human disease.

The mitochondrial threshold effect.

In some species, mild depletion of OXPHOS subunits can lead to lifespan extension, contrary to what is expected when considering the strong link between mitochondrial dysfunction and disease in humans (Dell'agnello *et al.*, 2007; Lapointe *et al*, 2009; Durieux *et al*, 2011; Houtkooper *et al*, 2013; Owusu-Ansah *et al*, 2013). This phenomenon is well-reported in *C. elegans*, since mutations in genes encoding ETC subunits (e.g. *cco-1, isp-1* and *nuo-6)* can lead to increased lifespan and increased resistance to oxidative stress (Feng *et al*, 2001; Rea *et al*, 2007; Yang & Hekimi, 2010; Houtkooper *et al.*, 2013). Similar lifespan extensions have also been reported in nematodes upon RNA interference against mitochondrial proteins (Dillin *et al*, 2002; Lee *et al*, 2003). While this effect is common in *C. elegans*, the beneficial effects of mild mitochondrial dysfunction have also been identified in other species. It has been shown that RNAi treatment against subunits of CI, CIII, CIV, or CV in *Drosophila melanogaster* can lead to lifespan extension. Furthermore, mutations in mice that result in mild mitochondrial dysfunction have been shown to enhance longevity and, in some cases, confer resistance to neurotoxicity (Dell'agnello *et al.*, 2007; Copeland *et al*, 2009; Lapointe *et al.*, 2009).

The “mitochondrial threshold effect” is a theory that outlines how organisms respond to mitochondrial dysfunction. The idea is that mitochondrial dysfunction activates compensatory mechanisms to overcome damage. If the dysfunction is mild, the compensatory mechanisms can promote survival despite the defects in energy production. Conversely, when the damage outweighs the level of compensation, animals develop disease and die earlier (Figure 4). In a disease context, it could be that differential activation of compensatory mechanisms may explain some of the variability in clinical presentation between individuals with similar genetic lesions. Thus, the identification of pathways that can account for this compensation may be useful for treatment of primary human mitochondrial disorders (Mazat *et al*, 1997; Rossignol *et al*, 2003; Rea *et al.*, 2007).

To date, research into mitochondrial mutations in *C. elegans* (and some other key model organisms) has revealed components of the compensatory mechanisms that overcome mitochondrial dysfunction. Mitochondrial damage and loss of membrane potential results in reduced efficiency of import and impaired processing of proteins in the mitochondria (Krayl *et al*, 2007; van der Laan *et al*, 2007). Proteins that are unable to be transported into the mitochondria accumulate in the cytosol and

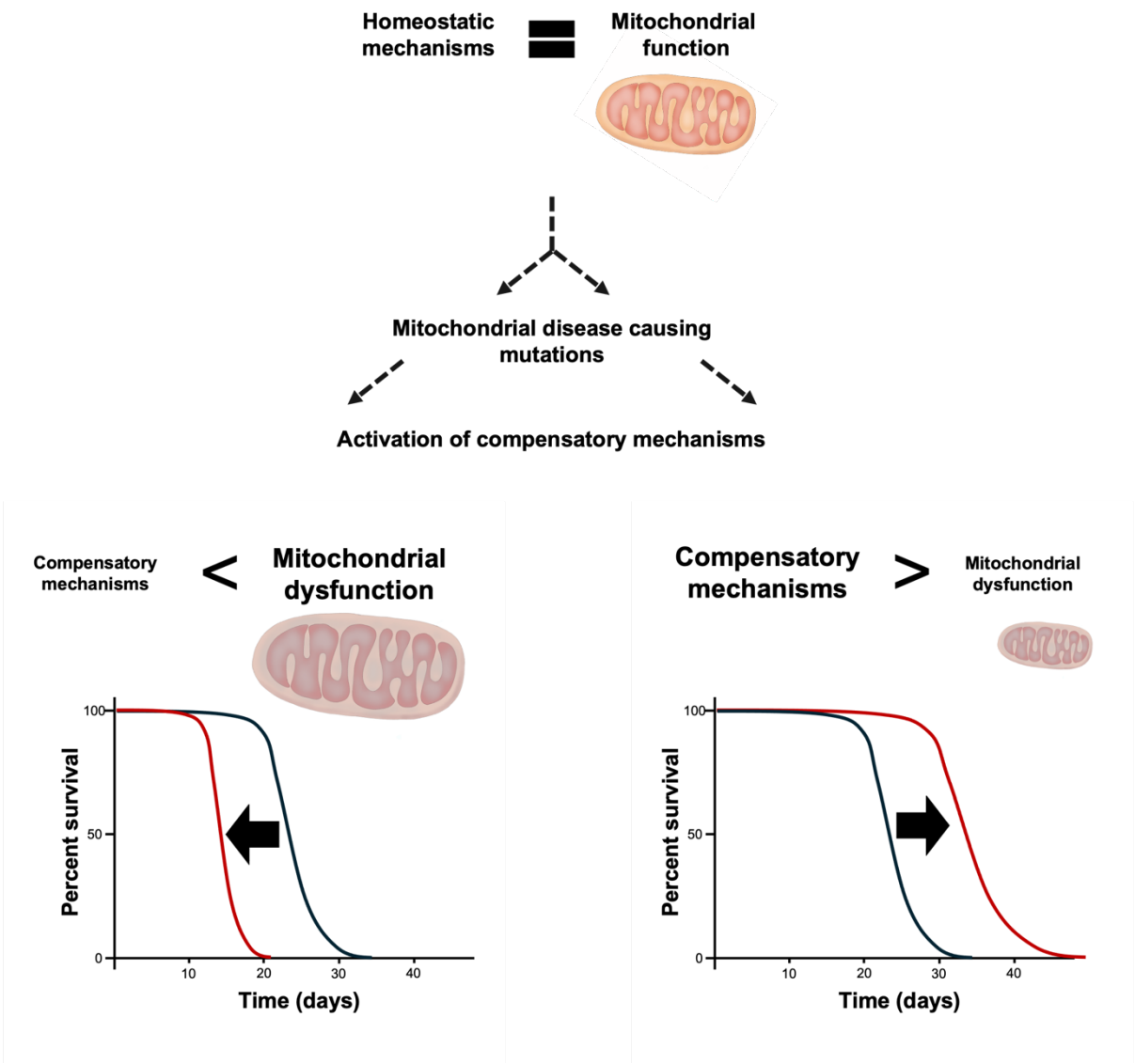

Figure 4. The mitochondrial threshold effect.
Mitochondrial dysfunction activate compensatory pathways which, below a certain threshold, can result in improved organismal health and lifespan extension. Dysfunction beyond this threshold results in reduced lifespan.

are degraded by the proteosome (Wrobel *et al*, 2015). In *C. elegans,* reduced import efficiency and degradation of the transcription factor ATFS-1 leads to its translocation to the nucleus and activation of the mitochondrial unfolded protein response (mtUPR), which aims to re-establish proper mitochondrial function. The mtUPR can be activated by a variety of stimuli including: reduced mtDNA content, accumulation of unfolded proteins inside the matrix, inhibition of mitochondrial chaperones or proteases, impairment of mitochondrial protein translation, and OXPHOS inhibition (Zhao *et al*, 2002; Nargund *et al*, 2012; Owusu-Ansah *et al.*, 2013; Liu *et al*, 2014; Lin & Haynes, 2016). The expression of chaperones (e.g. *hsp-6* and *hsp-60*), proteases, anti-oxidants, OXPHOS complex assembly factors, and glycolytic enzymes are all increased as part of the mtUPR (Haynes *et al*, 2010; Nargund *et al.*, 2012; Nargund *et al*, 2015; Rolland *et al*, 2019). Additional key proteins involved in the activation of the mtUPR are the transcription factors UBL-5 and DVE-1, the histone methyltransferase MET-2, the histone demethylases JMJD-1.2, JMJD-3.1 and HDA-1, and the nuclear co-factor LIN-65 (Benedetti *et al*, 2006; Haynes *et al*, 2007; Merkwirth *et al*, 2016; Tian *et al*, 2016; Shao *et al*, 2020).

Asides from mitochondrial dysfunction, multiple inducers of longevity have been identified in *C.* elegans, including dietary restriction, impaired insulin signalling, or germline ablation. These longevity-inducing conditions activate stress response pathways under the control of transcription factors, such as DAF-16, HLH-30, PHA-4, SKN-1, HIF-1 and HSF-1. These factors control transcription of numerous genes involved in pathways such as the endoplasmic reticulum UPR, the ubiquitin proteasome system, the heat shock response, and translation. In addition to the mtUPR, mitochondrial dysfunction also activates various aspects of these stress response pathways to restore cellular function (Lee *et al*, 2010; Park *et al*, 2010; Wei & Kenyon, 2016; Senchuk *et al*, 2018). Evidence suggests that ATFS-1 is not only required for mtUPR, but is also important for the activation of other stress response pathways in collaboration with SKN-1, HIF-1, and DAF-16 (Wu *et al*, 2018).

Inhibition of the insulin signalling pathway was the first discovered modulator of lifespan in *C. elegans* (Friedman & Johnson, 1988; Kenyon *et al*, 1993). Hypomorphic mutations in the gene encoding the insulin receptor DAF-2, or downstream targets such as AGE-1, alter the phosphorylation status of the transcription factor DAF-16, resulting in its translocation to the nucleus. A variety of posttranslational modification (PTMs) of DAF-16 have been identified that modulate

its activity, which have been demonstrated to be relevant for the integration of multiple upstream signals to influence longevity (Li *et al*, 2007; Takahashi *et al*, 2011; Chiang *et al*, 2012). DAF-16 is involved in the transcription of antioxidant genes such as *sod-3,* which is essential for lifespan extension of long-lived mitochondrial mutants *clk-1, nuo-6* and *isp-1* (Dues *et al*, 2017; Senchuk *et al.*, 2018; Wu *et al.*, 2018).

Activation of autophagy to induce longevity is controlled primarily by the transcription factors HLH-30 and PHA-4. Inhibition of mTOR or insulin signalling activates autophagy and lysosomal biogenesis via HLH-30 (Settembre *et al*, 2011; Roczniak-Ferguson *et al*, 2012). Similarly, dietary restriction via mutations in genes such as *eat-2*, or through restriction of food availability, increases lifespan in a PHA-4-dependent manner, by activating autophagy (Panowski *et al*, 2007; Hansen *et al*, 2008). Long-lived mitochondrial mutants such as *clk-1*(*e2519)* display increased expression and nuclear localisation of HLH-30, and downregulation of HLH-30 reduces lifespan (Lapierre *et al*, 2013). Furthermore, loss of function mutations in key autophagy genes abolishes lifespan extension in response to RNAi again CV subunit ATP-3 (Toth *et al*, 2008).

SKN-1 is involved in the response to oxidative stress and leads to the transcription of phase II detoxification genes such as *gst*-4. Furthermore, SKN-1 has been found to promote the production of the proteosome, aid in the activation of the endoplasmic UPR, and is involved in the activation of mitophagy and mitochondrial biogenesis in response to mitochondrial damage (Li *et al*, 2011; Glover-Cutter *et al*, 2013; Palikaras *et al*, 2015). Long-lived *nuo-6(qm200)* animals display increased expression of *gst-4,* however this seems to be dispensable for lifespan extension in this context (Wu *et al.*, 2018).

HIF-1 is involved in the response to hypoxia and induces the transcription of detoxification genes such as *nhr-57*. Long-lived animals with mutations in *nuo-6, clk-1,* and *isp-1* have increased generation of mitochondrial ROS, activation of HIF-1, and increased expression of *nhr-57.* Disruption of HIF-1-mediated signalling abolishes lifespan extension these mutants (Lee *et al.*, 2010; Dues *et al.*, 2017; Wu *et al.*, 2018).

The heat shock response is vital in proteostasis in the cytosol, and its main regulator is the transcription factor HSF-1. Key links between mitochondrial ETC

function and the heat shock response have been identified (Labbadia *et al*, 2017). RNAi against ETC components induces a specific phosphorylated form of HSF-1, and upregulates expression of HSF-1 target genes such as *hsp-16.2* (Williams *et al*, 2020). Furthermore, there is interplay between the mtUPR and the heat shock response, since downregulation of downstream components of the mtUPR triggers an HSF-1-dependent cytosolic stress response (Kim *et al*, 2016).

While the involvement these different transcriptional networks in lifespan extension in response to mitochondrial dysfunction is well documented, the role of specific pathways within these complex transcriptional networks have been relatively underexplored.

Neurodegeneration is linked with mitochondrial dysfunction

While inherited mutations in a variety of mitochondrial protein encoding genes often result in the disorders mentioned above, some of them have been also associated with neurodegenerative processes. Examples of mitochondrial proteins that are mutated in neurodegenerative diseases include MFN2 in Charcot-Marie-Tooth (CMT) subtype 2A, GDAP1 in CMT4A, OPA1 in dominant optic atrophy, and SOD1 in Amyotrophic Lateral Sclerosis (Rosen *et al*, 1993; Delettre *et al*, 2000; Baxter *et al*, 2002; Zuchner *et al*, 2004). Parkinson's disease is perhaps the neurodegenerative disease that is, genetically, most strongly associated with mitochondrial dysfunction. Mutations in the mitochondrial proteins Parkin, DJ-1, PINK1, LRRK2, and Pol γ all cause familial PD (Kitada *et al*, 1998; Bonifati *et al*, 2003; Luoma *et al*, 2004; Valente *et al*, 2004; Zimprich *et al*, 2004). Besides the genetic link between mitochondrial dysfunction and PD there is also strong association between PD and CI inhibition, since exposure to MPPP, MPTP, rotenone, and other CI inhibitors can induce parkinsonism (Davis *et al*, 1979; Langston *et al*, 1983; Betarbet *et al*, 2000).

In idiopathic neurodegenerative diseases and those with no genetic association with mitochondrial mutations, mitochondrial dysfunction is nevertheless an evident signature. For example, Alzheimer's disease (AD) post-mortem brain tissue displays reduced expression of components of the TCA cycle and OXPHOS pathway (Kish *et al*, 1992; Parker *et al*, 1994; Brooks *et al*, 2007). In addition to disrupted mitochondrial bioenergetics, AD pathology is associated with increased

oxidative stress, altered mtDNA integrity, altered fusion/fission dynamics, disrupted trafficking, impaired biogenesis, and impaired mitophagy (Bose & Beal, 2016; Monzio Compagnoni *et al*, 2020; Wang *et al*, 2020).

While the exact role of mitochondrial dysfunction in neurodegenerative disease has not been defined, it is clear that it features in pathology. It may be that age-related neurodegenerative diseases exist on a spectrum with classic mitochondrial disease, and that “mild” mitochondrial dysfunction over time leads to late-onset neurodegenerative disease, while “severe” mitochondrial dysfunction leads to early-onset disease.

Mitochondria at the forefront of Parkinson’s disease

Parkinson’s disease is a neurodegenerative disorder with motor symptoms including bradykinesia, resting tremors, dyskinesia (Figure 5A). In Parkinson’s disease (PD) and other synucleinopathies, the onset of movement defects is due to the loss of dopaminergic neurons of the substantia nigra pars compacta. Disease can arise spontaneously, as a result of environmental factors, or as a consequence of inherited genetic mutations (Figure 5B). Around 15% of PD cases are familial forms, with 5-10% of PD cases presenting with monogenic inheritance patterns (Luo *et al*, 2023). Identification of mutations associated with familial PD and synucleinopathy have provided useful insights into the molecular pathways that are disrupted in disease.

In the late 70s/early 80s, a group of individuals developed parkinsonism following intravenous injection of contaminated drugs. The culprit contaminants were identified as the compounds MPPP and MPTP, which were later found to be inhibitors of mitochondrial Complex I (Figure 5B) (Davis *et al.*, 1979; Langston *et al.*, 1983). Further inhibitors of complex I, such as rotenone (Betarbet *et al.*, 2000), pyridaben, fenpyroximate (Sherer *et al*, 2007), trichloroethylene (Guehl *et al*, 1999; Keane *et al*, 2019), and annonacin (Champy *et al*, 2004), were identified as the cause of selective degeneration of dopaminergic neurons and parkinsonism in experimental models (Burns *et al*, 1983; Heikkila *et al*, 1984). Complex I inhibition by these compounds can have multiple effects on the mitochondria, such as impairment of fission/fusion dynamics and increase in ROS generation (Barsoum *et al*, 2006; Thomas *et al*, 2011; Wang *et al*, 2011). Furthermore, there has been sporadic

evidence for the formation of α-Syn-positive inclusions, a hallmark feature of most forms of PD, following treatment of animals or cells with rotenone or MPTP (Betarbet *et al.*, 2000; Fornai *et al*, 2005).

Mutations in multiple genes have been documented to result in PD. Many of these have a direct role in mitochondrial function or homeostasis, while some have currently no known link to mitochondria. PINK1 and Parkin, for example, act together to trigger mitophagy in damaged mitochondria, and recessive mutations in either can lead to early-onset PD (Kitada *et al.*, 1998; Valente *et al.*, 2004). The loss of function of another PD-causing gene, *PARK7/*DJ-1, impairs mitophagy and results in a fragmented mitochondrial network and the accumulation of damaged mitochondria (Irrcher *et al*, 2010; Krebiehl *et al*, 2010). The mitochondrial network fragmentation caused by DJ-1 loss of function can be rescued by overexpression of PINK1 and Parkin (Irrcher *et al.*, 2010).

Additional supporting evidence of mitochondrial dysfunction in PD comes from post-mortem patient-derived tissue. Patient tissue often show evidence of oxidative damage (Bonifati *et al.*, 2003; Keeney *et al*, 2006; Andres-Mateos *et al*, 2007), complex I deficiency (Schapira *et al*, 1989; Schapira *et al*, 1990; Mann *et al*, 1992; Janetzky *et al*, 1994; Flones *et al*, 2024), and a reduction in the master regulator of mitochondrial biogenesis, PGC-1α (St-Pierre *et al*, 2006; Zheng *et al*, 2010).

While disruption in mitochondrial pathways forms a large part of PD pathogenesis, disruptions in additional pathways have been observed. These pathways include disrupted Ca^{2+} homeostasis, lysosomal function, vesicle trafficking, lipid homeostasis, and the induction of ER stress (Ryu *et al*, 2002; Outeiro & Lindquist, 2003; Gitler *et al*, 2008; Parihar *et al*, 2008; van Ham *et al*, 2008; Chu *et al*, 2009; Dehay *et al*, 2010; Colla *et al*, 2012; Selvaraj *et al*, 2012; Hurley *et al*, 2013; Caraveo *et al*, 2014; Luth *et al*, 2014; Galper *et al*, 2022; Luo *et al.*, 2023). Altered proteostasis is one of the most researched aspects of PD pathology besides mitochondrial dysfunction. This is because in many cases of PD there is the formation of intracellular inclusions called Lewy bodies and Lewy neurites, which largely consist of damaged membranes, as well as oligomers and fibrils of alpha-synuclein (Spillantini *et al*, 1997; Furukawa *et al*, 2002; McNaught *et al*, 2003; Chu *et al.*, 2009; Dehay *et al.*, 2010; Shahmoradian *et al*, 2019).

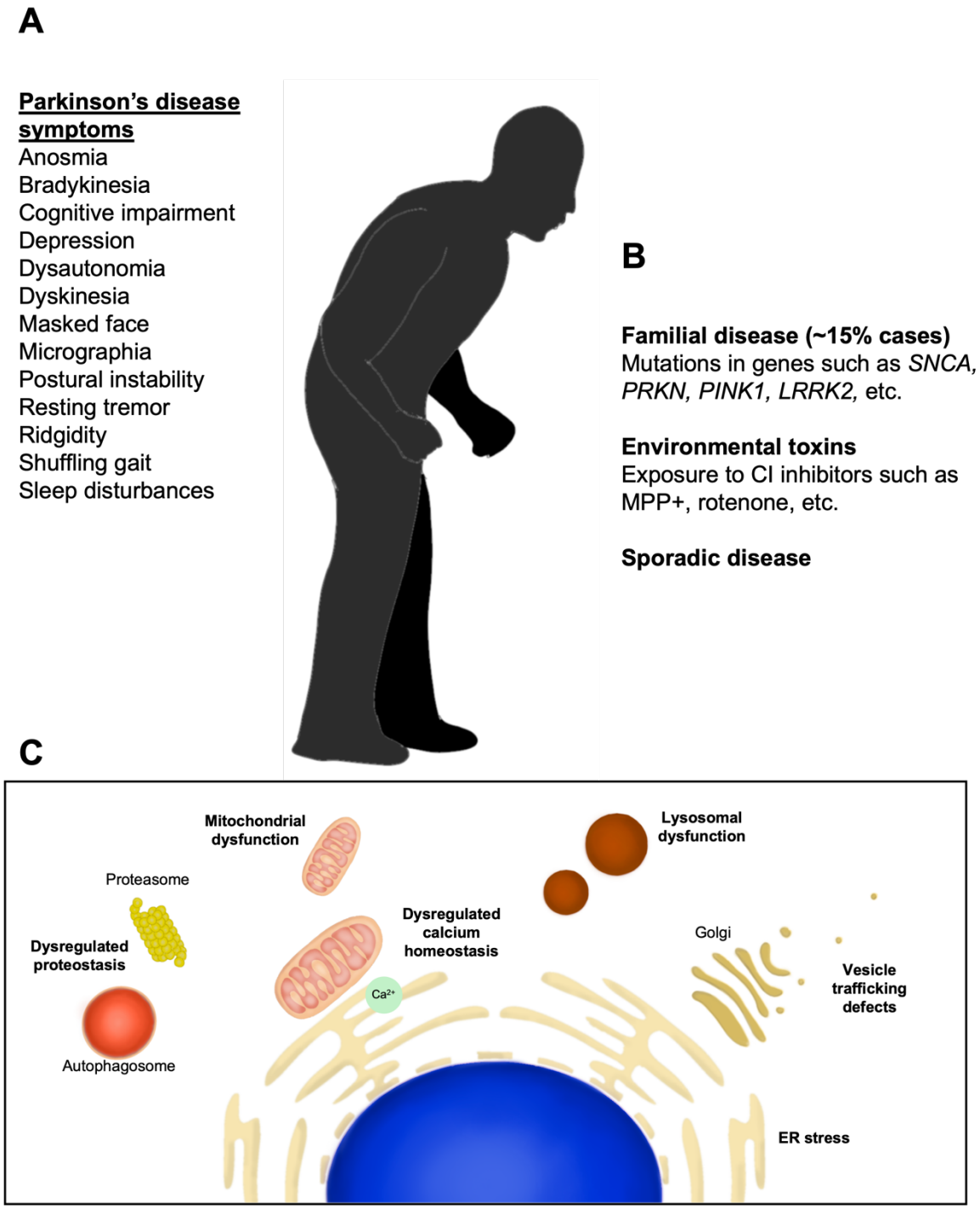

Figure 5. PD symptoms, genetic basis and dysregulated cellular processes. (A) Symptoms associated with Parkinson's disease. (B) Parkinson's disease can occur through inherited genetic mutations, exposure to toxins, or sporadically. (C) A variety of cellular pathways are disrupted in PD.

α-Syn and proteotoxicity in Parkinson's disease

α-Syn and PD pathology

The *SNCA* gene encodes the protein alpha-synuclein (α-Syn). Duplication, triplication, or point mutations in the *SNCA* gene causes PD (Polymeropoulos *et al*, 1997; Kruger *et al*, 1998; Singleton *et al*, 2003; Zarranz *et al*, 2004). α-Syn is a small, intrinsically disordered protein of 140 residues, and was first identified in the synapse and the nucleus of neurons innervating the electric organ of *T. californica*. While its presence and function within the nucleus is currently debated, it is thought that α-Syn regulates various steps of the synaptic vesicle cycle at the pre-synapse (Maroteaux *et al*, 1988; Spillantini *et al.*, 1997; Burre *et al*, 2010; Bendor *et al*, 2013; Burre *et al*, 2014; Atias *et al*, 2019).

In the pre-synapse, α-Syn associates with synaptic vesicles via its N-terminal region, leaving its C-terminal region to interact with binding partners such as synaptobrevin-2 and Synapsin 1. The N-terminal region of α-Syn forms an amphipathic α-helix conformation upon binding to lipid membranes of high curvature. Moreover, α-Syn displays a preference of binding with small vesicles of similar size to synaptic vesicles. Together, it seems that α-Syn may play a role in the maintenance of the size of recycling pools of synaptic vesicles and in inhibiting the docking of vesicles with the plasma membrane via its association with VAMP2/synaptobrevin-2. Triple synuclein KO or treatment with a pan-synuclein antibody depletes vesicles from active zone and reserve pools, while α-Syn overexpression within the range of gene duplication or triplication similarly impairs synaptic vesicle recycling and leads to reduction in the size of the reserve pool. Upon neuronal stimulation, α-Syn disperses from synaptic vesicles alongside Synapsin 1 and allows movement of vesicles to the active zone, however α-Syn dispersal is delayed and only occurs following exocytosis of vesicles. α-Syn has also been shown to play a role in "kiss-and-run" exocytosis, whereby vesicles transiently dock and fuse with the plasma membrane to release part of its contents (Davidson *et al*, 1998; Murphy *et al*, 2000; Eliezer *et al*, 2001; Chandra *et al*, 2003; Fortin *et al*, 2005; Middleton & Rhoades, 2010; Nemani *et al*, 2010; Diao *et al*, 2013; Wang *et al*, 2014; Logan *et al*, 2017; Sun *et al*, 2019; Fouke *et al*, 2021).

While α-Syn does not have a clear physiological role in mitochondrial function, it has been shown that α-Syn O/E may induce mitochondrial dysfunction (Parihar *et al.*, 2008; Banerjee *et al*, 2010; Chinta *et al*, 2010; Li *et al*, 2013; Luth *et al.*, 2014; Subramaniam *et al*, 2014; Tapias *et al*, 2017). In this regard, transgenic animals overexpressing α-Syn or carrying mutations in the *SNCA* gene are also sensitised to the exposure of MPTP or rotenone (Song *et al*, 2004; Nieto *et al*, 2006; Song *et al*, 2015), and conversely have increased resistance when they are lacking *SNCA* (Dauer *et al*, 2002; Klivenyi *et al*, 2006).

Recent evidence indicates α-Syn can interact with TOM20, an essential mediator of mitochondrial protein import, and inhibit its function (Di Maio *et al*, 2016). Furthermore, α-Syn is able to inhibit mitochondrial fusion processes, leading to overall fragmentation of the mitochondrial network (Kamp *et al*, 2010; Nakamura *et al*, 2011; Guardia-Laguarta *et al*, 2014). Since mitochondrial fusion/fission dynamics are essential for synaptic function and for positioning mitochondria in areas of high energy demand, it may be that α-Syn expression interferes with mitochondrial homeostasis, which is particularly detrimental to neurons (Li *et al*, 2004; Verstreken *et al*, 2005; Chang *et al*, 2006; Berthet *et al*, 2014). Together, this highlights a clear involvement of α-Syn in mitochondrial dysfunction associated with PD.

In addition to its influence on mitochondria, aggregation of α-Syn and the formation of Lewy bodies are some of the most studied aspects of disease pathology. It is thought that the aggregation of α-Syn and its neuropathological spreading throughout distinct brain regions is a causative feature of PD pathology (Braak *et al*, 2003; Volpicelli-Daley *et al*, 2011), while some believe that aggregation is just a by-product of other underlying dysfunctional processes, considering that not all familial PD cases display Lewy bodies (Doherty & Hardy, 2013; Doherty *et al*, 2013; Schulz-Schaeffer, 2015). Regardless, study of the cause and the mechanisms of protein aggregation is essential in understanding neurodegenerative processes.

Intrinsically disordered α-Syn and its ability to phase separate

Similar to other proteins that undergo aggregation, α-Syn contains intrinsically disordered regions (IDRs). These regions lack a defined structure, display low complexity and contain a limited number of amino acid residues, such as glycine, serine, glutamine, asparagine, phenylalanine and tyrosine (Gilks *et al*, 2004; Decker

et al, 2007; Reijns *et al*, 2008; Kato *et al*, 2012). Due to this low complexity, these proteins take many different conformations, which may make them more prone to fold in a pathological conformation. Despite the possibility of misfolding, it seems that IDRs have an essential evolutionary function.

The presence of IDRs in a protein often enables it to form biomolecular condensates, which allows proteins to organise themselves within the densely packed cellular milieu without the necessity of a lipid membrane (Nott *et al*, 2015). It is thought that these biomolecular condensates alter the activity of proteins, either through an increase in the local concentration, or conversely, to sequester molecules from reaction partners outside of the condensate (Strzelecka *et al*, 2010; Li *et al*, 2012; Banjade & Rosen, 2014; Tatomer *et al*, 2016; Franzmann *et al*, 2018; Case *et al*, 2019). Condensates may also act to buffer protein concentrations within the cell, act as a detection system for environmental changes, or to mechanically shape cellular contents (Figure 6A) (Riback *et al*, 2017; Shin *et al*, 2018; Klosin *et al*, 2020).

There are numerous examples of membraneless organelles/biomolecular condensation within the cells. Examples include nucleoli (Phair & Misteli, 2000; Audas *et al*, 2012; Feric *et al*, 2016; Frottin *et al*, 2019), Cajal bodies (Phair & Misteli, 2000), PML nuclear bodies (Mao *et al*, 2011; Nott *et al.*, 2015), DNA damage repair sites (Altmeyer *et al*, 2015; Patel *et al*, 2015), stress granules (Molliex *et al*, 2015; Yang *et al*, 2020), germ granules (Brangwynne *et al*, 2009), clusters of vesicles at the presynaptic terminal (Milovanovic *et al*, 2018; Hoffmann *et al*, 2021), and the synaptic active zones (Figure 6B) (Wu *et al*, 2019; McDonald *et al*, 2020). Some of these consist purely of a primary liquid phase, while some are more complex and contain multiple phases (Lang *et al*, 2010; Feric *et al.*, 2016; Jain *et al*, 2016).

Typically, biomolecular condensates consist of a scaffold, which is essential for condensate formation, and client molecules, which are dispensable and directly interact with the scaffold. Scaffolds play an important role in setting the saturation concentration at which a condensate occurs (Banani *et al*, 2016). Multiple factors can regulate the process of condensation, such as concentration, post-translational modifications, or the presence of additional proteins or lipid vesicles (Li *et al.*, 2012; Banjade & Rosen, 2014; Nott *et al.*, 2015; Weber & Brangwynne, 2015; Su *et al*, 2016; Milovanovic *et al.*, 2018; Martin *et al*, 2020; Ruff *et al*, 2021; Shimobayashi *et al*, 2021). Condensates can be removed via autophagy or other ATP-dependent

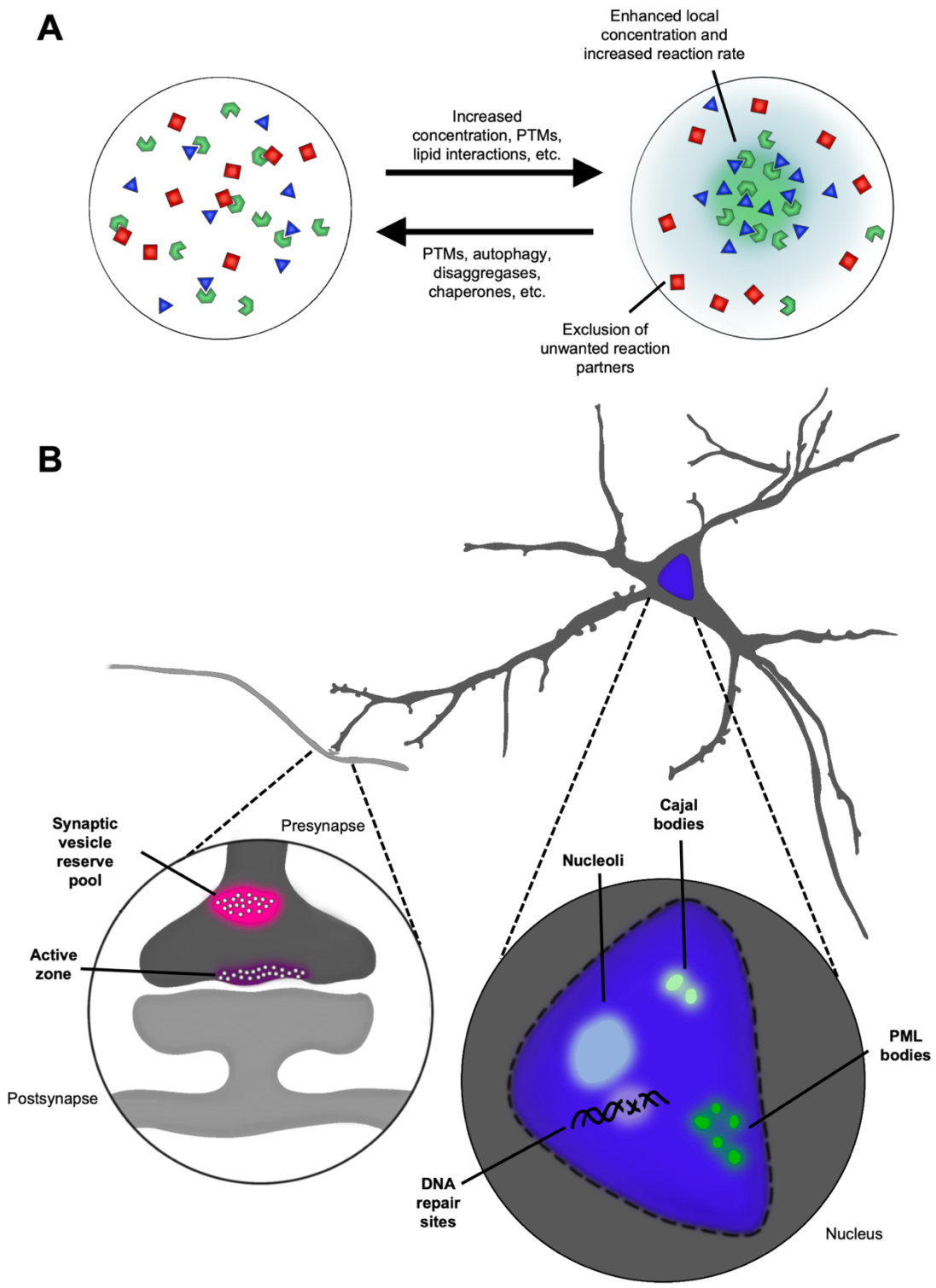

Figure 6. LLPS is a method to organise the contents to the cell.
(A) The process of liquid-liquid phase separation (LLPS) can be a method for enhancing activity of certain proteins or by sequesting them from certain protein-protein interactions. This process is regulated by a variety of factors. (B) LLPS has been implicated in multiple cellular regions and processe

machinery, such as chaperones and disaggregases (Figure 6A) (Buchan *et al*, 2013; Kroschwald *et al*, 2015; Jain *et al.*, 2016). Furthermore, high ATP concentrations have been shown to oppose LLPS and promote aggregation disassembly independently of its energy storage function (Patel *et al*, 2017; Hayes *et al*, 2018). Thus, it is possible that deficiency in the energy state of a cell may lead to unfavourable condensation processes.

The ability to phase separate is not only conferred by the presence of IDRs, but also by the presence of compatible, multivalent domains (Li *et al.*, 2012). The sticker-and-spacer model describes the constituents of biomolecular condensates as molecules formed of “sticker” regions that drive intermolecular interactions within the condensate, and “spacers” that link stickers together and provide flexibility but have no specific influence on the interactions (Semenov & Rubinstein, 1998; Wang *et al*, 2018; Choi *et al*, 2020).

One of the first, and most studied, examples of biomolecular condensation and liquid-liquid phase separation of multivalent proteins, is the formation of condensates of Nephrin, Nck, and N-WASP (Li *et al.*, 2012; Banjade & Rosen, 2014). In this example, Nephrin is a transmembrane protein with a cytoplasmic tail containing three tyrosine residues, which can be phosphorylated and interact with the SH2 domains of Nck. Nck contains three SH3 domains which can, in turn, interact with the six Proline-Rich Motifs (PRMs) of the proline-rich domain of N-WASP. Incubation of SH3 domain- and PRM domain- containing peptides is sufficient for LLPS to occur, with increasing valency decreasing the threshold concentration for condensation to occur. Conditions that promote LLPS of Nck and N-WASP also lead to a sharp increase in the rate of N-WASP-dependent Arp2/3 activation and actin polymerisation (Figure 7A) (Li *et al.*, 2012; Banjade & Rosen, 2014).

At the presynapse, Synapsin 1 and α-Syn phase separate to regulate synaptic vesicle release. In this example, Synapsin 1 forms a scaffold, with lower mobility, while α-Syn is a client with high mobility (Milovanovic *et al.*, 2018; Hoffmann *et al.*, 2021). The IDR of synapsin 1 is necessary and sufficient for condensate formation, but the size and rate of formation is increased in the presence of SH3 domain-containing proteins (Grb2 or Intersectin), molecular crowders, and negatively

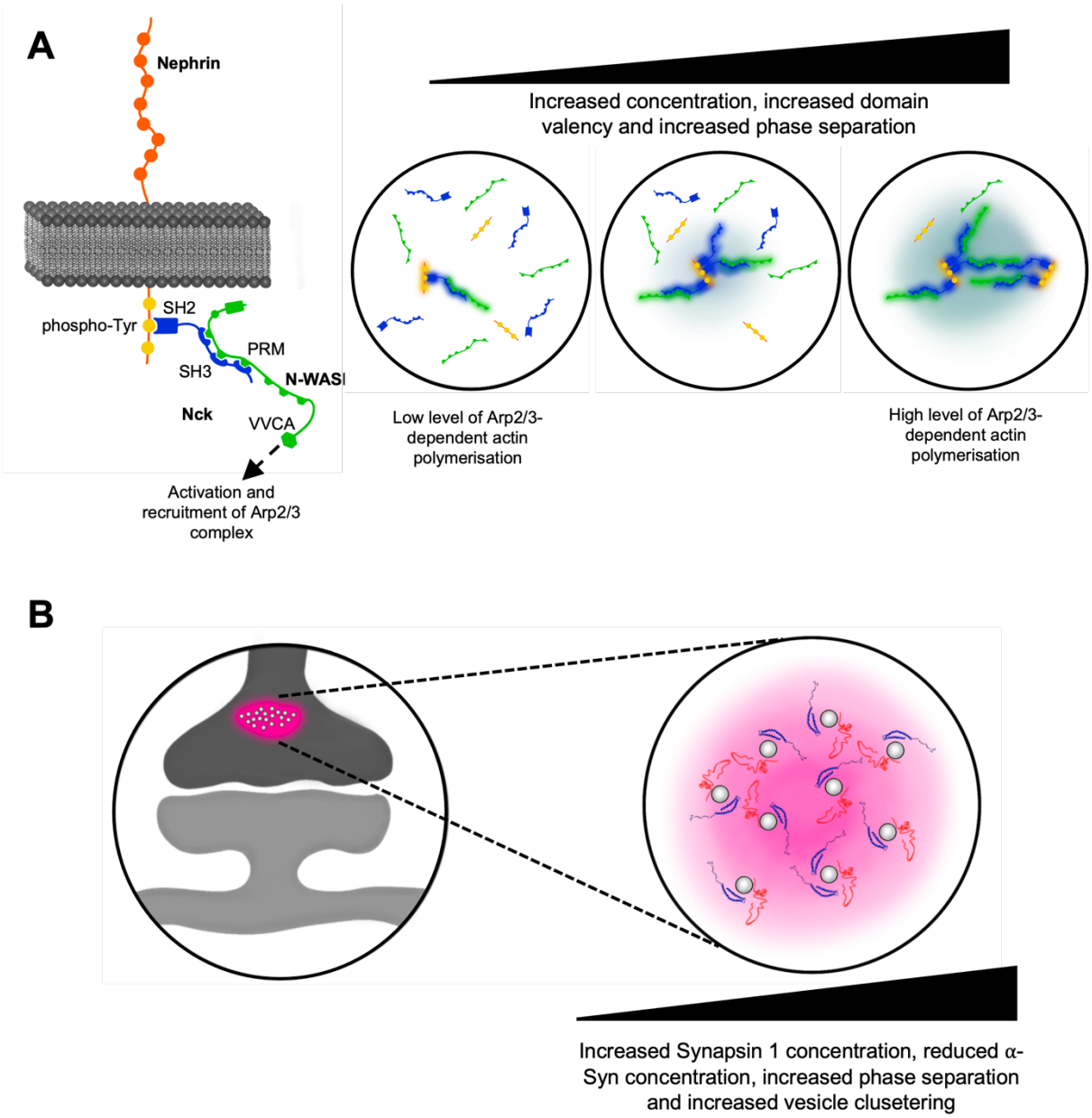

Figure 7. Factors that enhance LLPS increase molecular functions.
(A) The interaction between Nephrin, Nck and N-WASP results in the activation of N-WASP to recruit the Arp2/3 complex and nucleate branched actin filaments. Phosphorylated tyrosine residues on the C-terminal tail of Nephrin, the SH2 and SH3 domains of Nck, and the proline rich motif of N-WASP enable them to undergo LLPS, which enhances Arp2/3 recruitment. (B) Synapsin 1 (red) and α-Syn (blue) undergo LLPS to cluster synaptic vesicles. The balance of Synapsin 1 and α-Syn concentration is important for the LLPS and thus the amount of clustering.

charged vesicles (Milovanovic *et al.*, 2018). LLPS of synapsin 1 is able to sequester lipid vesicles, and when the IDR of synapsin 1 is phosphorylated by the kinase CaMKII, phase separation is disrupted, and the vesicles are dispersed (Milovanovic *et al.*, 2018; Hoffmann *et al.*, 2021). When α-Syn is overexpressed in the presence of endogenous levels of synapsin, there is reduced cycling of synaptic vesicles, however this reduction is abolished in neurons with a triple knockout of the synapsins (Atias *et al.*, 2019). Triple knockout of the synapsins leads to dispersion of synaptic vesicle clusters, while triple KO of synucleins leads to a higher clustering of the synaptic vesicles, suggesting that the balance of synapsin and α-Syn expression is important for the regulation of synaptic vesicle dynamics. Indeed, when higher concentrations of α-Syn are present compared to synapsin 1, phase separation is impaired (Figure 7B) (Hoffmann *et al.*, 2021). Another presynaptic protein Synaptophysin can also form condensates that contain vesicles, when overexpressed with Synapsin 1 in fibroblasts (Park *et al*, 2021).

If LLPS is essential for physiological properties of α-Syn and other neurodegenerative disease-associated proteins, why do these proteins also form aggregates in disease?

A LLPS model for Lewy body formation and disease

While LLPS is important for some cellular functions, it is also possible that condensates can mature into hydrogels over time and under certain conditions, leading to the nucleation of amyloid fibres and the formation of more solid-like structures, such as Lewy bodies (Han *et al*, 2012; Lin *et al*, 2015; Molliex *et al.*, 2015; Patel *et al.*, 2015; Xiang *et al*, 2015; Boke *et al*, 2016; Feric *et al.*, 2016; Piroska *et al*, 2023). In phase-separating, disease-related proteins, mutations can increase the propensity for the condensate to harden (Molliex *et al.*, 2015; Murakami *et al*, 2015; Patel *et al.*, 2015). Furthermore, loss of binding partners can increase the propensity of condensate hardening (Maharana *et al*, 2018). As previously mentioned, α-Syn is able to undergo LLPS, via two low complexity domains at the N-terminus (Ray *et al*, 2020). *In vitro* and *in vivo* studies have demonstrated that α-Syn forms biomolecular condensates that are mobile and liquid-like at early time points, but form amyloid-like, Proteinase K-resistant condensates at later time points (Ray *et al.*, 2020; Hardenberg *et al*, 2021; Piroska *et al.*, 2023). Furthermore, under

conditions that are thought to promote PD pathology (e.g. excess Cu^{2+}, Fe^{3+}) or when PD-causing mutations are present (α-Syn A53T and E46K), there is increased rate of condensate formation (Ray *et al.*, 2020). Liquid droplets can also act as a site of seeding and elongation of α-Syn fibrils in cells treated with PFFs (Figure 8) (Piroska *et al.*, 2023).

In addition to the formation of Lewy bodies by α-Syn LLPS, additional phase-separating protein have also been implicated in PD. As mentioned above, the protein N-WASP forms biomolecular condensates with Nepherin and Nck to activate the Arp2/3 complex and nucleate actin filaments (Li *et al.*, 2012; Banjade & Rosen, 2014). It has recently been shown that compound heterozygous mutations in the gene that encodes N-WASP leads to an early onset form of Parkinsonism. One mutation leads to the loss of the Arp2/3 binding domain of N-WASP, while the other disrupts the proline-rich domain (Kumar *et al*, 2021).

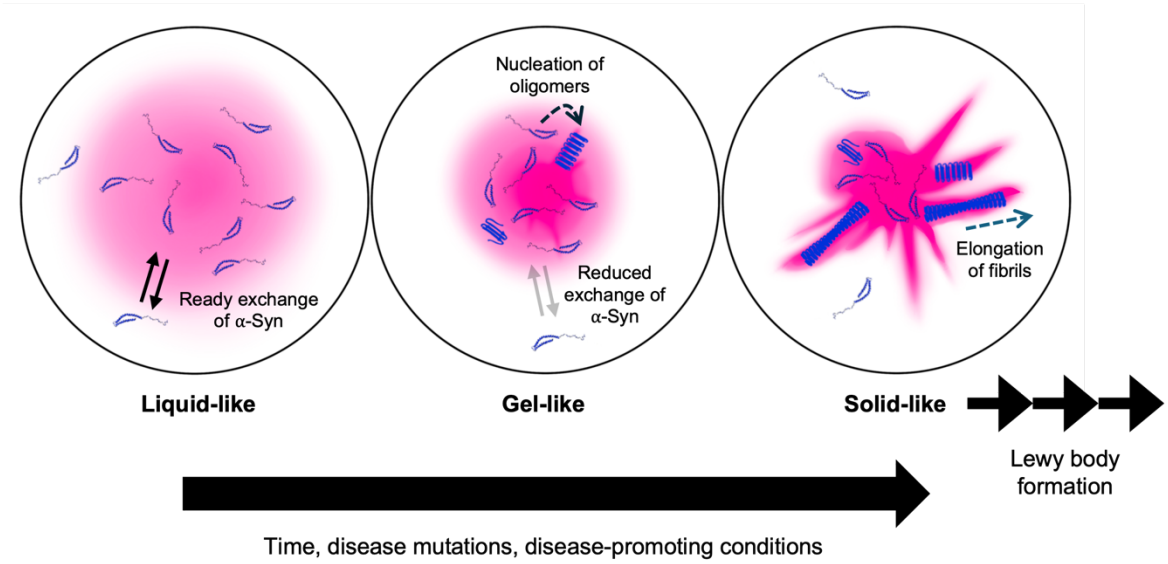

Figure 8. LLPS as a mode of Lewy body formation.
Aberrant α-Syn LLPS is a proposed model of Lewy body formation. Under certain conditions, condensates can shift from having liquid-like properties to a more gel- or solid-like state. Reduced motility of α-Syn in gel- or solid-like condensates can enable nucleation of oligomers of fibrils, which could eventually lead to Lewy body formation.

Loss of the Arp2/3 binding region will lead to a loss-of-function in terms of actin polymerisation, while disruption of the PRMs of the proline-rich domain will likely disrupt phase separation, therefore further decreasing actin polymerisation activity (Li *et al.*, 2012).

Together, it seems as there is growing evidence that aberrant LLPS, whether a loss of condensate formation or pathological condensate formation, plays a role in PD pathology.

Goals of thesis

Current evidence suggests that eukaryotic cells can compensate for mild mitochondrial dysfunction by promoting compensatory mechanisms that enable stress resilience. Based on this evidence, the first goal of my experimental work was to address the following open question:

1. **What molecular mechanisms counteract aberrant mitochondrial bioenergetics?**

Furthermore, since mitochondrial dysfunction and α-Syn proteotoxicity are common signatures of Parkinson's disease pathogenesis, the second part of my work aims to address the following question:

2. **What mechanisms contribute to mitochondrial dysfunction and proteotoxicity in neurodegenerative diseases, such as Parkinson's disease?**

Chapter I: SGPL1 stimulates VPS39 recruitment to the mitochondria in MICU1 deficient cells

Summary

Background:

Mitochondria modulate intracellular signalling through their ability to uptake calcium via the MCU complex, which consists of MCU, EMRE and MICU1/MICU2 (Kirichok *et al.*, 2004; Baughman *et al.*, 2011; De Stefani *et al.*, 2011; Plovanich *et al.*, 2013; Sancak *et al.*, 2013). Inherited mutations within *MICU1* or *MICU2* genes cause myopathies and severe neurodevelopmental disorders in humans (Logan *et al.*, 2014; Lewis-Smith *et al.*, 2016; Shamseldin *et al.*, 2017; Kohlschmidt *et al.*, 2021).

Objective:

To gain insight into the molecular mechanisms that organisms employ to counteract aberrant mitochondrial calcium uptake and mitochondrial bioenergetics.

Methods and results:

We employed CRISPR/Cas9 gene editing to generate *null* alleles of genes encoding for MCU complex subunits. We report that *micu-1(null)* animals display mitochondrial dysfunction, including reduced expression of CI and CIV subunits, and reduced respiration. Consistent with the mitochondrial threshold effect theory, we found that *micu-1(null)* mutants has an increased lifespan. We showed that genetic inhibition of *mcu-1* has no influence on *micu-1(null)* lifespan extension, suggesting that the lifespan extension is not due to aberrant mitochondrial Ca^{2+} uptake. Using transcriptomics, we found that *micu-1(null)* mutants had 3220 upregulated and 3132 downregulated transcripts compared to wt. However, comparative analyses of *micu-1(null);mcu-1(lof)* vs. *micu-1(null)* transcriptomes showed only minimal transcriptional changes, with 321 up- and 174 downregulated transcripts. Consistent with the lifespan data, this transcriptional signature further suggests that *micu-1(null)* lifespan extension is independent of the MCU complex.

We further showed in *micu-1(null)* animals that there is an activation of stress response pathways including the mitochondrial UPR, the oxidative stress response, and the hypoxia-induced stress response, which are commonly upregulated in response to lesions of OXPHOS subunits (Lee *et al.*, 2010; Senchuk *et al.*, 2018; Wu *et al.*, 2018). We showed that these stress responses are essential for lifespan extension in *micu-1(null)* animals by inhibiting the transcription factors that control these responses, using RNAi or loss-of-function mutations.

Using proteomic analysis, we identified 56 and 49 significantly up- and down-regulated proteins in *micu-1(null)* animals, which may contribute to the downstream compensatory pathways involved in lifespan extension. By performing an RNAi screen against the upregulated candidates, we found that *vps-39* and *spl-1* downregulation decreased the lifespan of *micu-1(null)* animals, while they had no effect on wt animals. VPS-39 is part of the HOPS complex and also forms part of the lysosome-mitochondria contact sites, while SPL-1 is an enzyme responsible for the catabolism of sphingosine-1-phosphate into phosphoethanolamine. The HOPS complex plays roles in the fusion of the autophagosome with the lysosome, while SPL-1 is thought to contribute to the induction of autophagy in neurons via the production of phosphatidylethanolamine (Mitroi *et al*, 2017; Gonzalez Montoro *et al*, 2018; van der Beek *et al*, 2019). Together we hypothesised that VPS-39 and SPL-1 may play a role in the activation of autophagy in *micu-1(null)* animals, thus contributing to lifespan extension. Indeed, we found that *vps-39* or *spl-1* RNAi decreased the number of mCherry::GFP::LGG-1 positive autolysosomes in *micu-1(null)* nematodes.

To further investigate the pathways that are affected upon downregulation of *vps-39* and *spl*-1, we collected *micu-1(null)* animals that had been grown on the corresponding RNAi and performed proteomic analysis. Compared to *micu-1(null)* animals grown on control RNAi, we found 50 and 26 differentially expressed proteins in *micu-1(null)* animals exposed to *vps-39* and *spl-1* RNAi*,* respectively. Of these differentially expressed proteins, around 60% were common to *micu-1(null)* animals exposed to *vps-39* or *spl-1* RNAi, suggesting that VPS-39 and SPL-1 act on similar pathways. Furthermore, downregulation of either resulted in a reduction in the number of autophagosomes and fragmentation of the mitochondrial network of *micu-1(null)* animals.

To determine whether the identified mechanisms could contribute to longevity pathways associated with other mitochondrial lesions, we used CI mutant *nuo-6(qm200)* nematodes. We showed that RNAi against *vps-39* and *spl-1* was also able to abolish lifespan extension, indicating that these mechanisms may contribute to longevity pathway activated by other mitochondrial lesions.

We showed that these pathways are conserved in mammals, as *MICU1 KO* cells showed an increased expression of the orthologous proteins VPS39 and SGPL1. Furthermore, we found that *MICU1 KO* cells had increased elongation of the mitochondrial network, increased autophagy, and impaired respiration.

Consistent with our *C. elegans* data, we observed increased proximity of lysosomes with mitochondria in *MICU1 KO* cells. This is likely a result of increased expression of VPS39, and its role in lysosome-mitochondria contact sites (Gonzalez Montoro *et al.*, 2018; van der Beek *et al.*, 2019). Consistent with this hypothesis, downregulation of either VPS39 or SGPL1 led to a reduction in lysosome-mitochondria contact sites. Finally, in an AIFM1 knock-in mouse model of mitochondrial disease, we also observed increased lysosome-mitochondria contact sites in the muscles, indicating that the upregulation of VPS39 and SGPL1 may be part of a widespread compensatory mechanism to counteract mitochondrial dysfunction.

Conclusions:

In conclusion, we show that VPS-39/VPS39 and SPL-1/SPGL1 are important components of the compensatory mechanisms that are activated in response to aberrant mitochondrial bioenergetics. We hypothesise that they act in parallel to regulate the synthesis and transfer of lipids, as the building blocks of new membranes for the biogenesis of autophagosomes, lysosomes and mitochondria. While we show that these proteins stimulate longevity in *C. elegans*, we did not test whether overexpression of VPS-39 or SPL-1 could promote the lifespan extension of short-lived mitochondrial mutants. This would be an important future avenue of research, since it may be that these short-lived animals fail to upregulate VPS-39 or SPL-1. We further show that the VPS-39/VPS39- and SPL-1/SPGL1-dependent compensatory mechanisms are evolutionarily conserved in human cells and in mouse tissue. Their upregulation occurs in response to *MICU1* downregulation as well as in an *AIFM1 knock-in* mouse model of severe myopathy. Accordingly, further

work should also assess these mechanisms in different metabolic syndromes and neurodegenerative diseases in humans, and discern whether disease severity is associated with the level of activation of VPS39 and SGPL1-related pathways.

Contributions:

Co first-authorship was shared between Lena Wischhof and myself. The majority of the *C. elegans* experiments were performed by me, while the *in vitro* and mouse tissue experiments were performed by Lena Wischhof.

I contributed to the conceptualisation, methodology, validation and investigation, and formal analysis of this study. Experimentally, I contributed significantly towards Figure 1, Figure 2D-P, and Figure 3.

Original Article

MOLECULAR METABOLISM

SGPL1 stimulates VPS39 recruitment to the mitochondria in MICU1 deficient cells

Joshua Jackson [1,7], Lena Wischhof [1,7], Enzo Scifo [1], Anna Pellizzer [1], Yiru Wang [1], Antonia Piazzesi [1], Debora Gentile [1], Sana Siddig [1], Miriam Stork [1], Chris E. Hopkins [2], Kristian Händler [1,3], Joachim Weis [4], Andreas Roos [5], Joachim L. Schultze [1,3,6], Pierluigi Nicotera [1], Dan Ehninger [1], Daniele Bano [1,*]

ABSTRACT

Objective: Mitochondrial "retrograde" signaling may stimulate organelle biogenesis as a compensatory adaptation to aberrant activity of the oxidative phosphorylation (OXPHOS) system. To maintain energy-consuming processes in OXPHOS deficient cells, alternative metabolic pathways are functionally coupled to the degradation, recycling and redistribution of biomolecules across distinct intracellular compartments. While transcriptional regulation of mitochondrial network expansion has been the focus of many studies, the molecular mechanisms promoting mitochondrial maintenance in energy-deprived cells remain poorly investigated.

Methods: We performed transcriptomics, quantitative proteomics and lifespan assays to identify pathways that are mechanistically linked to mitochondrial network expansion and homeostasis in *Caenorhabditis elegans* lacking the mitochondrial calcium uptake protein 1 (MICU-1/MICU1). To support our findings, we carried out biochemical and image analyses in mammalian cells and mouse-derived tissues.

Results: We report that *micu-1(null)* mutations impair the OXPHOS system and promote *C. elegans* longevity through a transcriptional program that is independent of the mitochondrial calcium uniporter MCU-1/MCU and the essential MCU regulator EMRE-1/EMRE. We identify sphingosine phosphate lyase SPL-1/SGPL1 and the ATFS-1-target HOPS complex subunit VPS-39/VPS39 as critical lifespan modulators of *micu-1(null)* mutant animals. Cross-species investigation indicates that SGPL1 upregulation stimulates VPS39 recruitment to the mitochondria, thereby enhancing mitochondria-lysosome contacts. Consistently, VPS39 downregulation compromises mitochondrial network maintenance and basal autophagic flux in MICU1 deficient cells. In mouse-derived muscles, we show that VPS39 recruitment to the mitochondria may represent a common signature associated with altered OXPHOS system.

Conclusions: Our findings reveal a previously unrecognized SGPL1/VPS39 axis that stimulates intracellular organelle interactions and sustains autophagy and mitochondrial homeostasis in OXPHOS deficient cells.

Keywords Autophagy; *Caenorhabditis elegans*; Longevity; MICU1; Mitochondria; Sphingosine signaling; VPS39

1. INTRODUCTION

Mitochondrial Ca^{2+} uptake finely tunes intracellular signaling. The transient Ca^{2+} accumulation in the matrix depends on mitochondrial membrane potential and occurs through a high conductance, ruthenium red-sensitive channel spanning the inner mitochondrial membrane (IMM) [1,2]. In all metazoans with a well-characterized Ca^{2+} signaling [3,4], electrogenic Ca^{2+} entry in the mitochondrial matrix depends on a multiprotein complex comprising three evolutionarily conserved components [5]. The ion-conducting pore consists of mitochondrial Ca^{2+} uniporter (MCU) oligomers [6,7] that associate with the essential MCU regulator (EMRE), a single-pass transmembrane protein that influences MCU activity and its inner membrane localization [8–11]. Within the mitochondrial intermembrane space, a membrane-embedded MCU-EMRE subcomplex interacts with the EF-hand containing mitochondrial calcium uptake protein 1 (MICU1) or its evolutionarily related paralogs MICU2 and MICU3 [12–18]. As MCU gatekeepers, MICU1 and its paralogs physically block MCU pore access and inhibit the electrogenic Ca^{2+} entry under resting conditions, thereby preventing mitochondrial Ca^{2+} overload [17–20]. Beside its regulatory role of the MCU complex, MICU1 localizes in the inner boundary membrane (IBM) of the IMM, thereby stabilizing cristae junctions along with optic atrophy 1 (OPA1) and mitochondrial contact site and cristae organizing system (MICOS) [14].

The pathophysiological relevance of MCU and its components has become even more evident since the identification in humans of

[1]German Center for Neurodegenerative Diseases (DZNE), Bonn, Germany [2]InVivoBiosystems, 1505 Westec Dr, Eugene, OR, USA [3]PRECISE Platform for Single Cell Genomics and Epigenomics, German Center for Neurodegenerative Diseases (DZNE), University of Bonn, Bonn, Germany [4]Institute of Neuropathology, RWTH Aachen University Hospital, Aachen, Germany [5]Universitätsklinikum Essen and Universität Duisburg-Essen, Essen, Germany [6]LIMES Institute, Department for Genomics and Immunoregulation, University of Bonn, Bonn, Germany

[7] Joshua Jackson and Lena Wischhof contributed equally to this work.

*Corresponding author. Deutsches Zentrum für Neurodegenerative Erkrankungen (DZNE), Venusberg-Campus 1, Gebäude 99, 53127, Bonn, Germany. E-mail: daniele.bano@dzne.de (D. Bano).

Received March 14, 2022 • Revision received April 8, 2022 • Accepted April 15, 2022 • Available online 19 April 2022

https://doi.org/10.1016/j.molmet.2022.101503

disease-causing loss-of-function mutations in *MICU1* and *MICU2* genes [21–24]. As for other mitochondrial diseases [25–28], *MICU1* and *MICU2* mutations lead to a variety of symptoms, including skeletal muscle weakness, fatigue, cognitive impairment, tremors and ataxia [21–24,29]. Patient-derived cells display aberrant mitochondrial OXPHOS and Ca^{2+} homeostasis along with other abnormalities, such as fragmented mitochondrial network, increased NAD(P)H levels [23] and enhanced sensitivity to oxidative stress [21]. A large number of *in vivo* studies have attempted to investigate the molecular mechanisms linked to dysfunctional MCU complex. Very surprisingly, *MCU* knockout mice are viable in a mixed background and display diminished pyruvate dehydrogenase (PDH) activity associated with reduced muscular strength [30]. To a similar extent, *EMRE* KO mice do not show obvious metabolic changes or altered skeletal muscle performance even under challenging conditions [9,15]. In contrast to *MCU* and *EMRE* KO mice, *MICU1* KO mice show high perinatal lethality with a few escapers that weigh 50% less than wild type littermates and display skeletal muscle degeneration and neurological defects [15,16]. Importantly, MICU1 deficient muscles exhibit clear signatures of mitochondrial dysfunction, with decreased succinate dehydrogenase (SDH)/cytochrome c oxidase (COX) staining, increased production of reactive oxygen species (ROS), low ATP levels and higher amounts of lactate [15]. Consistent with the role of MICU-family members in mitochondrial bioenergetics, it was shown that a loss-of-function (*lof*) of *MICU1*, but not the other MCU complex components, compromises the survival of *Drosophila melanogaster* larvae [31]. Notably, neither *MCU(lof)* nor *EMRE*(*lof)* suppresses the fly lethal phenotype due to *MICU1* deficiency [31]. Taken together, it seems that MICU1 may contribute to cellular homeostasis and metabolism through additional pathways that are MCU independent and partially uncoupled from mitochondrial Ca^{2+} uptake. However, further investigations in model organisms are necessary to identify evolutionarily conserved molecular signatures that are relevant to our understanding of syndromes associated with disease-causing *MICU1* and *MICU2* mutations.

To gain insights into MICU1 biology, we employed the nematode *Caenorhabditis elegans*. We herein report that MICU-1/MICU1 deficiency stimulates longevity independently of MCU. Using quantitative multiplexed tandem mass tags (TMT)-based mass spectrometry coupled to RNAi screenings in *C. elegans*, we identify sphingosine phosphate lyase SPL-1/SGPL1 and the HOPS complex subunit VPS-39/VPS39 as critical regulators of homeostatic processes mechanistically linked to the increased lifespan of *micu-1* mutant nematodes. In mammalian cells, MICU1 deficiency stimulates VPS39 recruitment to mitochondria, thereby enhancing the number of mitochondria-lysosome contact sites without altering mitochondria-ER tethering. Together, our findings provide new evidence of an MCU-independent role of MICU1 in metabolic remodeling and intracellular organelle homeostasis, the latter being of potential biological relevance in other diseases associated with aberrant mitochondrial bioenergetics.

2. MATERIALS AND METHODS

2.1. Antibodies

The following antibodies were used in our work: rabbit anti-NDUFB8 (Proteintech, 1479-1-AP); mouse anti-MTCO1 (Abcam, ab14705); mouse anti-total OXPHOS antibody cocktail (Abcam, ab110413); mouse anti-GFP (Roche, 11814460001); rabbit anti-VPS39 (Proteintech, 16219-1-AP and Novus Biologicals, NBP1-76535); mouse anti-KDEL (Millipore, 10C3); mouse anti-TOM40 (Santa Cruz, sc-365467); rabbit anti-TOM20 (Proteintech, 11802-1-AP); rabbit anti-LC3B (Sigma, L7543); rabbit anti-MICU1 (Sigma, PA5-83371); guinea pig anti-p62 (Progen, GP62-C); rabbit anti-pS473-AKT (Cell Signaling, 4060S), rabbit anti-AKT (Cell Signaling, 4685); rabbit anti-pT246-PRAS40 (Cell Signaling, 13175); anti-PRAS40 (Cell Signaling, 2691); rabbit anti-GAPDH (Santa Cruz, sc-25778); mouse anti-actin (Sigma, A5316 and abcam, ab14128); mouse anti-tubulin (Sigma, T6074); rabbit anti-SGPL1 (Atlas Antibodies, HPA021125); rabbit anti-AIF (Cell Signaling, 5318).

2.2. *C. elegans* strains and maintenance

Nematodes were maintained at 20 °C following standard culture methods. The following strains were used in this study: wild type N2 (Bristol), *atfs-1(tm4525)V*, BAN126 *zuls178[his-72p::his-72::GFP];* BAN299 *nuo-6(qm200)I;zcls14[myo-3p::GFP(mit)],* BAN338 *mcu-1(ju1154)IV;zcls13[hsp-6p::GFP]*, BAN362 *micu-1(bon20)IV/nT1 [qls51](IV;V)*, BAN369 *micu-1(bon20)IV/nT1[qls51](IV;V);zcls13[hsp-6p::GFP]*, BAN370 *micu-1(bon20)IV/nT1[qls51](IV;V);zuls178[his-72p::his-72::GFP]*, BAN372 *micu-1(bon20)IV/nT1[qls51](IV;V);bcls39 [lim-7p::ced-1::GFP + lin-15(+)]*, BAN373 *micu-1(bon20)IV/nT1 [qls51](IV;V);zcls14[myo-3p::GFP(mit)]*, BAN378 *micu-1(bon20)IV/nT1 [qls51](IV;V);mcu-1(ju1154)IV*, BAN380 *nuo-6(qm200)I;micu-1(bon20) IV/nT1[qls51](IV;V)*, BAN382 *micu-1(bon77)IV/nT1[qls51](IV;V)*, BAN397 *micu-1(bon20)IV/nT1[qls51](IV;V);atfs-1(tm4525)V*, BAN407 *emre-1(bon78)X*, BAN436 *age-1(hx546)III;micu-1(bon20)IV/nT1 [qls51](IV;V),* BAN448 *micu-1(bon20)IV/nT1[qls51](IV;V);sqls11[lgg-1p::mCherry::GFP::lgg-1 + rol-6)],* BAN449 *micu-1(bon20)IV;vps-39(ok2442)V/nT1[qls51](IV;V)*, BAN491 *glp-1(bn18)III;micu-1(bon20)/ nT1[[qls51](IV;V)*, BAN500 *micu-1(bon20)IV/nT1[qls51](IV;V);emre-1(bon78)X,* BAN501 *micu-1(bon20)IV/nT1[qls51](IV;V);mcu-1(ju1154) IV;emre-1(bon78)X,* DG2389 *glp-1(bn18)III*, CZ19982 *mcu-1(ju1154) IV*, MAH215 *sqls11[lgg-1p::mCherry::GFP::lgg-1 +rol-6)],* MD701 *bcls39[lim-7p::ced-1::GFP + lin-15(+)]*, MQ1333 *nuo-6(qm200)I*, SJ4100 *zcls13[hsp-6p::GFP]*, SJ4103 *zcls14[myo-3p::GFP(mit)],* TJ1052 *age-1(hx546)III.* Some strains were provided by the CGC, which is funded by NIH Office of Research Infrastructure Programs (P40 OD010440).

2.3. Cell culture

Human embryonic kidney HEK293 and HeLa cells were grown in DMEM (Gibco) supplemented with 10% fetal bovine serum and 1% penicillin/streptomycin (100 U/ml penicillin; 100 mg/ml streptomycin). For biochemical analysis, cells were seeded in 6-well plates at a density of 4×10^5 cells per well and collected on the following day. Cell pellets were then either processed directly for biochemical analysis or stored at −80 °C until further use. For immunostaining and PLA experiments, cells were seeded onto poly-L-lysine-coated coverslips in 12-well plates at a density of 6×10^4 cells per well and fixed with 4% PFA 48 h afterwards. Transient transfections were performed using transfection complexes. For plasmid and siRNA transfection, we used Turbofectin and 1 μg of plasmid DNA or RNAiMAX and siRNAs diluted in Opti-MEM, respectively. After 48 h, cells were fixed with 4% PFA and used for PLA experiments or immunostaining. The following plasmids were used: mEGFP-ER-5a (Addgene plasmid # 56455), mitochondrially targeted-GFP and mitochondrially targeted-DsRed. The following siRNAs were used at a final concentration of 50 nM: scramble (ID: AM4611), *siMICU1* (ID: 135594), *siSGPL1* (ID: 118700), *siVPS39* (ID:136872).

2.4. CRISPR/Cas9 genome editing

Young adult hermaphrodites were injected with a customized injection mix consisting of specific sgRNAs against target genes, Cas9 protein and a plasmid encoding *myo-2p::GFP* (NemaMetrix Inc., Eugene OR,

USA). F1 offspring were screened for GFP expression in the pharynx, while F2 were genotyped using specific oligonucleotides upstream and downstream the expected deletions. Mutants were backcrossed at least three times with wt N2 animals and, when necessary, stabilized using *nT1[qIs51]* balancer.

2.5. Imaging and image analysis

Imaging of nematodes was performed on a Zeiss LSM900 equipped with an Airyscan detector. All high-resolution images were acquired and processed using ZEN (Carl Zeiss). For gonad staining, gonads were extruded and fixed with 4% PFA for 5 min, washed with M9 buffer, stained with DAPI for 5 min, followed by further washing. Gonads were imaged with a 20x air objective. For imaging of mitochondria in *zcIs14 [myo-3p::gfp(mt)]* transgenic strains, age-matched animals were fixed with 4% PFA for 5 min, washed with M9 buffer, mounted on agarose pads and imaged posterior to the pharynx, using a 63x oil immersion objective. For imaging of *sqIs11[lgg-1p::mCherry::GFP::lgg-1 + rol-6)]* transgenic strains, adult nematodes were immobilized in levamisole on agarose pads and imaged with a 40x oil immersion objective. Z-stacks were taken at a thickness of 1 μm between focal planes, for a total thickness of 10 μm. Image analysis was performed using ImageJ on maximum intensity projections of Z-stacks. Red and green puncta were counted in the metacorpus of the pharynx using the Find Maxima function. Statistical analysis was performed using GraphPad Prism.

Image analyses of immunofluorescence-labelled and PLA-stained cells and tissue sections were carried out using a Zeiss LSM800 equipped with an Airyscan detector or a Zeiss LSM880 equipped with an Airyscan detector, using a 63x oil immersion objective. Z-stacks were taken at a thickness of 0.5 μm between focal planes. High-resolution images were acquired with ZEN (Carl Zeiss) and processed with the automated Airyscan processing algorithm in ZEN. Image analysis was done in ImageJ. Mitochondrial morphology was calculated after auto-threshold processing. Circularity and mitochondrial area were evaluated via the analyze particles plugin. For co-localization indices, Pearson's and Mander's coefficients were determined using the co-localization analysis plugin JACoP. PLA-dots were semi-automatically quantified as previously described [32].

2.6. Immunocytochemistry, proximity ligation assay (PLA) and LysoTracker staining

For immunocytochemistry, PFA-fixed cells were first incubated in blocking solution (0.5% Triton X-100, 10% normal goat serum) for 30 min at room temperature, followed by overnight incubation with primary antibodies. On the next day, cells were washed in PBS and incubated with appropriate Alexa Fluor-conjugated secondary antibodies (Invitrogen) for 2 h at room temperature. As a last step, cells were counterstained with DAPI and mounted onto microscope slides. PLA experiments were performed using Duolink® PLA fluorescence reagents (Sigma) according to the manufacturer's instructions and as previously described [32]. Briefly, cells and tissue samples were first permeabilized with 0.25% Triton X-100 in PBS, and then treated with Blocking solution for 1 h at 37 °C. Thereafter, samples were incubated with primary antibodies over night at 4 °C. Following three washes in Wash Buffer A, samples were then incubated with PLA probes for 1 h at 37 °C or, in case of tissue samples, for 24 h at 4 °C. Signal amplification was performed by incubation with amplification-polymerase solution for 100 min at 37 °C. After three washes in Wash Buffer B, cells were counterstained with DAPI and mounted onto microscope slides while tissue samples were incubated with anti-TOM20 antibody overnight. On the next day, sections were washed in PBS, incubated with appropriate secondary antibodies for 2 h at room temperature, and finally counterstained with DAPI. Imaging was then performed within 24 h.

For lysosomal labeling, mitochondria-targeted GFP-positive HEK293 and HeLa cells were seeded onto poly-L-lysine-coated coverslips. On the next day, medium was removed and replaced by pre-warmed growth medium containing LysoTracker Red DND-99 (Molecular probes, Life Technologies) at a concentration of 60 nM. Following 45 min of incubation at 37 °C, cells were fixed with 4% PFA, washed with PBS, mounted onto microscope slides and imaged immediately afterwards.

2.7. Lifespan assays and RNAi

All lifespan assays were carried out at 20 °C. RNAi experiments were performed by feeding with HT115 *E. coli* expressing dsRNA against target genes (Ahringer library, Source Bioscience LifeSciences). To obtain synchronized populations, gravid adult nematodes were bleached in hypochlorite solution and the resulting eggs transferred directly onto bacteria-seeded NGM plates. For lifespan-based RNAi screen, gravid *micu-1(bon20)/nT1[qIs51]* nematodes were bleached and eggs transferred onto HT115 *E. coli* expressing dsRNA against candidates. At L4/young adult stage, 50 *micu-1(bon20)* animals were transferred to a fresh plate for each RNAi condition. For all the other lifespan assays, nematodes were grown until L4/adult stage and then transferred to fresh plates in groups of 30 per plate. Animals were transferred every 2–4 days and scored at least every other day for touch-provoked movement until death. Animals that died abnormally (e.g., internal hatching, vulva protrusions) were scored as censored. Survival curves were generated using GraphPad Prism software (GraphPad Software Inc., San Diego, USA).

2.8. Mouse work

Aifm1(R200 del) knockin mice were generated as described previously [33]. Mice were housed in groups of two to four under a 12/12 h light/dark cycle with free access to food and tap water. All experiments were approved and performed in conformity to the guidelines of the State Agency for Nature, environment and Consumer Protection North Rhine Westphalia. At 6 months of age, animals were anaesthetized with an overdose of Ketamine: Xylazine and transcardially perfused with PBS followed by 4% PFA. Quadricep muscles were rapidly removed, post-fixed for 24 h in PFA, and stored in 30% sucrose solution until further processing. Muscle sections were cut on a cryostat at a thickness of 20 μM and stored at −20 °C until further use.

2.9. Next-generation RNA sequencing (NGS)

Adult nematodes were dissolved in 1 ml Trizol (Invitrogen) and total RNA was isolated via the miRNeasy Micro kit (Qiagen) according to the manufacturer's protocol. RNA concentration and integrity were determined by High Sensitivity RNA assay on a TapeStation 4200 system (Agilent). cDNA libraries were prepared from 5 ng total RNA using the SMART-seq2 protocol and tagmented with the Nextera XT kit (Illumina). Library purification and size selection was carried out with AMPure XP beads (Beckman–Coulter) and final library size distribution was measured via High Sensitivity D5000 assay on a TapeStation 4200 System (Agilent). Library concentration was determined using the HS dsDNA assay on a Qubit 3. Libraries were sequenced SR 75 cycles on a NextSeq500 system (Illumina) using High Output v2 chemistry. Base call files were converted to fastq format and demultiplexed using bcl2fastq v2.20. The 75 bp single-end reads were aligned to the *C. elegans* reference transcriptome WBcel235 by kallisto v0.44.0 using default parameters. Raw RNA seq data were deposited to GEO database under the common accession number GSE197286.

2.10. Oxygen consumption rate measurements (OCR)

OCR was measured using a Seahorse XFe24 Analyzer (Agilent). Synchronized animals were grown to first day of adulthood at 20 °C and transferred to heat-killed OP50 plates for 3 h to empty their gut of live bacteria. Each well of a Seahorse XFe24 Cell Culture Microplate was filled with 500 μl M9 buffer, and 50 animals transferred into each well, with a minimum of 3 wells per condition. OCR measurements were taken at basal conditions, and in response to addition of 20 μM FCCP, followed by 20 mM sodium azide (NaN_3).

Cells were seeded on cell culture microplates (Agilent Seahorse XF24) in growth medium 24 h, or in case of siRNA experiments 48 h, before the assay. On the day of the experiment, growth medium was replaced with Seahorse XF base medium supplemented with 1 mM pyruvate, 2 mM glutamine and 10 mM glucose or galactose. Before starting the measurements, cells were equilibrated for 60 min in a CO_2-free incubator at 37 °C. Following three baseline measurements, subsequent additions of 1 μM oligomycin, 1.5 μM FCCP and 0.5 μM rotenone/antimycin A were carried out as previously described. At the end of OCR and ECAR assessments, cells were collected and lysed in RIPA buffer (SIGMA), supplemented with protease and phosphatase inhibitors (Roche). Protein concentrations were determined via Bradford assay and OCR values were then normalized to the respective protein contents.

2.11. RNA extraction and quantitative real-time PCR

RT-PCR was used to quantify gene expression levels on synchronized populations. RNA extraction, purification and reverse transcription was performing using RNeasy RNA extraction kit (Qiagen) and qScript cDNA supermix (Quanta Biosciences). Quantitative RT-PCR was performed using Fast SYBR Green Master Mix (Applied Biosystems) in a Step One Plus Real Time PCR System (Applied Biosystems) and analyzed using comparative ΔΔCt method, normalized to mRNA levels of actin. Three technical replicates were performed for each biological replicate. The following oligonucleotides were used in this study: *sod-3* 5′- ccaaccagcgctgaaattcaatg-3′ and 5′-ggaaccgaagtcgcgcttaatag-3'; *nhr-57* 5′-tcggaatgaatccggaagt-3′ and 5′-atgcaggggaagatgaacag-3'; *gst-4* 5′-gatacttggcaagaaaatttggac-3′ and 5′-ttgatctacaattgaatcagcgtaa-3'; *vps-39* 5′-cgctttcccagacgcatttt-3′ and 5′-gtcgttttcggtagaggccc-3'; *spl-1* 5′-cagcgcctaacttcccatca-3′ and 5′-caggtatccggcgtcattca-3'; *beta-actin* 5′-tgtgatgccagatcttctccat-3′ and 5′-gagcacggtatcgtcaccaa-3'.

2.12. Sample preparation, LC-MS/MS measurements and database searching

Briefly, approximately 800 wt and *micu-1(bon20)/nT1[qIs51]* adult nematodes were collected at day 4 and 5 after hatching, respectively. Animals were washed twice with water and the pellets were kept at −80 °C. Samples were lysed in 200 μl Lysis buffer (50 mM HEPES (pH 7.4), 150 mM NaCl, 1 mM EDTA, 1.5% SDS, 1 mM DTT; supplemented with: 1 × protease and phosphatase inhibitor cocktail (ThermoScientific)). Lysis was aided by repeated cycles of sonication in a water bath (6 cycles of 1 min sonication (35 kHz) intermitted by 2 min incubation on ice). At least 40 μg of *C. elegans* protein lysates were reduced and alkylated prior to processing by a modified filter-aided sample preparation (FASP) protocol as previously described [34]. Samples were subjected to sequential overnight digestion with Lys-C (1:40 in 1.3 M Urea buffer) and Trypsin (1:20; in 50 mM ammonium bicarbonate) directly on the filters. Peptides were additionally precipitated using an equal volume of 2 M KCl for depletion of residual detergents, then cleaned and desalted on C18 stage tips, prior to resuspension in 20 μl of 50 mM HEPES (pH 8.5). Then, wt (OP50), *micu-1(bon20)* (OP50), *micu-1(bon20)* (on control RNAi), *micu-1(bon20)* (on *spl-1* RNAi), *micu-1(bon20)* (on *vps-39* RNAi) *C. elegans* peptides were labelled with 25 μl of diluted (14.75 mM) 126; 127N; 128N, 128C, 129N; and 129C, 130N, 130C (batches 1 and 2) TMT 10plex, respectively, for 1 h at RT. TMT signal was quenched by addition of 2 μl of 5% hydroxylamine to the reaction, vortexing for 20 s and incubating for 15 min at 25 °C with shaking (1000 rpm). TMT-labelled peptides were acidified with 45% (vol/vol) of 10% FA in 10% ACN, prior to combining samples at equal amounts for drying in a concentrator. Dried peptides were re-suspended in 300 μl of 0.1% TFA for subsequent high pH reverse phase fractionation (Perce kit). 8 peptide fractions (10, 12.5, 15, 20, 22.5, 25, 50, and 80%) ACN were collected, concentrated and re-suspended in 20 μl 5% FA for LC-MS analysis. MS runs were performed in triplicates.

Tryptic peptides were analyzed on a Dionex Ultimate 3000 RSLC nanosystem coupled to an Orbitrap Exploris 480 MS. They were injected at starting conditions of 95% eluent A (0.1% FA in water) and 5% eluent B (0.1% FA in 80% ACN). Peptides were loaded onto a trap column cartridge (Acclaim PepMap C18 100 Å, 5 mm × 300 μm i.d., #160454, Thermo Scientific) and separated by reversed-phase chromatography on a 50 cm μPAC C18 column (PharmaFluidics) using a 120 min linear increasing gradient from 8% to 25% of eluent B for 85 min, followed by a 28 min linear increase to 50% eluent B. The mass spectrometer was operated in data dependent and positive ion mode with MS1 spectra recorded at a resolution of 120 k with an automatic gain control (AGC) target value of 300% (3×10^6) ions, maxIT set to Auto and an intensity threshold of 1×10^4, using a mass scan range of 350—1550. Precursor ions for MS/MS were selected using a top speed method with a cycle time of 2 ms and normalized collision energy (NCE) of 36% (High-energy Collision Dissociation (HCD)), to activate both the reporter and parent ions for fragmentation. MS2 spectra were acquired at 45 k resolution using an AGC target value of 200% (2×10^5), and maxIT set to 86 ms. Dynamic exclusion was enabled and set at 45 s. Isolation width was set at 0.7 *m/z* and the fixed first mass to 110 *m/z* to ensure reporter ions were detected. Peptide match was set to off, and isotope exclusion was on. Charge-state exclusion rejected ions that had unassigned charge states, were singly charged or had a charge state above 5. Full MS data were acquired in the profile mode with fragment spectra recorded in the centroid mode.

Raw data files were processed with Proteome Discoverer™ software (v2.4.0.305, Thermo Scientific) using SEQUEST® HT search engine against the Swiss-Prot® *C. elegans database* (v2020-05-08). Peptides were identified by specifying Lys-C and trypsin as the proteases, with up to 2 missed cleavage sites allowed. Precursor mass tolerance was set to 10 ppm, and fragment mass tolerance to 0.02 Da MS2. Static modifications were set as carbamidomethylated cysteine and TMT6plex (229.163 Da; N-terminal, K), while dynamic modifications included methionine, oxidation and N-terminal protein acetylation, for all searches. Resulting peptide hits were filtered for maximum 1% FDR using the Percolator algorithm. The TMT10plex quantification method within Proteome Discoverer software was used to calculate the reporter ratios with mass tolerance ± 10 ppm and applying isotopic correction factors. Only peptide spectra containing all reporter ions were designated as "quantifiable spectra".

2.13. SDS-PAGE and western blotting

Adult nematodes were collected, washed in sterile H_2O and frozen in liquid nitrogen. *C. elegans* and cell pellets were thawed on ice and sonicated in ice-cold RIPA buffer (Sigma) with protease and phosphatase inhibitors. Total lysates were spun down, quantified using

Bradford reagent (Sigma), and boiled in 2X Laemmli buffer at 95 °C for 5 min. Samples were resolved on 10—15% poly-acrylamide gels and transferred onto nitrocellulose membranes using semi-dry transfer Trans-Blot Turbo™ (Bio-Rad). Immunoblots were developed in ECL and imaged using Chemidoc imaging system (Bio-Rad).

2.14. Statistics

GraphPad Prism Software was used for statistical analysis. Data were tested for normality distribution and statistical comparison of normal distributed data was performed with two-tailed Student's *t* test or one-way ANOVA, unless indicated differently. Non-normal distributed data were statistically compared using the Mann—Whitney U-test or Kruskal—Wallis test. Statistical significance was defined as $*p < 0.05$.

2.15. Thrashing assay

Synchronized nematodes at the first day of adulthood were used for thrashing assays. Individual animals were placed into a drop of M9 buffer, and each full back-and-forth lateral movement was counted for a total of 90 s. Thrashing was performed for 10 animals per strain, for each biological replicate.

3. RESULTS

3.1. MICU-1 deficiency extends *C. elegans* lifespan in an MCU-1 independent manner

As in other multicellular organisms, *C. elegans* expresses the three core components of the MCU complex: MCU-1/MCU, EMRE-1/EMRE and MICU-1/MICU1 (Figure 1A). Sequence alignments indicate that the nematode genome may also encode a partially conserved MICU-3/MICU3 as well as two poorly characterized SLC25A23 orthologs with predicted Ca^{2+} binding activity (Supplementary Figs. S1A—B). To assess the contribution of the MCU complex to *C. elegans* survival, we initially studied the lifespan of hermaphrodites homozygous for an existing *mcu-1(lof)* allele [35]. To our surprise, we found that *mcu-1* mutants lived as long as wild type (wt) nematodes (Figure 1B and Table S1), suggesting that MCU-1 is dispensable for *C. elegans* viability under standard laboratory conditions. Using CRISPR/Cas9-gene editing, we generated an *emre-1(lof)* allele consisting of an insertion in exon 2 that led to a truncated and potentially unstable protein lacking 38 amino acids (Supplementary Fig. S1C). We backcrossed this line, performed lifespan assays and observed that *emre-1* mutant nematodes also lived as long as wt animals (Figure 1C and Table S1). To complete our genetic survey, we then manipulated the expression of the *micu-1* gene by deleting a small portion of the promoter, the open reading frame and part of the 3′UTR (Supplementary Fig. S1D). An additional *micu-1* mutant allele was obtained by targeting most of the region between exon 1 and 3 (Supplementary Fig. S1E), since this strategy also abrogates the expression of all predicted MICU-1 isoforms. Similar to previously described mitochondrial mutants [36,37], homozygous *micu-1(null)* nematodes exhibited diminished motility and larval developmental delays (Supplementary Figs. S1F—G). While *mcu-1* and *emre-1* mutant animals did not show any obvious phenotypes, *micu-1(null)* nematodes had reduced syncytial gonads and did not develop oocytes when compared to wt animals (Supplementary Figs. S1H—I). As for an earlier *micu-1* mutant strain [38], we maintained our *micu-1(null)* mutations with the balancer *nT1[qIs51](IV;V)*. Confocal image analysis showed that *micu-1(null)* mutants had far fewer nuclei in their germlines compared to wt gonads (Supplementary Fig. S1H). Moreover, *micu-1* mutant gonads contained a large number of germ cells undergoing programmed cell death, as revealed by the intense CED-1:GFP fluorescence originating from sheath cells engulfing germ cell corpses in the pachytene and diplotene regions (Supplementary Fig. S1I). Of note, genetic manipulation of *mcu-1* or *emre-1* did not rescue the germline defects of *micu-1* mutants (Supplementary Fig. S1H). We found that *micu-1(bon20)(IV)/nT1 [qIs51](IV;V)* laid a comparable number of eggs to wt animals, with the population of hatched animals having genotypes that did not follow the Mendelian distribution (Supplementary Fig. S1J). Adult *micu-1(null)* mutants exhibited a fully differentiated vulva with no obvious abnormalities (Supplementary Fig. S1K).

Consistent with the "mitochondrial threshold effect" theory [39], mitochondrial lesions can either extend or decrease *C. elegans* lifespan, according to the ability of the organism to compensate for aberrant mitochondrial OXPHOS through transcriptional programs regulating stress response and metabolism [40—45]. Since MICU-1/MICU1 knockout compromises mitochondrial Ca^{2+} signaling and bioenergetics in mammalian and invertebrate cells [12,18,31,38], we reasoned that MICU-1/MICU1 deficiency could influence *C. elegans* survival similarly to other mitochondrial lesions [36,37,46]. In line with our hypothesis, we found that homozygous *micu-1(null)* hermaphrodites lived much longer than wt animals (Figure 1D—F and Table S1). Importantly, both *mcu-1(lof)* and/or *emre*-1 deficiency did not have a major impact on the lifespan extension of *micu-1* mutants (Figure 1F—H and Table S1), strongly suggesting that MICU-1 longevity does not require a functional MCU complex and MCU-dependent Ca^{2+} uptake. Next, we performed high-resolution confocal microscopy of *C. elegans* body-wall muscle cells expressing a mitochondrially localized GFP. We observed that wt animals began to accumulate abnormally enlarged, as well as fragmented mitochondria a few days after reaching adulthood (Figure 1I,J), whereas age-matched *micu-1(null)* mutants appeared to have a well-organized mitochondrial network with highly interconnected tubular structures similar to those described in other long-lived mitochondrial mutants [44,47,48]. Using an adapted Seahorse protocol [44,49], we measured oxygen consumption rate (OCR) and found that *micu-1(null)* mutants had a lower spare respiratory capacity compared to wt nematodes (Figure 1K,L). To assess the mitochondrial OXPHOS system in *micu-1* deficient nematodes, we ran immunoblot analyses and observed altered expression of mitochondrial complex I (CI) and complex IV (CIV) subunits in *micu-1(null)* mutants compared to wt (Figure 1M). Given this line of experimental evidence, we reasoned that the lifespan extension of *micu-1* mutants was probably dependent on lesions altering the expression of electron transport chain (ETC) subunits. Thus, we generated *nuo-6(qm200);micu-1(bon20)* double mutants and observed a tendency toward further lifespan extension compared to both *micu-1(bon20)* and *nuo-6(qm200)* animals (Figure 1N and Table S1), suggesting that aberrant ETC composition may not be the only contributing factor underlying *micu-1* longevity. Since MICU1 can be localized at cristae junctions and influences remodeling of the mitochondrial inner membrane [14], we assessed the survival of *micu-1(null)* mutants on bacteria expressing double strand RNAi against the mRNAs encoding the mitochondrial fusogen EAT-3/OPA1 [50] and MICOS complex subunit MOMA-1/APOOL/MIC27 [51]. We found that *eat-3* downregulation had a minor, although statistically significant, effect on *micu-1(null)* lifespan, while *moma-1* RNAi did not influence the survival of *micu-1* mutant animals (Figure 1O, Supplementary Figure S1L-M and Table S1). These data suggest that additional IMM remodeling following EAT-3/OPA1 downregulation may further influence the longevity pathways linked to MICU-1 deficiency. In summary, our findings indicate that *micu-1(null)* mutations alter the maintenance and function of the OXPHOS system in *C. elegans*, recapitulating some of the

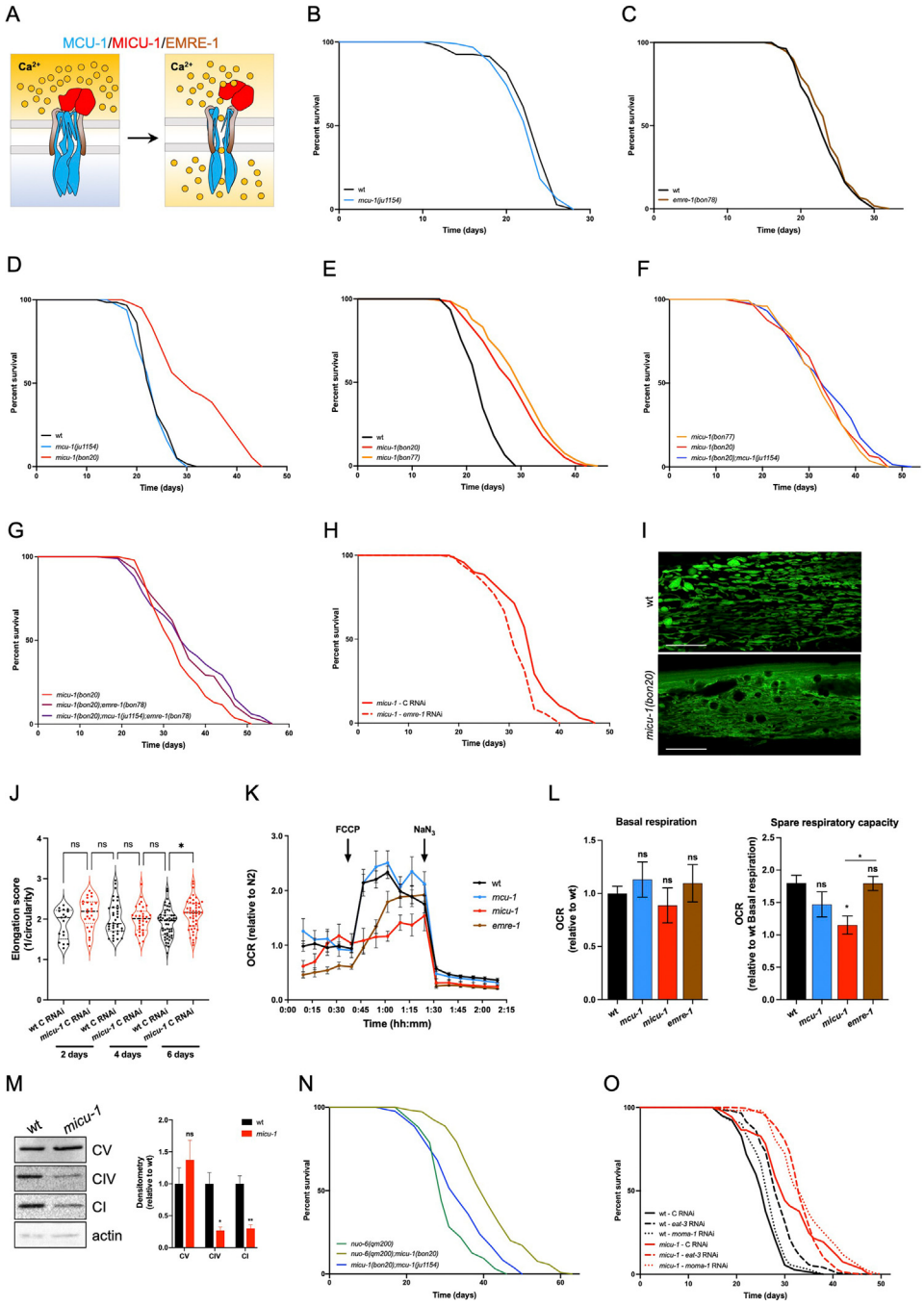

Figure 1: *micu-1(null)* alleles extend *C. elegans* lifespan independently of MCU complex. (A) Schematic representation of the *C. elegans* mitochondrial calcium uniporter (MCU) complex. MICU-1 homo- or heterodimers (red) bind MCU-1 (blue) and EMRE-1 (brown) subunits. Upon Ca^{2+} binding, MICU-1 regulates MCU-1 permeability and Ca^{2+} influx into the mitochondrial matrix. (B—C) Representative survival curves of wt versus (B) *mcu-1(ju1154)* and (C) *emre-1(bon78)* mutant nematodes. (D—E) Representative survival curves of wt animals compared to (D) *mcu-1(ju1154)* and *micu-1(bon20)*, (E) *micu-1(bon20)* and *micu-1(bon77)* nematodes. (F—G) Lifespan assay of *micu-1(bon20)* vs (F) *micu-1(bon20);mcu-1(ju1154)* and *micu-1(bon77)*, (G) *micu-1(bon20);emre-1(bon78)* and *micu-1(bon20);mcu-1(ju1154);emre-1(bon78)*. (H) Representative survival curves of *micu-1(bon20)* grown on control and RNAi against *emre-1*. (I) Confocal images of 9-day-old control and *micu-1(bon20)* animals expressing *zcls14[myo-3p::GFP(mit)]* transgene. Mitochondria are visualized as GFP-positive structures (scale bar = 10 μm). (J) Quantification of mitochondrial elongation in *zcls14[myo-3p::GFP(mit)]* expressing control (wt) and *micu-1(bon20)* animals at 2, 4 and 6 days after adulthood (Kruskal—Wallis ANOVA, Dunn's multiple comparison test: ns = not significant, $*p < 0.05$, n = 17—53 animals from at least 3 independent experiments). To be consistent with other experiments (see figure 3I), the assessment of mitochondrial elongation was performed on animals grown on control RNAi. (K) Seahorse OCR profiles of wt, *mcu-1(ju1154)*, *micu-1(bon20)* and *emre-1(bon78)* animals. (L) Basal respiration and spare respiratory capacity of animals at day 1 of adulthood (mean ± S.E.M., Kruskal—Wallis test: ns = not significant, $*p < 0.05$, n = 3). (M) Immunoblot analyses of samples from wt and *micu-1(bon20)* animals using antibodies against CV subunit ATP5A, CIV subunit CTC-1/MTCO1, CI subunit NUO-2/NDUFS3 and actin (as loading control). Densitometry is reported on the right (mean ± S.E.M., unpaired Student's t-test: ns = not significant, $*p < 0.05$, $**p < 0.01$, n = 3). (N) Representative survival curve of *nuo-6(qm200)*, *nuo-6(qm200);micu-1(bon20)* and *micu-1(bon20);mcu-1(ju1154)* mutant nematodes. (O) Representative lifespan assay of wt and *micu-1(bon20)* mutants grown on control (solid lines), *eat*-3 (dashed lines) and *moma-1* (dotted lines) RNAi.

mitochondrial defects observed in higher organisms carrying *MICU1* or *MICU2* lesions.

3.2. MICU-1 loss stimulates stress response pathways

Mitochondrial dysfunction during development can stimulate transcriptional regulation of stress response pathways that confer *C. elegans* longevity [40,41,52—54]. To explore the mechanisms underlying lifespan-extending properties of MICU-1 deficiency, we performed next-generation sequencing (NGS) of RNAs extracted from adult nematodes. Similar to other long-lived mitochondrial mutants [44,45], the *micu-1(null)* mutation led to profound transcriptional changes comprising of 3220 upregulated and 3132 downregulated genes compared to wt animals (Figure 2A—C). Many of the dysregulated genes encode for mitochondrial proteins, including ETC components (Supplementary Fig. S2A). Consistent with our lifespan assays, *mcu-1(lof)* had a negligible contribution to the gene expression profiles linked to MICU-1 deficiency (*micu-1(bon20);mcu-1(ju1154)* vs *micu-1(bon20)*: 321 upregulated and 174 downregulated genes; Figure 2B—C), further emphasizing that MCU-1 participates only marginally in lifespan-extending programs established in *micu-1(null)* nematodes. Ingenuity pathway analysis (IPA) of up- and downregulated genes further revealed protein synthesis and xenobiotic metabolism as significantly overrepresented pathways in the transcriptome of *micu-1(bon20)* compared to wt nematodes (Supplementary Figs. S2B—D), as reported in other *C. elegans* models of mitochondrial deficiency [44,55,56].

A vast body of literature indicates that decreased mitochondrial function evokes a nuclear encoded stress response associated with longevity [41,42]. Since *micu-1* mutants show clear signatures of mitochondrial dysfunction (Figure 1K—M), we measured the expression of the unfolded protein response (UPR^{mt}) reporter *zcls13[hsp-6p::gfp]* and other stress-response markers (i.e., *sod-3*, *gst-4* and *nhr-57*) using immunoblots and quantitative RT-PCR, respectively. Compared to control and *mcu-1* mutant animals, we found that *hsp-6p::gfp* expression was strongly induced in *micu-1(null)* nematodes (Figure 2D). Similar to CI deficient *nuo-6(qm200)* mutants, MICU-1 loss led to enhanced expression of the DAF-16/ATFS-1 target *sod-3* and the SKN-1 target *gst-4*, while the HIF-1 target *nhr-57* was only marginally affected (Figure 2E—G). Consistent with a minor role of MCU-1 in the transcriptional profile of *micu-1(null)* nematodes, we observed that *sod-3* and *gst-4* genes were upregulated independently of MCU-1 activity (Figure 2E—F). Given these lines of evidence, we next tested the contribution of mitochondria-to-nucleus "retrograde" stress response to *micu-1* longevity by genetically altering the expression of ATFS-1, an upstream transcriptional regulator of UPR^{mt} [57,58], and the ROS responsive transcription factor SKN-1/NRF2 [59,60]. We showed that *atfs-1(lof)* as well as *skn-1* RNAi significantly inhibited the lifespan extension of *micu-1* mutants (Figure 2H—J and Table S1). To complete our epistatic analyses, we also assessed the contribution of other transcription factors that were previously reported to influence lifespan-extending programs in nematodes [54,61—63]. Specifically, we silenced the expression of heat shock factor HSF-1, which regulates proteostasis in mitochondrial deficient animals [64], and the diet-restriction regulator PHA-4/FOXA [65]. In line with their roles in longevity pathways linked to mitochondria, these two transcription factors contributed to the lifespan extension of *micu-1* mutant nematodes (Figure 2K,L and Table S1). As was the case for other mitochondrial mutants [36,44], inhibition of the insulin/IGF-1 signaling pathway through hypomorphic *age-1* mutation further extended *micu-1* lifespan, while DAF-16/FOXO downregulation did not modify their survival (Figure 2M—O and Table S1). Together, these epistatic analyses suggest that *micu-1(null)* mutants have several transcriptional signatures commonly observed in other long-lived mitochondrial animals.

Since *micu-1(null)* nematodes have defective germline and are sterile (Supplementary Figs. S1H—J), we tested the contribution of germline deficiency on *micu-1(null)* lifespan. To do so, we employed a temperature-sensitive *glp-1* mutation that impairs gonadogenesis in *C. elegans* hermaphrodites, stimulates DAF-16 activity (Supplementary Fig. S2E) and leads to longevity [66,67]. Upon exposure to a restrictive temperature that compromised the germline, we found that the median lifespan of *glp-1;micu-1* double mutants was comparable to the survival of *glp-1* single mutants and *micu-1(null)* nematodes (Figure 2P and Table S1). This non-addictive effect of *glp-1* mutation suggests that signals from the germline may contribute to *micu-1* longevity pathways.

3.3. SPL-1 and VPS-39 upregulation underlies cellular homeostasis and longevity of *micu-1* mutant nematodes

To uncover novel regulatory pathways linked to MICU-1, we performed TMT-based mass spectrometry (MS) analyses of peptides extracted from wt and *micu-1(bon20)* mutant *C. elegans* samples from two distinct biological replicates (see materials and methods section for details). A total of 1563 and 1849 proteins were identified from the combined cytosolic and membrane fractions of the two biological replicates, with medium—high confidence (combined q value ≤ 0.05) (Supplementary Figs. S3A—D and Supplementary Tables S2—3). By integrating the two independent datasets, we found 56 down- and 49 up-regulated proteins in young *micu-1(null)* mutant animals compared to age-matched wt nematodes (Figure 3A; threshold = fold change 1.5, p value < 0.05). Gene ontology analysis of the overlapping significantly downregulated proteins in *micu-1*, by PANTHER (GO Consortium, http://geneontology.org/) revealed: protein refolding (GO:0080058, adjusted p-value: 2.19E-02); translation (GO:0006412, adjusted p-value: 1.24E-04); and determination of lifespan (GO:0008340, adjusted p-value: 5.78E-03), as the most enriched biological processes. Upregulated proteins were associated with enrichment of transsulfuration (GO:0019346, adjusted p-value: 4.86E-02). Among the significantly dysregulated proteins, we found 15 ribosomal components and two translation elongation factors (Supplementary Fig. S3E), implying a decreased protein synthesis as predicted by our IPA analysis of RNA sequencing data (Supplementary Figs. S2B—D). We detected significant expression changes of mitochondrial respiratory complexes (Supplementary Figs. S3E—F) and other mitochondrial proteins, including factors that contribute to cristae remodeling (i.e., F54A3.5/MICOS10, MOMA-1/APOOL), as well as mitochondrial or cytosolic enzymes involved in carbon metabolism, such as nucleotide biosynthesis (ADSS-1, AHCY-1), lipid and carbohydrate catabolism (i.e., MDH-2, ALDO-2, GPDH-2, GPD-1) (Supplementary Fig. S3E). Furthermore, *micu-1* mutants had a diminished expression of voltage-dependent anion channel VDAC-1 and protein arginine N-methyltransferase PRMT-1 (Supplementary Fig. S3E). The former participates in mitochondrial Ca^{2+} uptake and ER coupling [68], while the latter is an important regulator of MICU1 activity and its affinity to Ca^{2+} and to the MCU/EMRE1 subcomplex [14]. Consistent with previous evidence in patient-derived samples [24], we observed aberrant expression of structural proteins, such as cytoskeleton components, extracellular matrix molecules (e.g., collagen) and proteins associated with the nuclear envelope (Supplementary Fig. S3E).

Taking advantage of *C. elegans* genetic tractability, we sought to determine the relevance of the upregulated proteins in *micu-1* lifespan.

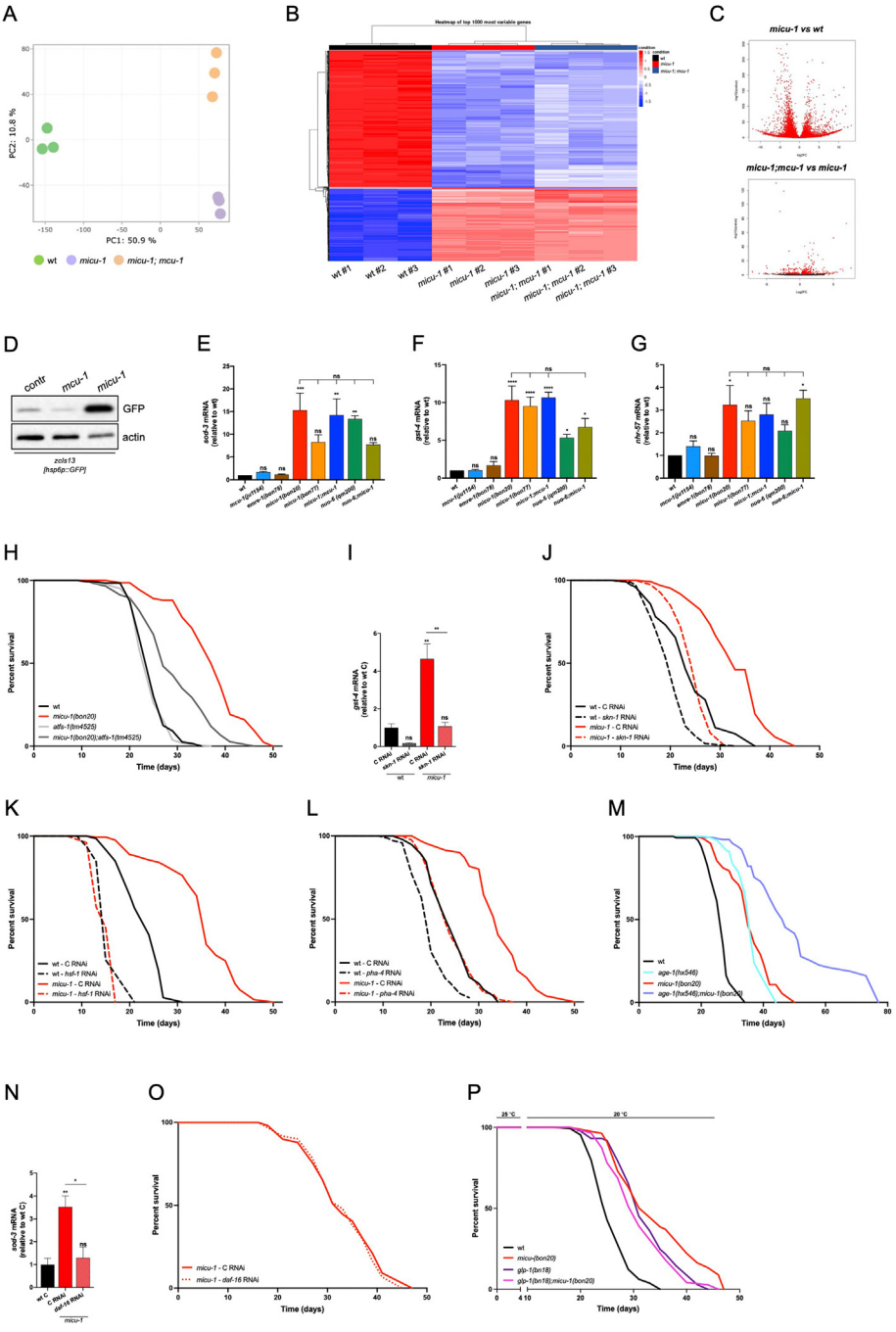

Figure 2: *micu-1(lof)* induces a transcription-dependent stress response. (A) Principal component analysis of normalized RNA-seq data. Each dot represents an RNA-seq sample of the indicated genotype. Samples with similar gene expression profiles cluster together. (B) Heatmap showing the top 1000 differentially expressed genes in *micu-1* and *micu-1;mcu-1* mutants relative to wt animals. (C) Volcano plot of significantly dysregulated genes in *micu-1(bon20)* vs. wt (top panel) and *micu-1(bon20);mcu-1(ju1154)* vs. *micu-1(bon20)* (bottom panel). Compared to wt, 3220 genes were significantly up-regulated and 3132 genes significantly down-regulated in *micu-1* mutants. In *micu-1;mcu-1* double mutants compared to *micu-1(null)* animals, only a total of 495 genes were differentially expressed (321 upregulated and 174 downregulated genes). (D) Representative WB of samples from animals expressing the *zcls13[hsp-6p::gfp]* transgene. Immunoblots were performed using antibodies against GFP and actin (as loading control). (E–G) RT-PCR of (E) *sod-3,* (F) *gst-4* and (G) *nhr-57* genes in animals at day 1 of adulthood (mean ± S.E.M., one-way ANOVA, Tukey's multiple comparisons test: ns = not significant, $*p < 0.05$, $**p < 0.01$, $***p < 0.001$ $****p < 0.0001$, n = 3–5). (H) Representative survival curves of wt, *micu-1*, *atsf-1* and *micu-1;atfs-1* mutant nematodes. (I) RT-PCR of *gst-4* expression in wt and *micu-1(bon20)* animals exposed to control and *skn-1* RNAi constructs from hatching until adulthood (mean ± S.E.M., one-way ANOVA, Tukey's multiple comparisons test: ns = not significant, $**p < 0.01$, n = 3). (J–L) Representative survival curves of wt and *micu-1(bon20)* animals exposed to control (solid lines) and (J) *skn-1,* (K) *hsf-1* and (L) *pha-4* RNAi (dashed lines) from hatching. (M) Representative survival curves of wt, *age-1*, *micu-1* and *age-1;micu-1* animals. (N) RT-PCR of *sod-3* gene expression in wt and *micu-1(bon20)* adult animals exposed to control and *daf-16* RNAi (mean ± S.E.M., one-way ANOVA, Tukey's multiple comparisons test: ns = not significant, $*p < 0.05$, $**p < 0.01$, n = 3). (O) Lifespan assay of *micu-1(bon20)* animals grown on control (solid line) and *daf-16* RNAi (dashed line) from hatching. (P) Representative survival curves of wt, *micu-1(bon20)*, *glp-1(bn18)* and *glp-1(bn18);micu-1(bon20)* animals grown at 25 °C until adulthood, then shifted to 20 °C until all animals were dead. Exposure to 25 °C from hatching results in germline-less *glp-1* animals and lifespan extension.

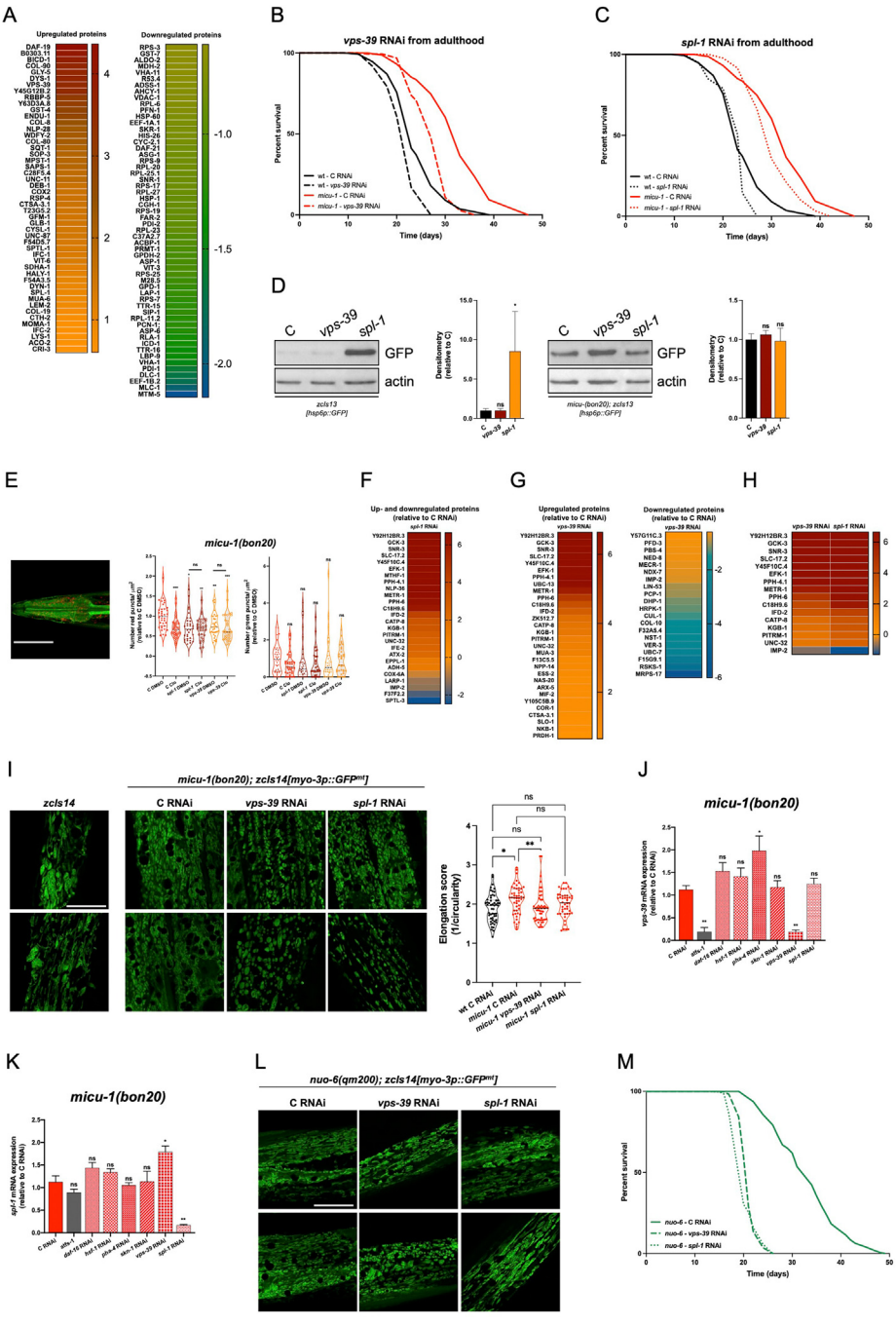

Figure 3: SPL-1/SGPL1 and VPS-39/VPS39 expression contributes to the lifespan extension of *micu-1(null)* mutants. (A) Heatmap of statistically upregulated (left) and downregulated (right) proteins in *micu-1(bon20)* mutants compared to wt. Fold changes are color coded and are indicated on the right of each heatmap. (B–C) Lifespan assay of wt and *micu-1(bon20)* mutant animals exposed to control (solid lines), (B) *vps-39* (dashed lines) and (C) *spl-1* (dotted lines) RNAi from adulthood. For wt and *micu-1(bon20)* on control RNAi, representative curves come from the same experiment and figures were split for the sake of clarity (for each individual experiment, see Supplementary Table S1). (D) WB analysis of *zcls13[hsp-6p::gfp]* transgene expression in control and *micu-1(bon20)* mutant nematodes exposed to the indicated RNAi. Immunoblots were developed using antibodies against GFP and actin (as loading control). Densitometry is reported on the right of each WB panel (Kruskal–Wallis ANOVA, Dunn's multiple comparison test, $*p < 0.05$, n = 3–4). (E) Confocal image of the head of a nematode expressing *sqIs11[[lgg-1p::mCherry::GFP::lgg-1+ rol-6]*. Statistical analysis of mCherry-positive (left violin graph) and GFP-positive (right violin graph) puncta in wt and *micu-1(bon20)* animals exposed to control, *spl-1* and *vsp-39* RNAi. Extracted eggs were grown on RNAi plates until the first day of adulthood. Animals were then exposed for 4 h to DMSO or 50 μg/ml clomipramine (Clo) and immediately imaged for mCherry-positive puncta (Kruskal–Wallis, Dunn's multiple comparison test: ns = not significant, $*p < 0.05$, $**p < 0.01$, n = 33–36 animals from 3 independent experiments). (F–G) Heatmaps of differentially regulated proteins in *micu-1(bon20)* animals exposed to (F) *spl-1* and (G) *vps-39* RNAi from hatching, compared to control RNAi. (H) Heatmap of common differentially expressed proteins in *micu-1(bon20)* animals grown on *vps-39* or *spl-1* RNAi. (I) High-resolution confocal images of 9-day-old control and 10-day-old *micu-1(bon20)* animals expressing *zcls14[myo-3p::GFP(mit)]* transgene, with quantification of mitochondrial elongation. (Kruskal–Wallis ANOVA, Dunn's multiple comparison test: ns = not significant, $*p < 0.05$, $**p < 0.01$, n = 46–53 animals from 3 independent experiments, scale bar = 10 μm). RNAi treatment is indicated. (J–K) RT-PCR of (J) *vps-39* and (K) *spl*-1 mRNA expression in *micu-1(bon20)* carrying *atfs-1(tm4525)* mutation (gray bars) or exposed to the indicated RNAi from hatching, relative to control RNAi (one-way ANOVA, Tukey's multiple comparisons test: ns = not significant, $*p < 0.05$, $**p < 0.01$, n = 3). (L) High-resolution confocal images of 7-day-old *nuo-6 (qm200)* animals expressing *zcls14[myo-3p::GFP(mt)]* transgene, following exposure to control, *vps-39*, or *spl-1* RNAi from hatching. Scale bar = 10 μm. (M) Lifespan assay of *nuo-6 (qm200)* mutant nematodes grown on control, *vps-39* and *spl-1* RNAi from hatching.

For the available 37 RNAi clones, we carried out a small-scale screen and identified *dyn-1*, *vps-39*, *spl-1* and *lem-2* RNAi as potential modifiers of *micu-1* survival (Supplementary Fig. S3G). To refine our investigation, we performed epistatic analysis on larger populations and with appropriate biological replicates. Since some of the RNAi (e.g., *dyn-1* RNAi) altered *C. elegans* development, we adopted a RNAi protocol that interferes with gene expression starting at adulthood, even though this approach does not impact early programs in larvae that are often considered to be critical in establishing longevity of mitochondrial mutant nematodes [36,58]. We grew animals until adulthood on control *E. coli* and then moved adults to plates seeded with dsRNA-expressing bacteria (see materials and methods section for details). Despite the diminished RNAi effect of our experimental paradigm, we observed a significant lifespan reduction in *micu-1(null)* animals exposed to *dyn-1*, *spl-1* and *vps-39* RNAi, while *lem-2* and RNAi starting from adulthood did not significantly alter animal survival (Figure 3B,C, Supplementary Figs. S3H—I and Table S1). We also tested these RNAi on wt animals and found that only *dyn-1* downregulation considerably affected their survival (Figure 3B,C, Supplementary Figs. S3H—I and Table S1). Because DYN-1 deficiency had this confounding effect on wt, we focused our attention on sphingosine phosphate lyase (SPL-1) and vacuolar protein sorting-associated protein 39 homolog (VPS-39).

SPL-1 is a component of the sphingolipid degradative pathway and cleaves sphingosine 1-phosphase (S1P) into hexadecenal and phosphoethanolamine (Supplementary Fig. S3J), thereby regulating sphingolipid metabolism, intracellular calcium mobilization through S1P and stress response in a ceramide-dependent manner [55,69,70]. Yeast Vps39 is part of the homotypic fusion and vacuole protein sorting (HOPS) complex, which controls membrane tethering of yeast lysosome (i.e., vacuole)-late endosome and yeast lysosome-mitochondria [71]. Moreover, the VPS39-containing HOPS complex modulates intracellular autophagic flux [71] as well as mitochondria degradation (i.e., mitophagy) through the interaction between Vps39 and Tom40 at the outer membrane [72,73]. Based on these considerations, we initially set out to measure *zcls13[hsp-6p::gfp]* expression in animals exposed to *spl-1* and *vps-39* RNAi, since sphingosine and ethanolamine pathways are highly upregulated in *micu-1(null)* mutants compared to wt (Supplementary Figs. S3J—K). Consistent with previous lines of evidence [55,69,70], *spl-1* RNAi enhanced *zcls13[hsp-6p::gfp]* expression in control animals (Figure 3D), possibly through increased ceramide availability that would sustain UPR^{mt} [55]. Conversely, *micu-1(null)* mutants grown on *vps-39* and *spl-1* RNAi exhibited negligible changes in *zcls13[hsp-6p::gfp]* expression compared to control RNAi (Figure 3D), suggesting that UPR^{mt} is fully engaged as a result of SPTL-1 and SPL-1 upregulation (Figure 3A and Supplementary Figs. S3E and S3K), thereby overriding the effect of *vps-39* and *spl-1* RNAi.

A previous genetic screen demonstrated that *dyn-1* and *vps-39* are in the same genetic pathway involved in the maturation of phagosomes during the engulfment and removal of dead corpses in adult hermaphrodite gonads [74]. Because of this role of VPS-39/Vps39 in phagosome biogenesis [74] and in yeast autophagy [73], we investigated the autophagic flux in control and *micu-1* mutant animals expressing the transgene *sqls11[lgg-1p::mCherry::GFP::lgg-1+ rol-6]* [75]. As originally described [75], tandem fluorescent tagged LGG1 is recruited to nascent phagophores and upon fusion with lysosomes, can be degraded into GFP-tagged LGG-1. We grew *sqls11[lgg-1p::mCherry::GFP::lgg-1+ rol-6]* expressing animals on control, *spl-1* and *vps-39* RNAi. Before high-resolution confocal image analysis, adults were briefly exposed to DMSO or to the antidepressant clomipramine as a potent autophagic inhibitor [76,77]. Since GFP is quenched upon autophagosome fusion with lysosomes, we visualized mature autolysosomes stained as red structures [75]. We quantified the number of mCherry-positive puncta in the head of nematodes exposed from hatching to control or RNAi against *spl-1* or *vps-39* (Figure 3E). We found that downregulation of both *spl-1* or *vps-39* inhibited autophagosome formation and autophagic flux to the same extent of clomipramine (Figure 3E). To further corroborate our line of evidence, we generated *micu-1(bon20)IV;vps-39(ok2442)V/nT1 [qIs51](IV;V)*. However, we could retrieve only a few *micu-1;vps-39* double mutant escapers out of thousands of nematodes, suggesting that a *vps-39(null)* mutation is incompatible with the survival of *micu-1(null) C. elegans*. Taken together, our findings suggest that SPL-1 and VPS-39 sustain autophagy, possibly by providing phosphatidylethanolamine to phagophore membranes as recently shown in other experimental settings [78—81].

To further investigate the putative synergism between SPL-1 and VPS-39, we exposed *micu-1(null)* mutants to control, *spl-1* and *vps-39* RNAi starting from hatching. We then extracted proteins from 5-day-old animals and performed TMT-based MS analysis, using homogenates from control RNAi-treated nematodes as a reference. Based on MS analysis of three biological replicates run in duplicates, we identified 1394 proteins with medium—high confidence (p value ≤ 0.05). We found that *spl-1* and *vps-39* silenced *micu-1* animals had 26 and 50 differentially expressed proteins (Figure 3F,G and Supplementary Table S4), respectively. Among the differentially expressed proteins uniquely found in *spl-1* RNAi *micu-1* mutants, we measured upregulation of EPPL-1/ETNPPL ethanolamine-phosphate phospho-lyase (i.e., an enzyme that catalyzes the breakdown of phosphoethanolamine) and downregulation of serine palmitoyl transferase SPTL-3/SPTLC2/SPTLC3 (i.e., an ER-localized enzyme that regulates sphingolipid biosynthesis) (Figure 3F—H and Supplementary Figs. S3J—K). This evidence suggests that SPL-1 downregulation decreases sphingolipid signaling and phosphatidylethanolamine synthesis (Supplementary Fig. S3K). Strikingly, ~60% of the differentially expressed proteins in SPL-1 deficient nematodes had a similar trend in *micu-1* mutants exposed to *vps-39* RNAi (Figure 3H and Supplementary Figure S3L), further indicating that SPL-1 and VPS-39 act on common pathways. Among the differentially expressed proteins common in the two datasets (Figure 3H and Supplementary Figure S3L), we noticed changes of intracellular signaling cascade components (i.e., GCK-3/STK39, KGB-1/MAPK10/JNK3, PPH-4/PPP4C, PPH-6/PPP6C) along with the elongation factor 2 kinase EFK-1/EEF2K, the latter being an AMPK downstream target that, through inhibition of protein synthesis, can stimulate survival of cells and nematodes in response to nutrient deprivation and sustained energy crisis [82]. Additionally, we observed an increased expression of methionine synthase METR-1/MTR (Figure 3H and Supplementary Figure S3L), an enzyme that by connecting methionine folate cycles and transsulfuration pathway, can stimulate mitochondrial biogenesis as a compensatory mechanism to alleviate lysosomal dysfunction [83]. Other evident changes of evolutionarily conserved proteins included pitrilysin metallopeptidase PITRM1, a matrix-localized peptidase that contributes to mitochondrial proteome homeostasis by degrading aggregate-prone and presequence peptides [84,85], the H^+/sialic acid cotransporter SLC17A5, a H^+/nitrate cotransporter causally linked to rare forms of lysosomal storage disorders [86], and the V-type proton ATPase UNC-32/ATP6V0A1, a subunit of the lysosomal ATPase that stimulates vacuolar acidification [87] (Figure 3H and Supplementary Figure S3L). To complete our investigation and frame our findings in the context of mitochondria-to-nucleus "retrograde" signaling, we assessed

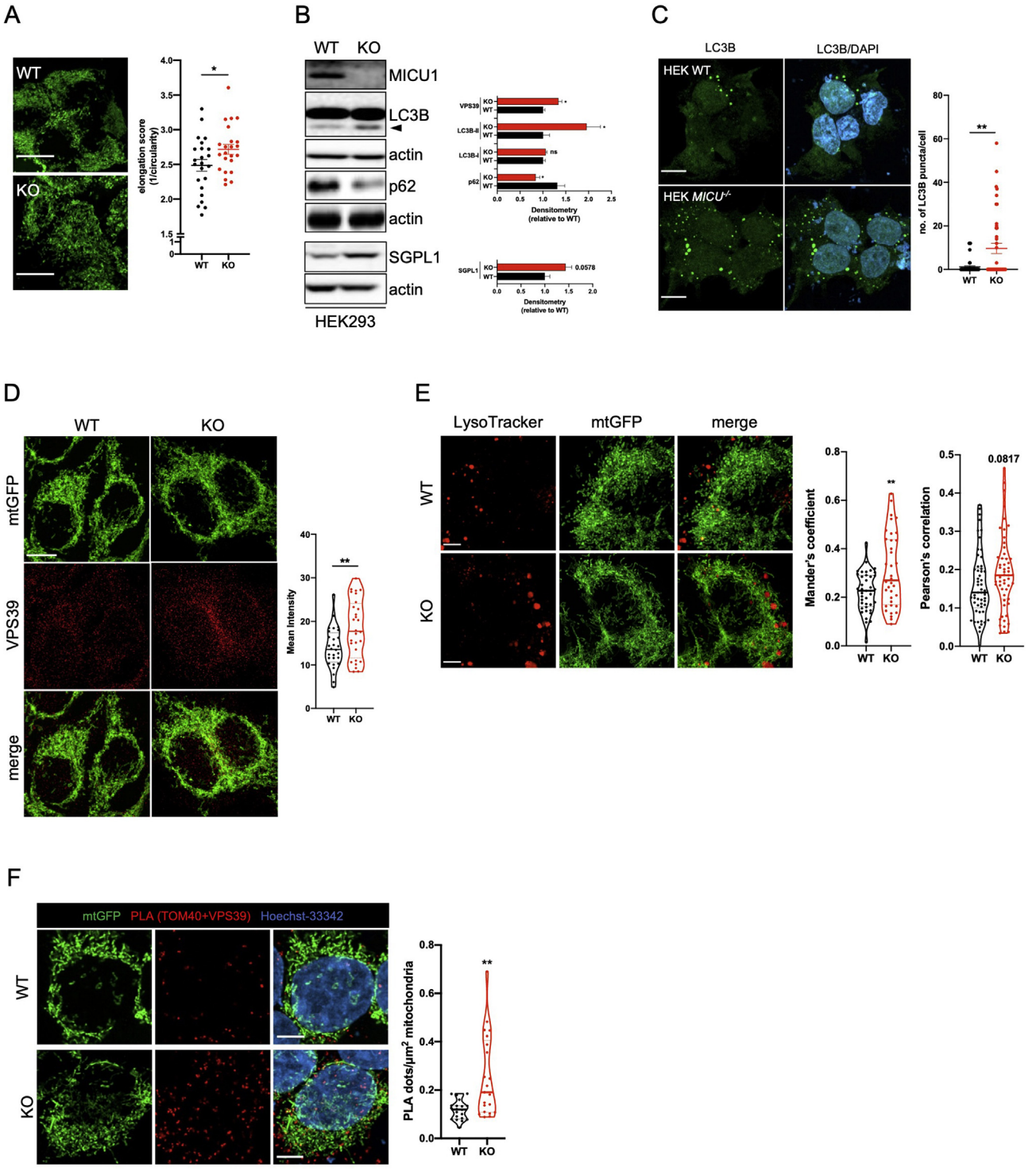

Figure 4: MICU1 KO stimulates mitochondrial recruitment of VPS39. (A) Confocal images and quantification of mitochondrial elongation in WT and MICU1 KO HEK293 cells overexpressing mitochondrially targeted GFP (Student's t-test, $^{*}p < 0.05$, n = 3, n > 20 cells/condition. Scale bar = 10 μm). (B) Western blot analyses of samples from WT and MICU1 KO cells. Immunoblots were performed using antibodies against MICU1, LC3B, p62, SGPL1 and actin (as loading control). Head arrow indicates lipidated LC3B at ~16 kDa. Densitometry is reported on the right (fold differences relative to WT cells: Mann Whitney and Student's t-test, $^{*}p < 0.05$, n = 3–5). Data are represented as mean ± S.E.M. (C) Confocal images and quantification of LC3B puncta/cell in WT and MICU1 KO HEK293 cells (Mann–Whitney test, $^{**}p < 0.01$, n > 40 cells/condition). Scale bar = 10 μm. DAPI was used to stain nuclei (blue). (D) Confocal imaging of WT and MICU1 KO cells overexpressing mitochondrially targeted GFP (mtGFP) and stained with VPS39 antibody (scale bar = 10 μm). Quantification of VPS39 staining is shown on the right (Student's t-test, $^{**}p < 0.01$, n = 28 cells/condition). (E) LysoTracker-stained WT and MICU1 KO HEK293 cells overexpressing mtGFP (scale bar = 10 μm). Lysosome-mitochondria overlap was quantified using Mander's and Pearson's correlation coefficient (Student's t-test, $^{**}p < 0.01$, n = 3, WT:54 cells, KO:55 cells). (F) Proximity ligation assay (PLA) between VPS39 and TOM40 in WT and MICU1 KO HEK293 cells overexpressing mtGFP (scale bar = 10 μm). The number of PLA dots per cell was normalized to the mitochondrial area (Mann–Whitney U-test, $^{**}p < 0.01$, n = 3, WT: 20 cells, KO: 21 cells).

mitochondrial morphology upon *spl-1* and *vps-39* silencing and found that *spl-1* downregulation had a slight, though statistically not significant effect on mitochondrial network, whereas VPS-39 was required for the proper maintenance of the mitochondrial morphology in *micu-1* mutant nematodes (Figure 3I). Next, we investigated the transcriptional regulation of *vps-39* and *spl-1* in *micu-1(null)* mutants. Following our previous epistatic analysis of the transcription factors involved in *micu-1* longevity (Figure 2H—L), we found that ATFS-1 loss significantly compromised *vps-39* expression in *micu-1(null)* animals, while downregulation of PHA-4, a transcription factor previously described as regulator of autophagy during dietary restriction [65,88], slightly enhanced *vps-39* expression (Figure 3J). These data strongly suggest that *vps-39* gene expression is under the transcriptional regulation of ATFS-1 and is therefore a component of the ATFS-1-dependent mitochondria-to-nucleus retrograde signaling. Conversely, neither *atfs-1(lof)* nor downregulation of other transcription factors influenced *spl-1* expression (Figure 3K). Of note, a very mild *spl-1* upregulation was detected in *vps-39* deficient *micu-1* mutant nematodes (Figure 3K). Neither *vps-39* nor *spl-1* RNAi could rescue the germline defects observed in *micu-1(null)* mutants (Supplementary Figs. S4A—B). Together, our findings describe a previously unknown SPL-1/VPS-39 signaling axis that, through sphingolipid metabolism and autophagy, may contribute to mitochondrial network expansion underlying lifespan-extending programs in *micu-1* deficient *C. elegans*.

Finally, to determine whether *spl-1* and *vps-39* RNAi could influence mitochondrial maintenance also in other long-lived mitochondrial mutants, we employed *nuo-6(qm200)* expressing mitochondrial GFP in body wall muscle cells. In line with our data in *micu-1(null)* animals, we observed that SPL-1 and VPS-39 promoted the proper organization of the mitochondrial network in *nuo-6* mutant nematodes (Figure 3L). Notably, *spl-1* and *vps-39* RNAi reduced *nuo-6* longevity (Figure 3M), indicating that SPL-1/VPS-39 signaling may play a role in animals carrying genetic lesions of complex I.

3.4. VPS39 localization to the mitochondria is associated with enhanced autophagic flux in MICU1 deficient HEK293 cells

To gain deeper insights into evolutionarily conserved cellular processes mechanistically linked to MICU1 deficiency, we employed WT and MICU1 KO HEK293 cells as an *in vitro* mammalian model [89]. Conventional Seahorse measurements showed a clear decreased OCR in MICU1 KO cells grown in either glucose- or galactose-containing media (Supplementary Figs. S5A—B). The diminished mitochondrial respiration and the loss of mitochondrial respiratory complex subunits correlated with an increased extracellular acidification rate as an accepted proxy of enhanced glycolysis (Supplementary Figs. S5C—D). Using a newly validated proximity ligation assay (PLA)-based protocol [32], we performed *in situ* analysis of mitochondrial CI—CIV proximity as an indicator of mitochondrial respiratory supercomplexes (RSCs). We observed that MICU1 KO cells exhibited less CI, CIV-containing RSCs (Supplementary Fig. S5E), further confirming lesions of the mitochondrial OXPHOS system. Having characterized the bioenergetic profiles of these cells, we moved forward to substantiate our molecular evidence obtained in *C. elegans*. In WT and MICU1 KO HEK293 cells, we overexpressed mitochondria-targeted GFP and assessed mitochondrial morphology, thereby noticing that MICU1 KO mitochondria had slightly more elongated structures (Figure 4A). High-resolution confocal imaging showed no major changes of mitochondria-endoplasmic reticulum (ER) contacts in MICU1 KO cells compared to controls (Supplementary Fig. S5F). To support this evidence, we performed PLA between the mitochondrial translocase of the outer membrane TOM20 and ER localized KDEL-containing proteins. We quantified PLA dots and observed no differences between WT and MICU1 KO cells (Supplementary Fig. S5G), suggesting that MICU1 deficiency does not alter mitochondria-ER contact sites.

We ran immunoblot analysis and found that, consistent with our data in nematodes, SGPL1 was considerably upregulated in MICU1 KO cells compared to WT ones (Figure 4B). Strikingly, these cells also had an increased basal level of autophagosome-associated lipidated LC3B [90] and a decreased amount of ubiquitin binding protein p62 (Figure 4B), a well-known receptor that promotes cargo delivery to the autophagosome which is selectively degraded during autophagy [91,92]. Such enhanced autophagic flux was neither linked to altered mTOR/Akt activity nor to obvious changes in AMPK signaling (Supplementary Figs. S6A—B). Consistent with our immunoblots (Figure 4B), high-resolution confocal image analysis revealed an increased number of LC3B-positive structures (Figure 4C) that were accompanied by more VPS39-positive dots in MICU1 KO cells compared to controls (Figure 4D). Next, we stained mitochondria and lysosomes in WT and MICU1 KO cells. We observed that MICU1 KO cells had an increased number of LysoTracker-positive vesicles, which may be interpreted as enhanced lysosomal content, with a consequent expansion of contacts between GFP-positive mitochondria and LysoTracker-stained vesicles (Figure 4E). Since Vps39 interacts with Tom40 and relocalizes to mitochondria in yeast during starvation [73,93], we set up a PLA between TOM40 and VPS39, then quantified PLA dots over the mitochondrial area. Using two independent sets of VPS39 antibodies, we found that VPS39 redistributed to mitochondria in MICU1 KO cells (Figure 4F and data not shown). Taken together, our findings reveal evolutionarily conserved molecular signatures that are mechanistically linked to MICU1 dysfunction. While MICU1 KO does not profoundly affect mitochondria-ER tethering, it increases the number of mitochondria-lysosome contact sites in HEK293 cells. Consistent with our data in *C. elegans*, MICU1 KO stimulates the autophagic flux in HEK293 cells grown in glucose, promoting VPS39 upregulation and its interaction with mitochondria as previously described in yeast [73].

3.5. SGPL1 controls mitochondria-tethered VPS39 in MICU1 deficient HeLa cells

To address the mechanistic contribution of SGPL1 and VPS39 to MICU1-dependent processes, we attempted to genetically modulate their expression using synthetic small interfering RNAs (siRNAs). However, we could not obtain sufficient downregulation of the two target genes due to the fast replication rate of HEK293 cells. To overcome this limitation, we employed tumorigenic HeLa cells, in which we manipulated gene expression in a highly efficient manner (Figure 5A,B and Supplementary Fig. S6C). To be consistent with our study in HEK293 cells, we carried out experiments in HeLa cells grown in glucose-containing medium. We found that MICU1 deficient HeLa cells exhibited a decreased OCR, although milder compared to cells grown in galactose-containing medium (Figure 5C). In standard growing conditions, *MICU1* downregulation stimulated LC3B lipidation in HeLa cells, although it did not result in a significant decrease of p62 levels (Figure 5B). Notably, siRNA against *VPS39* abrogated LC3B lipidation in MICU1 deficient cells, while it upregulated lipidated LC3B in control HeLa cells (Figure 5B). No significant differences of p62 levels were observed compared to controls, possibly because autophagy is not highly upregulated in cells grown in glucose- and serum-containing medium [94,95]. Our interpretation of this dataset is that VPS39 influences MICU1-dependent recruitment of LC3B to nascent phagophores. Having profiled the bioenergetics and autophagy levels of MICU1 deficient HeLa cells, we set out to confirm the SGPL1/VPS39 signaling axis and its role in cellular homeostasis (Figure 5D), as

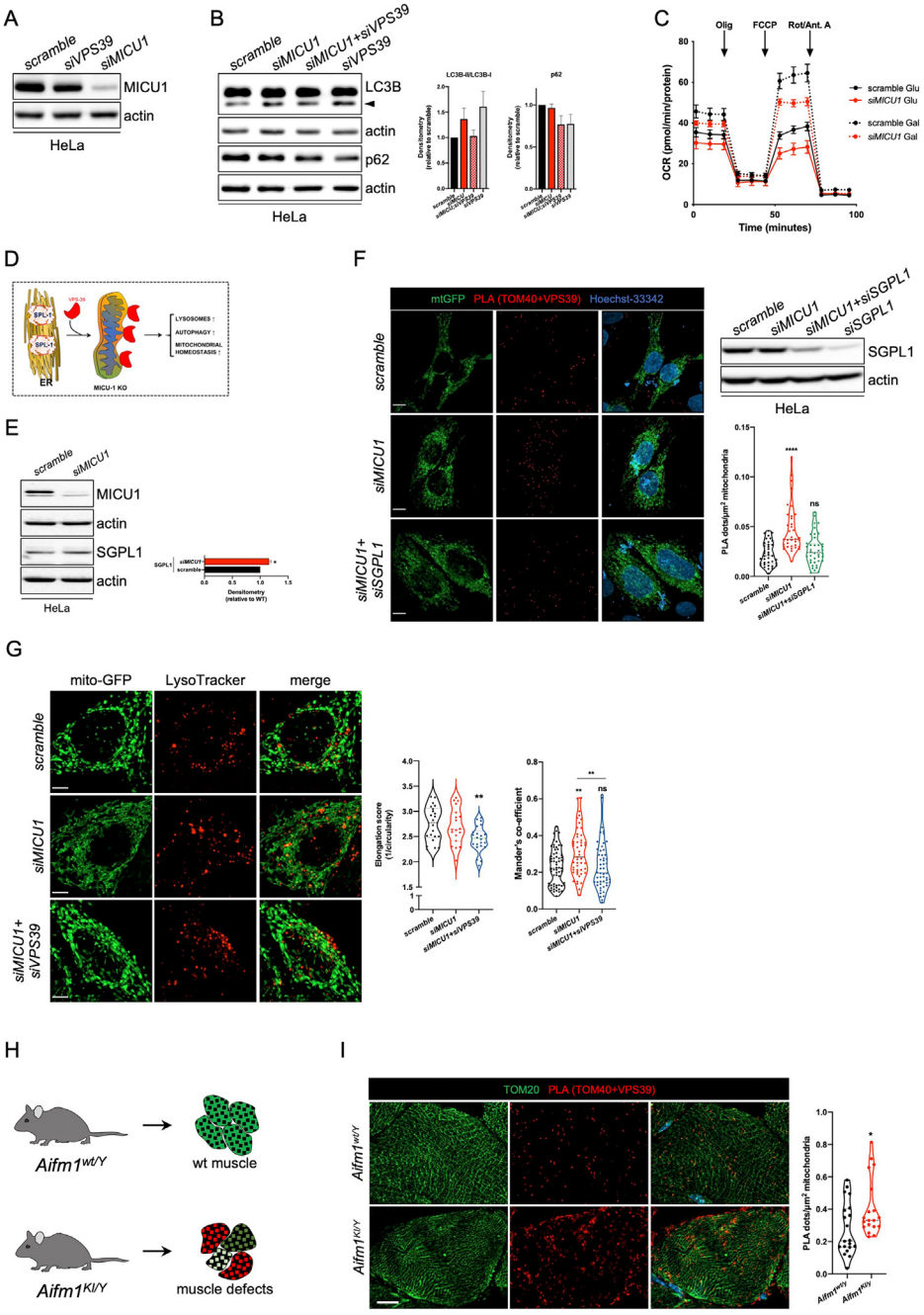

Figure 5: SGPL1 influences mitochondrial recruitment of VPS39 in mitochondrial deficient cells. (A) Western blot analyses of samples from HeLa cells transfected with siRNAs against *VPS39* (*siVPS39*) and *MICU1* (*siMICU1*). Scramble siRNA was used as control. Immunoblots were developed using antibodies against MICU1 and actin (as loading control). (B) Western blot analyses of HeLa cells transfected with scramble or siRNA against *MICU1* and/or *VPS39*. Immunoblots were developed using antibodies against LC3B (head arrow indicates lipidated LC3B), p62 and actin (as loading control). Densitometry is reported on the right (Student's t-test, $*p < 0.05$, n = 3). Data are represented as mean ± S.E.M. (C) OCR of HeLa cells transfected with siRNAs against *MICU1* and grown in glucose- or galactose-containing medium (n = 1). (D) Schematic representation of SGPL1-dependent recruitment of VPS39 to the mitochondria and its expected effects on lysosome-mitochondria contacts, autophagy and mitochondrial homeostasis. (E) Representative immunoblots of HeLa cells transfected with siRNA against *MICU1*. Immunoblots were developed using antibodies against MICU1, SGPL1 and actin (as loading control). Densitometry is reported on the right (Student's t-test, $*p < 0.05$, n = 3). (F) Proximity ligation assay (PLA) of mtGFP-overexpressing HeLa cells transfected with scramble, siRNAs against *MICU1* (s*iMICU1*) and/or *SGPL1* (*siSGPL1*). PLA dots per cell were normalized to the mitochondrial area (Kruskal–Wallis test, $****p < 0.0001$, n = 2, scramble: 38 cells, *siMICU1*: 36 cells, *siMICU1* + *siSGPL1*: 40 cells). Scale bar = 10 µm. Representative WB analysis of siRNA transfected HeLa cells is reported on top right. (G) LysoTracker staining in mtGFP-overexpressing HeLa cells transfected with scramble, *siMICU1* and/or *siVPS39*. Mitochondrial morphology was analyzed based on the mtGFP-signal and lysosome-mitochondria overlap was quantified via Mander's coefficient (Kruskal–Wallis test, $**p < 0.01$, n = 3, scramble: 42 cells, *siMICU1*: 49 cells, *siMICU1*+*siVPS39*: 54 cells). Scale bar = 10 µm. (H) Schematic representation of the transgenic mice and derived muscle tissues used in this work. *Aifm1*$^{KI/Y}$ are males carrying the disease-causing *Aifm1(R200 del)* mutation, whereas *Aifm1*$^{wt/Y}$ are wt littermates. (I) PLA (TOM40+VPS39) staining of muscle sections derived from 6-month-old mice. Mitochondria were counterstained using an antibody against TOM20 (scale bar = 10 µm). Quantification of the PLA dots/µm^2 mitochondria is reported on the right (Mann–Whitney U-test, $*p < 0.05$, n = 2 mice/genotype with 10 muscle fibers/mouse).

previously demonstrated in our experiments using *C. elegans* and HEK293 cells. To do so, we performed PLA (TOM40+VPS39) staining followed by high-resolution confocal image analysis. We quantified the number of PLA (TOM40+VPS39) dots and found that siRNA against *SGPL1* reduced VPS39 proximity to TOM40 (Figure 5E,F), further supporting our hypothesis that SGPL1 activity is required for VPS39 association to mitochondria (Figure 5D). We transfected HeLa cells with mitochondrial GFP and siRNAs. We found that *MICU1* downregulation enhanced the colocalization of LysoTracker-positive structures with GFP-labelled mitochondria (Figure 5G). However, *VPS39* downregulation impaired lysosome-mitochondria contacts in MICU1 deficient HeLa cells (Figure 5G), resulting in aberrant mitochondrial morphology as observed in nematodes. Together, this experimental evidence mechanistically links VPS39 localization in proximity of the mitochondria with the remodeling of mitochondria-lysosome contact sites in MICU1 deficient cells.

Finally, to demonstrate that these newly identified molecular signatures may be commonly observed in cells carrying mitochondrial lesions, we employed muscle tissues from wt and transgenic mice expressing a disease-causing *Aifm1(R200 del)* mutation (Figure 5H) [28,33]. These knockin mice develop severe myopathy due to apoptosis-inducing factor (AIF) loss and consequent aberrant expression of ETC components [32,33,49,96]. We ran immunoblot analysis and showed that AIF loss stimulated VPS39 expression in 6-month-old muscles (Supplementary Fig. S6D). We carried out PLA staining and quantified TOM40-VSP39 proximity in control and AIF deficient muscle fibers. In symptomatic *Aifm1(R200 del)* knockin animals, we found that OXPHOS deficiency promoted VPS39 redistribution to the mitochondria (Figure 5I), which was reflected by a higher number of PLA dots compared to controls. Thus, our cross-species analysis indicates that SGPL1-dependent redistribution of VPS39 to mitochondria may be a detectable common signature in cells carrying mitochondrial lesions.

4. DISCUSSION

Mitochondrial energy production is finely tuned to accurately interpret cellular needs. During embryogenesis or in tumors, dividing cells employ mitochondria to produce biomass, while they generate a large amount of ATP by redirecting glucose and other substrates to the glycolytic pathway. Conversely, ATP is mostly generated through mitochondrial OXPHOS in cells undergoing postmitotic differentiation or grown in presence of non-fermenting carbon substrates (e.g., galactose) [97–99]. Such plasticity in adjusting mitochondrial bioenergetics is a key adaptive mechanism that eukaryotic cells exploit in response to environmental changes, altered nutritional conditions, toxic stimuli and stress signals [41]. To coordinate mitochondrial bioenergetics, the nuclear genome must encode thousands of proteins that, upon correct import and folding, potentiate mitochondrial function and eventually scale up mitochondrial mass. This nucleus-to-mitochondria communication, generally known as anterograde signaling [100], depends on a sophisticated array of transcription factors regulating the functional properties of the organelles. To accurately and dynamically coordinate such broad metabolic rewiring, the expression of nuclear-encoded mitochondrial proteins triggers evolutionarily conserved mitochondria-to-nucleus "retrograde" signals that act as necessary inputs to adjust the intensity and temporal resolution of the anterograde signaling [41,42,52,101]. According to the physiological context, this highly interconnected regulatory network of communication between the nucleus and mitochondria ultimately determines cell division, growth, lineage commitment and differentiation. Notably, this bidirectional regulation of the mitochondrial proteome represents also a protective mechanism to adjust mitochondrial activity and homeostasis upon injury, ETC inhibition and stress due to the accumulation of unfolded proteins or other toxic species. In this regard, mitochondria-to-nucleus "retrograde" signals, including the unfolded protein response (UPR^{mt}) [102,103], may confer healthspan and longevity of an organism when they occur within a certain time window during development [36,37,46]. Although UPR^{mt} is not a predictor of *C. elegans* lifespan [104], its transcriptional inhibition can abrogate lifespan-extending programs in animals carrying genetic lesions or exposed to mitochondrial toxins [45,57,58,105–108]. By failing in responding to the necessary adjustment of mitochondrial activity, cells lose their fitness and experience severe damage because protective compensatory mechanisms are not sufficient to prevent the accumulation of toxic species. While UPR^{mt} is essential for the expansion of the mitochondrial network during development and in development-dependent processes underlying longevity [36,58,109], its contribution becomes less obvious in human pathology. Albeit these mechanisms help to overcome mitochondrial dysfunction in nematodes, the scenario is different in higher organisms, since these processes may become a maladaptive response that compromises cellular homeostasis in organs suffering from a chronic bioenergetic crisis [110]. As a consequence of increased mitochondrial mass due to uncontrolled biogenesis or impaired removal of defective organelles, cells are forced to balance their transcriptional output with compensatory processes that should prevent the progressive accumulation of damaged mitochondria, ultimately depleting the already scarce resources. Because of their clinical implications in metabolic disorders, these poorly elucidated processes are extremely relevant in biomedicine and deserve further attention.

We herein investigate novel molecular mechanisms linked to mitochondrial dysfunction by employing a *C. elegans* model of MICU1 deficiency, given the strong relevance of MICU1/MICU2 in human pathophysiology [21–24,29]. We demonstrate that *micu-1(null)* mutations lead to developmental defects, including abnormal cell death in the mitotic and pachytene zones of the gonads, impaired oocyte production and slow growth. As in higher organisms, we report that altered expression of OXPHOS subunits is linked to diminished mitochondrial respiration in *C. elegans*. Similar to other mitochondrial mutants, the significant lifespan extension of *micu-1(null)* nematodes requires the establishment of a mitochondria-to-nucleus stress response that relies on various transcription factors (i.e., ATFS-1, SKN-1, HSF-1 and PHA-4), whereas it is not dependent on components of the insulin/IGF-1 cascade (i.e., AGE-1 and DAF-16). While MICU-1 deficiency induces mitochondrial dysfunction and pro-longevity stress response, genetic ablation of *micu-1* negatively affects the proper maintenance of the germline to a level which is not comparable to other mitochondrial mutants that have been previously described. Another additional intriguing aspect is that neither the lifespan extension of *micu-1(null)* nematodes nor the degenerative processes in the meiotic zone or the transcriptional control of pro-longevity genes depend on a functional MCU complex. Thus, the dispensable MCU contribution to the observed phenotypes prompted us to further investigate MICU-1/MICU1 function beyond its widely reported participation in Ca^{2+} signaling. In this regard, our quantitative proteomics and epistatic analyses unveil previously underestimated processes in which MICU-1/MICU1 is engaged. We report that *micu-1(null)* mutations stimulate the expression of sphingosine phosphate lyase SPL-1/SGPL1 (i.e., an enzyme involved in sphingolipid degradation), which possibly acts upstream the mitochondrial network expansion underlying longevity of mitochondrial mutant nematodes. Given that the basal mitochondrial matrix Ca^{2+} is comparable between control and *micu-1(null)* mutant animals under resting conditions [38], one possible

explanation is that SPL-1 upregulation may also act as a compensatory mechanism to prevent excessive Ca^{2+} mobilization, since SPL-1-mediated degradation of S1P would attenuate Ca^{2+} release from intracellular stores (e.g., ER) [70]. As an alternative scenario, SPL-1 upregulation may stimulate phosphoethanolamine biosynthesis (as suggested by our proteomics) and trafficking between the ER and mitochondria, with the contact points between the two intracellular compartments acting as physical bridges necessary to sustain the transfer of phospholipids to lysosomes and/or nascent phagophores containing membrane anchored lipidated LGG-1/LC3 [79]. In support of this hypothesis and in line with previous evidence in other experimental models [78,80,81], genetic inhibition of *spl-1* diminishes the autophagic flux in *C. elegans*, possibly because it exhausts mitochondrial membranes required to sustain autophagosome biogenesis in a system chronically under energy crisis and forced to recycle nutrients as shown in cultured cells [81]. It is certainly exciting to find that MICU-1/MICU1 deficiency induces SPL-1/SGPL1 and VPS-39/VPS39 upregulation in both *C. elegans* and mammalian cells. In this regard, our study conclusively describes how the mitochondria-to-nucleus "retrograde" program can expand mitochondrial mass and efficiently support their homeostasis [58,109]. We show that the bZIP transcription factor ATFS-1 regulates *vps-39* expression, meaning that this gene is an integral component of those longevity programs associated with the "mitochondrial threshold effect" [39]. As unveiled by our cross-species investigation, we mechanistically establish that SGPL1 stimulates mitochondria-tethered VPS39 to contribute to functional remodeling of intracellular organelle interactions. Specifically, we conclusively elucidate that decreased SGPL1 expression inhibits the binding of VPS39 to TOM40, while VPS-39/VPS39 downregulation compromises the maintenance of the expanded mitochondrial network in MICU-1/MICU1 deficient cells, thereby altering the contacts between mitochondria and lysosomes. Of note, the increased VPS39 expression and localization to mitochondria does not have a profound effect on ER-mitochondria tethering, probably also because of mitochondrial elongation in response to sustained autophagy as previously reported [111]. We speculate that, as shown in *Saccharomyces cerevisiae* [73,93], mitochondria-tethered VPS39 may influence lipid exchange and eventually mitophagy. Consistent with the role of SPL-1/SGPL1 in autophagy (our data and [78]), we report that VPS-39/VPS39 downregulation diminishes the autophagosome numbers in MICU-1 deficient nematodes and the autophagic flux in cells grown in glucose- and serum-containing medium (i.e., not under starving conditions).

In the context of human pathophysiology, we speculate that MCU inhibition would not be sufficient as a therapeutic intervention for inherited mitochondrial diseases with altered MICU1/MICU2 function. Although difficult, it would be very informative to test whether manipulation of the sphingosine pathway by ethanolamine supplementation may have a beneficial effect in patients. Furthermore, our proof-of-principle evidence in nematodes and transgenic mice suggests that the importance of our findings may go beyond diseases linked to MICU1/MICU2 deficiency and be relevant to other metabolic disorders. Future studies will explore and clarify this possibility in detail.

5. CONCLUSION

In summary, we propose that the SGPL1/VPS39 axis contributes to mitochondria-nucleus "retrograde" signals and deciphers the energetic states of the cell, thereby attenuating maladaptive processes that are adopted to counteract aberrant mitochondrial OXPHOS.

AUTHOR CONTRIBUTION

Conceptualization, JJ, LW, DB; Methodology, JJ, LW, DB; Validation and Investigation, JJ, LW, ES, AnPe, YW, AnPi, DG, SS, MS, DB; Formal Analysis, JJ, LW, ES; Resources, KH, CEH, JW, AR, JLS, DE; Writing, DB; Visualization, LW, ES, DB; Supervision, LW, DB; Project Administration, DB; Funding Acquisition, PN and DB.

ACKNOWLEDGEMENTS

We wish to thank our DZNE colleagues at LMF; Prof. Ina Vorberg (DZNE), Prof. Donato Di Monte (DZNE) and Prof. Gerhild van Echten-Deckert (University of Bonn) for their useful suggestions; Ms. Christiane Bartling-Kirsch (DZNE), Ms. Anaïs Marsal-Cots (DZNE), Ms. Elena Schlimgen, Mr. Nick Atanelov, Ms. Elide Lo Cacciato and Dr. Tannaz Norizadeh Abbariki for their technical assistance. We thank Dr. Diego De Stefani and Dr. Agnese De Mario (University of Padova, Padova, Italy) for providing MICU1 KO HEK293 cells. This research was supported by the DZNE institutional budget, the CoEN (Carbon-Model, 3018) initiative and the Helmholtz cross-program topic "Aging and Metabolic Programming (AMPro)". PN and DB are members of the DFG Cluster of Excellence ImmunoSensation funded by the Deutsche Forschungsgemeinschaft (DFG, German Research Foundation) under Germany's Excellence Strategy – EXC2151 – 390873048. JJ and DB are members of the Mitochondrial Dysfunction in Parkinson's Consortium (PD-MitoQUANT). PD-MitoQUANT has received funding from the Innovative Medicines Initiative 2 Joint Undertaking under grant agreement No. 821522. This Joint Undertaking receives support from the European Union's Horizon 2020 research and innovation programme and EFPIA.

CONFLICT OF INTEREST

None declared.

APPENDIX A. SUPPLEMENTARY DATA

Supplementary data to this article can be found online at https://doi.org/10.1016/j.molmet.2022.101503.

REFERENCES

[1] Kirichok, Y., Krapivinsky, G., Clapham, D.E., 2004. The mitochondrial calcium uniporter is a highly selective ion channel. Nature 427(6972):360–364.
[2] Vasington, F.D., Murphy, J.V., 1962. Ca ion uptake by rat kidney mitochondria and its dependence on respiration and phosphorylation. Journal of Biological Chemistry 237:2670–2677.
[3] Bick, A.G., Calvo, S.E., Mootha, V.K., 2012. Evolutionary diversity of the mitochondrial calcium uniporter. Science 336(6083):886.
[4] Pittis, A.A., Goh, V., Cebrian-Serrano, A., Wettmarshausen, J., Perocchi, F., Gabaldon, T., 2020. Discovery of EMRE in fungi resolves the true evolutionary history of the mitochondrial calcium uniporter. Nature Communications 11(1):4031.
[5] De Stefani, D., Rizzuto, R., Pozzan, T., 2016. Enjoy the trip: calcium in mitochondria back and forth. Annual Review of Biochemistry 85:161–192.
[6] Baughman, J.M., Perocchi, F., Girgis, H.S., Plovanich, M., Belcher-Timme, C.A., Sancak, Y., et al., 2011. Integrative genomics identifies MCU as an essential component of the mitochondrial calcium uniporter. Nature 476(7360):341–345.
[7] De Stefani, D., Raffaello, A., Teardo, E., Szabo, I., Rizzuto, R., 2011. A forty-kilodalton protein of the inner membrane is the mitochondrial calcium uniporter. Nature 476(7360):336–340.

[8] Sancak, Y., Markhard, A.L., Kitami, T., Kovacs-Bogdan, E., Kamer, K.J., Udeshi, N.D., et al., 2013. EMRE is an essential component of the mitochondrial calcium uniporter complex. Science 342(6164):1379–1382.

[9] Liu, J.C., Syder, N.C., Ghorashi, N.S., Willingham, T.B., Parks, R.J., Sun, J., et al., 2020. EMRE is essential for mitochondrial calcium uniporter activity in a mouse model. JCI Insight.

[10] Wang, Y., Nguyen, N.X., She, J., Zeng, W., Yang, Y., Bai, X.C., et al., 2019. Structural mechanism of EMRE-dependent gating of the human mitochondrial calcium uniporter. Cell 177(5):1252–1261 e1213.

[11] Vais, H., Mallilankaraman, K., Mak, D.D., Hoff, H., Payne, R., Tanis, J.E., et al., 2016. EMRE is a matrix Ca(2+) sensor that governs gatekeeping of the mitochondrial Ca(2+) uniporter. Cell Reports 14(3):403–410.

[12] Perocchi, F., Gohil, V.M., Girgis, H.S., Bao, X.R., McCombs, J.E., Palmer, A.E., et al., 2010. MICU1 encodes a mitochondrial EF hand protein required for Ca(2+) uptake. Nature 467(7313):291–296.

[13] Vais, H., Payne, R., Paudel, U., Li, C., Foskett, J.K., 2020. Coupled transmembrane mechanisms control MCU-mediated mitochondrial Ca(2+) uptake. Proceedings of the National Academy of Sciences of the United States of America 117(35):21731–21739.

[14] Gottschalk, B., Klec, C., Leitinger, G., Bernhart, E., Rost, R., Bischof, H., et al., 2019. MICU1 controls cristae junction and spatially anchors mitochondrial Ca(2+) uniporter complex. Nature Communications 10(1):3732.

[15] Liu, J.C., Liu, J., Holmstrom, K.M., Menazza, S., Parks, R.J., Fergusson, M.M., et al., 2016. MICU1 serves as a molecular gatekeeper to prevent in vivo mitochondrial calcium overload. Cell Reports 16(6):1561–1573.

[16] Antony, A.N., Paillard, M., Moffat, C., Juskeviciute, E., Correnti, J., Bolon, B., et al., 2016. MICU1 regulation of mitochondrial Ca(2+) uptake dictates survival and tissue regeneration. Nature Communications 7:10955.

[17] Csordas, G., Golenar, T., Seifert, E.L., Kamer, K.J., Sancak, Y., Perocchi, F., et al., 2013. MICU1 controls both the threshold and cooperative activation of the mitochondrial Ca(2)(+) uniporter. Cell Metabolism 17(6):976–987.

[18] Mallilankaraman, K., Doonan, P., Cardenas, C., Chandramoorthy, H.C., Muller, M., Miller, R., et al., 2012. MICU1 is an essential gatekeeper for MCU-mediated mitochondrial Ca(2+) uptake that regulates cell survival. Cell 151(3):630–644.

[19] Orrenius, S., Zhivotovsky, B., Nicotera, P., 2003. Regulation of cell death: the calcium-apoptosis link. Nature Reviews Molecular Cell Biology 4(7):552–565.

[20] Nicotera, P., Orrenius, S., 1992. Ca2+ and cell death. Annals of the New York Academy of Sciences 648:17–27.

[21] Shamseldin, H.E., Alasmari, A., Salih, M.A., Samman, M.M., Mian, S.A., Alshidi, T., et al., 2017. A null mutation in MICU2 causes abnormal mitochondrial calcium homeostasis and a severe neurodevelopmental disorder. Brain 140(11):2806–2813.

[22] Lewis-Smith, D., Kamer, K.J., Griffin, H., Childs, A.M., Pysden, K., Titov, D., et al., 2016. Homozygous deletion in MICU1 presenting with fatigue and lethargy in childhood. Neurology Genetics 2(2):e59.

[23] Logan, C.V., Szabadkai, G., Sharpe, J.A., Parry, D.A., Torelli, S., Childs, A.M., et al., 2014. Loss-of-function mutations in MICU1 cause a brain and muscle disorder linked to primary alterations in mitochondrial calcium signaling. Nature Genetics 46(2):188–193.

[24] Kohlschmidt, N., Elbracht, M., Czech, A., Hausler, M., Phan, V., Topf, A., et al., 2021. Molecular pathophysiology of human MICU1-deficiency. Neuropathology and Applied Neurobiology.

[25] Frazier, A.E., Thorburn, D.R., Compton, A.G., 2019. Mitochondrial energy generation disorders: genes, mechanisms, and clues to pathology. Journal of Biological Chemistry 294(14):5386–5395.

[26] Gorman, G.S., Chinnery, P.F., DiMauro, S., Hirano, M., Koga, Y., McFarland, R., et al., 2016. Mitochondrial diseases. Nature Reviews Disease Primers 2:16080.

[27] Koopman, W.J., Beyrath, J., Fung, C.W., Koene, S., Rodenburg, R.J., Willems, P.H., et al., 2016. Mitochondrial disorders in children: toward development of small-molecule treatment strategies. EMBO Molecular Medicine 8(4):311–327.

[28] Bano, D., Prehn, J.H.M., 2018. Apoptosis-inducing factor (AIF) in physiology and disease: the tale of a repented natural born killer. EBioMedicine 30:29–37.

[29] Wilton, K.M., Morales-Rosado, J.A., Selcen, D., Muthusamy, K., Ewing, S., Agre, K., et al., 2020. Developmental brain abnormalities and acute encephalopathy in a patient with myopathy with extrapyramidal signs secondary to pathogenic variants in MICU1. JIMD Report 53(1):22–28.

[30] Pan, X., Liu, J., Nguyen, T., Liu, C., Sun, J., Teng, Y., et al., 2013. The physiological role of mitochondrial calcium revealed by mice lacking the mitochondrial calcium uniporter. Nature Cell Biology 15(12):1464–1472.

[31] Tufi, R., Gleeson, T.P., von Stockum, S., Hewitt, V.L., Lee, J.J., Terriente-Felix, A., et al., 2019. Comprehensive genetic characterization of mitochondrial Ca(2+) uniporter components reveals their different physiological requirements in vivo. Cell Reports 27(5):1541–1550 e1545.

[32] Bertan, F., Wischhof, L., Scifo, E., Guranda, M., Jackson, J., Marsal-Cots, A., et al., 2020. Comparative profiling of N-respirasomes predicts aberrant mitochondrial bioenergetics at single-cell resolution. bioRxiv.

[33] Wischhof, L., Gioran, A., Sonntag-Bensch, D., Piazzesi, A., Stork, M., Nicotera, P., et al., 2018. A disease-associated Aifm1 variant induces severe myopathy in knockin mice. Molecular Metabolism 13:10–23.

[34] Scifo, E., Szwajda, A., Soliymani, R., Pezzini, F., Bianchi, M., Dapkunas, A., et al., 2015. Proteomic analysis of the palmitoyl protein thioesterase 1 interactome in SH-SY5Y human neuroblastoma cells. Journal of Proteomics 123:42–53.

[35] Xu, S., Chisholm, A.D., 2014. C. elegans epidermal wounding induces a mitochondrial ROS burst that promotes wound repair. Developmental Cell 31(1):48–60.

[36] Dillin, A., Hsu, A.L., Arantes-Oliveira, N., Lehrer-Graiwer, J., Hsin, H., Fraser, A.G., et al., 2002. Rates of behavior and aging specified by mitochondrial function during development. Science 298(5602):2398–2401.

[37] Rea, S.L., Ventura, N., Johnson, T.E., 2007. Relationship between mitochondrial electron transport chain dysfunction, development, and life extension in Caenorhabditis elegans. PLoS Biology 5(10):e259.

[38] Tang, N.H., Kim, K.W., Xu, S., Blazie, S.M., Yee, B.A., Yeo, G.W., et al., 2020. The mRNA decay factor CAR-1/LSM14 regulates axon regeneration via mitochondrial calcium dynamics. Current Biology 30(5):865–876 e867.

[39] Rossignol, R., Faustin, B., Rocher, C., Malgat, M., Mazat, J.P., Letellier, T., 2003. Mitochondrial threshold effects. Biochemical Journal 370(Pt 3):751–762.

[40] Wang, Y., Hekimi, S., 2015. Mitochondrial dysfunction and longevity in animals: untangling the knot. Science 350(6265):1204–1207.

[41] Bar-Ziv, R., Bolas, T., Dillin, A., 2020. Systemic effects of mitochondrial stress. EMBO Reports 21(6):e50094.

[42] Lin, Y.F., Haynes, C.M., 2016. Metabolism and the UPR(mt). Molecular Cell 61(5):677–682.

[43] Piazzesi, A., Wang, Y., Jackson, J., Wischhof, L., Zeisler-Diehl, V., Scifo, E., et al., 2022. CEST-2.2 overexpression alters lipid metabolism and extends longevity of mitochondrial mutants. EMBO Reports e52606.

[44] Gioran, A., Piazzesi, A., Bertan, F., Schroer, J., Wischhof, L., Nicotera, P., et al., 2019. Multi-omics identify xanthine as a pro-survival metabolite for nematodes with mitochondrial dysfunction. The EMBO Journal 38(6).

[45] Piazzesi, A., Papic, D., Bertan, F., Salomoni, P., Nicotera, P., Bano, D., 2016. Replication-independent histone variant H3.3 controls animal lifespan through the regulation of pro-longevity transcriptional programs. Cell Reports 17(4):987–996.

[46] Feng, J., Bussiere, F., Hekimi, S., 2001. Mitochondrial electron transport is a key determinant of life span in Caenorhabditis elegans. Developmental Cell 1(5):633–644.

[47] Lee, S.S., Lee, R.Y., Fraser, A.G., Kamath, R.S., Ahringer, J., Ruvkun, G., 2003. A systematic RNAi screen identifies a critical role for mitochondria in C. elegans longevity. Nature Genetics 33(1):40—48.
[48] Chaudhari, S.N., Kipreos, E.T., 2017. Increased mitochondrial fusion allows the survival of older animals in diverse C. elegans longevity pathways. Nature Communications 8(1):182.
[49] Troulinaki, K., Buttner, S., Marsal Cots, A., Maida, S., Meyer, K., Bertan, F., et al., 2018. WAH-1/AIF regulates mitochondrial oxidative phosphorylation in the nematode Caenorhabditis elegans. Cell Death & Disease 4:2.
[50] Kanazawa, T., Zappaterra, M.D., Hasegawa, A., Wright, A.P., Newman-Smith, E.D., Buttle, K.F., et al., 2008. The C. elegans Opa1 homologue EAT-3 is essential for resistance to free radicals. PLoS Genetics 4(2):e1000022.
[51] Head, B.P., Zulaika, M., Ryazantsev, S., van der Bliek, A.M., 2011. A novel mitochondrial outer membrane protein, MOMA-1, that affects cristae morphology in Caenorhabditis elegans. Molecular Biology of the Cell 22(6): 831—841.
[52] Shpilka, T., Haynes, C.M., 2018. The mitochondrial UPR: mechanisms, physiological functions and implications in ageing. Nature Reviews Molecular Cell Biology 19(2):109—120.
[53] Riera, C.E., Dillin, A., 2015. Tipping the metabolic scales towards increased longevity in mammals. Nature Cell Biology 17(3):196—203.
[54] Troulinaki, K., Bano, D., 2012. Mitochondrial deficiency: a double-edged sword for aging and neurodegeneration. Frontiers in Genetics 3:244.
[55] Liu, Y., Samuel, B.S., Breen, P.C., Ruvkun, G., 2014. Caenorhabditis elegans pathways that surveil and defend mitochondria. Nature 508(7496):406—410.
[56] Mao, K., Ji, F., Breen, P., Sewell, A., Han, M., Sadreyev, R., et al., 2019. Mitochondrial dysfunction in C. elegans activates mitochondrial relocalization and nuclear hormone receptor-dependent detoxification genes. Cell Metabolism 29(5):1182—1191 e1184.
[57] Nargund, A.M., Pellegrino, M.W., Fiorese, C.J., Baker, B.M., Haynes, C.M., 2012. Mitochondrial import efficiency of ATFS-1 regulates mitochondrial UPR activation. Science 337(6094):587—590.
[58] Shpilka, T., Du, Y., Yang, Q., Melber, A., Uma Naresh, N., Lavelle, J., et al., 2021. UPR(mt) scales mitochondrial network expansion with protein synthesis via mitochondrial import in Caenorhabditis elegans. Nature Communications 12(1):479.
[59] Tullet, J.M., Hertweck, M., An, J.H., Baker, J., Hwang, J.Y., Liu, S., et al., 2008. Direct inhibition of the longevity-promoting factor SKN-1 by insulin-like signaling in C. elegans. Cell 132(6):1025—1038.
[60] Walker, A.K., See, R., Batchelder, C., Kophengnavong, T., Gronniger, J.T., Shi, Y., et al., 2000. A conserved transcription motif suggesting functional parallels between Caenorhabditis elegans SKN-1 and Cap'n'Collar-related basic leucine zipper proteins. Journal of Biological Chemistry 275(29): 22166—22171.
[61] Kenyon, C.J., 2010. The genetics of ageing. Nature 464(7288):504—512.
[62] Fontana, L., Partridge, L., Longo, V.D., 2010. Extending healthy life span–from yeast to humans. Science 328(5976):321—326.
[63] Sen, P., Shah, P.P., Nativio, R., Berger, S.L., 2016. Epigenetic mechanisms of longevity and aging. Cell 166(4):822—839.
[64] Williams, R., Laskovs, M., Williams, R.I., Mahadevan, A., Labbadia, J., 2020. A mitochondrial stress-specific form of HSF1 protects against age-related proteostasis collapse. Developmental Cell 54(6):758—772 e755.
[65] Panowski, S.H., Wolff, S., Aguilaniu, H., Durieux, J., Dillin, A., 2007. PHA-4/Foxa mediates diet-restriction-induced longevity of C. elegans. Nature 447(7144):550—555.
[66] Austin, J., Kimble, J., 1987. glp-1 is required in the germ line for regulation of the decision between mitosis and meiosis in C. elegans. Cell 51(4):589—599.
[67] Arantes-Oliveira, N., Apfeld, J., Dillin, A., Kenyon, C., 2002. Regulation of lifespan by germ-line stem cells in Caenorhabditis elegans. Science 295(5554): 502—505.
[68] Szabadkai, G., Bianchi, K., Varnai, P., De Stefani, D., Wieckowski, M.R., Cavagna, D., et al., 2006. Chaperone-mediated coupling of endoplasmic reticulum and mitochondrial Ca2+ channels. The Journal of Cell Biology 175(6):901—911.
[69] Kim, H.E., Grant, A.R., Simic, M.S., Kohnz, R.A., Nomura, D.K., Durieux, J., et al., 2016. Lipid biosynthesis coordinates a mitochondrial-to-cytosolic stress response. Cell 166(6):1539—1552 e1516.
[70] Spiegel, S., Milstien, S., 2003. Sphingosine-1-phosphate: an enigmatic signalling lipid. Nature Reviews Molecular Cell Biology 4(5):397—407.
[71] van der Beek, J., Jonker, C., van der Welle, R., Liv, N., Klumperman, J., 2019. CORVET, CHEVI and HOPS - multisubunit tethers of the endo-lysosomal system in health and disease. Journal of Cell Science 132(10).
[72] Heo, J.M., Harper, N.J., Paulo, J.A., Li, M., Xu, Q., Coughlin, M., et al., 2019. Integrated proteogenetic analysis reveals the landscape of a mitochondrial-autophagosome synapse during PARK2-dependent mitophagy. Science Advances 5(11):eaay4624.
[73] Gonzalez Montoro, A., Auffarth, K., Honscher, C., Bohnert, M., Becker, T., Warscheid, B., et al., 2018. Vps39 interacts with Tom40 to establish one of two functionally distinct vacuole-mitochondria contact sites. Developmental Cell 45(5):621—636 e627.
[74] Kinchen, J.M., Doukoumetzidis, K., Almendinger, J., Stergiou, L., Tosello-Trampont, A., Sifri, C.D., et al., 2008. A pathway for phagosome maturation during engulfment of apoptotic cells. Nature Cell Biology 10(5):556—566.
[75] Chang, J.T., Kumsta, C., Hellman, A.B., Adams, L.M., Hansen, M., 2017. Spatiotemporal regulation of autophagy during Caenorhabditis elegans aging. Elife 6.
[76] Cavaliere, F., Fornarelli, A., Bertan, F., Russo, R., Marsal-Cots, A., Morrone, L.A., et al., 2019. The tricyclic antidepressant clomipramine inhibits neuronal autophagic flux. Scientific Reports 9(1):4881.
[77] Rossi, M., Munarriz, E.R., Bartesaghi, S., Milanese, M., Dinsdale, D., Guerra-Martin, M.A., et al., 2009. Desmethylclomipramine induces the accumulation of autophagy markers by blocking autophagic flux. Journal of Cell Science 122(Pt 18):3330—3339.
[78] Mitroi, D.N., Karunakaran, I., Graler, M., Saba, J.D., Ehninger, D., Ledesma, M.D., et al., 2017. SGPL1 (sphingosine phosphate lyase 1) modulates neuronal autophagy via phosphatidylethanolamine production. Autophagy 13(5):885—899.
[79] Acoba, M.G., Senoo, N., Claypool, S.M., 2020. Phospholipid ebb and flow makes mitochondria go. The Journal of Cell Biology 219(8).
[80] Rockenfeller, P., Koska, M., Pietrocola, F., Minois, N., Knittelfelder, O., Sica, V., et al., 2015. Phosphatidylethanolamine positively regulates autophagy and longevity. Cell Death & Differentiation 22(3):499—508.
[81] Hailey, D.W., Rambold, A.S., Satpute-Krishnan, P., Mitra, K., Sougrat, R., Kim, P.K., et al., 2010. Mitochondria supply membranes for autophagosome biogenesis during starvation. Cell 141(4):656—667.
[82] Leprivier, G., Remke, M., Rotblat, B., Dubuc, A., Mateo, A.R., Kool, M., et al., 2013. The eEF2 kinase confers resistance to nutrient deprivation by blocking translation elongation. Cell 153(5):1064—1079.
[83] Wei, W., Ruvkun, G., 2020. Lysosomal activity regulates Caenorhabditis elegans mitochondrial dynamics through vitamin B12 metabolism. Proceedings of the National Academy of Sciences of the United States of America 117(33):19970—19981.
[84] Mossmann, D., Vogtle, F.N., Taskin, A.A., Teixeira, P.F., Ring, J., Burkhart, J.M., et al., 2014. Amyloid-beta peptide induces mitochondrial dysfunction by inhibition of preprotein maturation. Cell Metabolism 20(4): 662—669.
[85] Perez, M.J., Ivanyuk, D., Panagiotakopoulou, V., Di Napoli, G., Kalb, S., Brunetti, D., et al., 2020. Loss of function of the mitochondrial peptidase PITRM1 induces proteotoxic stress and Alzheimer's disease-like pathology in human cerebral organoids. Molecular Psychiatry.

[86] Verheijen, F.W., Verbeek, E., Aula, N., Beerens, C.E., Havelaar, A.C., Joosse, M., et al., 1999. A new gene, encoding an anion transporter, is mutated in sialic acid storage diseases. Nature Genetics 23(4):462—465.

[87] Oka, T., Toyomura, T., Honjo, K., Wada, Y., Futai, M., 2001. Four subunit a isoforms of Caenorhabditis elegans vacuolar H+-ATPase. Cell-specific expression during development. Journal of Biological Chemistry 276(35): 33079—33085.

[88] Hansen, M., Chandra, A., Mitic, L.L., Onken, B., Driscoll, M., Kenyon, C., 2008. A role for autophagy in the extension of lifespan by dietary restriction in C. elegans. PLoS Genetics 4(2):e24.

[89] Kamer, K.J., Mootha, V.K., 2014. MICU1 and MICU2 play nonredundant roles in the regulation of the mitochondrial calcium uniporter. EMBO Reports 15(3): 299—307.

[90] Kabeya, Y., Mizushima, N., Ueno, T., Yamamoto, A., Kirisako, T., Noda, T., et al., 2000. LC3, a mammalian homologue of yeast Apg8p, is localized in autophagosome membranes after processing. The EMBO Journal 19(21): 5720—5728.

[91] Kirkin, V., McEwan, D.G., Novak, I., Dikic, I., 2009. A role for ubiquitin in selective autophagy. Molecular Cell 34(3):259—269.

[92] Seibenhener, M.L., Babu, J.R., Geetha, T., Wong, H.C., Krishna, N.R., Wooten, M.W., 2004. Sequestosome 1/p62 is a polyubiquitin chain binding protein involved in ubiquitin proteasome degradation. Molecular and Cellular Biology 24(18):8055—8068.

[93] Iadarola, D.M., Basu Ball, W., Trivedi, P.P., Fu, G., Nan, B., Gohil, V.M., 2020. Vps39 is required for ethanolamine-stimulated elevation in mitochondrial phosphatidylethanolamine. Biochimica et Biophysica Acta (BBA) - Molecular and Cell Biology of Lipids 1865(6):158655.

[94] Levine, B., Kroemer, G., 2019. Biological functions of autophagy genes: a disease perspective. Cell 176(1—2):11—42.

[95] Dikic, I., Elazar, Z., 2018. Mechanism and medical implications of mammalian autophagy. Nature Reviews Molecular Cell Biology 19(6):349—364.

[96] Meyer, K., Buettner, S., Ghezzi, D., Zeviani, M., Bano, D., Nicotera, P., 2015. Loss of apoptosis-inducing factor critically affects MIA40 function. Cell Death & Disease 6:e1814.

[97] Nunnari, J., Suomalainen, A., 2012. Mitochondria: in sickness and in health. Cell 148(6):1145—1159.

[98] Pavlova, N.N., Thompson, C.B., 2016. The emerging hallmarks of cancer metabolism. Cell Metabolism 23(1):27—47.

[99] Vander Heiden, M.G., Cantley, L.C., Thompson, C.B., 2009. Understanding the Warburg effect: the metabolic requirements of cell proliferation. Science 324(5930):1029—1033.

[100] Quiros, P.M., Mottis, A., Auwerx, J., 2016. Mitonuclear communication in homeostasis and stress. Nature Reviews Molecular Cell Biology 17(4):213—226.

[101] D'Amico, D., Sorrentino, V., Auwerx, J., 2017. Cytosolic proteostasis networks of the mitochondrial stress response. Trends in Biochemical Sciences 42(9):712—725.

[102] Zhao, Q., Wang, J., Levichkin, I.V., Stasinopoulos, S., Ryan, M.T., Hoogenraad, N.J., 2002. A mitochondrial specific stress response in mammalian cells. The EMBO Journal 21(17):4411—4419.

[103] Haynes, C.M., Ron, D., 2010. The mitochondrial UPR - protecting organelle protein homeostasis. Journal of Cell Science 123(Pt 22):3849—3855.

[104] Bennett, C.F., Vander Wende, H., Simko, M., Klum, S., Barfield, S., Choi, H., et al., 2014. Activation of the mitochondrial unfolded protein response does not predict longevity in Caenorhabditis elegans. Nature Communications 5:3483.

[105] Labbadia, J., Brielmann, R.M., Neto, M.F., Lin, Y.F., Haynes, C.M., Morimoto, R.I., 2017. Mitochondrial stress restores the heat shock response and prevents proteostasis collapse during aging. Cell Reports 21(6):1481—1494.

[106] Benedetti, C., Haynes, C.M., Yang, Y., Harding, H.P., Ron, D., 2006. Ubiquitin-like protein 5 positively regulates chaperone gene expression in the mitochondrial unfolded protein response. Genetics 174(1):229—239.

[107] Nargund, A.M., Fiorese, C.J., Pellegrino, M.W., Deng, P., Haynes, C.M., 2015. Mitochondrial and nuclear accumulation of the transcription factor ATFS-1 promotes OXPHOS recovery during the UPR(mt). Molecular Cell 58(1):123—133.

[108] Tian, Y., Garcia, G., Bian, Q., Steffen, K.K., Joe, L., Wolff, S., et al., 2016. Mitochondrial stress induces chromatin reorganization to promote longevity and UPR(mt). Cell 165(5):1197—1208.

[109] Palikaras, K., Lionaki, E., Tavernarakis, N., 2015. Coordination of mitophagy and mitochondrial biogenesis during ageing in C. elegans. Nature 521(7553): 525—528.

[110] Uittenbogaard, M., Chiaramello, A., 2014. Mitochondrial biogenesis: a therapeutic target for neurodevelopmental disorders and neurodegenerative diseases. Current Pharmaceutical Design 20(35):5574—5593.

[111] Gomes, L.C., Di Benedetto, G., Scorrano, L., 2011. During autophagy mitochondria elongate, are spared from degradation and sustain cell viability. Nature Cell Biology 13(5):589—598.

Chapter II: Actin-nucleation promoting factor N-WASP influences alpha-synuclein condensates and pathology

Summary

Background:

Neurodegenerative diseases are often characterised by the presence of insoluble inclusions. In patients with Parkinson's disease (PD) and other synucleinopathies, patient-derived tissues often display the presence of α-Syn-positive inclusions such as Lewy bodies or Lewy neurites. Despite the extensive efforts of the scientific community, the molecular mechanisms underlying α-Syn inclusion formation are poorly understood (Spillantini *et al.*, 1997; Shahmoradian *et al.*, 2019). A growing hypothesis is that aberrant liquid-liquid phase separation (LLPS) contributes to the process of inclusion formation, since α-Syn is able to undergo LLPS under physiological conditions (Ray *et al.*, 2020; Hoffmann *et al.*, 2021; Piroska *et al.*, 2023).

Furthermore, several lines of evidence suggest that mitochondrial defects contribute to PD pathology (Davis *et al.*, 1979; Langston *et al.*, 1983; Kitada *et al.*, 1998; Valente *et al.*, 2004; Irrcher *et al.*, 2010). Yet, the connection between α-Syn and mitochondrial dysfunction in PD is not fully understood. In this regard, it is unclear how mitochondrial dysfunction may contribute to aberrant α-Syn folding and inclusion formation.

Objective:

To investigate the molecular factors that contribute to mitochondrial dysfunction and proteotoxicity in PD.

Methods and results:

As a starting point of our study, we decided to assess the interactome of α-Syn to identify modifiers of its function. Using two parallel assays, we identified actin-binding proteins and other cytoskeletal proteins to be a relatively large group of α-Syn interacting partners. From these interactors, we focused on N-WASP, an actin

nucleation promoting factor that was shown to be mutated in family members affected by early-onset PD (Kumar *et al.*, 2021).

We found that α-Syn and N-WASP colocalise at the pre-synapse in neuronal cell cultures, however we did not detect an interaction in HEK293T cells using coimmunoprecipitation, likely due to a weak or transient interaction.

A feature of many synaptic proteins, such as Synapsin 1 and Synaptophysin, is the ability to form biomolecular condensates (Milovanovic *et al.*, 2018; Park *et al.*, 2021). Since N-WASP has also been shown to undergo phase separation (Li *et al.*, 2012), we sought to test whether it could be recruited to condensates of Synapsin 1 or Synaptophysin. We confirmed that N-WASP is recruited to Synapsin 1 condensates using a combination of neuronal and HEK293 cell cultures.

When we assessed whether α-Syn, Synapsin 1, and N-WASP could be recruited to the same condensates, we found that most condensates only contained α-Syn/Synapsin 1 or N-WASP/Synapsin 1, but not all three proteins together. Inhibition of N-WASP activity using Wiskostatin, or downregulation using siRNA, led to a depletion of α-Syn from Synapsin 1 condensates. Furthermore, downregulation of N-WASP led to reduced size of Synapsin 1 condensates. Together, this data suggests that N-WASP plays an important role in regulation of α-Syn/Synapsin 1 biomolecular condensates, which may be important for their role in synaptic function.

Using a *C. elegans* model of α-Syn pathology, we characterised the outcome of *in vivo loss-of-function* of WSP-1, the nematode ortholog of N-WASP. We found that *wsp-1(lof)* and *α-Syn O/E* had negative effects on locomotion and lifespan, under different growth conditions. *wsp-1(lof)* did not have any significant effect on the expression of α-Syn and did not have a consistent effect on α-Syn condensate size or number in different growth conditions. However, *wsp-1(lof)* consistently reduced the mobility of α-Syn condensates across different growth conditions and ages.

To test the influence of *α-Syn O/E* and *wsp-1(lof)* on *C. elegans* health, we performed proteomic analysis on wt, *wsp-1(lof)*, *α-Syn O/E* and *wsp-1(lof); α-Syn O/E* animals. We showed that *wsp-1(lof), α-Syn O/E*, and *wsp-1(lof); α-Syn O/E* animals show a similar signature of mitochondrial impairment and metabolic alterations.

We assessed mitochondrial respiration using Seahorse, and found that, *wsp-1, α-Syn O/E*, and *wsp-1; α-Syn O/E* animals had reduced respiration compared to

wt animals. To assess whether reduced mitochondrial function was linked to the reduced mobility of α-Syn condensates as seen in *wsp-1; α-Syn O/E* animals, we utilised the CI mutant strain *gas-1(fc21).* Contrary to our expectation, CI deficiency increased *α-Syn* condensate mobility, indicating that mitochondrial dysfunction may drive condensates to a less aggregate-prone state.

Since proteomic analysis indicated a reduced lipid metabolism, we sought to assess the neutral lipid content using Oil Red O staining. We found a reduced accumulation of neutral lipids in *wsp-1* and *wsp-1; α-Syn O/E* animals in both growth temperatures, and a reduction in *α-Syn O/E* animals only at 25ºC. We assessed whether modifying lipid storage by overexpressing *fat-7* could alter α-Syn condensate mobility. Surprisingly, *fat-7* O/E had little effect on α-Syn LLPS. Since proteomic analysis indicated increased expression of proteins involved in muscle function, we assessed condensate mobility in *α-Syn* O/E animals exposed to RNAi against selected muscle function proteins. Similarly, we saw no evidence for contribution to condensate mobility.

Conclusions:

It has been hypothesised that the formation of α-Syn-positive inclusions depends on aberrant biomolecular condensates of α-Syn, which can mature into a more solid-like, aggregated state in some conditions (Ray *et al.*, 2020; Piroska *et al.*, 2023). Here we provide evidence that WSP-1/N-WASP plays a role in balancing the formation of Synapsin 1/α-Syn liquid condensates and maintaining solubility of α-Syn within condensates. Loss of WSP-1/N-WASP may promote the transition of α-Syn-containing condensates into a more hydrogel-like state, which have been shown to increase the propensity of α-Syn to form pathogenic fibrils. Furthermore, we demonstrate that loss of WSP-1/N-WASP or α-Syn overexpression act independently to induce mitochondrial and metabolic alterations, which is particularly interesting considering that mitochondrial dysfunction is a feature of PD pathology. Finally, we demonstrate that, under the conditions tested, aberrant CI activity does not impair α-Syn LLPS and does not shift the balance of α-Syn condensates towards a more solid-like state.

Contributions:

I contributed to the conceptualisation, investigation, validation, formal analysis, writing, and visualisation of this study. Experimentally, I contributed significantly towards Figure 1C-E, Figure 1 G-I, Figure 4, Figure 5, and Figure 6.

CDDpress

www.nature.com/cddis

ARTICLE OPEN

Actin-nucleation promoting factor N-WASP influences alpha-synuclein condensates and pathology

Joshua Jackson[1,8], Christian Hoffmann[2,3,8], Enzo Scifo[1,8], Han Wang[2], Lena Wischhof[1], Antonia Piazzesi[1], Mrityunjoy Mondal[1], Hanna Shields[1], Xuesi Zhou[4], Magali Mondin[5], Eanna B. Ryan[6], Hermann Döring[7], Jochen H. M. Prehn[6], Klemens Rottner[7], Gregory Giannone[4], Pierluigi Nicotera[1], Dan Ehninger[1]✉, Dragomir Milovanovic[2,3]✉ and Daniele Bano[1]✉

Abnormal intraneuronal accumulation of soluble and insoluble α-synuclein (α-Syn) is one of the main pathological hallmarks of synucleinopathies, such as Parkinson's disease (PD). It has been well documented that the reversible liquid-liquid phase separation of α-Syn can modulate synaptic vesicle condensates at the presynaptic terminals. However, α-Syn can also form liquid-like droplets that may convert into amyloid-enriched hydrogels or fibrillar polymorphs under stressful conditions. To advance our understanding on the mechanisms underlying α-Syn phase transition, we employed a series of unbiased proteomic analyses and found that actin and actin regulators are part of the α-Syn interactome. We focused on Neural Wiskott-Aldrich syndrome protein (N-WASP) because of its association with a rare early-onset familial form of PD. In cultured cells, we demonstrate that N-WASP undergoes phase separation and can be recruited to synapsin 1 liquid-like droplets, whereas it is excluded from α-Syn/synapsin 1 condensates. Consistently, we provide evidence that *wsp-1/WASL loss of function* alters the number and dynamics of α-Syn inclusions in the nematode *Caenorhabditis elegans*. Together, our findings indicate that N-WASP expression may create permissive conditions that promote α-Syn condensates and their potentially deleterious conversion into toxic species.

Cell Death and Disease (2024)15:304 ; https://doi.org/10.1038/s41419-024-06686-7

INTRODUCTION

Synucleinopathies are a clinically heterogeneous group of neurodegenerative diseases in which misfolded and/or aggregated α-Syn abnormally accumulates in cytoplasmic deposits generally known as Lewy bodies (LB) [1, 2]. Post-mortem assessment of patients with idiopathic PD or dementia with Lewy bodies (DLB) reveals α-Syn-positive deposits in well-defined regions, such as the *substantia nigra* (SN) *pars compacta*. The progressive accumulation of α-Syn-containing LB is associated with the degeneration of vulnerable neurons and the consequent onset of motor disabilities [3]. In addition to the presence of LB pathology, tissues from PD patients often show mitochondrial defects and signs of oxidative stress that are assumed to be part of the detrimental cascade leading to dopaminergic neuronal death [4]. While familial forms of PD have a clear etiology, idiopathic PD is considered a complex multifactorial age-related disorder in which aberrant α-Syn accumulation is one of the main hallmarks and causes of neurodegeneration [5]. Given the relevance in human pathophysiology, the molecular mechanisms underlying α-Syn pathology in PD and other synucleinopathies remain a topic of intense investigation, as they represent targets for therapeutic interventions.

Human α-Syn is an intrinsically disordered cytosolic protein consisting of 140 amino acids. Normally, α-Syn is highly expressed in neural cells and localizes at the presynaptic terminals, where it is highly abundant and modulates synaptic vesicle (SV) trafficking by promoting membrane curvature and chaperoning the formation of SNARE complexes [6, 7]. Recent evidence suggests that high concentrations of α-Syn promote its liquid-liquid phase separation (LLPS), with liquid-like droplets that could convert into amyloid-enriched hydrogel under certain conditions [8, 9]. Additionally, α-Syn condensates may act as reservoirs of highly concentrated α-Syn monomers that can contribute to the growth of fibrillar polymorphs, as it occurs in cells that are exposed to exogenous preformed fibrils [10]. It has been proposed that LLPS is a thermodynamic process in which macromolecules assemble into distinct subcellular compartments lacking a membrane or a scaffold [11]. In functionally healthy neurons, clusters of SVs at the synapses are shown to assemble by LLPS through their interaction with synapsins, a highly abundant family of synaptic phosphoproteins [12–14]. Synapsin 1 is an SV-associated protein that interacts with α-Syn when upregulated or overexpressed [15, 16]. Moreover, synapsin 1 establishes a functional coupling with α-Syn

[1]German Center for Neurodegenerative Diseases (DZNE), Bonn, Germany. [2]German Center for Neurodegenerative Diseases (DZNE), Berlin, Germany. [3]Einstein Center for Neuroscience, Charité-Universitätsmedizin Berlin, Corporate Member of Freie Universität Berlin, Humboldt-Universität Berlin, and Berlin Institute of Health, Berlin, Germany. [4]University Bordeaux, CNRS, Interdisciplinary Institute for Neuroscience, IINS, UMR 5297, Bordeaux, France. [5]University Bordeaux, CNRS, INSERM, BIC, UAR 3420, F-33000 Bordeaux, France. [6]RCSI Centre for Systems Medicine and Department of Physiology and Medical Physics, RCSI University of Medicine and Health Sciences; SFI FutureNeuro Research Centre, Dublin 2, Ireland. [7]Division of Molecular Cell Biology, Zoological Institute, Technische Universität Braunschweig; Department of Cell Biology, Helmholtz Centre for Infection Research, Braunschweig, Germany. [8]These authors contributed equally: Joshua Jackson, Christian Hoffmann, Enzo Scifo. ✉email: dan.ehninger@dzne.de; dragomir.milovanovic@dzne.de; daniele.bano@dzne.de

Edited by Gerry Melino

Received: 6 September 2023 Revised: 7 April 2024 Accepted: 16 April 2024
Published online: 30 April 2024

on the SV surface [17], thereby regulating vesicle recycling and abundance at the presynaptic terminals [18]. Although α-Syn partially retains its high mobility within the crowded environment at the nerve compartments, it is actively recruited and reversibly sequestered by SV/synapsin 1 condensates [19]. Interestingly, high molar ratios of α-Syn alter the assembly kinetics of SV/synapsin 1 condensates [19, 20], further indicating that expression changes of α-Syn may impact the biophysical properties of other synaptic molecules.

Clinical evidence indicates that duplication and triplication of *SNCA* gene can cause familial forms of PD [1]. Consistent with its toxic effect when aberrantly accumulated, it is known that α-Syn upregulation can occur upon stress or synaptic damage [21, 22], which may promote α-Syn mislocalization, interactions with non-conventional molecular partners and association with lipid bilayer membranes. Over time, these binding molecules can exert an influence on α-Syn's conformational state, along with its recruitment and incorporation into functional liquid condensates or amyloid-like hydrogels [1, 6, 19, 23]. At least in experimental models, intracerebral inoculation of α-Syn toxic species or aggregates can rapidly lead to progressive neurodegeneration and parkinsonism [24, 25], further emphasizing the strong mechanistic link between aberrant α-Syn homeostasis and PD. Despite these functionally relevant consequences, the mechanisms that abolish the native localization of α-Syn from the synaptic boutons and drive its aberrant condensation in neuronal cell bodies remain unclear.

Given the contribution of α-Syn to PD and other neurodegenerative diseases, we hypothesized that a better understanding of the α-Syn interactome may help to reveal molecular processes linked to α-Syn LLPS and possibly to α-Syn toxicity. Thus, we set out a series of proteomic analyses and an unbiased in vitro protein-protein profiling of α-Syn interactors. We found that many α-Syn interaction partners are actin and actin-binding proteins, including members of the Wiskott-Aldrich syndrome (WAS) protein family, such as WASF1 and WASF3. We focused on the Neural Wiskott-Aldrich syndrome protein (N-WASP), an actin nucleation factor that binds and activates the Arp2/3 complex [26]. It is known that N-WASP can undergo liquid-like density phase transition [27, 28], which enhances its dwell time on the membrane and its positive influences on Arp2/3-dependent actin assembly [29]. Since compound heterozygous *WASL* mutations segregate in family members with early-onset PD [30], we sought to explore the biological consequence of N-WASP deficiency. We found that N-WASP expression can modify the size and number of α-Syn- and synapsin 1-containing liquid condensates. Furthermore, *wsp-1/WASL loss of function (lof)* lowers the tolerance of *Caenorhabditis elegans* to α-Syn overexpression. Together, these data describe the contribution of N-WASP to α-Syn homeostasis and LLPS, which may help to explain in part the early onset of PD in individuals expressing pathogenic N-WASP variants.

RESULTS

Actin and actin-binding proteins are part of the α-Syn interactome

To identify novel modulators of α-Syn LLPS in an unbiased manner, we initially performed co-immunoprecipitation experiments using HEK293 cells transiently overexpressing HA-tagged α-Syn. Upon incubation of cell homogenates with a validated HA antibody, we co-immunoprecipitated proteins that were then analyzed by liquid chromatography/mass spectrometry (LC–MS/MS) (Fig. 1A). We detected 347 proteins that were exclusively found in the HA-tagged α-Syn condition (Supplementary Table ST1). Of the detected proteins, 42 were actin, cytoskeletal proteins, and actin-binding factors (Supplementary Table ST1). Identified actin or actin-binding cytoskeletal proteins included ARPC3, TMOD1, LMOD1, SHROOM3, MYH11, MYH7 and ACTN2. Amongst the non-motor actin-binding proteins, we detected DBNL, CFL2, WASF1, EPB41L3, WASF3, and CORO1A (Fig. 1B and Supplementary Table ST1). GO BP analysis by ClueGO indicated that the 5 most significantly enriched terms included actin-myosin filament sliding (adj p value = 1.89 E-6) with 41.18% associated proteins (MYH2, MYH4, MYH7, MYH8, MYL1, MYL11, TPM1) detectable in our α-Syn co-IP dataset (Supplementary table ST2). In addition, 7.31% of the proteins (AGBL4, AP3M2, BICD2, CCDC186, CLIP3, HDAC6, HOOK2, KIF17, KIF1B, KIF5A, KIFAP3, MAK, MYO15A, MYO1A, PCM1, WASF1) linked to cytoskeleton-dependent intracellular transport (adj p value = 4.80 E-4) were also identified (Supplementary table ST2). Together, these data indicate that α-Syn has a certain binding propensity toward actin and other cytoskeletal factors.

To corroborate our findings using an additional method, we employed high-content protein microchips consisting of more than 9.000 human polypeptides. Following the same approach as described in one of our prior works [31], two separate microarrays were incubated with 5 or 50 ng of monomeric α-Syn. After development with primary and fluorescently labeled secondary antibodies, we identified 158 putative polypeptides that could physically interact with α-Syn in vitro (Fig. 1C and Supplementary Table ST3). Additionally, we carried out another protein microarray screen using fibrillar α-Syn and found 159 interacting polypeptides (Fig. 1D), of which 91 proteins were common hits with the monomeric α-Syn dataset (Fig. 1E and Supplementary Table ST3). Among these putative 91 α-Syn interactors, 5 proteins (GABARAPL2, NPM1, POLB, TWF1, WASL/N-WASP) were associated with the cytoskeleton and/or actin-binding factors, of which N-WASP was of particular interest because of its propensity to undergo a density phase transition and to bind the actin nucleator Arp2/3 complex [27, 29]. Given the causal relationship between pathogenic *WASL* mutations and inherited PD [30], we tested if N-WASP could physically bind α-Syn, since these two proteins highly co-localized in cultured cells (Fig. 1F). We set up a series of co-immunoprecipitations (co-IPs) using homogenates from HEK293T cells overexpressing HA-tagged YFP or HA-tagged α-Syn (Fig. 1G). After a mild exposure with the reversible crosslinker dithiobis (succinimidyl propionate) (DSP), we lysed the cells and carried out co-IPs using a validated primary antibody against HA. Subsequent SDS-PAGE and western blot analyses showed that N-WASP and α-Syn did not co-immunoprecipitate (Fig. 1H, I). This set of data suggests that α-Syn and N-WASP can physically bind in vitro, although their interaction is relatively weak and possibly transient in cultured cells.

N-WASP forms condensates in cells

N-WASP promotes actin remodeling at both pre-and post-synaptic terminals [32]. Using a validated antibody against N-WASP (Supplementary figure S1A-C), we found that N-WASP perfectly co-localized with the SV integral membrane glycoprotein synaptophysin in primary hippocampal neurons (Fig. 2A). Since proteins undergoing LLPS form condensates when fused to oligomerization domains that decrease their saturation concentration (i.e., the minimal concentration at which proteins phase separate), we fused N-WASP to the light-sensitive flavin adenine dinucleotide-binding protein cryptochrome-2 (Cry2) as in previous studies [33, 34]. Optogenetic activation of Cry2-mCherry fused to N-WASP caused rapid cluster formation of the protein in HEK cells (Fig. 2B) in a fashion not normally seen with Cry2-mCherry alone [35]. When we performed live-cell imaging of Cry2-mCherry-N-WASP and Synaptophysin-miRFP in primary hippocampal cell cultures, we further observed that N-WASP co-localized with synaptophysin-positive pre-synaptic compartments (Fig. 2C). To study the dynamic properties of N-WASP in neuronal projections, we fused the photoconvertible fluorophore mEos3.2 to the N-terminus of N-WASP. Upon overexpression in hippocampal neurons, we performed single-particle tracking (Fig. 2D, E) and

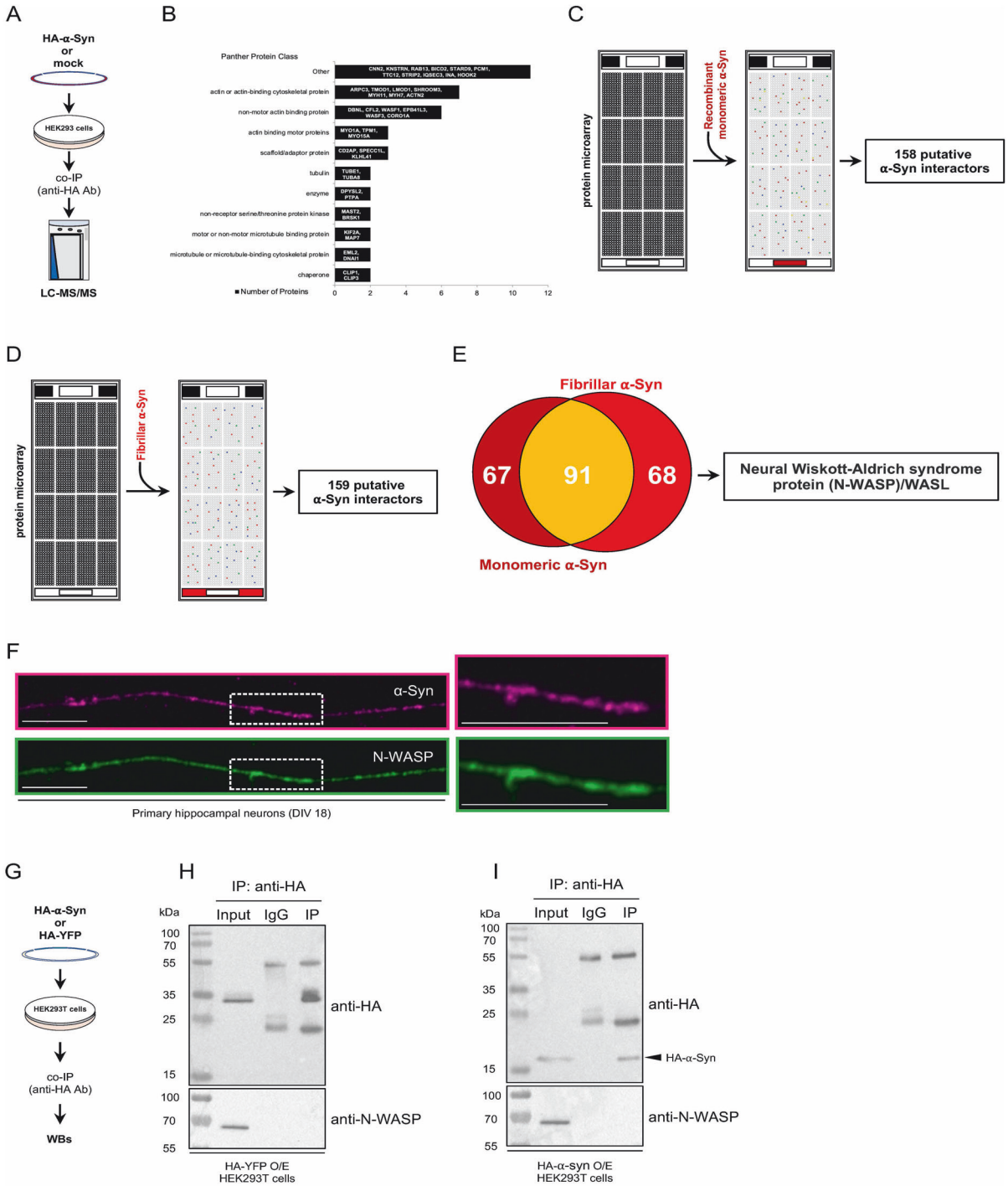

Fig. 1 Proteomic analyses reveal novel α-Syn interactors. A Schematic representation of the co-immunoprecipitation experiment. Co-immunoprecipitated proteins were obtained using an antibody against HA, which was incubated with lysates from control and transiently transfected HEK293/Expi293 cells overexpressing HA-tagged α-Syn. Detection of α-Syn-interacting proteins was performed by LC–MS/MS. **B** Panther protein class of immunoprecipitated cytoskeleton-associated proteins. Schematic representation of the experimental workflow. Protein microchips were incubated with recombinant **C** monomeric or **D** fibrillar α-Syn and, after incubation with a primary antibody against α-Syn, developed using a fluorescent-labeled secondary antibody. Out of ~9000 polypeptides, **C** 158 and **D** 159 putative α-Syn-interacting polypeptides were retrieved. **E** Venn diagram of common and unique interactors of monomeric and/or fibrillar α-Syn. N-WASP was detected in both assays. **F** Representative image of a primary hippocampal neuron stained with antibodies against α-Syn (magenta) and N-WASP (green). Scale bars = 10 µm. **G** Schematic representation of co-IP strategy using HEK293T cells. Co-IPs were performed using homogenates of **H** HA-YFP O/E and **I** HA-α-Syn O/E HEK293T cells, which were incubated with an anti-HA antibody in the presence of Sepharose beads. Immunoblots were developed using anti-N-WASP and anti-HA antibodies.

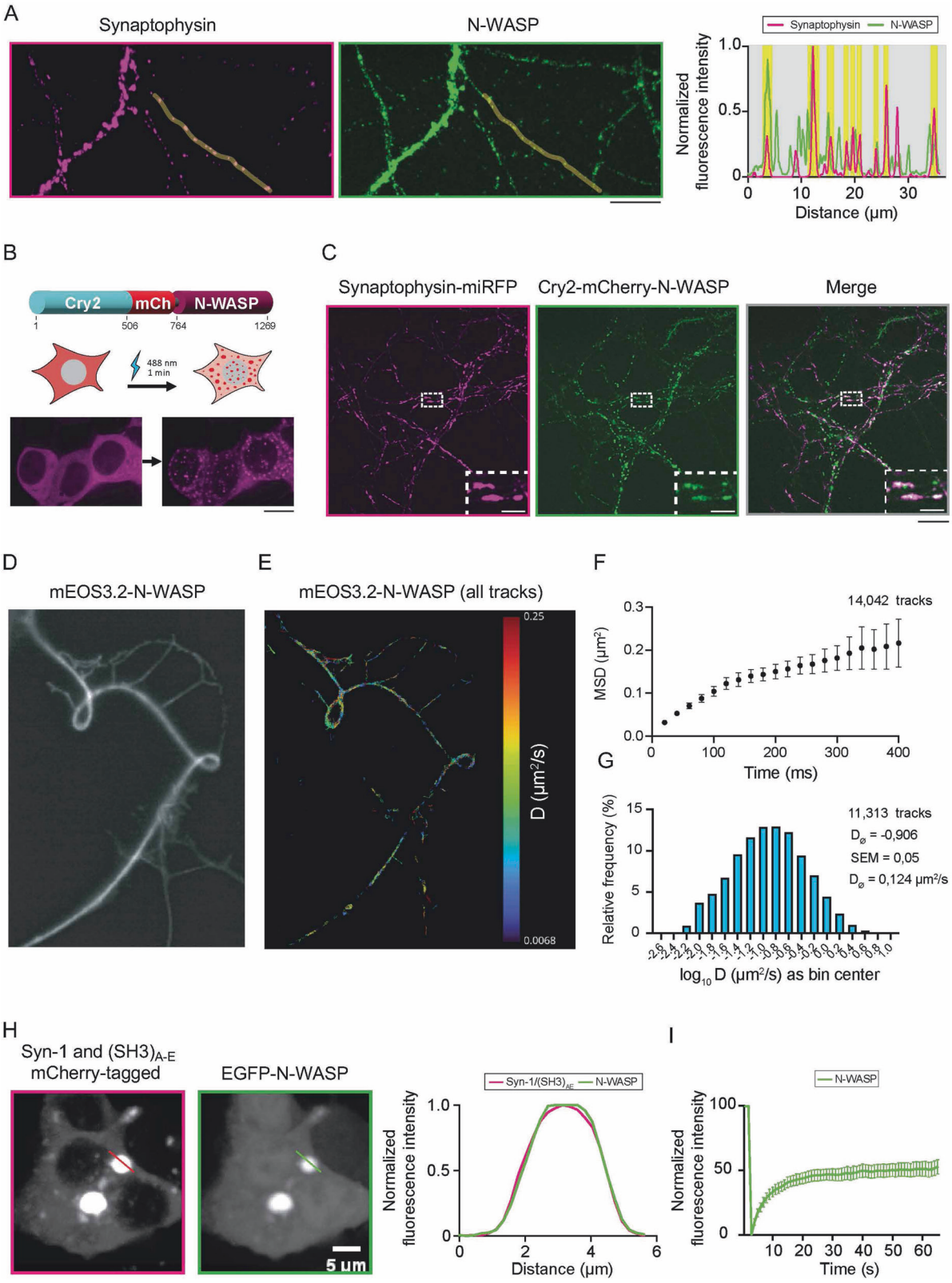

found that, although confined in an area of around 0.2 µm^2 (Fig. 2F), N-WASP retained a high motility ($D = 0.124$ µm^2 s^{-1}; Fig. 2G). These data indicate that N-WASP is a highly dynamic molecule that maintains fluid-like properties even in discrete neuronal sub-compartments.

Next, we assessed how N-WASP behaves in the presence of SV condensates by employing a minimal reconstitution system similar to the one used in our previous papers [36, 37]. For this purpose, we co-expressed mCherry-synapsin 1 (Syn-1) and a concatemer of SH3 domains of intersectin also tagged with

Fig. 2 Single-molecule tracking reveals N-WASP behavior in cultured cells. A Immunostaining and confocal imaging analysis of synaptophysin and N-WASP in mouse-derived hippocampal neurons. Scale bar = 10 µm. Line profiles on the right show respective colocalization analyses of endogenous synaptophysin (magenta) and N-WASP (green) along the line indicated in representative images. **B** Photoactivation (1 min with 488 nm-laser) of Cry2-mCherry-N-WASP leads to the formation of condensates in cells. Top: scheme of the construct. Bottom: representative images of HEK cells before and after activation. Scale bar = 10 µm. **C** Confocal imaging of rat-derived primary hippocampal neurons 14 days in vitro expressing Cry2-mCherry-N-WASP and Synaptophysin-miRFP. Inset: magnified region indicating the accumulation of N-WASP at the pre-synapses. Scale bars = 20 µm (entire image) and 5 µm (inset). **D** Representative fluorescence image of a neuron expressing mEos3.2-N-WASP. **E** Single-molecule tracks reconstructed for the image shown in 2D after photoconversion of mEos3.2 and color-coded for the measured diffusion coefficients. **F** Mean-square displacement (MSD) curve for 14,042 tracks (from four distinct regions) indicates the confined motion of mEos3.2-N-WASP. **G** Distribution of diffusion coefficients for mEOS3.2-tagged N-WASP from 11,313 tracks analyzed (mobile fraction). The average diffusion coefficient was 0.124 $\mu m^2 s^{-1}$. **H** Representative images of HEK293 cells expressing mCherry-Syn-1 with SH3-concatamer of intersectin $(SH3)_{A\text{-}E}$, and EGFP-N-WASP. On the right, colocalization analysis of mCherry-Syn-1/$(SH3)_{A\text{-}E}$ (magenta) and EGFP-N-WASP (green) along the lines indicated in representative images (left). **I** Fluorescence recovery after photobleaching of EGFP-N-WASP (average ± SEM) from three independent transfections indicates swift fluorescence recovery (~50%).

mCherry $(SH3)_{A\text{-}E}$, that readily co-assemble into condensates in mammalian cells [37]. In HEK293 cells, EGFP-N-WASP co-localized with mCherry-Syn-1 within condensates (Fig. 2H). Importantly, N-WASP maintained its high mobility within these condensates, as shown by the rapid fluorescence recovery after laser photobleaching of the GFP-positive droplets (i.e., 50% mobile fraction, $t_{1/2}$~8 s) (Fig. 2I). Upon ectopic expression, Syn-1 and α-Syn also co-assembled into condensates [19]. The endogenous N-WASP was also enriched in these condensates in both murine and human cells (Supplementary Fig. S1D–G). Together, these data demonstrate the dynamic behavior of N-WASP in Syn-1/SV condensates in cultured cells.

N-WASP deficiency influences the formation of α-Syn condensates

In healthy neurons, α-Syn is highly abundant at the synapse [6, 7, 38] and can form liquid-liquid condensates with Syn-1 [19]. To test if N-WASP and α-Syn can be recruited together to synapsin 1-driven condensates, we overexpressed BFP-tagged α-Syn, EGFP-tagged N-WASP, mCherry-tagged Syn-1 and $(SH3)_{A\text{-}E}$ in mammalian cells. We observed that Syn-1/$(SH3)_{A\text{-}E}$ condensates that contained N-WASP lacked α-Syn and, conversely, distinct condensates harboring α-Syn largely lacked N-WASP (Fig. 3A). Next, we assessed whether N-WASP-containing structures were indeed condensates rather than aggregate-like inclusions. To achieve this, cells were treated with the aliphatic alcohol 1,6-hexanediol, which broadly disrupts hydrophobic interactions present in condensates [39]. Live-cell imaging experiments showed little evidence of aggregate formation, since treatment with 1,6-HD could largely abolish condensates (Fig. 3B). Building on our observations that α-Syn and N-WASP did not always co-condense in the same structures, we tested whether N-WASP inhibition could influence the sequestering of α-Syn into Syn-1 condensates. As a first proof-of-principle experiment, we incubated cells with the carbazole derivative wiskostatin which is capable of binding and inhibiting N-WASP [40]. In wiskostatin-treated cells, we observed a marked reduction in the number and size of condensates, along with the depletion of α-Syn from the remaining condensates (Fig. 3C–E). To confirm these observations, we downregulated N-WASP using short interfering RNA (siRNA) and found that diminished N-WASP expression led to a reduction in the fraction and size of Syn-1 condensates that were positive for α-Syn (Fig. 3F–H). Together, these data suggest that N-WASP can influence α-Syn recruitment into Syn-1-containing condensates.

WSP-1/N-WASP expression modulates α-Syn pathology in *C. elegans*

To investigate if N-WASP can influence α-Syn homeostasis in vivo, we employed *C. elegans* strains carrying the transgene *pkIs2386[unc-54p::α-Syn:YFP]* and expressing YFP-tagged α-Syn in the body wall muscle cells. As a well-established model for studying proteotoxicity in vivo in nematodes [41], we initially assessed locomotion at standard experimental conditions (20 °C) and found that *wsp-1(lof)* mutants showed no obvious differences compared to wt animals, whereas α-Syn O/E nematodes exhibited locomotor defects (Fig. 4A). Based on our thrashing assays, the genetic inhibition of WSP-1 protein expression by *wsp-1(lof)* allele [42] did not worsen the phenotype of α-Syn O/E nematodes (Fig. 4A). We also grew animals at a warmer temperature starting from hatching, since it is known that at 25 °C nematodes exhibit faster development, reduced lifespan and changes in proteostasis [43, 44]. Compared to wt animals, *wps-1(lof)*, *α-Syn O/E* and *wps-1(lof);α-Syn O/E* equally compromised *C. elegans* locomotion at 25 °C (Fig. 4B), suggesting that WSP-1 deficiency had a minor effect on thrashing defects due to α-Syn O/E. However, while α-Syn O/E had a marginal lifespan effect at 20 °C, it negatively impacted *C. elegans* survival at 25 °C (Fig. 4C, D and Supplementary table ST4). In each experiment, *wsp-1(lof)* compromised *C. elegans* survival at both temperatures and had an additive negative effect on α-Syn O/E lifespan at higher temperatures (Fig. 4C, D and Supplementary Table ST4). Statistical analysis of median lifespan suggested that *wsp-1(lof)* and α-Syn O/E may act independently on organismal survival (Supplementary Table ST4). Of note, α-Syn O/E had a negligible developmental effect in short-lived *wsp-1(lof)* animals that were grown at warmer temperature (Fig. 4E).

Having assessed a few phenotypes linked to α-Syn O/E and *wsp-1(lof)* in *C. elegans*, we sought to test whether WSP-1 deficiency could shift the balance of α-Syn inclusions from liquid-like condensates to more toxic species, knowing that over time α-Syn inclusions convert into intracellular amyloid-like aggregates in the body wall muscles of *C. elegans* [9]. We performed western blot analysis and showed that *wsp-1(lof)* did not affect the expression of the transgene encoding YFP-tagged α-Syn neither at 20 °C nor at 25 °C (Fig. 4F, G). We quantified the number and size of α-Syn inclusions in nematodes grown at 20 °C and found that *wsp-1(lof)* promoted the formation of larger α-Syn-containing inclusions compared to those in control animals (Fig. 4H). We performed FRAP analysis in young and relatively old (12 days after hatching) animals and found that *wsp-1(lof)* negatively affected α-Syn::YFP mobility in *C. elegans* muscle cells (Fig. 4I, J). At a warmer temperature, adult *wsp-1(lof)* animals showed an increased number of smaller α-Syn::YFP inclusions compared to controls (Fig. 4K). Importantly, genetic inhibition of WSP-1 protein expression reduced α-Syn::YFP mobility compared to control nematodes (Fig. 4L). Together, our data suggest that WSP-1/N-WASP deficiency can diminish the mobile fraction of α-Syn::YFP within inclusions and may possibly promote α-Syn conversion into amyloid-like hydrogels.

In PD pathology, α-Syn readily forms insoluble fibrils that propagate among neurons and surrounding glia [45]. To assess the burden caused by preformed fibrils (PFFs) of α-Syn in N-WASP deficient cells, we employed induced-pluripotent stem cell

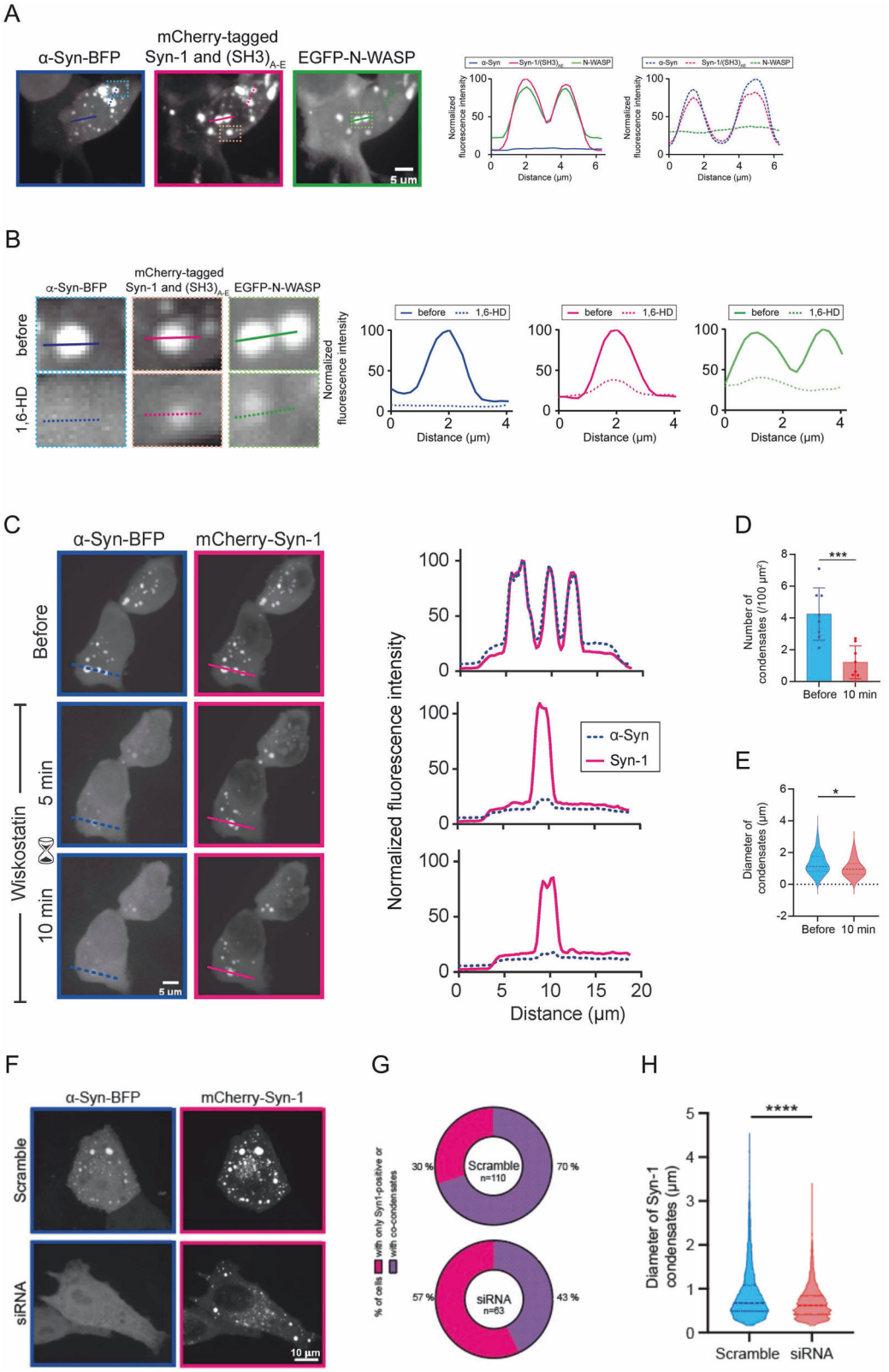

(iPSC)-derived dopaminergic neurons and found that N-WASP downregulation further undermined the maintenance of neurite branches upon exposure to exogenous α-Syn PFFs (Supplementary Fig. 2A, B), suggesting that N-WASP dysfunction may promote α-Syn pathology.

Inhibition of mitochondrial complex I does not phenocopy *wsp-1(lof)* effects on α-Syn pathology

To better understand how WSP-1/N-WASP modulates α-Syn phase transition in *C. elegans*, we decided to perform additional LC-MS/MS experiments on animals grown at 20 °C and 25 °C (Fig. 5A).

Fig. 3 N-WASP influences α-Syn LLPS. A Representative images of HEK293 cells expressing α-Syn-BFP, mCherry-Syn-1 with SH3-concatamer of intersectin $(SH3)_{A-E}$ and EGFP-N-WASP. Panels on the right show respective colocalization analyses of α-Syn-BFP (blue), mCherry-Syn-1 (magenta), and EGFP-N-WASP (green) along the lines indicated in representative images. **B** Treatment with 1,6-hexanediol (1,6-HD) leads to dispersion of fluorescence signal from the condensate. Left: condensates before (top) and after (bottom) the addition of 3% 1,6-HD. Right: line profiles over condensates for α-Syn (blue), synapsin condensates (magenta), and N-WASP (green) before (full line) or after 1,6-HD (dashed line) treatment. **C** Wiskostatin treatment (10 μM final concentration) leads to selective dispersion of α-Syn-BFP (α-Syn-BFP) from synapsin condensates (mCherry-Syn-1). On the left, representative images before, 5 min, and 10 min after treatment. On the right, line profiles of the condensates are shown (magenta, syn-1; blue, α-Syn). Number (**D**) and diameter (**E**) of mCherry-Syn-1 condensates condensates decrease upon wiskostatin treatment in a statistically significant fashion (paired *t*-test, two-tailed, confidence level: 95%). **F** Transfection of siRNA against N-WASP reduces the formation of synapsin condensates. Representative images of HeLa cells expressing α-Syn-BFP and mCherry-Syn-1 condensates further transfected with scrambled (control, top) or N-WASP-directed siRNAs (bottom). Scale bar = 10 μm. **G** Fraction of cells containing α-Syn within condensates of Syn-1 decreases strongly upon N-WASP knockdown. **H** The diameters of mCherry-Syn-1 condensates display a statistically significant decrease upon N-WASP knockdown (Kolmogorov–Smirnov test, two-tailed, confidence level: 95%).

Compared to wt animals grown at 20 °C, we identified 246, 253, and 258 differentially expressed proteins in *wsp-1(lof), α-Syn O/E*, and *wsp-1(lof);α-Syn O/E*, respectively (Fig. 5B and Supplementary table ST5). At 25 °C, we obtained 265, 279, and 253 differentially expressed proteins in *wsp-1(lof), α-Syn O/E*, and *wsp-1(lof);α-Syn O/E*, respectively (Fig. 5C and Supplementary table ST5). All these three mutant strains displayed an upregulation of proteins related to muscle function among the most obvious changes (Fig. 5D and Supplementary table ST6). Moreover, many proteins involved in mitochondrial metabolism were downregulated in *wsp-1(lof)* and *α-Syn O/E* compared to wt at 25 °C. We observed depletion of proteins involved in metabolism, including lipid and amino acid metabolism, that were more prominent in *α-Syn O/E*, and *wsp-1(lof);α-Syn O/E* compared to *wsp-1(lof)* animals grown at 25 °C (Fig. 5E and Supplementary table ST6). Together, our data suggest that aberrant metabolism may accompany the pathology due to α-Syn O/E and WSP-1/N-WASP deficiency.

To validate some of these *in-silico* predictions, we decided to genetically manipulate a few metabolic pathways in nematodes grown at the two different temperatures (Fig. 5F). Since aberrant mitochondrial activity is associated with many synucleinopathies [4, 46], we measured oxygen consumption rate (OCR) using a Seahorse Analyzer (Fig. 5G). At normal growing conditions (20 °C), α-Syn O/E animals had the tendency to respire less than wt, with a basal OCR and spare respiratory capacity similar to those detected in *wsp-1(lof);α-Syn O/E* animals (Fig. 5H–J). Interestingly, animals carrying a *wsp-1(lof)* showed a reduced spare respiratory capacity compared to wt animals (Fig. 5J). Notably, α-Syn O/E further exacerbated the mitochondrial respiratory defects of *wsp-1(lof)* mutant animals when grown at 25 °C (Fig. 5K–M). Together, these data suggest that WSP-1/N-WASP deficiency impairs mitochondrial respiration, with α-Syn O/E having an additive effect only in certain conditions. To determine if inhibition of mitochondrial bioenergetics may phenocopy the effect of *wsp-1(lof)* on α-Syn phase transition, we employed *gas-1(fc21)* mutant nematodes, which also exhibit reduced mitochondrial respiration and shortened lifespan compared to wildtype as shown in our previous studies [47–49]. Surprisingly, FRAP experiments at different ages and temperatures showed that α-Syn::YFP was relatively more mobile in *gas-1* mutants compared to control nematodes (Fig. 5N-Q). At least in *C. elegans*, mitochondrial inhibition does not recapitulate the changes of α-Syn mobility caused by WSP-1 deficiency, possibly indicating that WSP-1 influences α-Syn pathology independently of its effects on mitochondrial bioenergetics.

Next, we assessed neutral lipids and carried out Oil Red O (ORO) staining in our four strains. We found that *wsp-1(lof)* and *wsp-1(lof);α-Syn O/E* animals had a reduced ORO staining at both 20 °C and 25 °C compared to wt, whereas *α-Syn O/E* animals showed lower signal only at 25 °C (Fig. 6A, B). To alter lipid metabolism in *C. elegans*, we used an extrachromosomal array overexpressing FAT-7 (Fig. 6C), a fatty acid desaturase that converts stearic acid into oleic acid and promotes *C. elegans* lifespan extension [50]. Although FAT-7 was expressed only in the intestine, it could increase the overall lipid content in the transgenic nematodes compared to wt ones (Fig. 6D). We carried out FRAP experiments in α-Syn::YFP O/E animals and found that FAT-7 expression in the gut was not sufficient to modify the mobility of α-Syn::YFP condensates in the muscle cells of neither control nor *wsp-1(lof)* mutant nematodes (Fig. 6E–G). This dataset suggests that changes in lipid metabolism may not be the main driver of α-Syn liquid phase transition.

Finally, we tested whether proteins related to muscle function may modulate condensates in animals grown at 20 °C, given that this term was upregulated in *wsp-1(lof);α-Syn O/E* animals at this temperature (Fig. 5D and Supplementary table ST6). Using a validated RNAi feeding protocol starting from hatching as described in our previous studies [47, 48, 51], we downregulated *F15G9.1, F42H10.3, myo-1*, and *tni-4* genes in *α-Syn O/E* and *wsp-1(lof);α-Syn O/E* animals (Fig. 6H). Our RNAi experiments showed negligible changes in FRAP of α-Syn::YFP liquid-like droplets in young as well as older adult animals (Fig. 6I, J). Similarly, there was no rescue of condensate mobility following downregulation of the candidates in *wsp-1(lof);α-Syn O/E* animals, neither in younger animals nor in older animals (Fig. 6I–L). In summary, our data suggest that some of the proteomic changes may contribute to the pathological phenotype of WSP-1/N-WASP deficiency, however they are not the main cause of α-Syn LLPS and its eventual transition into amyloid-like hydrogel (Fig. 6M).

DISCUSSION

Synucleinopathies are common age-related neurodegenerative diseases, with PD accounting for the high incidence in people aged 80 years or older [52, 53]. Despite the advance of knowledge in the scientific community, our understanding of α-Syn interactome changes in certain biological contexts (e.g., aging) as well as upon exposure to environmental cues remains very limited. Similarly, it remains elusive which molecular mechanisms govern the liquid phase transition and aggregation of α-Syn.

Here, we investigate the interactome of α-Syn and report new evidence connecting α-Syn with cytoskeleton components. Our findings are in line with previous studies showing that wild type and mutant α-Syn can interact with actin [54] and actin-binding proteins such as gelsolin or spectrin [54–56]. Consistent with prior evidence, α-Syn interaction with actin and actin-binding proteins includes dysregulation of actin dynamics, altered exo- and endocytosis, and reduced mitochondrial function [54, 56]. In addition to α-Syn-dependent regulation of the actin cytoskeleton, other PD-related proteins, such as Parkin/PARK2 [57, 58] and VPS35/PARK17 [59], have also been shown to influence the remodeling of the actin cytoskeleton. In an attempt to elucidate mechanistically the biological meaning of this network of interactions, we show that N-WASP expression and activity can modify the recruitment of α-Syn into liquid-like condensates in cultured cells. Consistent with a role of N-WASP in modulating

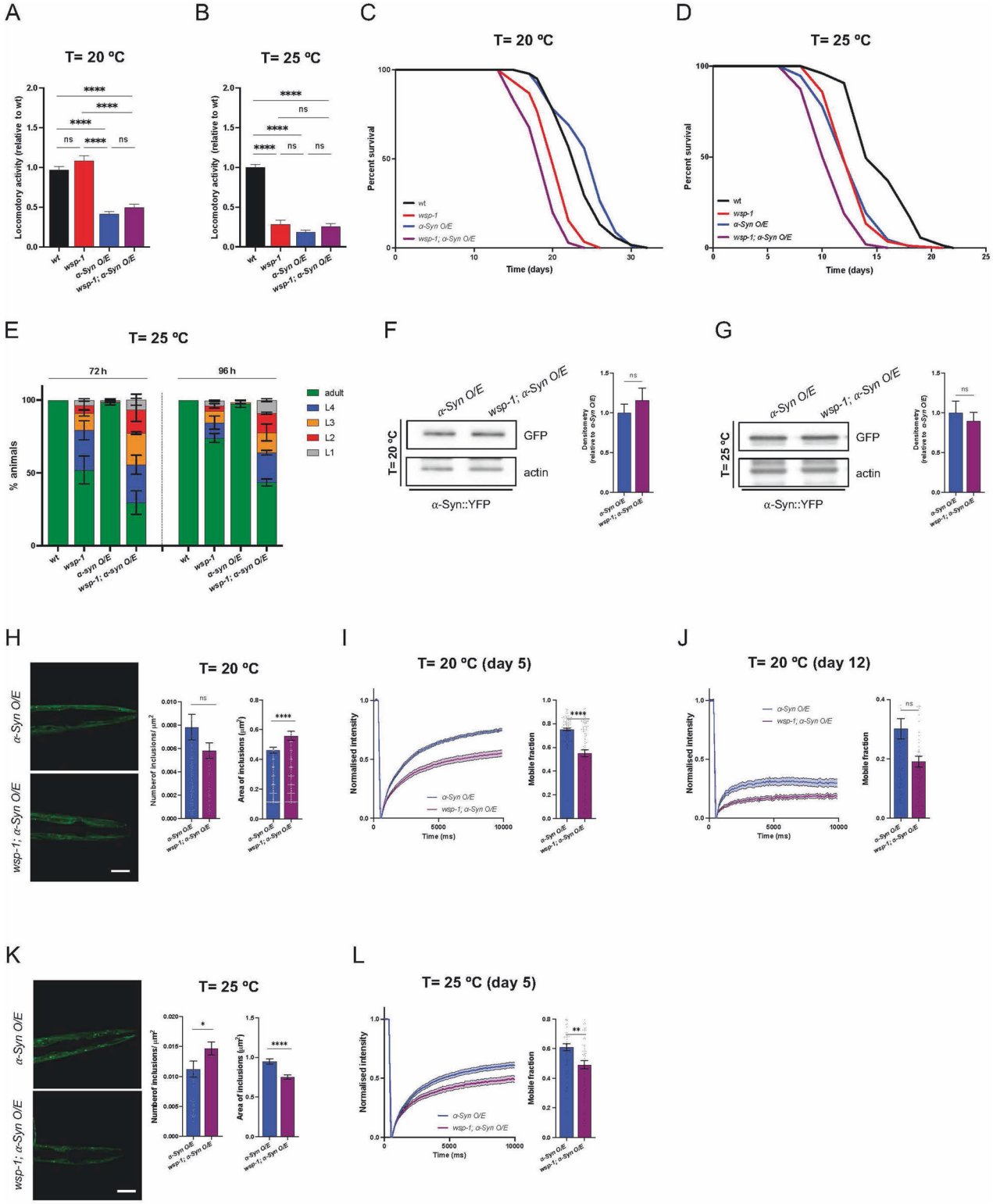

α-Syn recruitment into intracellular inclusions, we provide a first line of evidence demonstrating that WSP-1 deficiency can promote α-Syn pathology in *C. elegans*. Indeed, when we exposed nematodes to different experimental paradigms, we found that α-Syn O/E is relatively well tolerated and does not have a negative impact on development. However, α-Syn seems to become more toxic in WSP-1 deficient cells, possibly because it converts into less mobile condensates that, over time, may transform into pathogenic species. This in vivo evidence suggests that disease-causing *WASL* mutations may define the threshold of susceptibility to α-Syn expression, thereby predisposing an organism to α-Syn proteotoxicity. Consistent with the complex etiology and epidemiology of PD [60], it may be that N-WASP loss of function variants represent one of the genetic predispositions promoting α-Syn pathology under stress and environmental challenges. Although further studies are necessary, our findings indicate a direct

Fig. 4 *wsp-1(lof)* negatively affects the dynamics of α-Syn-containing condensates in *C. elegans*. Locomotor activity of **A** 7-day-old and **B** 4-day-old wt (black), *wsp-1(lof)* (red), *α-Syn O/E* (blue), and *wsp-1(lof);α-Syn O/E* (purple) animals grown at **A** 20 °C or **B** 25 °C. Each bar represents mean±SEM (One-way ANOVA with Tukey's multiple comparison test, ns not significant, ****$p < 0.0001$; number of animals = 24 (**A**) and 16-36 (**B**) from 3 (**A**) and 5 (**B**) experiments). **C**, **D** Representative lifespan assays of wt, *wsp-1(lof)*, *α-Syn O/E*, and *wsp-1(lof);α-Syn O/E* animals grown at the indicated temperatures. **E** Developmental assay at 25 °C. The percentage of the population at the indicated larval stages at 72 h (left panel) and 96 h (right panel) after hatching. Bars represent mean±SEM. Representative western blots (left) and densitometry (right) of α-Syn::YFP protein expression, in 5-day-old *α-Syn O/E* and *wsp-1(lof);α-Syn O/E* animals grown (**F**) at 20 °C and (**G**) 25 °C. Bars represent mean ± SEM (Unpaired *t*-test, ns not significant, $n = 3$). **H** Representative images and quantification of the number and size of α-Syn::YFP inclusions in the heads of 10-day-old *α-Syn O/E* and *wsp-1(lof);α-Syn O/E* animals grown at 20 °C. Scale bar = 40 μm. Bars represent mean±SEM (Mann–Whitney test, ns not significant, ****$p < 0.0001$, $n = 61$–72 animals from 4 independent experiments). FRAP traces (left) and quantification of mobile fraction (right) of individual α-Syn::YFP inclusions in *α-Syn O/E* and *wsp-1(lof);α-Syn O/E* animals grown for **I** 5 and **J** 12 days at 20 °C. Lines represent mean normalized intensity±SEM and bars represent mean ± SEM (Mann–Whitney test, ns not significant, ****$p < 0.0001$; **I** $n = 94$–95 inclusions, $n = 3$ biological replicates; **J** $n = 92$–100 inclusions, $n = 3$ biological replicates). **K** Representative images of 5-day-old nematodes grown at 25 °C (scale bar = 40 μm). Quantification of inclusion number and size is reported as mean±SEM (Mann–Whitney test, *$p < 0.05$, ****$p < 0.0001$, n = 45-50 inclusions, $n = 3$ biological replicates). **L** FRAP traces (left) and quantification of mobile fraction (right) of individual α-Syn::YFP inclusions in 5-day-old *α-Syn O/E* and *wsp-1(lof);α-Syn O/E* animals grown at 25 °C. Lines and bars represent mean±SEM (Mann–Whitney test, **$p < 0.01$, $n = 68$–75 inclusions, $n = 3$ biological replicates).

relationship between α-Syn expression and N-WASP deficiency, which may partially explain the causative genetic link of compound heterozygous *WASL* mutations with an early onset familial form of PD [30].

While the role of the cytoskeleton is emerging as an important player in synucleinopathies, a vast literature has reported genetic mutations linking mitochondria with parkinsonism and/or inherited PD [4, 61–63]. Given these lines of evidence, we investigated the impact of *wsp-1(lof)* on mitochondria in *C. elegans*. We report that genetic inhibition of *wsp-1/WASL* can impair mitochondrial respiration and worsen metabolic defects due to α-Syn overexpression. Although we could not conclusively elucidate the molecular mechanisms underlying these observations, our findings recapitulate some of the mitochondrial defects that are often associated with synucleinopathies. At least in nematodes, it seems that aberrant mitochondrial respiration may be exacerbated by the cumulative effects of WSP-1/N-WASP deficiency and α-Syn overexpression. Despite the influence of *wsp-1(lof)* on mitochondrial respiration, complex I deficiency alone was not sufficient to recapitulate the α-Syn::YFP phase transition changes observed in *wsp-1(lof)* animals. Rather than through metabolic changes as upstream effects, we speculate that WSP-1/N-WASP deficiency may prime the susceptibility of the proteome to additional stress, which may further shift the proteostatic balance of α-Syn, its propensity to undergo LLPS and eventually its toxic aggregation. In addition to the proteome collapse, cells may undergo further metabolic challenges due to aberrant mitochondrial bioenergetics as a consequence of N-WASP deficiency. To support this scenario, it has been shown that aberrant expression of the WAS family member WASp causes mitochondrial network fragmentation and loss of mitochondrial respiration in haemopoietic cells [64]. As in our experimental paradigms, the loss of a WAS family member may critically affect the threshold at which cells can buffer stress, since defective cytoskeleton remodeling may compromise mitochondrial dynamics, trafficking and biogenesis, with obvious consequences on cellular homeostasis and survival.

Taken together, our cross-species study broadens the molecular landscape of the α-Syn interactome and offers a first experimental framework to better understand how actin remodelers may contribute to α-Syn phase transition into toxic species.

EXPERIMENTAL PROCEDURES

Antibodies

The following primary antibodies were used in this study: mouse anti-alpha-synuclein (Bio Legend, 4B12/Synuclein, 807801), mouse anti-alpha-synuclein (Invitrogen, AHB0261), mouse anti-GFP (Roche, 11814460001), mouse anti-HA (Sigma, HA-7, H9658), rabbit anti-HA (Sigma, H6908), rabbit anti-N-WASP (Cell Signaling, 30D10, #4848), rabbit anti-N-WASP (polyclonal raised against peptide 385–401) [65], rabbit anti-N-WASP (Invitrogen, PA5-52198), mouse anti-synaptophysin 1 (SySy, 7.2, 101 0011), mouse anti-actin (Abcam, ab14128). Secondary antibodies used in this study were: HRP-conjugated anti-mouse secondary (Thermo Fisher Scientific), HRP-conjugated anti-rabbit secondary (Promega, W4011), Alexa Fluor™ 488-conjugated goat anti-mouse IgG (Invitrogen, A-11001), Alexa Fluor™ 568-conjugated goat anti-rabbit IgG (Invitrogen, A-11011) and Abberior STAR 488-conjugated goat anti-rabbit IgG (Abberior).

Caenorhabditis elegans strains

The following strains were used in this study: wild type N2 (Bristol), BAN419 *gas-1(fc21)X;pkIs2386[unc-54p::α-syn::YFP+unc-119(+)]*, BAN534 *wsp-1(gm324)IV*, BAN550 *wsp-1(gm324)IV;pkIs2386[unc-54p::α-syn::YFP+unc-119(+)]*, BAN686 *shEx34[myo-3p::mCherry]*, BAN688 *pkIs2386[unc-54p::alpha synuclein::YFP + unc-119(+)];shEx34[myo-3p::mCherry]*, BAN689 *wsp-1(gm324)IV;pkIs2386[unc-54p::alpha synuclein::YFP + unc-119(+)];shEx34[myo-3p::mCherry]*, BAN690 *shEx1[ges-1p::fat-7 + myo-3p::mCherry]*, BAN692 *pkIs2386[unc-54p::alpha synuclein::YFP + unc-119(+)];shEx1[ges-1p::fat-7 + myo-3p::mCherry]*, BAN693 *wsp-1(gm324)IV;pkIs2386[unc-54p::alpha synuclein::YFP + unc-119(+)];shEx1[ges-1p::fat-7 + myo-3p::mCherry]*, NL5901 *pkIs2386[unc-54p::α-syn::YFP+unc-119(+)]*. Nematodes were maintained following standard culture methods as in some of our previous studies [47, 48, 51]. All RNAi experiments were performed at indicated temperatures by feeding nematodes with HT115 *E. coli* expressing dsRNA against target genes. Some strains were provided by the CGC, which is funded by the NIH Office of Research Infrastructure Programs (P40 OD010440).

Cell cultures

HeLa cells and human embryonic kidney HEK293 and HEK293T cells were grown in DMEM (Gibco) supplemented with 10% fetal bovine serum and 1% penicillin/streptomycin (100 U/ml penicillin; 100 mg/ml streptomycin). Cells were transfected with 2 μg of plasmid DNA using either Lipofectamine 2000 (Thermo Fisher Scientific) or Turbofectin (Origene) following the manufacturer's instructions. For experiments in HeLa cells downregulating N-WASP, the siRNA (siRNA ID: 137396; Thermo Fisher Scientific) was transfected with Lipofectamine RNAiMAX (Thermo FisherScientific), 24 h prior to plasmid transfection with Lipofectamine 2000 for the transient protein expression. For co-IP mass spectrometry sample preparation, suspension cultures of Expi293F™ cells (HEK derivative) were used. Cultures were maintained in an Expi expression medium as described in the manufacturer's protocol (8% CO_2, 37 °C, 125 rpm). For protein expression, suspension cultures (30 ml) were transfected with 30 μg of plasmid DNA following the ExpiFectamine transfection guidelines.

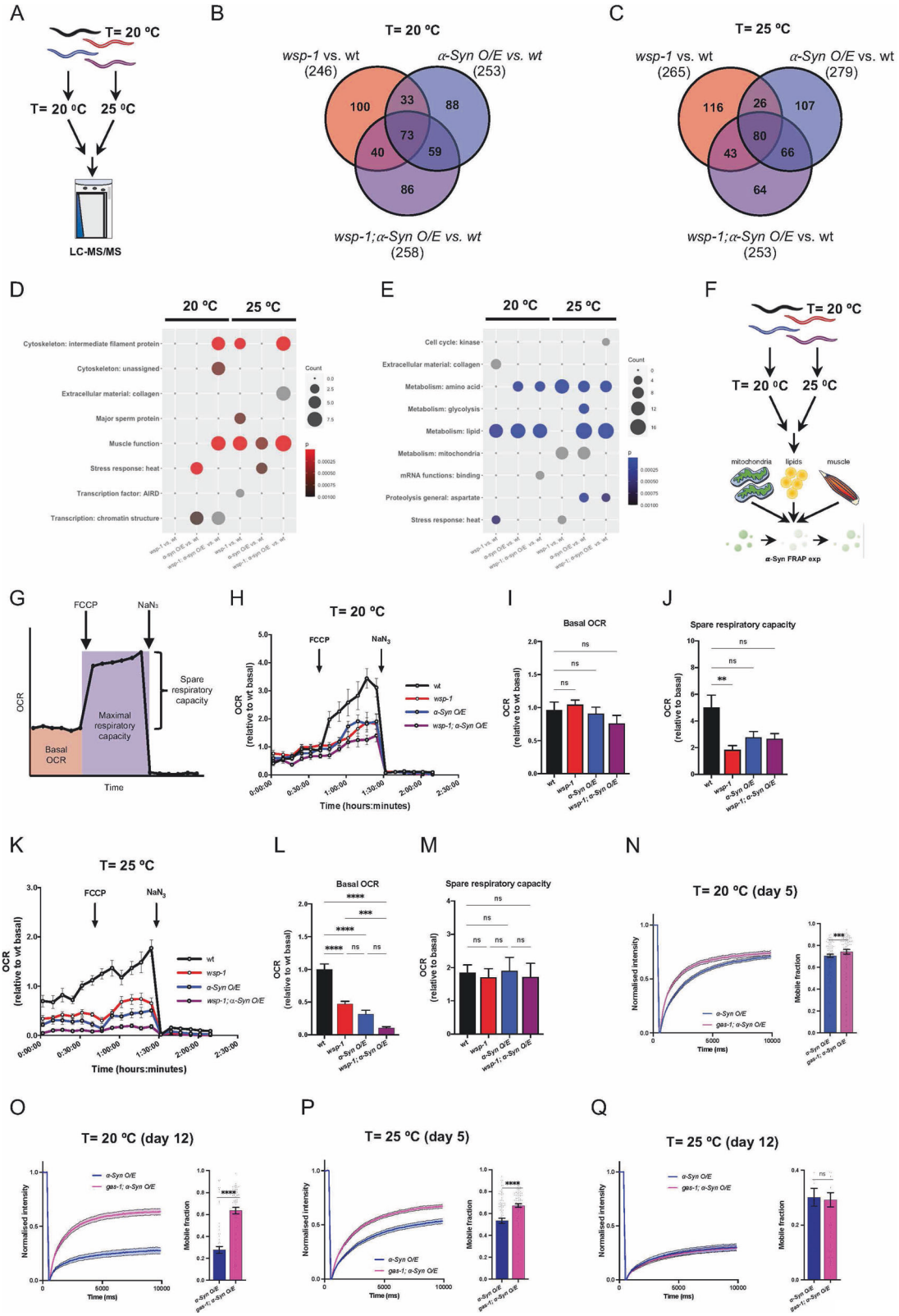

B16-F1 cells were routinely grown in Dulbecco's Modified Eagles Medium (DMEM, Gibco) supplemented with 10% FBS and 2 mM L-glutamine (Gibco) at 37 °C and in 5% CO_2 atmosphere. CRISPR/Cas9-mediated disruption in B16-F1 cells of the *Wasl* encoding N-WASP was achieved essentially following standard procedures [66] and transfection of a vector harboring a CRISPR-gRNA sequence targeting exon 1 (5′-GAGAGACTCGTTCTCTTGCG-3′). Monoclonal cell lines were expanded from single-cell clones followed by screening for the absence of N-WASP expression by Western blotting (not shown). Selected clones devoid of N-WASP

Fig. 5 Mitochondrial complex I deficiency stimulates α-Syn::YFP LLPS. A Schematic representation of the LC-MS/MS experiment. Venn diagrams indicating the number of differentially expressed proteins (relative to wt) in *wsp-1(lof)*, *α-Syn O/E*, and *wsp-1(lof);α-Syn O/E* animals grown at **B** 20 °C and **C** 25 °C. Bubble plots showing the significant WormCat categories that were **D** upregulated or **E** downregulated in the indicated comparisons. Bubble size indicates the number of differentially expressed proteins in the corresponding category, and bubble color corresponds to *p* value. **F** Schematic summary of the experiments performed using wt and mutant nematodes grown at 20 °C or 25 °C. **G** Schematic representation of an OCR trace and how basal respiration and maximal respiratory capacity were calculated. **H** OCR traces of 5-day-old animals grown at 20 °C. Each point reports mean±SEM across replicates ($n = 15–19$ from 4 experiments). Quantification of **I** basal OCR and **J** spare respiratory capacity in 5-day-old animals grown at 20 °C. Bars represent mean ± SEM (Kruskal–Wallis test with Dunn's multiple comparison test, ns not significant, $^{**}p < 0.01$, $n = 15–19$ from 4 independent experiments). **K** Representative OCR traces of 5-day-old animals grown at 25 °C. Each point reports mean±SEM across replicates ($n = 9–12$ from 3 independent experiments). Quantification of **L** basal OCR and **M** spare respiratory capacity of 5-day-old wt animals grown at 25 °C. Bars represent mean±SEM (One-way ANOVA with Tukey's multiple comparison test, ns not significant, $^{***}p < 0.001$, $^{****}p < 0.0001$, $n = 9–12$ from 3 experiments). FRAP of α-Syn::YFP inclusions in the head region of (**N**, **P**) 5-day- and (**O**, **Q**) 12-day-old animals grown at **N**, **O** 20 °C or **P**, **Q** 25 °C. Left, normalized recovery curves of *α- Syn O/E* (blue) and *gas-1;α-Syn O/E* (pink). Right, quantification of the mobile fraction of individual inclusions. Lines and bars represent mean ± SEM (Mann–Whitney test, ns not significant, $^{***}p < 0.001$, $^{****}p < 0.0001$, number of inclusions = 94–95 (**N**), 70–71 (**O**), 95–100 (**P**), 66–68 (**Q**), from 3 biological replicates).

expression (Supplementary figure S1A) were confirmed to lack any *WasI* wildtype allele by genotyping, as follows: sequences resulting from PCR amplification of the *WasI* targeting region potentially harboring the site of disruption were subjected to Sanger sequencing and analysis by TIDE sequence trace decomposition [67]. N-WASP expression was also assessed by western blot using a previously characterized triple KO cell line lacking Sra1, PIR121/CYFIP, and N-WASP [65] (Supplementary Fig. S1A).

Primary hippocampal neurons were prepared from P0 wild-type mice (C57BL6/J) as previously described [19]. Neurons were seeded on coverslips and transfected using a standard calcium phosphate protocol. For single molecule tracking experiments, primary rat hippocampal neurons were used.

Induced-pluripotent stem cell (iPSC)-derived midbrain dopaminergic neurons (mDANs) were generated from smNPCs, as previously described [68, 69]. Briefly, iPSC cultures were dissociated using accutase, centrifuged and resuspended in neural induction medium (DMEM-F12 (Invitrogen) 1:200 N2 supplement (Invitrogen), 1:100 B27 supplement without vitamin A (Invitrogen), 2 mM of GlutaMax, 10 µM of SB-431542, 1 µM of dorsomorphin, 0.5 µM of purmorphamine, and 3 µM CHIR99021), supplemented with 10 µM of ROCK inhibitor (Tocris). Cells were cultured in nonadherent plates for 3 days, and on days 4–5, medium was changed to smNPC maintenance medium (neural induction medium lacking SB-431542 and dorsomorphin, with 150 µM of ascorbic acid added). On day 6, embryoid bodies were triturated by pipetting and plated into Matrigel-coated 12-well plates. Cells were split using accutase and passaged for at least 6 splits to remove non-smNPC cells from the cultures. Subsequent differentiation into mDANs was initiated approximately 2 days after the previous passage. Medium was changed to mDAN induction medium (DMEM-F12 (Invitrogen) 1:200 N2 supplement (Invitrogen), 1:100 B27 supplement without vitamin A (Invitrogen), 100 ng/ml FGF8 (Invitrogen), 1 µM purmorphamine, and 200 µM Ascorbic Acid), and changed every 2–3 days. After 8 days, medium was changed to mDAN maturation medium (DMEM-F12 (Invitrogen) 1:200 N2 supplement (Invitrogen), 1:100 B27 supplement without vitamin A (Invitrogen), 10 ng/ml BDNF (PeproTech), 10 ng/ml GDNF (Peprotech), 1 ng/ml TGF-b3, 200 µM Ascorbic Acid, and 500 µM dbcAMP (Sigma)). On days 8-10, maturation medium was supplemented with 0.5 µM purmorphamine. On day 9, cultured cells were split 1:3 into small clumps using accutase. Cells were maintained in mDAN maturation medium until day 21. Transfection of shRNA (VectorBuilder, ID VB010000-9346qaz and VB900072-7764yby) was performed at day 10 with Lipofectamine 3000 (Invitrogen), and medium was changed the following day. For mDAN treatment, recombinant human α-synuclein (A140C) was purified from bacteria and labeled with Alexa Fluor™ 647 C_2 Maleimide (Thermo Fisher Scientific) as previously described [19]. The preformed fibrils were prepared by mixing 10:1 (unlabeled-to-labeled) α-synuclein, as previously described [70]. Freshly sonicated α-Syn-Alexa Fluor 647 PFFs (100 nM final concentration) were added on day 14. On day 21, mDANs were fixed with warm 4% PFA/4% sucrose.

Co-immunoprecipitation for mass spectrometry analysis

Expi293 cells expressing either HA-tagged α-synuclein or mock controls were harvested 3 days after transfection. Cells were lysed in a buffer that contained 25 mM Tris-HCl pH 7.4, 150 mM NaCl, and 0.5 mM TCEP (buffer A) supplemented with complete EDTA-free Protease Inhibitor Cocktail (Roche) by three consecutive cycles of freezing and thawing. Soluble protein was separated from cellular debris by centrifugation at 20,000 × *g* at 4 °C for 45 min. Approximately 2000 µg of soluble protein supernatant was subjected to 100 µl of pre-equilibrated anti-HA agarose beads (Thermo Fisher Scientific, 26181) in a Poly-Prep® gravity flow chromatography column (Biorad) at 4 °C for 1.5 h with slow rotating agitation. Then, beads were washed with 10 ml of wash buffer (buffer A), and bound proteins were eluted with hot, non-reducing 2x SDS-PAGE loading buffer (125 mM Tris-HCl pH 6.8, 20% glycerol, 4% SDS, and 0.1% bromophenol blue).

Co-immunoprecipitations and western blot analysis

Co-IPs were performed using Immunoprecipitation kit (Abcam; catalog no.: ab206996) following the manufacturer's instructions. Briefly, cells expressing HA-α-Syn or HA-YFP (48 h after transfection) were washed once with PBS and incubated with 2 mM dithiobis (succinimidyl propionate) (Thermo Fisher Scientific, PG82081) for 30 min for reversible crosslinking. The crosslinking reaction was stopped by incubating the cells with 25 mM Tris for 15 min. Cells were then washed with PBS and harvested in 500 µl cold nondenaturing lysis buffer (Abcam, ab206996). Cells were lysed at 4 °C for 30 min on a rotatory mixer. Lysates were cleared by centrifugation at 10,000 × *g* for 10 min, and protein concentration was determined using a Bradford assay. Approximately 500 µg of total protein was incubated with an anti-HA antibody (1:100) overnight at 4 °C on a rotatory mixer. Then, 40 µl of A/G Sepharose bead slurry was added to the protein–antibody mix and incubated for 1 h at 4 °C. Beads were then collected and washed by slow-speed centrifugation. Bound proteins were eluted from the beads by adding 40 µl 2× SDS-PAGE loading buffer (125 mM Tris-HCl pH 6.8, 4% SDS, 20% glycerol, 10% 2-mercaptoethanol, and 0.005% bromophenol blue) and boiling for 5 min.

Samples were resolved on 12% poly-acrylamide gels and transferred onto nitrocellulose membranes using semi-dry transfer Trans-Blot Turbo (Bio-Rad). Protein detection was performed using the following primary antibodies at a dilution of 1:1000, followed by HRP-conjugated secondary antibodies at a 1:2000 dilution. Immunoblots were developed in ECL and imaged using Chemidoc imaging system (Bio-Rad).

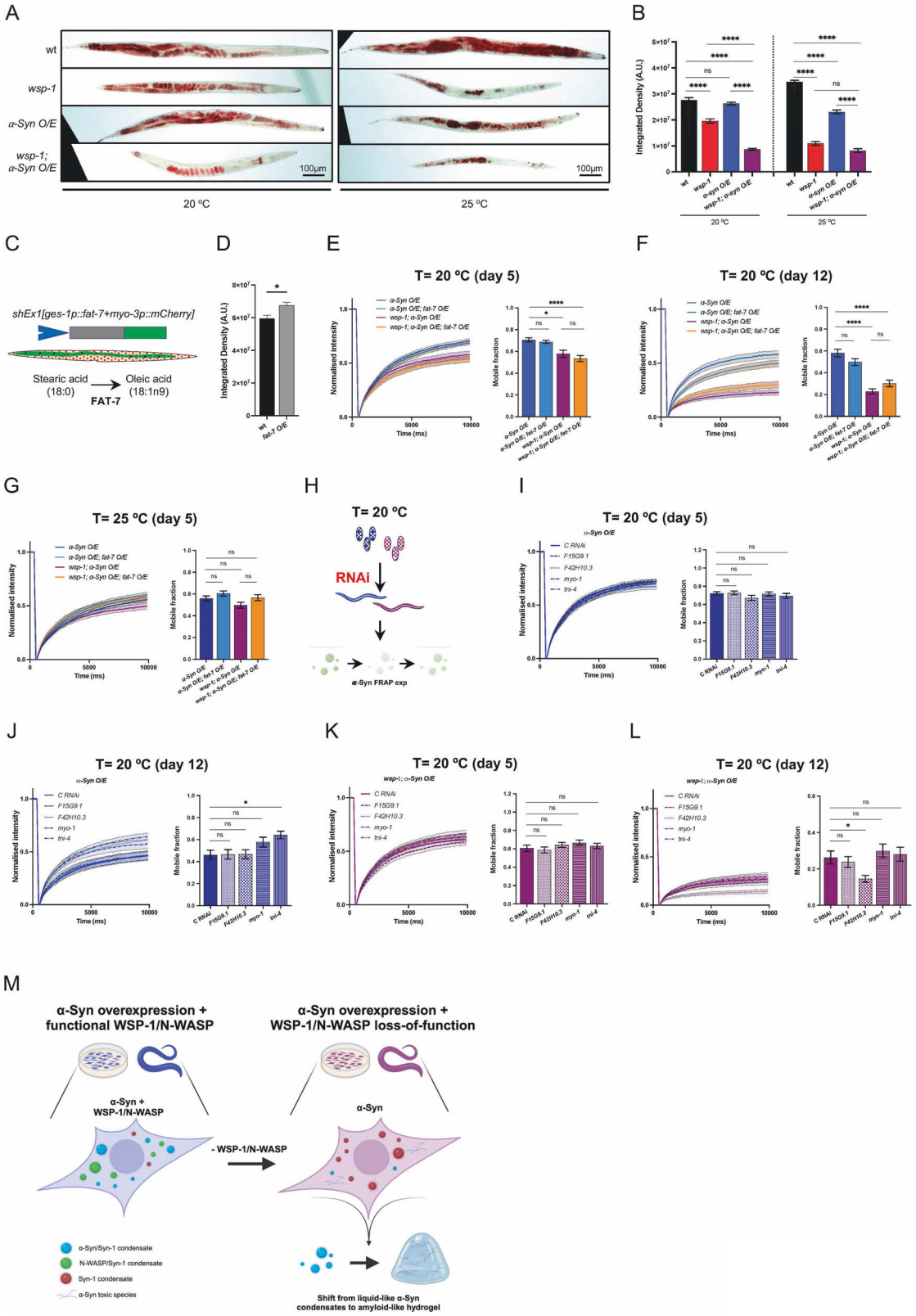

Confocal analysis and FRAP in vivo

Nematodes were transferred into a drop of 20 mM levamisole on a glass slide with a pad of 2% agarose, and a glass coverslip was gently placed on top. Animals were imaged for a maximum of 20 min following mounting on the slide. Z-stack images of alpha-synuclein inclusions were acquired from the head region, using a 20× objective and a Zeiss LSM900 confocal microscope. Inclusion size and number were assessed on maximum Z projections using ImageJ.

For FRAP analysis, animals were imaged using a 20× objective with 4× crop. Individual inclusions in the head to the animal were

Fig. 6 Changes in lipid content and muscle function accompany α-Syn::YFP LLPS. Representative **A** Oil Red O staining (scale bar = 100 µm) and **B** its quantification in wt, *wsp-1(lof)*, *α -Syn O/E*, and *wsp-1(lof);α-Syn O/E* animals grown at 20 °C or 25 °C. Each bar represents mean±SEM (Kruskal–Wallis test with Dunn's multiple comparison test, ns not significant, ****$p < 0.0001$, n = 50–60 animals from 3 independent experiments). **C** Schematic representation of the *shEx1[ges-1p::fat-7+myo-3p::mCherry]* transgene expressing FAT-7 in *C. elegans* intestine. FAT-7 desaturates stearic acid into oleic acid. **D** Quantification of ORO staining in wt and *fat-7 O/E* animals grown at 20 °C. Each bar represents mean ± SEM (Student's t-test, *$p < 0.05$, $n = 36$ animals from 3 independent experiments). (Fluorescent recovery after photobleaching of α-Syn::YFP inclusions in the head region of **E**, **G** 5-day- and **F** 12-day-old animals grown at **E**, **F** 20 °C and **G** 25 °C. Left: normalized recovery curves of *α-Syn O/E* (blue), *α-Syn O/E;fat-7 O/E* (light blue), *wsp-1(lof);α-Syn O/E* (purple), and *wsp-1(lof);α-Syn O/E; fat-7 O/E* (orange). Right: quantification of the mobile fraction of individual inclusions. Lines and bars represent the mean±SEM (Kruskal–Wallis with Dunn's multiple comparison test, ns not significant, *$p < 0.05$, ****$p < 0.0001$, number of inclusions = 54–63 (**E**), 62–78 (**F**), 58–61 (**G**), $n = 3$ biological replicates). **H** Schematic summary of FRAP experiments performed using *α-Syn O/E* and *wsp-1(lof);α-Syn O/E* nematodes grown on RNAi at 20 °C. Fluorescent recovery after photobleaching of α-Syn::YFP inclusions in the head region of animals grown at 20 °C. On the left, normalized recovery curves are reported for **I**, **J** *α-Syn O/E* or **K**, **L** *wsp-1(lof);α-Syn O/E* animals grown on RNAi against control, *F15G9.1, F42H10.3, myo-1, tni-4*. On the right of each panel, quantification of the mobile fraction of individual inclusions are reported. Lines and bars represent the mean ±SEM (Kruskal-Wallis with Dunn's multiple comparison test, ns none-significant, *$p < 0.05$, number of inclusions = 45–48 (**I**), 36-47 (**J**), 4748 (**K**), 47-48 (**L**), $n = 3$ biological replicates). **M** Schematic summary of our findings. The expression of Syn-1 promotes the formation of intracellular condensates that can recruit either α-Syn or N-WASP. Loss of WSP-1/N-WASP negatively affects the recruitment of α-Syn to Syn-1-containing condensates, possibly shifting the propensity of α-Syn to form amyloid-like hydrogel. Created with BioRender.com.

selected. Following image acquisition of 5 frames (<120 ms per frame), inclusions were photobleached, and subsequent fluorescent recovery was assessed for a further 95 frames. Intensity measurements of bleached region, whole cell, and background regions were performed using ImageJ. FRAP recovery curves were normalized using EasyFRAP web [71]. The mobile fraction was calculated using the final intensity of normalized recovery curve.

Confocal live-cell imaging

Live-cell imaging was performed on a Nikon spinning disk confocal CSU-X microscope (Nikon Europe B.V., Düsseldorf, NRW, Germany) equipped with a temperature stage at 37 °C and a 5% CO_2 saturation. A planar Apo objective 60x oil, NA 1.49 was used. Excitation wavelengths were: 405 nm for BFP; 488 nm for EGFP; 561 nm for mCherry. Image Analysis was done using ImageJ (Version: 1.8.0_172/1.53c).

For N-WASP condensation experiments, HEK293 cells were transfected with 2 µg of pCry2-mCh-N-WASP plasmid using Lipofectamine 2000. After 20 h, cells were imaged by confocal live-cell imaging (561 nm for mCherry) before and after photoactivation for 1 min (488 nm for Cry2, laser intensity at 2.4 mW output).

Gene ontology biological process pathway enrichment analysis by ClueGO and WormCat

Alpha-synuclein interaction partners were subjected to pathway enrichment analysis by ClueGO (v2.5.9), a plug-in application in Cytoscape [72] (v.3.9.1) (https://cytoscape.org,). The following parameters were used for ClueGO analysis, analysis mode: ClueGO (Functional Analysis); Loaded Marker List (*Homo sapiens* - 9606); ClueGO settings: Ontologies/Pathways (GO GO_BiologicalProcess-EBI-UniProt-GOA-ACAP-ARAP_25.05.2022), Evidence: All; Network specificity: medium; use of GO term Fusion; *p* value threshold ≤ 0.05 for pathway significance; GO Tree interval: 3 (minimum) and 8 (maximum) levels, GO term/pathway selection: 3 genes (minimum), 4% genes, and kappa score of 0.4, for GO term, pathway connectivity.

WormbaseIDs from upregulated and downregulated proteins obtained from proteomic analysis of nematode samples were entered into the online tool WormCat 2.0 [73]. Significant Category 2 pathways were plotted using *R* (v. 4.3.1).

Lifespan analysis

Synchronized *C. elegans* populations were obtained by incubating gravid adult nematodes with hypochlorite solution, with the resulting eggs that were then transferred onto bacteria-seeded NGM plates. At L4/young adult stage, at least 180 animals (30 animals per plate) were transferred to fresh plates. Animals were transferred every 2 days until egg laying ceased, in order to eliminate offspring. Scoring for dead animals was performed every second day. Death was counted as a lack of touch-evoked movement, and censored animals were counted due to abnormal death (e.g., due to internal hatching). Survival curves were plotted and statistical analysis was performed using GraphPad Prism (GraphPad Software Inc., San Diego, USA).

Human protein-protein interaction profiling

Protein-Protein Interaction Profiling Service was performed on ProtoArray™ Human Protein Microarrays v5.1 (ThermoFisher Scientific, USA) as previously described [31]. Briefly, microarrays were incubated with blocking buffer (50 mM Hepes, 200 mM NaCl, 0.08% Triton X 100, 25% glycerol, 20 mM glutathione, 1.0 mM DTT, and 1× synthetic block) at 4 °C for 1 h under gentle shaking. Following blocking, arrays were incubated with either monomeric or fibrillar human α-Syn, at two concentrations (5 and 50 ng/µl) diluted in probe buffer (1× PBS, 0.1% Tween-20, and 1× synthetic block) for 90 min at 4 °C. As a positive control, a microarray was incubated with 50 ng/ml of array control protein (*i.e.*, yeast calmodulin kinase 1 with a biotin and V5 tags at the N terminus) diluted in probe buffer, and for a negative control one microarray was incubated with probe buffer alone. Following 5 washes with probe buffer at room temperature, microarrays were incubated with anti-α-Syn antibody in probe buffer for 90 min at 4 °C, followed by secondary antibody for 90 min at 4 °C. Following a final wash with probe buffer, arrays were washed with distilled water, dried by centrifugation at 1000 rpm for 1 min, and scanned using an Axon 4000B fluorescent microarray scanner (Molecular Devices). Candidate interactors were considered when the following conditions were satisfied: (a) the fluorescent intensity value was at least 20-fold higher than the corresponding negative control; (b) the normalized fluorescent signal was greater than three standard deviations; (c) the signal-to-noise ratio was higher than 0.5; and (d) the replicate spot coefficient of variation was lower than 50%.

Immunohistochemistry in cells

Cells on glass coverslips were washed once in PBS before fixing with 4% PFA in PBS for 15 min. Following three washes with PBS, cells were permeabilized and blocked with PBS containing 3% (w/v) BSA, 10 mM glycine, and 0.1% saponin (PBS/B) for 30 min. After blocking, coverslips were washed twice with PBS containing 0.1% saponin (PBS/S). Primary antibody incubation (in PBS/B) was performed for 2 h (dilution 1:500), followed by two PBS/S washes and subsequent incubation with fluorescently labeled secondary antibodies (dilution 1:500) in PBS/B for 45 min. After incubation, coverslips were washed three times with PBS/S and mounted on glass microscope slides using Fluoroshield with DAPI (Sigma, F6057) for imaging. For sample mounting samples, Fluoroshield

without DAPI was used (Sigma, F6182). For immunohistochemistry of primary neurons, coverslips were washed once gently with PBS before fixing neurons with 4% PFA in PBS containing 4% (w/v) sucrose, 1 mM $MgCl_2$, and 0.1 mM $CaCl_2$ for 20 min at room temperature. Following three washes with PBS, cells were permeabilized with PBS containing 0.1% (v/v) Triton-X 100 (PBT) for 5 min. After blocking for 30 min in Blocker™ Casein (Thermo Fisher, 37528) supplemented with 0.1% Triton-X 100 (βCasT), coverslips were washed once in PBT. Primary antibody incubation (dilution: 1:500 in βCasT) was performed for 2 h, followed by two PBT washes and subsequent incubation with fluorescently labeled secondary antibodies (dilution: 1:400 in βCasT) for 45 min. After incubation, the coverslips were washed three times with PBT and mounted on glass microscope slides using Fluoroshield with DAPI (Sigma, F6057) for imaging.

Oil Red O (ORO) neutral lipid staining

Nematodes were washed off NGM plates, washed 3 times with H_2O, flash-frozen in liquid nitrogen, and stored at −80 °C until required. On the day prior to staining, ORO stock solution (0.5% w/v in isopropanol) was diluted to 60% in distilled H_2O and left at room temperature overnight. On the day of staining, ORO solution was filtered twice to remove insoluble precipitate. Pellets were thawed on ice and fixed with 4% PFA at 4 °C on a rotary mixer for 20 min. Fixed worms were washed in PBS, and subsequently dehydrated in 60% isopropanol. To each sample, 1 ml of ORO working solution was added and incubated overnight at room temperature on a rotary mixer. Stained animals were washed 3 times in PBS, and resuspended in 50 µl glycerol, before mounting on a glass slide. Images were acquired using Zeiss Epi-Scope1-Apotome. Staining intensity was measured using ImageJ.

Oxygen consumption rate (OCR) measurements

OCR was measured using a Seahorse XFe24 Analyzer (Agilent), using a modified protocol as previously described [47, 51]. Briefly, synchronized animals were grown for 5 days at either 20 °C or 25 °C and transferred to freeze-killed OP50 plates for 2 h to empty their gut of live bacteria. Hydrated XFe24 sensor cartridges were calibrated, and the assay was run, at either 20 °C or 25 °C, depending on the initial growth conditions of the animals. Each well of a Seahorse XFe24 Cell Culture Microplate was filled with 500 µl M9 buffer, and 30 animals transferred into each well, with a minimum of 3 wells per condition. OCR measurements were taken at basal conditions, and in response to addition of 20 µM FCCP, followed by 20 mM sodium azide (NaN_3).

PALM imaging of neurons and Single Particle Tracking (SPT)

The PALM microscope was a Nikon Ti Eclipse (Nikon France S.A.S., Champigny-sur-Marne, France) equipped with a Perfect Focus System (PFS), a motorized stage TI-S-ER, and an 18zimuthal Ilas^2 TIRF arm (Gataca Systems, Massy, France) coupled to a laser bench containing 405 nm (100 mW), 491 nm (150 mW), 532 nm (1 W), 561 nm (200 mW) and 642 nm (1 W) diodes. Images were recorded using objective Apo TIRF 100x oil NA 1.49 and a FusionBT sCMOS camera (Hamamatsu Photonics, Massy, France). Photo-conversion experiments were done using the Ilas^2 scanner system and a 405 nm laser diode while Illumination of the converted mEos3.2 fluorescent protein was exited using the 561 nm laser diode. To record protein trajectories streams of 4000 frames with an exposure time of 50 ms were acquired. The 37 °C atmosphere was created with an incubator box and an air heating system (Life Imaging Services, Basel, Switzerland). This system was controlled by MetaMorph software (Molecular Devices, Sunnyvale, USA).

SPT PALM experiments were analyzed using PALMTracer software, a MetaMorph (Molecular Devices, Sunnyvale, USA) add-on developed at the Interdisciplinary Institute of Neuroscience by Corey Butler (IINS -UMR5297 -CNRS/University of Bordeaux), Adel Mohamed Kechkar (Ecole Nationale Supérieure de Biotechnologie, Constantine, Algeria) and Jean-Baptiste Sibarita (IINS -UMR5297 -CNRS/University of Bordeaux). Briefly, single-molecule localization was achieved using wavelet segmentation, and then filtered out based on the quality of a 2D Gaussian fit. SPT analysis was then done based on the detections using reconnection algorithms and for MSD and D calculations on reconnected trajectories [74, 75].

Plasmids and DNA cloning

The following plasmids were used: α-synuclein-BFP [19], mCherry-Synapsin 1 and mCherry-(SH3) $_{A\text{-}E}$ [12], GFP-N-WASP (Addgene plasmid # 47406; kindly provided by Peter McPherson). mEOS3.2-N-WASP was generated by PCR of N-WASP from GFP-N-WASP (primer fwd: ATCACTCGAGTGAGCTCGGGCCAGCAG, primer rv: ATCAACTGCAGAATTCGAAGCTTTCAG) and subcloning into a pmEOS3.2-C1 backbone using *Xho*I and *Pst*I. pCry2-mCh-N-WASP was generated by restriction enzyme-based cloning (*Kpn*I/*Xho*I) of the N-WASP coding sequence into a pCry2-mCherry backbone plasmid [34].

Sample preparation, LC–MS/MS measurements, database searching, and SAINT analysis

Co-IP elution fractions were run using SDS-PAGE. In Gel digestion-Molecular weight bands were dissected from 18% SDS PAGE gels of anti-HA CoIP elution fractions derived from Expi293 cells either expressing empty HA-tagged vector or HA-tagged human SNCA wt. Excised gel bands were destained with 1:1 destain solutions A and B (Silverquest kit, #LC6070, Sigma Aldrich), reduced with 10 mM DTT and 2 mM TCEP in 100 mM ammonium bicarbonate and alkylated using 50 mM IAA in 100 mM ammonium bicarbonate for 30 min at room temperature and in the dark. In gel digestion was performed overnight at 30 °C with sufficient Trypsin (20 ng/µl; in 50 mM ammonium bicarbonate) to completely cover the gel pieces. Peptides were extracted from the gel slices by adding an equal volume of extraction buffer (1:2 (vol/vol) of 5% formic acid/ acetronitrile) and incubation at 37 °C with shaking for 15 min. Filter-aided sample preparation- young adult wt(N2), BAN534 *wsp-1(gm324)IV*, BAN550 *wsp-1(gm324)IV;pkIs2386[unc-54p::α-Syn::YFP+unc-119(+)] and* NL5901 *pkIs2386[unc-54p::α-Syn::YFP+unc-119(+)]* animals grown at 20 °C or 25 °C, were collected in water, spun down and stored at -80 °C until further processing. Samples were lysed in 200 µl Lysis buffer (50 mM HEPES (pH 7.4), 150 mM NaCl, 1 mM EDTA, 1.5% SDS, 1 mM DTT; supplemented with 1× protease and phosphatase inhibitor cocktail (ThermoScientific)). Lysis was aided by repeated cycles of sonication in a water bath (6 cycles of 1 min sonication (35 kHz) intermitted by 2 min incubation on ice). Approximately 20 µg of *C. elegans* protein lysates were reduced and alkylated prior to processing by a modified filter-aided sample preparation (FASP) protocol as previously described [76]. Samples were digested overnight with Trypsin (1:20; in 50 mM ammonium bicarbonate) directly on the filters, at 30 °C and precipitated using an equal volume of 2 M KCl for depletion of residual detergents. Tryptic peptides were then cleaned, desalted on C18 stage tips and re-suspended in 20 µl 1% FA for LC-MS analysis. Extracted peptides were dried in a vacuum centrifuge and re-suspended in 30 µl of 5% formic acid for LC-MS analysis. MS runs were performed with at least 3 biological replicates.

Tryptic peptides were analyzed on a Dionex Ultimate 3000 RSLC nanosystem coupled to an Orbitrap Exploris 480 MS. Peptides were injected at starting conditions of 95% eluent A (0.1% FA in water) and 5% eluent B (0.1% FA in 80% ACN), with a flow rate of 300 nL/min. They were loaded onto a trap column cartridge (Acclaim PepMap C18, 100 Å, 5 mm × 300 µm i.d., #160454, Thermo Scientific) and separated by reversed-phase chromatography on an Acclaim PepMap C18, 100 Å, 75 µm × 25 cm (both columns from Thermo Scientific) using a 75 min linear increasing gradient from 5% to 31% of eluent B followed by a 20 min linear

increase to 50% eluent B. The mass spectrometer was operated in data dependent and positive ion mode with MS1 spectra recorded at a resolution of 120 K, mass scan range of 375–1550, automatic gain control (AGC) target value of 300% (3×10^6) ions, maxIT of 25 ms, charge state of 2–7, dynamic exclusion of 60 s with exclusion after 1 time and a mass tolerance of 10 ppm. Precursor ions for MS/MS were selected using a top-speed method with a cycle time of 2 s. A decision tree was used to acquire MS2 spectra with a minimum precursor signal intensity threshold of 3×10^5 for scan priority one and an intensity range of 1×10^4 to 3×10^5 for scan priority two. Data-dependent MS2 scan settings were as follows: isolation window of 2 *m/z*, normalized collision energy (NCE) of 30% (High-energy Collision Dissociation (HCD), 7.5 K and 15 K resolution, AGC target value of 100% (1×10^5), maxIT set to 20 and 50 ms, for scan priority one and two, respectively. Full MS data were acquired in the profile mode with fragment spectra recorded in the centroid mode.

Raw data files were processed with Proteome Discoverer™ software (v2.5.0.400, Thermo Scientific) using SEQUEST® HT search engine against the Swiss-Prot® *Homo sapiens* (v2021-06-20) or *Caenorhabditis elegans* (v2022-12-14) databases. Peptides were identified by specifying trypsin as the protease, with up to 2 missed cleavage sites allowed and restricting peptide length between 7 and 30 amino acids. Precursor mass tolerance was set to 10 ppm, and fragment mass tolerance to 0.02 Da MS2. Static modifications were set as carbamidomethylated cysteine, while dynamic modifications included methionine and N-terminal loss of methionine, for all searches. Peptide and protein FDR were set to 1% by the peptide and protein validator nodes in the Consensus workflow. Default settings of individual nodes were used if not otherwise specified. In the Spectrum Selector node, the Lowest Charge State = 2 and Highest Charge State = 6 were used. The INFERYS rescoring node was set to automatic mode, and the resulting peptide hits were filtered for maximum 1% FDR using the Percolator algorithm in the Processing workflow. A second-stage search was activated to identify semi-tryptic peptides. Both unique and razor peptides were selected for protein quantification. Proteins identified by site, reverse or potential contaminants were filtered out prior to analysis.

SAINT analysis of SNCA IP was performed as previously described [77]. Briefly PSMs of at least 3 biological replicates of HA only (control) and human SNCA associated protein complexes were uploaded into CRAPome with the following settings: Organism- H. sapiens, Experiment Type- Single step Epitope tag AP MS and Quantitation type- SPC. Probabilistic SAINT Score (SP), SAINT analysis was performed with user controls, averaging of biological replicates and 10 virtual controls. Prey proteins with a Probabilistic SAINT Score (SP) ≥ 0.5 were considered SNCA IP.

Raw MS data are publicly available under the following accession numbers- ProteomeXchange (PXD050719) and jPOST* (JPST002992) [78].

Sholl analysis

Fixed mDANs on coverslips were washed with PBS, stained with Hoechst, and mounted on glass slides using a fluorescent mounting medium (Dako). Individual cells expressing EGFP (successfully transfected with shRNA) were imaged using LSM900 with a 20x objective. For PFF-treated cells, the presence of Alexa Fluor 647 within the cell was confirmed prior to imaging. Sholl analysis was performed using the ImageJ Neuroanatomy plugin, on maximum Z projections, with a step size of 2um. Graphs were plotted using GraphPad Prism (GraphPad Software Inc., San Diego, USA). A linear mixed effect model was applied for statistical analysis by applying a published code adaption for R [79] and (https://zenodo.org/records/1158612).

Thrashing assay

Individual animals were transferred into a drop of M9 buffer on a glass slide. Each full-body bends (left to right to left again) were counted for a total of 90 s for each animal. Body bends for 8 animals per strain per experiment were assessed.

DATA AVAILABILITY

Raw MS data are publicly available under the following accession numbers- ProteomeXchange (PXD050719) and jPOST* (JPST002992).

REFERENCES

1. Goedert M, Jakes R, Spillantini MG. The synucleinopathies: twenty years on. J Parkinsons Dis. 2017;7:S51–S69.
2. Spillantini MG, Schmidt ML, Lee VM, Trojanowski JQ, Jakes R, Goedert M. Alpha-synuclein in Lewy bodies. Nature. 1997;388:839–40.
3. Del Tredici K, Braak H. Review: Sporadic Parkinson's disease: development and distribution of alpha-synuclein pathology. Neuropathol Appl Neurobiol. 2016;42:33–50.
4. Monzio Compagnoni G, Di Fonzo A, Corti S, Comi GP, Bresolin N, Masliah E. The role of mitochondria in neurodegenerative diseases: the lesson from Alzheimer's disease and Parkinson's disease. Mol Neurobiol. 2020;57:2959–80.
5. Tan EK, Chao YX, West A, Chan LL, Poewe W, Jankovic J. Parkinson disease and the immune system - associations, mechanisms and therapeutics. Nat Rev Neurol. 2020;16:303–18.
6. Burre J, Sharma M, Sudhof TC. Cell biology and pathophysiology of alpha-synuclein. Cold Spring Harb Perspect Med. 2018;8:a024091.
7. Wilhelm BG, Mandad S, Truckenbrodt S, Krohnert K, Schafer C, Rammner B, et al. Composition of isolated synaptic boutons reveals the amounts of vesicle trafficking proteins. Science. 2014;344:1023–8.
8. Ray S, Singh N, Kumar R, Patel K, Pandey S, Datta D, et al. alpha-Synuclein aggregation nucleates through liquid-liquid phase separation. Nat Chem. 2020;12:705–16.
9. Hardenberg MC, Sinnige T, Casford S, Dada ST, Poudel C, Robinson EA, et al. Observation of an alpha-synuclein liquid droplet state and its maturation into Lewy body-like assemblies. J Mol Cell Biol. 2021;13:282–94.
10. Piroska L, Fenyi A, Thomas S, Plamont MA, Redeker V, Melki R, et al. alpha-Synuclein liquid condensates fuel fibrillar alpha-synuclein growth. Sci Adv. 2023;9:eadg5663.
11. Banani SF, Lee HO, Hyman AA, Rosen MK. Biomolecular condensates: organizers of cellular biochemistry. Nat Rev Mol Cell Biol. 2017;18:285–98.
12. Milovanovic D, Wu Y, Bian X, De Camilli P. A liquid phase of synapsin and lipid vesicles. Science. 2018;361:604–7.
13. Pechstein A, Tomilin N, Fredrich K, Vorontsova O, Sopova E, Evergren E, et al. Vesicle clustering in a living synapse depends on a synapsin region that mediates phase separation. Cell Rep. 2020;30:2594–602 e3.
14. Sansevrino R, Hoffmann C, Milovanovic D. Condensate biology of synaptic vesicle clusters. Trends Neurosci. 2023;46:293–306.
15. Atias M, Tevet Y, Sun J, Stavsky A, Tal S, Kahn J, et al. Synapsins regulate alpha-synuclein functions. Proc Natl Acad Sci USA. 2019;116:11116–8.
16. Woods WS, Boettcher JM, Zhou DH, Kloepper KD, Hartman KL, Ladror DT, et al. Conformation-specific binding of alpha-synuclein to novel protein partners detected by phage display and NMR spectroscopy. J Biol Chem. 2007;282:34555–67.
17. Perego E, Reshetniak S, Lorenz C, Hoffmann C, Milovanovic D, Rizzoli SO, et al. A minimalist model to measure interactions between proteins and synaptic vesicles. Sci Rep. 2020;10:21086.
18. Nemani VM, Lu W, Berge V, Nakamura K, Onoa B, Lee MK, et al. Increased expression of alpha-synuclein reduces neurotransmitter release by inhibiting synaptic vesicle reclustering after endocytosis. Neuron. 2010;65:66–79.
19. Hoffmann C, Sansevrino R, Morabito G, Logan C, Vabulas RM, Ulusoy A, et al. Synapsin condensates recruit alpha-synuclein. J Mol Biol. 2021;433:166961.
20. Fouke KE, Wegman ME, Weber SA, Brady EB, Roman-Vendrell C, Morgan JR. Synuclein regulates synaptic vesicle clustering and docking at a vertebrate synapse. Front Cell Dev Biol. 2021;9:774650.
21. Giasson BI, Duda JE, Murray IV, Chen Q, Souza JM, Hurtig HI, et al. Oxidative damage linked to neurodegeneration by selective alpha-synuclein nitration in synucleinopathy lesions. Science. 2000;290:985–9.
22. Manning-Bog AB, McCormack AL, Li J, Uversky VN, Fink AL, Di Monte DA. The herbicide paraquat causes up-regulation and aggregation of alpha-synuclein in mice: paraquat and alpha-synuclein. J Biol Chem. 2002;277:1641–4.
23. Wong YC, Krainc D. alpha-synuclein toxicity in neurodegeneration: mechanism and therapeutic strategies. Nat Med. 2017;23:1–13.
24. Luk KC, Kehm V, Carroll J, Zhang B, O'Brien P, Trojanowski JQ, et al. Pathological alpha-synuclein transmission initiates Parkinson-like neurodegeneration in non-transgenic mice. Science. 2012;338:949–53.

25. Winner B, Jappelli R, Maji SK, Desplats PA, Boyer L, Aigner S, et al. In vivo demonstration that alpha-synuclein oligomers are toxic. Proc Natl Acad Sci USA. 2011;108:4194–9.
26. Alekhina O, Burstein E, Billadeau DD. Cellular functions of WASP family proteins at a glance. J Cell Sci. 2017;130:2235–41.
27. Li P, Banjade S, Cheng HC, Kim S, Chen B, Guo L, et al. Phase transitions in the assembly of multivalent signalling proteins. Nature. 2012;483:336–40.
28. Su X, Ditlev JA, Hui E, Xing W, Banjade S, Okrut J, et al. Phase separation of signaling molecules promotes T cell receptor signal transduction. Science. 2016;352:595–9.
29. Case LB, Zhang X, Ditlev JA, Rosen MK. Stoichiometry controls activity of phase-separated clusters of actin signaling proteins. Science. 2019;363:1093–7.
30. Kumar S, Abbas MM, Govindappa ST, Muthane UB, Behari M, Pandey S, et al. Compound heterozygous variants in Wiskott-Aldrich syndrome like (WASL) gene segregating in a family with early onset Parkinson's disease. Parkinsonism Relat Disord. 2021;84:61–7.
31. Wischhof L, Adhikari A, Mondal M, Marsal-Cots A, Biernat J, Mandelkow EM, et al. Unbiased proteomic profiling reveals the IP3R modulator AHCYL1/IRBIT as a novel interactor of microtubule-associated protein tau. J Biol Chem. 2022;298:101774.
32. Wegner AM, Nebhan CA, Hu L, Majumdar D, Meier KM, Weaver AM, et al. N-wasp and the arp2/3 complex are critical regulators of actin in the development of dendritic spines and synapses. J Biol Chem. 2008;283:15912–20.
33. Shin Y, Berry J, Pannucci N, Haataja MP, Toettcher JE, Brangwynne CP. Spatiotemporal control of intracellular phase transitions using light-activated optoDroplets. Cell. 2017;168:159–71 e14.
34. Trnka F, Hoffmann C, Wang H, Sansevrino R, Rankovic B, Rost BR, et al. Aberrant phase separation of FUS leads to lysosome sequestering and acidification. Front Cell Dev Biol. 2021;9:716919.
35. Lee S, Park H, Kyung T, Kim NY, Kim S, Kim J, et al. Reversible protein inactivation by optogenetic trapping in cells. Nat Methods. 2014;11:633–6.
36. Park D, Wu Y, Lee SE, Kim G, Jeong S, Milovanovic D, et al. Cooperative function of synaptophysin and synapsin in the generation of synaptic vesicle-like clusters in non-neuronal cells. Nat Commun. 2021;12:263.
37. Hoffmann C, Rentsch J, Tsunoyama TA, Chhabra A, Aguilar Perez G, Chowdhury R, et al. Synapsin condensation controls synaptic vesicle sequestering and dynamics. Nat Commun. 2023;14:6730.
38. Murphy DD, Rueter SM, Trojanowski JQ, Lee VM. Synucleins are developmentally expressed, and alpha-synuclein regulates the size of the presynaptic vesicular pool in primary hippocampal neurons. J Neurosci. 2000;20:3214–20.
39. Schmidt HB, Gorlich D. Nup98 FG domains from diverse species spontaneously phase-separate into particles with nuclear pore-like permselectivity. Elife. 2015;4:e04251.
40. Peterson JR, Bickford LC, Morgan D, Kim AS, Ouerfelli O, Kirschner MW, et al. Chemical inhibition of N-WASP by stabilization of a native autoinhibited conformation. Nat Struct Mol Biol. 2004;11:747–55.
41. van Ham TJ, Thijssen KL, Breitling R, Hofstra RM, Plasterk RH, Nollen EA. *C. elegans* model identifies genetic modifiers of alpha-synuclein inclusion formation during aging. PLoS Genet. 2008;4:e1000027.
42. Withee J, Galligan B, Hawkins N, Garriga G. *Caenorhabditis elegans* WASP and Ena/VASP proteins play compensatory roles in morphogenesis and neuronal cell migration. Genetics. 2004;167:1165–76.
43. Klass MR. Aging in the nematode Caenorhabditis elegans: major biological and environmental factors influencing life span. Mech Ageing Dev. 1977;6:413–29.
44. Ben-Zvi A, Miller EA, Morimoto RI. Collapse of proteostasis represents an early molecular event in *Caenorhabditis elegans* aging. Proc Natl Acad Sci USA. 2009;106:14914–9.
45. Peng C, Trojanowski JQ, Lee VM. Protein transmission in neurodegenerative disease. Nat Rev Neurol. 2020;16:199–212.
46. Nguyen M, Wong YC, Ysselstein D, Severino A, Krainc D. Synaptic, mitochondrial, and lysosomal dysfunction in Parkinson's disease. Trends Neurosci. 2019;42:140–9.
47. Piazzesi A, Wang Y, Jackson J, Wischhof L, Zeisler-Diehl V, Scifo E, et al. CEST-2.2 overexpression alters lipid metabolism and extends longevity of mitochondrial mutants. EMBO Rep. 2022;23:e52606.
48. Gioran A, Piazzesi A, Bertan F, Schroer J, Wischhof L, Nicotera P, et al. Multi-omics identify xanthine as a pro-survival metabolite for nematodes with mitochondrial dysfunction. EMBO J. 2019;38:e99558.
49. Troulinaki K, Buttner S, Marsal Cots A, Maida S, Meyer K, Bertan F, et al. WAH-1/AIF regulates mitochondrial oxidative phosphorylation in the nematode Caenorhabditis elegans. Cell Death Discov. 2018;4:2.
50. Han S, Schroeder EA, Silva-Garcia CG, Hebestreit K, Mair WB, Brunet A. Monounsaturated fatty acids link H3K4me3 modifiers to C. elegans lifespan. Nature. 2017;544:185–90.
51. Jackson J, Wischhof L, Scifo E, Pellizzer A, Wang Y, Piazzesi A, et al. SGPL1 stimulates VPS39 recruitment to the mitochondria in MICU1 deficient cells. Mol Metab. 2022;61:101503.
52. Bloem BR, Okun MS, Klein C. Parkinson's disease. Lancet. 2021;397:2284–303.
53. Ou Z, Pan J, Tang S, Duan D, Yu D, Nong H, et al. Global trends in the incidence, prevalence, and years lived with disability of Parkinson's disease in 204 countries/territories from 1990 to 2019. Front Public Health. 2021;9:776847.
54. Sousa VL, Bellani S, Giannandrea M, Yousuf M, Valtorta F, Meldolesi J, et al. alpha-synuclein and its A30P mutant affect actin cytoskeletal structure and dynamics. Mol Biol Cell. 2009;20:3725–39.
55. Welander H, Bontha SV, Nasstrom T, Karlsson M, Nikolajeff F, Danzer K, et al. Gelsolin co-occurs with Lewy bodies in vivo and accelerates alpha-synuclein aggregation in vitro. Biochem Biophys Res Commun. 2011;412:32–8.
56. Ordonez DG, Lee MK, Feany MB. alpha-synuclein induces mitochondrial dysfunction through spectrin and the actin cytoskeleton. Neuron. 2018;97:108–24 e6.
57. Kim KH, Son JH. PINK1 gene knockdown leads to increased binding of parkin with actin filament. Neurosci Lett. 2010;468:272–6.
58. Huynh DP, Scoles DR, Ho TH, Del Bigio MR, Pulst SM. Parkin is associated with actin filaments in neuronal and nonneural cells. Ann Neurol. 2000;48:737–44.
59. Korolchuk VI, Schutz MM, Gomez-Llorente C, Rocha J, Lansu NR, Collins SM, et al. Drosophila Vps35 function is necessary for normal endocytic trafficking and actin cytoskeleton organisation. J Cell Sci. 2007;120:4367–76.
60. de Lau LM, Breteler MM. Epidemiology of Parkinson's disease. Lancet Neurol. 2006;5:525–35.
61. Bose A, Beal MF. Mitochondrial dysfunction in Parkinson's disease. J Neurochem. 2016;139:216–31.
62. Chen C, Turnbull DM, Reeve AK. Mitochondrial dysfunction in Parkinson's disease-cause or consequence? Biology. 2019;8:38.
63. Schon EA, Przedborski S. Mitochondria: the next (neurode)generation. Neuron. 2011;70:1033–53.
64. Rivers E, Rai R, Lotscher J, Hollinshead M, Markelj G, Thaventhiran J, et al. Wiskott Aldrich syndrome protein regulates non-selective autophagy and mitochondrial homeostasis in human myeloid cells. Elife. 2020;9:e55547.
65. Kage F, Doring H, Mietkowska M, Schaks M, Gruner F, Stahnke S, et al. Lamellipodia-like actin networks in cells lacking WAVE regulatory complex. J Cell Sci. 2022;135:jcs260364.
66. Schaks M, Singh SP, Kage F, Thomason P, Klunemann T, Steffen A, et al. Distinct interaction sites of Rac GTPase with WAVE regulatory complex have non-redundant functions in vivo. Curr Biol. 2018;28:3674–84 e6.
67. Brinkman EK, Chen T, Amendola M, van Steensel B. Easy quantitative assessment of genome editing by sequence trace decomposition. Nucleic Acids Res. 2014;42:e168.
68. Wischhof L, Lee HM, Tutas J, Overkott C, Tedt E, Stork M, et al. BCL7A-containing SWI/SNF/BAF complexes modulate mitochondrial bioenergetics during neural progenitor differentiation. EMBO J. 2022;41:e110595.
69. Reinhardt P, Glatza M, Hemmer K, Tsytsyura Y, Thiel CS, Hoing S, et al. Derivation and expansion using only small molecules of human neural progenitors for neurodegenerative disease modeling. PLoS ONE. 2013;8:e59252.
70. Volpicelli-Daley LA, Luk KC, Lee VM. Addition of exogenous alpha-synuclein preformed fibrils to primary neuronal cultures to seed recruitment of endogenous alpha-synuclein to Lewy body and Lewy neurite-like aggregates. Nat Protoc. 2014;9:2135–46.
71. Koulouras G, Panagopoulos A, Rapsomaniki MA, Giakoumakis NN, Taraviras S, Lygerou Z. EasyFRAP-web: a web-based tool for the analysis of fluorescence recovery after photobleaching data. Nucleic Acids Res. 2018;46:W467–W72.
72. Shannon P, Markiel A, Ozier O, Baliga NS, Wang JT, Ramage D, et al. Cytoscape: a software environment for integrated models of biomolecular interaction networks. Genome Res. 2003;13:2498–504.
73. Holdorf AD, Higgins DP, Hart AC, Boag PR, Pazour GJ, Walhout AJM, et al. WormCat: an online tool for annotation and visualization of *Caenorhabditis elegans* genome-scale data. Genetics. 2020;214:279–94.
74. Racine V, Sachse M, Salamero J, Fraisier V, Trubuil A, Sibarita JB. Visualization and quantification of vesicle trafficking on a three-dimensional cytoskeleton network in living cells. J Microsc. 2007;225:214–28.
75. Kechkar A, Nair D, Heilemann M, Choquet D, Sibarita JB. Real-time analysis and visualization for single-molecule based super-resolution microscopy. PLoS ONE. 2013;8:e62918.
76. Scifo E, Szwajda A, Soliymani R, Pezzini F, Bianchi M, Dapkunas A, et al. Proteomic analysis of the palmitoyl protein thioesterase 1 interactome in SH-SY5Y human neuroblastoma cells. J Proteom. 2015;123:42–53.
77. Mellacheruvu D, Wright Z, Couzens AL, Lambert JP, St-Denis NA, Li T, et al. The CRAPome: a contaminant repository for affinity purification-mass spectrometry data. Nat Methods. 2013;10:730–6.

78. Okuda S, Watanabe Y, Moriya Y, Kawano S, Yamamoto T, Matsumoto M, et al. jPOSTrepo: an international standard data repository for proteomes. Nucleic Acids Res. 2017;45:D1107–D11.
79. Wilson MD, Sethi S, Lein PJ, Keil KP. Valid statistical approaches for analyzing sholl data: mixed effects versus simple linear models. J Neurosci Methods. 2017;279:33–43.

ACKNOWLEDGEMENTS

We wish to thank our DZNE colleagues at LMF; Prof. Ina Vorberg (DZNE) and Prof. Donato Di Monte (DZNE) for their useful suggestions; Prof. Ulf Dettmer (Harvard) for discussion; Ms. Christiane Bartling-Kirsch(DZNE) for her technical assistance; Mr. Aleksandr Korobeinikov and Mr. Gerard Aguilar Pérez (DZNE) for the fibrillar alpha-synuclein used for iPSC experiments. We are immensely thankful to Prof. Erwan Bezard (CNRS, University of Bordeaux, France) for kindly providing monomeric and fibrillar alpha-synuclein used for the protoarrays. This research was supported by the DZNE institutional budget. PN and DB are members of the DFG Cluster of Excellence ImmunoSensation funded by the Deutsche Forschungsgemeinschaft (DFG, German Research Foundation) under Germany's Excellence Strategy – EXC2151 – 390873048. JJ, JHMP, and DB were members of the Mitochondrial Dysfunction in Parkinson's Consortium (PD-MitoQUANT). PD-MitoQUANT has received funding from the Innovative Medicines Initiative 2 Joint Undertaking under grant agreement No. 821522. This Joint Undertaking receives support from the European Union's Horizon 2020 research and innovation program and EFPIA and Parkinson's UK. DM is supported by start-up funds from DZNE, grants from the German Research Foundation (MI 2104), French-BioImaging and Euro-Bioimaging (FBI-1743/2154), and the Human Frontiers Science Organization (RGEC32/2023). HS received support from the Fulbright U.S. Student Program, funded by the U.S. Department of State and German-American Fulbright Commission. CH is supported by a fellowship of the Innovative Minds Program of the German Dementia Association; HW is supported by the Oversea Study Program of Guangzhou Elite Project (SJ2020/2/JY202025). HD was supported by the German Research Foundation (Research Training Group GRK2223 to KR).

AUTHOR CONTRIBUTIONS

Joshua Jackson: Conceptualization, investigation, validation, formal analysis, writing-original draft, visualization. Christian Hoffmann: conceptualization, investigation, validation, formal analysis, writing-original draft, visualization. Enzo Scifo: Investigation, writing-original draft. Han Wang: Formal analysis, visualization. Lena Wischhof: Investigation. Antonia Piazzesi: investigation. Mrityunjoy Mondal: Investigation. Hanna Shields: Investigation. Xuesi Zhou: Formal analysis (single molecule tracking). Magali Mondin: Formal analysis (single molecule tracking). Eanna B. Ryan: Formal analysis. Hermann Döring: Reagents. Jochen H.M. Prehn: Funding acquisition. Klemens Rottner: Reagents, Funding acquisition. Gregory Giannone: Formal analysis (single molecule tracking). Pierluigi Nicotera: Funding acquisition. Dan Ehninger: Supervision. Dragomir Milovanovic: Conceptualization, Formal analysis, Writing-Original Draft, Visualization, Supervision, Project administration, Funding acquisition. Daniele Bano: Conceptualization, Formal analysis, Writing-Original Draft, Visualization, Supervision, Project administration, Funding acquisition.

FUNDING

Open Access funding enabled and organized by Projekt DEAL.

COMPETING INTERESTS

The authors declare no competing interests.

ADDITIONAL INFORMATION

Supplementary information The online version contains supplementary material available at https://doi.org/10.1038/s41419-024-06686-7.

Correspondence and requests for materials should be addressed to Dan Ehninger, Dragomir Milovanovic or Daniele Bano.

Reprints and permission information is available at http://www.nature.com/reprints

Publisher's note Springer Nature remains neutral with regard to jurisdictional claims in published maps and institutional affiliations.

Conclusions and outlook

In this thesis, my goal was to address the following questions:

1. **What molecular mechanisms counteract aberrant mitochondrial bioenergetics?**

2. **What mechanisms contribute to mitochondrial dysfunction and proteotoxicity in synucleinopathies such as Parkinson's disease?**

In Chapter I of my experimental work, we aimed to address the first goal of the thesis. We demonstrated that *micu-1* loss induces a mitochondrial bioenergetic defect in *C. elegans,* which activates molecular mechanisms that upregulate the proteins SPL-1 and VPS-39. Some of these molecular signatures are evolutionarily conserved in human cells. We found that SPL-1/SGPL1 and VPS-39/VPS39 act in parallel to support an increase in lysosomal and mitochondrial biogenesis, along with enhanced autophagy. We hypothesised that the role of these proteins is to stimulate the production and transfer of membrane lipids, via the enzymatic activity of SPL-1/SGPL1 and the role of VPS-39/VPS39 in mitochondria-lysosome contacts, respectively (Spiegel & Milstien, 2003; Gonzalez Montoro *et al.*, 2018; Iadarola *et al*, 2020). We found that these conserved mechanisms were present in different long-lived *C. elegans* mitochondrial mutants, in MICU1 KO cultured cells and in a mouse model of myopathy.

In our study, we provided evidence that genetic inhibition of MCU does not cause detectable mitochondrial defects in *C. elegans* at basal conditions. Importantly, MCU loss does not rescue most of the phenotypes associated with MICU1 deficiency. This observation may be important for the treatment of MICU1-related disease, and highlights that the MCU complex may not be an appropriate therapeutic target.

The outcome of MICU1 KO seems to be independent of its function in the MCU complex. We reasoned that MICU1 loss negatively affects mitochondrial bioenergetics by its role in cristae remodelling. In support of this line of thinking, recent studies have shown that MICU1 inhibition can lead to the widening of cristae junctions and decreased membrane potential in mammalian cells (Gottschalk *et al.*,

2019; Gottschalk *et al.*, 2022; Tomar *et al.*, 2023). Consistently, mutations in subunits of the cristae-regulating MICOS complex also lead to energy defects and mitochondrial disease in humans (Eramo *et al*, 2020; Khosravi & Harner, 2020). Further investigation into the role of MICU1 in cristae organisation should be carried out, to improve our understanding of diseases caused by *MICU1* mutations.

Future work should also aim to further investigate the role of VPS39 and SGPL1 in human mitochondrial syndromes and neurodegenerative diseases. A particularly interesting aspect of this study is the involvement of mitochondria-lysosome contact sites in compensating for mitochondrial dysfunction. The exact function of these VPS39-dependent mitochondria-lysosome contact sites are currently poorly understood and mainly addressed in yeast. In our models, we show that these contact sites contribute to mitochondrial network expansion in response to OXPHOS inhibition. Therefore, the identification of specific molecular species that are transferred at these contact sites will add to our understanding of the mechanisms that regulate mitochondrial biogenesis.

Finally, the activation of these pathways in patients should be assessed, to investigate whether the magnitude of activation correlates with disease severity. For example, it could be that patients with more severe pathology fail to upregulate VPS39 and SGPL1 expression or fail to increase the number of mitochondria-lysosome contact sites. If this is the case, modulation of these pathways may act as a beneficial target to enhance mitochondrial function for the treatment of mitochondrial disease.

Mitochondrial defects are often observed in a variety of neurodegenerative diseases. Thus, in the second chapter of this thesis, we aimed to understand the mechanisms that contribute to mitochondrial dysfunction and proteotoxicity in the neurodegenerative disease Parkinson's disease. We identified the actin nucleation promoting factor WSP-1/N-WASP as a modulator of α-Syn biomolecular condensates. Loss of activity in WSP-1/N-WASP leads to depletion of α-Syn from condensates of its physiological interaction partner Synapsin 1 and reduces the mobility of α-Syn in condensates in *C. elegans* (Hoffmann *et al.*, 2021). We hypothesise that N-WASP is involved in the recruitment of α-Syn into Synapsin 1 condensates at the synapse, and that loss of activity leads to depletion of α-Syn from

the synapse, allowing for aberrant LLPS in other cellular compartments which may contribute to pathological inclusion formation.

As an initial observation in our study, we found that a α-Syn interacts with a relatively large group of cytoskeleton-associated proteins, particularly actin-associated proteins. Other studies have previously shown that α-Syn interacts with some actin-binding proteins, such as spectrin and gelsolin, however the physiological function of these interactions are largely unknown (Welander *et al*, 2011; Ordonez *et al*, 2018). There is growing evidence to support that the cytoskeleton can influence the behaviour of biomolecular condensates, and *vice versa* (Mohapatra & Wegmann, 2023). Furthermore, the actin cytoskeleton has been shown to be important in the synapse as a molecular scaffold for synaptic vesicle clusters, the regulation of the vesicle cycle, and the regulation of endocytosis (Gentile *et al*, 2022). It could be possible that actin-regulating proteins in general are involved in LLPS at the synapse. This could be further explored in future studies, not only to help understand the physiological processes occurring in the synapse, but also to help us understand diseases that affect synapse function.

Compound heterozygous mutations in N-WASP have been identified in patients with early-onset PD. One of the identified mutations leads to skipping of exon 10, and subsequent loss of part of the N-WASP VCA domain. The VCA domain is responsible for the interaction of N-WASP with actin and the Arp2/3 complex, which will impact the induction of actin polymerisation. The second mutation is a P380L missense mutation, which is found in the proline-rich region of the protein (Kumar *et al.*, 2021). Evidence suggests that the proline rich region of N-WASP is important for its ability to phase separate, which in turn aids in its ability to recruit and activate the Arp2/3 complex (Li *et al.*, 2012). These two mutations in N-WASP are likely a loss of function in their ability to efficiently activate Arp2/3-dependent actin nucleation. Future work could investigate whether additional mutations that influence N-WASP phase separation, or other modifiers of N-WASP activity, are also associated with parkinsonism. Furthermore, it would also be important to identify whether any other mutations in N-WASP also affect the recruitment of α-Syn into synapsin 1 condensates, or whether they lead to hardening of α-Syn condensates.

With respect to the effect of WSP-1/N-WASP on mitochondrial function, we found that WSP-1 loss of function and α-Syn overexpression resulted in a similar

decrease in expression of mitochondrial and metabolic proteins. Consistent with this proteomic signature, we showed that *wsp-1(lof)* and *α-Syn O/E* had impaired mitochondrial respiration and reduced storage of neutral lipids. At least in some experimental conditions, the outcome of *wsp-1(lof)* and *α-Syn O/E* had an additive effect. To date, the connection between the actin cytoskeleton and mitochondrial function remains a topic of interest. Some evidence suggests that actin plays an essential in the response to acute mitochondrial damage and depolarisation, and promotes rapid glycolytic activation to recover ATP production (Kruppa *et al*, 2018; Chakrabarti *et al*, 2022; Fung *et al*, 2022). It could be that N-WASP and other actin-regulatory proteins are important for mitochondrial function and certain metabolic pathways, and that impairment in their function may contribute to mitochondrial dysfunction in diseases such as PD.

Since WSP-1 loss of function seems to have a dual role in regulating α-Syn condensates and mitochondrial metabolism in *C. elegans*, we hypothesised that altered mitochondrial function itself may lead to aberrant LLPS of α-Syn. To test this, we assessed the mobility of α-Syn condensates in CI deficient *gas-1(fc21)* nematodes. Contrary to our expectations, the *gas-1(fc21)* mutation increased mobility of α-Syn condensates, suggesting that mitochondrial dysfunction may promote the maintenance of a liquid-like state of α-Syn condensates. Having said that, it would be important to clarify the role of mitochondrial function in the regulation of biomolecular condensates. This would further help us to understand the contribution of mitochondrial dysfunction in proteostasis and neurodegenerative processes.

Together, this thesis work has contributed to the growing understanding of the mechanisms that compensate for aberrant mitochondrial energy production and demonstrates the notable importance of mitochondria-lysosome contact sites. Furthermore, it draws attention to the relatively understudied involvement of cytoskeletal proteins in α-Syn physiology, biomolecular condensation processes, and mitochondrial function.

Acknowledgements

Firstly, I would like to thank the members of AG Bano, past and present, for creating such an amazing working environment over the years. I would like to thank Antonia for all the support at the start of my journey in the lab, and for introducing me to the wonderful world of *C. elegans.* I am particularly grateful for Lena and Christiane, for their wealth of knowledge, assistance in the lab, scientific discussions, and for their friendship.

Additionally, I would like to thank everyone that contributed to the manuscripts presented in this thesis, especially for the amazing work and support from my main collaborators, Lena Wischoff, Christian Hoffmann, and Enzo Scifo. Thank you to all the staff in the DZNE that helped to keep my research running smoothly, especially those in the Media Kitchen and those at the Light Microscopy Facility. I would also like to thank PD-MitoQUANT, who funded part of my research.

I would like to thank Dr. Daniele Bano for opportunity to conduct my research in his lab, and his guidance throughout the years. Thank you to Prof. Dr. Dr. Pierluigi Nicotera, Prof. Dr. Joachim Schultze, Prof. Dr. Dietmar Schmucker, and Priv-Doz. Dr. Dan Ehninger for agreeing to be part of my doctoral committee.

Finally, thanks to my friends and family, near and far, who have provided endless support and motivation throughout this chapter of my life.

References

Altmeyer M, Neelsen KJ, Teloni F, Pozdnyakova I, Pellegrino S, Grofte M, Rask MD, Streicher W, Jungmichel S, Nielsen ML *et al* (2015) Liquid demixing of intrinsically disordered proteins is seeded by poly(ADP-ribose). *Nat Commun* 6: 8088

Anderson S, Bankier AT, Barrell BG, de Bruijn MH, Coulson AR, Drouin J, Eperon IC, Nierlich DP, Roe BA, Sanger F *et al* (1981) Sequence and organization of the human mitochondrial genome. *Nature* 290: 457-465

Andres-Mateos E, Perier C, Zhang L, Blanchard-Fillion B, Greco TM, Thomas B, Ko HS, Sasaki M, Ischiropoulos H, Przedborski S *et al* (2007) DJ-1 gene deletion reveals that DJ-1 is an atypical peroxiredoxin-like peroxidase. *Proc Natl Acad Sci U S A* 104: 14807-14812

Anflous-Pharayra K, Lee N, Armstrong DL, Craigen WJ (2011) VDAC3 has differing mitochondrial functions in two types of striated muscles. *Biochim Biophys Acta* 1807: 150-156

Antony AN, Paillard M, Moffat C, Juskeviciute E, Correnti J, Bolon B, Rubin E, Csordas G, Seifert EL, Hoek JB *et al* (2016) MICU1 regulation of mitochondrial Ca(2+) uptake dictates survival and tissue regeneration. *Nat Commun* 7: 10955

Atias M, Tevet Y, Sun J, Stavsky A, Tal S, Kahn J, Roy S, Gitler D (2019) Synapsins regulate alpha-synuclein functions. *Proc Natl Acad Sci U S A* 116: 11116-11118

Audas TE, Jacob MD, Lee S (2012) Immobilization of proteins in the nucleolus by ribosomal intergenic spacer noncoding RNA. *Mol Cell* 45: 147-157

Austin S, Mekis R, Mohammed SEM, Scalise M, Wang WA, Galluccio M, Pfeiffer C, Borovec T, Parapatics K, Vitko D *et al* (2022) TMBIM5 is the Ca(2+) /H(+) antiporter of mammalian mitochondria. *EMBO Rep* 23: e54978

Baines CP, Kaiser RA, Sheiko T, Craigen WJ, Molkentin JD (2007) Voltage-dependent anion channels are dispensable for mitochondrial-dependent cell death. *Nat Cell Biol* 9: 550-555

Bakare AB, Lesnefsky EJ, Iyer S (2021) Leigh Syndrome: A Tale of Two Genomes. *Front Physiol* 12: 693734

Banani SF, Rice AM, Peeples WB, Lin Y, Jain S, Parker R, Rosen MK (2016) Compositional Control of Phase-Separated Cellular Bodies. *Cell* 166: 651-663

Banerjee K, Sinha M, Pham Cle L, Jana S, Chanda D, Cappai R, Chakrabarti S (2010) Alpha-synuclein induced membrane depolarization and loss of phosphorylation capacity of isolated rat brain mitochondria: implications in Parkinson's disease. *FEBS Lett* 584: 1571-1576

Banjade S, Rosen MK (2014) Phase transitions of multivalent proteins can promote clustering of membrane receptors. *Elife* 3

Bano D, Prehn JHM (2018) Apoptosis-Inducing Factor (AIF) in Physiology and Disease: The Tale of a Repented Natural Born Killer. *EBioMedicine* 30: 29-37

Barsoum MJ, Yuan H, Gerencser AA, Liot G, Kushnareva Y, Graber S, Kovacs I, Lee WD, Waggoner J, Cui J *et al* (2006) Nitric oxide-induced mitochondrial fission is regulated by dynamin-related GTPases in neurons. *EMBO J* 25: 3900-3911

Baughman JM, Perocchi F, Girgis HS, Plovanich M, Belcher-Timme CA, Sancak Y, Bao XR, Strittmatter L, Goldberger O, Bogorad RL *et al* (2011) Integrative genomics identifies MCU as an essential component of the mitochondrial calcium uniporter. *Nature* 476: 341-345

Baumgartner HK, Gerasimenko JV, Thorne C, Ferdek P, Pozzan T, Tepikin AV, Petersen OH, Sutton R, Watson AJ, Gerasimenko OV (2009) Calcium elevation in mitochondria is the main Ca2+ requirement for mitochondrial permeability transition pore (mPTP) opening. *J Biol Chem* 284: 20796-20803

Baxter RV, Ben Othmane K, Rochelle JM, Stajich JE, Hulette C, Dew-Knight S, Hentati F, Ben Hamida M, Bel S, Stenger JE *et al* (2002) Ganglioside-induced differentiation-associated protein-1 is mutant in Charcot-Marie-Tooth disease type 4A/8q21. *Nat Genet* 30: 21-22

Bendor JT, Logan TP, Edwards RH (2013) The function of alpha-synuclein. *Neuron* 79: 1044-1066

Benedetti C, Haynes CM, Yang Y, Harding HP, Ron D (2006) Ubiquitin-like protein 5 positively regulates chaperone gene expression in the mitochondrial unfolded protein response. *Genetics* 174: 229-239

Bernardi P, Gerle C, Halestrap AP, Jonas EA, Karch J, Mnatsakanyan N, Pavlov E, Sheu SS, Soukas AA (2023) Identity, structure, and function of the mitochondrial permeability transition pore: controversies, consensus, recent advances, and future directions. *Cell Death Differ* 30: 1869-1885

Berridge MJ, Lipp P, Bootman MD (2000) The versatility and universality of calcium signalling. *Nat Rev Mol Cell Biol* 1: 11-21

Bertan F, Wischhof L, Scifo E, Guranda M, Jackson J, Marsal-Cots A, Piazzesi A, Stork M, Peitz M, Prehn JHM *et al* (2021) Comparative analysis of CI- and CIV-containing respiratory supercomplexes at single-cell resolution. *Cell Rep Methods* 1: 100002

Berthet A, Margolis EB, Zhang J, Hsieh I, Zhang J, Hnasko TS, Ahmad J, Edwards RH, Sesaki H, Huang EJ *et al* (2014) Loss of mitochondrial fission depletes axonal mitochondria in midbrain dopamine neurons. *J Neurosci* 34: 14304-14317

Betarbet R, Sherer TB, MacKenzie G, Garcia-Osuna M, Panov AV, Greenamyre JT (2000) Chronic systemic pesticide exposure reproduces features of Parkinson's disease. *Nat Neurosci* 3: 1301-1306

Bick AG, Calvo SE, Mootha VK (2012) Evolutionary diversity of the mitochondrial calcium uniporter. *Science* 336: 886

Bitarafan F, Khodaeian M, Amjadi Sardehaei E, Darvishi FZ, Almadani N, Nilipour Y, Garshasbi M (2021) Identification of a novel MICU1 nonsense variant causes myopathy with extrapyramidal signs in an Iranian consanguineous family. *Mol Cell Pediatr* 8: 6

Blachly-Dyson E, Baldini A, Litt M, McCabe ER, Forte M (1994) Human genes encoding the voltage-dependent anion channel (VDAC) of the outer mitochondrial membrane: mapping and identification of two new isoforms. *Genomics* 20: 62-67

Blachly-Dyson E, Zambronicz EB, Yu WH, Adams V, McCabe ER, Adelman J, Colombini M, Forte M (1993) Cloning and functional expression in yeast of two human isoforms of the outer mitochondrial membrane channel, the voltage-dependent anion channel. *J Biol Chem* 268: 1835-1841

Blok MJ, van den Bosch BJ, Jongen E, Hendrickx A, de Die-Smulders CE, Hoogendijk JE, Brusse E, de Visser M, Poll-The BT, Bierau J *et al* (2009) The unfolding clinical spectrum of POLG mutations. *J Med Genet* 46: 776-785

Boke E, Ruer M, Wuhr M, Coughlin M, Lemaitre R, Gygi SP, Alberti S, Drechsel D, Hyman AA, Mitchison TJ (2016) Amyloid-like Self-Assembly of a Cellular Compartment. *Cell* 166: 637-650

Bonifati V, Rizzu P, van Baren MJ, Schaap O, Breedveld GJ, Krieger E, Dekker MC, Squitieri F, Ibanez P, Joosse M *et al* (2003) Mutations in the DJ-1 gene associated with autosomal recessive early-onset parkinsonism. *Science* 299: 256-259

Bonora M, Giorgi C, Pinton P (2022) Molecular mechanisms and consequences of mitochondrial permeability transition. *Nat Rev Mol Cell Biol* 23: 266-285

Bonora M, Morganti C, Morciano G, Pedriali G, Lebiedzinska-Arciszewska M, Aquila G, Giorgi C, Rizzo P, Campo G, Ferrari R *et al* (2017) Mitochondrial permeability transition involves dissociation of F(1)F(O) ATP synthase dimers and C-ring conformation. *EMBO Rep* 18: 1077-1089

Bootman MD, Bultynck G (2020) Fundamentals of Cellular Calcium Signaling: A Primer. *Cold Spring Harb Perspect Biol* 12

Bose A, Beal MF (2016) Mitochondrial dysfunction in Parkinson's disease. *J Neurochem* 139 Suppl 1: 216-231

Braak H, Del Tredici K, Rub U, de Vos RA, Jansen Steur EN, Braak E (2003) Staging of brain pathology related to sporadic Parkinson's disease. *Neurobiol Aging* 24: 197-211

Brangwynne CP, Eckmann CR, Courson DS, Rybarska A, Hoege C, Gharakhani J, Julicher F, Hyman AA (2009) Germline P granules are liquid droplets that localize by controlled dissolution/condensation. *Science* 324: 1729-1732

Brooks WM, Lynch PJ, Ingle CC, Hatton A, Emson PC, Faull RL, Starkey MP (2007) Gene expression profiles of metabolic enzyme transcripts in Alzheimer's disease. *Brain Res* 1127: 127-135

Buchan JR, Kolaitis RM, Taylor JP, Parker R (2013) Eukaryotic stress granules are cleared by autophagy and Cdc48/VCP function. *Cell* 153: 1461-1474

Burns RS, Chiueh CC, Markey SP, Ebert MH, Jacobowitz DM, Kopin IJ (1983) A primate model of parkinsonism: selective destruction of dopaminergic neurons in the pars compacta of the substantia nigra by N-methyl-4-phenyl-1,2,3,6-tetrahydropyridine. *Proc Natl Acad Sci U S A* 80: 4546-4550

Burre J, Sharma M, Sudhof TC (2014) alpha-Synuclein assembles into higher-order multimers upon membrane binding to promote SNARE complex formation. *Proc Natl Acad Sci U S A* 111: E4274-4283

Burre J, Sharma M, Tsetsenis T, Buchman V, Etherton MR, Sudhof TC (2010) Alpha-synuclein promotes SNARE-complex assembly in vivo and in vitro. *Science* 329: 1663-1667

Byrne E, Dennett X, Trounce I, Henderson R (1985) Partial cytochrome oxidase (aa3) deficiency in chronic progressive external ophthalmoplegia. Histochemical and biochemical studies. *J Neurol Sci* 71: 257-271

Calvo SE, Clauser KR, Mootha VK (2016) MitoCarta2.0: an updated inventory of mammalian mitochondrial proteins. *Nucleic Acids Res* 44: D1251-1257

Caraveo G, Auluck PK, Whitesell L, Chung CY, Baru V, Mosharov EV, Yan X, Ben-Johny M, Soste M, Picotti P *et al* (2014) Calcineurin determines toxic versus beneficial responses to alpha-synuclein. *Proc Natl Acad Sci U S A* 111: E3544-3552

Carreras-Sureda A, Jana F, Urra H, Durand S, Mortenson DE, Sagredo A, Bustos G, Hazari Y, Ramos-Fernandez E, Sassano ML *et al* (2019) Non-canonical function of IRE1alpha determines mitochondria-associated endoplasmic reticulum composition to control calcium transfer and bioenergetics. *Nat Cell Biol* 21: 755-767

Case LB, Zhang X, Ditlev JA, Rosen MK (2019) Stoichiometry controls activity of phase-separated clusters of actin signaling proteins. *Science* 363: 1093-1097

Chakrabarti R, Fung TS, Kang T, Elonkirjo PW, Suomalainen A, Usherwood EJ, Higgs HN (2022) Mitochondrial dysfunction triggers actin polymerization necessary for rapid glycolytic activation. *J Cell Biol* 221

Champy P, Hoglinger GU, Feger J, Gleye C, Hocquemiller R, Laurens A, Guerineau V, Laprevote O, Medja F, Lombes A *et al* (2004) Annonacin, a lipophilic inhibitor of mitochondrial complex I, induces nigral and striatal neurodegeneration in rats: possible relevance for atypical parkinsonism in Guadeloupe. *J Neurochem* 88: 63-69

Chandra S, Chen X, Rizo J, Jahn R, Sudhof TC (2003) A broken alpha -helix in folded alpha -Synuclein. *J Biol Chem* 278: 15313-15318

Chandran R, Kumar M, Kesavan L, Jacob RS, Gunasekaran S, Lakshmi S, Sadasivan C, Omkumar RV (2019) Cellular calcium signaling in the aging brain. *J Chem Neuroanat* 95: 95-114

Chang DT, Honick AS, Reynolds IJ (2006) Mitochondrial trafficking to synapses in cultured primary cortical neurons. *J Neurosci* 26: 7035-7045

Cheng EH, Sheiko TV, Fisher JK, Craigen WJ, Korsmeyer SJ (2003) VDAC2 inhibits BAK activation and mitochondrial apoptosis. *Science* 301: 513-517

Chiang WC, Tishkoff DX, Yang B, Wilson-Grady J, Yu X, Mazer T, Eckersdorff M, Gygi SP, Lombard DB, Hsu AL (2012) C. elegans SIRT6/7 homolog SIR-2.4 promotes DAF-16 relocalization and function during stress. *PLoS Genet* 8: e1002948

Chinta SJ, Mallajosyula JK, Rane A, Andersen JK (2010) Mitochondrial alpha-synuclein accumulation impairs complex I function in dopaminergic neurons and results in increased mitophagy in vivo. *Neurosci Lett* 486: 235-239

Choi JM, Holehouse AS, Pappu RV (2020) Physical Principles Underlying the Complex Biology of Intracellular Phase Transitions. *Annu Rev Biophys* 49: 107-133

Chu Y, Dodiya H, Aebischer P, Olanow CW, Kordower JH (2009) Alterations in lysosomal and proteasomal markers in Parkinson's disease: relationship to alpha-synuclein inclusions. *Neurobiol Dis* 35: 385-398

Clapham DE (2007) Calcium signaling. *Cell* 131: 1047-1058

Colla E, Coune P, Liu Y, Pletnikova O, Troncoso JC, Iwatsubo T, Schneider BL, Lee MK (2012) Endoplasmic reticulum stress is important for the manifestations of alpha-synucleinopathy in vivo. *J Neurosci* 32: 3306-3320

Copeland JM, Cho J, Lo T, Jr., Hur JH, Bahadorani S, Arabyan T, Rabie J, Soh J, Walker DW (2009) Extension of Drosophila life span by RNAi of the mitochondrial respiratory chain. *Curr Biol* 19: 1591-1598

Csordas G, Golenar T, Seifert EL, Kamer KJ, Sancak Y, Perocchi F, Moffat C, Weaver D, de la Fuente Perez S, Bogorad R *et al* (2013) MICU1 controls both the threshold and cooperative activation of the mitochondrial Ca(2)(+) uniporter. *Cell Metab* 17: 976-987

Dauer W, Kholodilov N, Vila M, Trillat AC, Goodchild R, Larsen KE, Staal R, Tieu K, Schmitz Y, Yuan CA *et al* (2002) Resistance of alpha -synuclein null mice to the parkinsonian neurotoxin MPTP. *Proc Natl Acad Sci U S A* 99: 14524-14529

Davidson WS, Jonas A, Clayton DF, George JM (1998) Stabilization of alpha-synuclein secondary structure upon binding to synthetic membranes. *J Biol Chem* 273: 9443-9449

Davis GC, Williams AC, Markey SP, Ebert MH, Caine ED, Reichert CM, Kopin IJ (1979) Chronic Parkinsonism secondary to intravenous injection of meperidine analogues. *Psychiatry Res* 1: 249-254

De Stefani D, Raffaello A, Teardo E, Szabo I, Rizzuto R (2011) A forty-kilodalton protein of the inner membrane is the mitochondrial calcium uniporter. *Nature* 476: 336-340

De Stefani D, Rizzuto R, Pozzan T (2016) Enjoy the Trip: Calcium in Mitochondria Back and Forth. *Annu Rev Biochem* 85: 161-192

Debattisti V, Horn A, Singh R, Seifert EL, Hogarth MW, Mazala DA, Huang KT, Horvath R, Jaiswal JK, Hajnoczky G (2019) Dysregulation of Mitochondrial Ca(2+) Uptake and Sarcolemma Repair Underlie Muscle Weakness and Wasting in Patients and Mice Lacking MICU1. *Cell Rep* 29: 1274-1286 e1276

Decker CJ, Teixeira D, Parker R (2007) Edc3p and a glutamine/asparagine-rich domain of Lsm4p function in processing body assembly in Saccharomyces cerevisiae. *J Cell Biol* 179: 437-449

Dehay B, Bove J, Rodriguez-Muela N, Perier C, Recasens A, Boya P, Vila M (2010) Pathogenic lysosomal depletion in Parkinson's disease. *J Neurosci* 30: 12535-12544

Delettre C, Lenaers G, Griffoin JM, Gigarel N, Lorenzo C, Belenguer P, Pelloquin L, Grosgeorge J, Turc-Carel C, Perret E *et al* (2000) Nuclear gene OPA1, encoding a mitochondrial dynamin-related protein, is mutated in dominant optic atrophy. *Nat Genet* 26: 207-210

Dell'agnello C, Leo S, Agostino A, Szabadkai G, Tiveron C, Zulian A, Prelle A, Roubertoux P, Rizzuto R, Zeviani M (2007) Increased longevity and refractoriness to Ca(2+)-dependent neurodegeneration in Surf1 knockout mice. *Hum Mol Genet* 16: 431-444

Di Maio R, Barrett PJ, Hoffman EK, Barrett CW, Zharikov A, Borah A, Hu X, McCoy J, Chu CT, Burton EA *et al* (2016) alpha-Synuclein binds to TOM20 and inhibits mitochondrial protein import in Parkinson's disease. *Sci Transl Med* 8: 342ra378

Diao J, Burre J, Vivona S, Cipriano DJ, Sharma M, Kyoung M, Sudhof TC, Brunger AT (2013) Native alpha-synuclein induces clustering of synaptic-vesicle mimics via binding to phospholipids and synaptobrevin-2/VAMP2. *Elife* 2: e00592

Dillin A, Hsu AL, Arantes-Oliveira N, Lehrer-Graiwer J, Hsin H, Fraser AG, Kamath RS, Ahringer J, Kenyon C (2002) Rates of behavior and aging specified by mitochondrial function during development. *Science* 298: 2398-2401

DiMauro S, Mendell JR, Sahenk Z, Bachman D, Scarpa A, Scofield RM, Reiner C (1980) Fatal infantile mitochondrial myopathy and renal dysfunction due to cytochrome-c-oxidase deficiency. *Neurology* 30: 795-804

Doherty KM, Hardy J (2013) Parkin disease and the Lewy body conundrum. *Mov Disord* 28: 702-704

Doherty KM, Silveira-Moriyama L, Parkkinen L, Healy DG, Farrell M, Mencacci NE, Ahmed Z, Brett FM, Hardy J, Quinn N *et al* (2013) Parkin disease: a clinicopathologic entity? *JAMA Neurol* 70: 571-579

Dues DJ, Schaar CE, Johnson BK, Bowman MJ, Winn ME, Senchuk MM, Van Raamsdonk JM (2017) Uncoupling of oxidative stress resistance and lifespan in long-lived isp-1 mitochondrial mutants in Caenorhabditis elegans. *Free Radic Biol Med* 108: 362-373

Durieux J, Wolff S, Dillin A (2011) The cell-non-autonomous nature of electron transport chain-mediated longevity. *Cell* 144: 79-91

Eliezer D, Kutluay E, Bussell R, Jr., Browne G (2001) Conformational properties of alpha-synuclein in its free and lipid-associated states. *J Mol Biol* 307: 1061-1073

Enriquez JA (2016) Supramolecular Organization of Respiratory Complexes. *Annu Rev Physiol* 78: 533-561

Eramo MJ, Lisnyak V, Formosa LE, Ryan MT (2020) The 'mitochondrial contact site and cristae organising system' (MICOS) in health and human disease. *J Biochem* 167: 243-255

Feng J, Bussiere F, Hekimi S (2001) Mitochondrial electron transport is a key determinant of life span in Caenorhabditis elegans. *Dev Cell* 1: 633-644

Feno S, Rizzuto R, Raffaello A, Vecellio Reane D (2021) The molecular complexity of the Mitochondrial Calcium Uniporter. *Cell Calcium* 93: 102322

Feric M, Vaidya N, Harmon TS, Mitrea DM, Zhu L, Richardson TM, Kriwacki RW, Pappu RV, Brangwynne CP (2016) Coexisting Liquid Phases Underlie Nucleolar Subcompartments. *Cell* 165: 1686-1697

Flones IH, Toker L, Sandnes DA, Castelli M, Mostafavi S, Lura N, Shadad O, Fernandez-Vizarra E, Painous C, Perez-Soriano A *et al* (2024) Mitochondrial complex I deficiency stratifies idiopathic Parkinson's disease. *Nat Commun* 15: 3631

Fornai F, Schluter OM, Lenzi P, Gesi M, Ruffoli R, Ferrucci M, Lazzeri G, Busceti CL, Pontarelli F, Battaglia G *et al* (2005) Parkinson-like syndrome induced by continuous MPTP infusion: convergent roles of the ubiquitin-proteasome system and alpha-synuclein. *Proc Natl Acad Sci U S A* 102: 3413-3418

Fortin DL, Nemani VM, Voglmaier SM, Anthony MD, Ryan TA, Edwards RH (2005) Neural activity controls the synaptic accumulation of alpha-synuclein. *J Neurosci* 25: 10913-10921

Fouke KE, Wegman ME, Weber SA, Brady EB, Román-Vendrell C, Morgan JR (2021) Synuclein Regulates Synaptic Vesicle Clustering and Docking at a Vertebrate Synapse. *Frontiers in Cell and Developmental Biology* 9

Franzmann TM, Jahnel M, Pozniakovsky A, Mahamid J, Holehouse AS, Nuske E, Richter D, Baumeister W, Grill SW, Pappu RV *et al* (2018) Phase separation of a yeast prion protein promotes cellular fitness. *Science* 359

Frazier AE, Thorburn DR, Compton AG (2019) Mitochondrial energy generation disorders: genes, mechanisms, and clues to pathology. *J Biol Chem* 294: 5386-5395

Friedman DB, Johnson TE (1988) A mutation in the age-1 gene in Caenorhabditis elegans lengthens life and reduces hermaphrodite fertility. *Genetics* 118: 75-86

Frottin F, Schueder F, Tiwary S, Gupta R, Korner R, Schlichthaerle T, Cox J, Jungmann R, Hartl FU, Hipp MS (2019) The nucleolus functions as a phase-separated protein quality control compartment. *Science* 365: 342-347

Fung TS, Chakrabarti R, Kollasser J, Rottner K, Stradal TEB, Kage F, Higgs HN (2022) Parallel kinase pathways stimulate actin polymerization at depolarized mitochondria. *Curr Biol* 32: 1577-1592 e1578

Furukawa Y, Vigouroux S, Wong H, Guttman M, Rajput AH, Ang L, Briand M, Kish SJ, Briand Y (2002) Brain proteasomal function in sporadic Parkinson's disease and related disorders. *Ann Neurol* 51: 779-782

Galper J, Dean NJ, Pickford R, Lewis SJG, Halliday GM, Kim WS, Dzamko N (2022) Lipid pathway dysfunction is prevalent in patients with Parkinson's disease. *Brain* 145: 3472-3487

Garbincius JF, Salik O, Cohen HM, Choya-Foces C, Mangold AS, Makhoul AD, Schmidt AE, Khalil DY, Doolittle JJ, Wilkinson AS *et al* (2023) TMEM65 regulates NCLX-dependent mitochondrial calcium efflux. *bioRxiv*

Gentile JE, Carrizales MG, Koleske AJ (2022) Control of Synapse Structure and Function by Actin and Its Regulators. *Cells* 11

Ghezzi D, Sevrioukova I, Invernizzi F, Lamperti C, Mora M, D'Adamo P, Novara F, Zuffardi O, Uziel G, Zeviani M (2010) Severe X-linked mitochondrial encephalomyopathy associated with a mutation in apoptosis-inducing factor. *Am J Hum Genet* 86: 639-649

Gilks N, Kedersha N, Ayodele M, Shen L, Stoecklin G, Dember LM, Anderson P (2004) Stress granule assembly is mediated by prion-like aggregation of TIA-1. *Mol Biol Cell* 15: 5383-5398

Giorgi C, Baldassari F, Bononi A, Bonora M, De Marchi E, Marchi S, Missiroli S, Patergnani S, Rimessi A, Suski JM *et al* (2012) Mitochondrial Ca(2+) and apoptosis. *Cell Calcium* 52: 36-43

Gitler AD, Bevis BJ, Shorter J, Strathearn KE, Hamamichi S, Su LJ, Caldwell KA, Caldwell GA, Rochet JC, McCaffery JM *et al* (2008) The Parkinson's disease protein alpha-synuclein disrupts cellular Rab homeostasis. *Proc Natl Acad Sci U S A* 105: 145-150

Glancy B, Willis WT, Chess DJ, Balaban RS (2013) Effect of calcium on the oxidative phosphorylation cascade in skeletal muscle mitochondria. *Biochemistry* 52: 2793-2809

Glover-Cutter KM, Lin S, Blackwell TK (2013) Integration of the unfolded protein and oxidative stress responses through SKN-1/Nrf. *PLoS Genet* 9: e1003701

Gomori G (1950) A rapid one-step trichrome stain. *Am J Clin Pathol* 20: 661-664

Gonzalez Montoro A, Auffarth K, Honscher C, Bohnert M, Becker T, Warscheid B, Reggiori F, van der Laan M, Frohlich F, Ungermann C (2018) Vps39 Interacts with Tom40 to Establish One of Two Functionally Distinct Vacuole-Mitochondria Contact Sites. *Dev Cell* 45: 621-636 e627

Goto Y, Nonaka I, Horai S (1990) A mutation in the tRNA(Leu)(UUR) gene associated with the MELAS subgroup of mitochondrial encephalomyopathies. *Nature* 348: 651-653

Gottschalk B, Klec C, Leitinger G, Bernhart E, Rost R, Bischof H, Madreiter-Sokolowski CT, Radulovic S, Eroglu E, Sattler W *et al* (2019) MICU1 controls cristae junction and spatially anchors mitochondrial Ca(2+) uniporter complex. *Nat Commun* 10: 3732

Gottschalk B, Koshenov Z, Waldeck-Weiermair M, Radulovic S, Oflaz FE, Hirtl M, Bachkoenig OA, Leitinger G, Malli R, Graier WF (2022) MICU1 controls spatial membrane potential gradients and guides Ca(2+) fluxes within mitochondrial substructures. *Commun Biol* 5: 649

Gray MW (2012) Mitochondrial evolution. *Cold Spring Harb Perspect Biol* 4: a011403

Guardia-Laguarta C, Area-Gomez E, Rub C, Liu Y, Magrane J, Becker D, Voos W, Schon EA, Przedborski S (2014) alpha-Synuclein is localized to mitochondria-associated ER membranes. *J Neurosci* 34: 249-259

Guehl D, Bezard E, Dovero S, Boraud T, Bioulac B, Gross C (1999) Trichloroethylene and parkinsonism: a human and experimental observation. *Eur J Neurol* 6: 609-611

Han TW, Kato M, Xie S, Wu LC, Mirzaei H, Pei J, Chen M, Xie Y, Allen J, Xiao G *et al* (2012) Cell-free formation of RNA granules: bound RNAs identify features and components of cellular assemblies. *Cell* 149: 768-779

Hansen M, Chandra A, Mitic LL, Onken B, Driscoll M, Kenyon C (2008) A role for autophagy in the extension of lifespan by dietary restriction in C. elegans. *PLoS Genet* 4: e24

Hardenberg MC, Sinnige T, Casford S, Dada ST, Poudel C, Robinson EA, Fuxreiter M, Kaminksi CF, Kaminski Schierle GS, Nollen EAA *et al* (2021) Observation of an α-synuclein liquid droplet state and its maturation into Lewy body-like assemblies. *J Mol Cell Biol* 13: 282-294

Hayes MH, Peuchen EH, Dovichi NJ, Weeks DL (2018) Dual roles for ATP in the regulation of phase separated protein aggregates in Xenopus oocyte nucleoli. *Elife* 7

Haynes CM, Petrova K, Benedetti C, Yang Y, Ron D (2007) ClpP mediates activation of a mitochondrial unfolded protein response in C. elegans. *Dev Cell* 13: 467-480

Haynes CM, Yang Y, Blais SP, Neubert TA, Ron D (2010) The matrix peptide exporter HAF-1 signals a mitochondrial UPR by activating the transcription factor ZC376.7 in C. elegans. *Mol Cell* 37: 529-540

Heikkila RE, Hess A, Duvoisin RC (1984) Dopaminergic neurotoxicity of 1-methyl-4-phenyl-1,2,5,6-tetrahydropyridine in mice. *Science* 224: 1451-1453

Hirano M, Emmanuele V, Quinzii CM (2018) Emerging therapies for mitochondrial diseases. *Essays Biochem* 62: 467-481

Hoffman NE, Chandramoorthy HC, Shanmughapriya S, Zhang XQ, Vallem S, Doonan PJ, Malliankaraman K, Guo S, Rajan S, Elrod JW *et al* (2014) SLC25A23 augments mitochondrial Ca(2)(+) uptake, interacts with MCU, and induces oxidative stress-mediated cell death. *Mol Biol Cell* 25: 936-947

Hoffmann C, Sansevrino R, Morabito G, Logan C, Vabulas RM, Ulusoy A, Ganzella M, Milovanovic D (2021) Synapsin Condensates Recruit alpha-Synuclein. *J Mol Biol* 433: 166961

Houtkooper RH, Mouchiroud L, Ryu D, Moullan N, Katsyuba E, Knott G, Williams RW, Auwerx J (2013) Mitonuclear protein imbalance as a conserved longevity mechanism. *Nature* 497: 451-457

Hurley MJ, Brandon B, Gentleman SM, Dexter DT (2013) Parkinson's disease is associated with altered expression of CaV1 channels and calcium-binding proteins. *Brain* 136: 2077-2097

Hwang MS, Schwall CT, Pazarentzos E, Datler C, Alder NN, Grimm S (2014) Mitochondrial Ca(2+) influx targets cardiolipin to disintegrate respiratory chain complex II for cell death induction. *Cell Death Differ* 21: 1733-1745

Hynynen J, Komulainen T, Tukiainen E, Nordin A, Arola J, Kalviainen R, Jutila L, Roytta M, Hinttala R, Majamaa K *et al* (2014) Acute liver failure after valproate exposure in patients with POLG1 mutations and the prognosis after liver transplantation. *Liver Transpl* 20: 1402-1412

Iadarola DM, Basu Ball W, Trivedi PP, Fu G, Nan B, Gohil VM (2020) Vps39 is required for ethanolamine-stimulated elevation in mitochondrial phosphatidylethanolamine. *Biochim Biophys Acta Mol Cell Biol Lipids* 1865: 158655

Irrcher I, Aleyasin H, Seifert EL, Hewitt SJ, Chhabra S, Phillips M, Lutz AK, Rousseaux MW, Bevilacqua L, Jahani-Asl A *et al* (2010) Loss of the Parkinson's disease-linked gene DJ-1 perturbs mitochondrial dynamics. *Hum Mol Genet* 19: 3734-3746

Jackson J, Hoffmann C, Scifo E, Wang H, Wischhof L, Piazzesi A, Mondal M, Shields H, Zhou X, Mondin M *et al* (2024) Actin-nucleation promoting factor N-WASP influences alpha-synuclein condensates and pathology. *Cell Death Dis* 15: 304

Jackson J, Wischhof L, Scifo E, Pellizzer A, Wang Y, Piazzesi A, Gentile D, Siddig S, Stork M, Hopkins CE *et al* (2022) SGPL1 stimulates VPS39 recruitment to the mitochondria in MICU1 deficient cells. *Mol Metab* 61: 101503

Jain S, Wheeler JR, Walters RW, Agrawal A, Barsic A, Parker R (2016) ATPase-Modulated Stress Granules Contain a Diverse Proteome and Substructure. *Cell* 164: 487-498

Janetzky B, Hauck S, Youdim MB, Riederer P, Jellinger K, Pantucek F, Zochling R, Boissl KW, Reichmann H (1994) Unaltered aconitase activity, but decreased complex I activity in substantia nigra pars compacta of patients with Parkinson's disease. *Neurosci Lett* 169: 126-128

Kalko SG, Paco S, Jou C, Rodríguez MA, Meznaric M, Rogac M, Jekovec-Vrhovsek M, Sciacco M, Moggio M, Fagiolari G *et al* (2014) Transcriptomic profiling of TK2 deficient human skeletal muscle suggests a role for the p53 signalling pathway and identifies growth and differentiation factor-15 as a potential novel biomarker for mitochondrial myopathies. *BMC Genomics* 15: 91

Kamer KJ, Mootha VK (2014) MICU1 and MICU2 play nonredundant roles in the regulation of the mitochondrial calcium uniporter. *EMBO Rep* 15: 299-307

Kamp F, Exner N, Lutz AK, Wender N, Hegermann J, Brunner B, Nuscher B, Bartels T, Giese A, Beyer K *et al* (2010) Inhibition of mitochondrial fusion by alpha-synuclein is rescued by PINK1, Parkin and DJ-1. *EMBO J* 29: 3571-3589

Kang Y, Hepojoki J, Maldonado RS, Mito T, Terzioglu M, Manninen T, Kant R, Singh S, Othman A, Verma R *et al* (2024) Ancestral allele of DNA polymerase gamma modifies antiviral tolerance. *Nature* 628: 844-853

Kato M, Han TW, Xie S, Shi K, Du X, Wu LC, Mirzaei H, Goldsmith EJ, Longgood J, Pei J *et al* (2012) Cell-free formation of RNA granules: low complexity sequence domains form dynamic fibers within hydrogels. *Cell* 149: 753-767

Katona M, Bartok A, Nichtova Z, Csordas G, Berezhnaya E, Weaver D, Ghosh A, Varnai P, Yule DI, Hajnoczky G (2022) Capture at the ER-mitochondrial contacts licenses IP(3) receptors to stimulate local Ca(2+) transfer and oxidative metabolism. *Nat Commun* 13: 6779

Kawarai T, Yamazaki H, Yamakami K, Tsukamoto-Miyashiro A, Kodama M, Rumore R, Caltagirone C, Nishino I, Orlacchio A (2020) A novel AIFM1 missense mutation in a Japanese patient with ataxic sensory neuronopathy and hearing impairment. *J Neurol Sci* 409: 116584

Keane PC, Hanson PS, Patterson L, Blain PG, Hepplewhite P, Khundakar AA, Judge SJ, Kahle PJ, LeBeau FEN, Morris CM (2019) Trichloroethylene and its metabolite TaClo lead to degeneration of substantia nigra dopaminergic neurones: Effects in wild type and human A30P mutant alpha-synuclein mice. *Neurosci Lett* 711: 134437

Keeney PM, Xie J, Capaldi RA, Bennett JP, Jr. (2006) Parkinson's disease brain mitochondrial complex I has oxidatively damaged subunits and is functionally impaired and misassembled. *J Neurosci* 26: 5256-5264

Kenyon C, Chang J, Gensch E, Rudner A, Tabtiang R (1993) A C. elegans mutant that lives twice as long as wild type. *Nature* 366: 461-464

Khosravi S, Harner ME (2020) The MICOS complex, a structural element of mitochondria with versatile functions. *Biol Chem* 401: 765-778

Kim HE, Grant AR, Simic MS, Kohnz RA, Nomura DK, Durieux J, Riera CE, Sanchez M, Kapernick E, Wolff S *et al* (2016) Lipid Biosynthesis Coordinates a Mitochondrial-to-Cytosolic Stress Response. *Cell* 166: 1539-1552 e1516

Kirichok Y, Krapivinsky G, Clapham DE (2004) The mitochondrial calcium uniporter is a highly selective ion channel. *Nature* 427: 360-364

Kish SJ, Bergeron C, Rajput A, Dozic S, Mastrogiacomo F, Chang LJ, Wilson JM, DiStefano LM, Nobrega JN (1992) Brain cytochrome oxidase in Alzheimer's disease. *J Neurochem* 59: 776-779

Kitada T, Asakawa S, Hattori N, Matsumine H, Yamamura Y, Minoshima S, Yokochi M, Mizuno Y, Shimizu N (1998) Mutations in the parkin gene cause autosomal recessive juvenile parkinsonism. *Nature* 392: 605-608

Klein JA, Longo-Guess CM, Rossmann MP, Seburn KL, Hurd RE, Frankel WN, Bronson RT, Ackerman SL (2002) The harlequin mouse mutation downregulates apoptosis-inducing factor. *Nature* 419: 367-374

Klivenyi P, Siwek D, Gardian G, Yang L, Starkov A, Cleren C, Ferrante RJ, Kowall NW, Abeliovich A, Beal MF (2006) Mice lacking alpha-synuclein are resistant to mitochondrial toxins. *Neurobiol Dis* 21: 541-548

Klosin A, Oltsch F, Harmon T, Honigmann A, Julicher F, Hyman AA, Zechner C (2020) Phase separation provides a mechanism to reduce noise in cells. *Science* 367: 464-468

Kohlschmidt N, Elbracht M, Czech A, Hausler M, Phan V, Topf A, Huang KT, Bartok A, Eggermann K, Zippel S *et al* (2021) Molecular pathophysiology of human MICU1-deficiency. *Neuropathol Appl Neurobiol*

Kovacs-Bogdan E, Sancak Y, Kamer KJ, Plovanich M, Jambhekar A, Huber RJ, Myre MA, Blower MD, Mootha VK (2014) Reconstitution of the mitochondrial calcium uniporter in yeast. *Proc Natl Acad Sci U S A* 111: 8985-8990

Krayl M, Lim JH, Martin F, Guiard B, Voos W (2007) A cooperative action of the ATP-dependent import motor complex and the inner membrane potential drives mitochondrial preprotein import. *Mol Cell Biol* 27: 411-425

Krebiehl G, Ruckerbauer S, Burbulla LF, Kieper N, Maurer B, Waak J, Wolburg H, Gizatullina Z, Gellerich FN, Woitalla D *et al* (2010) Reduced basal autophagy and impaired mitochondrial dynamics due to loss of Parkinson's disease-associated protein DJ-1. *PLoS One* 5: e9367

Kroschwald S, Maharana S, Mateju D, Malinovska L, Nuske E, Poser I, Richter D, Alberti S (2015) Promiscuous interactions and protein disaggregases determine the material state of stress-inducible RNP granules. *Elife* 4: e06807

Kruger R, Kuhn W, Muller T, Woitalla D, Graeber M, Kosel S, Przuntek H, Epplen JT, Schols L, Riess O (1998) Ala30Pro mutation in the gene encoding alpha-synuclein in Parkinson's disease. *Nat Genet* 18: 106-108

Kruppa AJ, Kishi-Itakura C, Masters TA, Rorbach JE, Grice GL, Kendrick-Jones J, Nathan JA, Minczuk M, Buss F (2018) Myosin VI-Dependent Actin Cages Encapsulate Parkin-Positive Damaged Mitochondria. *Dev Cell* 44: 484-499 e486

Kruse SE, Watt WC, Marcinek DJ, Kapur RP, Schenkman KA, Palmiter RD (2008) Mice with mitochondrial complex I deficiency develop a fatal encephalomyopathy. *Cell Metab* 7: 312-320

Kumar S, Abbas MM, Govindappa ST, Muthane UB, Behari M, Pandey S, Juyal RC, Thelma BK (2021) Compound heterozygous variants in Wiskott-Aldrich syndrome like (WASL) gene segregating in a family with early onset Parkinson's disease. *Parkinsonism Relat Disord* 84: 61-67

Labbadia J, Brielmann RM, Neto MF, Lin YF, Haynes CM, Morimoto RI (2017) Mitochondrial Stress Restores the Heat Shock Response and Prevents Proteostasis Collapse during Aging. *Cell Rep* 21: 1481-1494

Lake NJ, Compton AG, Rahman S, Thorburn DR (2016) Leigh syndrome: One disorder, more than 75 monogenic causes. *Ann Neurol* 79: 190-203

Lang M, Jegou T, Chung I, Richter K, Munch S, Udvarhelyi A, Cremer C, Hemmerich P, Engelhardt J, Hell SW *et al* (2010) Three-dimensional organization of promyelocytic leukemia nuclear bodies. *J Cell Sci* 123: 392-400

Langston JW, Ballard P, Tetrud JW, Irwin I (1983) Chronic Parkinsonism in humans due to a product of meperidine-analog synthesis. *Science* 219: 979-980

Lapierre LR, De Magalhaes Filho CD, McQuary PR, Chu CC, Visvikis O, Chang JT, Gelino S, Ong B, Davis AE, Irazoqui JE *et al* (2013) The TFEB orthologue HLH-30 regulates autophagy and modulates longevity in Caenorhabditis elegans. *Nat Commun* 4: 2267

Lapointe J, Stepanyan Z, Bigras E, Hekimi S (2009) Reversal of the mitochondrial phenotype and slow development of oxidative biomarkers of aging in long-lived Mclk1+/- mice. *J Biol Chem* 284: 20364-20374

Larsson NG, Wang J, Wilhelmsson H, Oldfors A, Rustin P, Lewandoski M, Barsh GS, Clayton DA (1998) Mitochondrial transcription factor A is necessary for mtDNA maintenance and embryogenesis in mice. *Nat Genet* 18: 231-236

Lee SJ, Hwang AB, Kenyon C (2010) Inhibition of respiration extends C. elegans life span via reactive oxygen species that increase HIF-1 activity. *Curr Biol* 20: 2131-2136

Lee SS, Lee RY, Fraser AG, Kamath RS, Ahringer J, Ruvkun G (2003) A systematic RNAi screen identifies a critical role for mitochondria in C. elegans longevity. *Nat Genet* 33: 40-48

Leigh D (1951) Subacute necrotizing encephalomyelopathy in an infant. *J Neurol Neurosurg Psychiatry* 14: 216-221

Letts JA, Sazanov LA (2017) Clarifying the supercomplex: the higher-order organization of the mitochondrial electron transport chain. *Nat Struct Mol Biol* 24: 800-808

Lewis-Smith D, Kamer KJ, Griffin H, Childs AM, Pysden K, Titov D, Duff J, Pyle A, Taylor RW, Yu-Wai-Man P *et al* (2016) Homozygous deletion in MICU1 presenting with fatigue and lethargy in childhood. *Neurol Genet* 2: e59

Li L, Nadanaciva S, Berger Z, Shen W, Paumier K, Schwartz J, Mou K, Loos P, Milici AJ, Dunlop J *et al* (2013) Human A53T alpha-synuclein causes reversible deficits in mitochondrial function and dynamics in primary mouse cortical neurons. *PLoS One* 8: e85815

Li P, Banjade S, Cheng HC, Kim S, Chen B, Guo L, Llaguno M, Hollingsworth JV, King DS, Banani SF *et al* (2012) Phase transitions in the assembly of multivalent signalling proteins. *Nature* 483: 336-340

Li W, Gao B, Lee SM, Bennett K, Fang D (2007) RLE-1, an E3 ubiquitin ligase, regulates C. elegans aging by catalyzing DAF-16 polyubiquitination. *Dev Cell* 12: 235-246

Li X, Matilainen O, Jin C, Glover-Cutter KM, Holmberg CI, Blackwell TK (2011) Specific SKN-1/Nrf stress responses to perturbations in translation elongation and proteasome activity. *PLoS Genet* 7: e1002119

Li Y, Huang TT, Carlson EJ, Melov S, Ursell PC, Olson JL, Noble LJ, Yoshimura MP, Berger C, Chan PH *et al* (1995) Dilated cardiomyopathy and neonatal lethality in mutant mice lacking manganese superoxide dismutase. *Nat Genet* 11: 376-381

Li Z, Okamoto K, Hayashi Y, Sheng M (2004) The importance of dendritic mitochondria in the morphogenesis and plasticity of spines and synapses. *Cell* 119: 873-887

Lin Y, Ji K, Ma X, Liu S, Li W, Zhao Y, Yan C (2020) Accuracy of FGF-21 and GDF-15 for the diagnosis of mitochondrial disorders: A meta-analysis. *Ann Clin Transl Neurol* 7: 1204-1213

Lin Y, Protter DS, Rosen MK, Parker R (2015) Formation and Maturation of Phase-Separated Liquid Droplets by RNA-Binding Proteins. *Mol Cell* 60: 208-219

Lin YF, Haynes CM (2016) Metabolism and the UPR(mt). *Mol Cell* 61: 677-682

Liu JC, Liu J, Holmstrom KM, Menazza S, Parks RJ, Fergusson MM, Yu ZX, Springer DA, Halsey C, Liu C *et al* (2016) MICU1 Serves as a Molecular Gatekeeper to Prevent In Vivo Mitochondrial Calcium Overload. *Cell Rep* 16: 1561-1573

Liu JC, Syder NC, Ghorashi NS, Willingham TB, Parks RJ, Sun J, Fergusson MM, Liu J, Holmstrom KM, Menazza S *et al* (2020) EMRE is essential for mitochondrial calcium uniporter activity in a mouse model. *JCI Insight* 5

Liu Y, Ma X, Fujioka H, Liu J, Chen S, Zhu X (2019) DJ-1 regulates the integrity and function of ER-mitochondria association through interaction with IP3R3-Grp75-VDAC1. *Proc Natl Acad Sci U S A* 116: 25322-25328

Liu Y, Samuel BS, Breen PC, Ruvkun G (2014) Caenorhabditis elegans pathways that surveil and defend mitochondria. *Nature* 508: 406-410

Logan CV, Szabadkai G, Sharpe JA, Parry DA, Torelli S, Childs AM, Kriek M, Phadke R, Johnson CA, Roberts NY *et al* (2014) Loss-of-function mutations in MICU1 cause a brain and muscle disorder linked to primary alterations in mitochondrial calcium signaling. *Nat Genet* 46: 188-193

Logan T, Bendor J, Toupin C, Thorn K, Edwards RH (2017) alpha-Synuclein promotes dilation of the exocytotic fusion pore. *Nat Neurosci* 20: 681-689

Luo S, Wang D, Zhang Z (2023) Post-translational modification and mitochondrial function in Parkinson's disease. *Front Mol Neurosci* 16: 1329554

Luoma P, Melberg A, Rinne JO, Kaukonen JA, Nupponen NN, Chalmers RM, Oldfors A, Rautakorpi I, Peltonen L, Majamaa K *et al* (2004) Parkinsonism, premature menopause, and mitochondrial DNA polymerase gamma mutations: clinical and molecular genetic study. *Lancet* 364: 875-882

Luongo TS, Lambert JP, Gross P, Nwokedi M, Lombardi AA, Shanmughapriya S, Carpenter AC, Kolmetzky D, Gao E, van Berlo JH *et al* (2017) The mitochondrial Na(+)/Ca(2+) exchanger is essential for Ca(2+) homeostasis and viability. *Nature* 545: 93-97

Luth ES, Stavrovskaya IG, Bartels T, Kristal BS, Selkoe DJ (2014) Soluble, prefibrillar alpha-synuclein oligomers promote complex I-dependent, Ca2+-induced mitochondrial dysfunction. *J Biol Chem* 289: 21490-21507

Magri A, Belfiore R, Reina S, Tomasello MF, Di Rosa MC, Guarino F, Leggio L, De Pinto V, Messina A (2016) Hexokinase I N-terminal based peptide prevents the VDAC1-SOD1 G93A interaction and re-establishes ALS cell viability. *Sci Rep* 6: 34802

Maharana S, Wang J, Papadopoulos DK, Richter D, Pozniakovsky A, Poser I, Bickle M, Rizk S, Guillen-Boixet J, Franzmann TM *et al* (2018) RNA buffers the phase separation behavior of prion-like RNA binding proteins. *Science* 360: 918-921

Mallilankaraman K, Cardenas C, Doonan PJ, Chandramoorthy HC, Irrinki KM, Golenar T, Csordas G, Madireddi P, Yang J, Muller M *et al* (2012a) MCUR1 is an essential component of mitochondrial Ca2+ uptake that regulates cellular metabolism. *Nat Cell Biol* 14: 1336-1343

Mallilankaraman K, Doonan P, Cardenas C, Chandramoorthy HC, Muller M, Miller R, Hoffman NE, Gandhirajan RK, Molgo J, Birnbaum MJ *et al* (2012b) MICU1 is an essential gatekeeper for MCU-mediated mitochondrial Ca(2+) uptake that regulates cell survival. *Cell* 151: 630-644

Mancuso M, Orsucci D, Angelini C, Bertini E, Carelli V, Comi GP, Minetti C, Moggio M, Mongini T, Servidei S *et al* (2013) Phenotypic heterogeneity of the 8344A>G mtDNA "MERRF" mutation. *Neurology* 80: 2049-2054

Manczak M, Reddy PH (2012) Abnormal interaction of VDAC1 with amyloid beta and phosphorylated tau causes mitochondrial dysfunction in Alzheimer's disease. *Hum Mol Genet* 21: 5131-5146

Mann VM, Cooper JM, Krige D, Daniel SE, Schapira AH, Marsden CD (1992) Brain, skeletal muscle and platelet homogenate mitochondrial function in Parkinson's disease. *Brain* 115 (Pt 2): 333-342

Mao YS, Zhang B, Spector DL (2011) Biogenesis and function of nuclear bodies. *Trends Genet* 27: 295-306

Maresca A, Del Dotto V, Romagnoli M, La Morgia C, Di Vito L, Capristo M, Valentino ML, Carelli V, Group E-MS (2020) Expanding and validating the biomarkers for mitochondrial diseases. *J Mol Med (Berl)* 98: 1467-1478

Maroteaux L, Campanelli JT, Scheller RH (1988) Synuclein: a neuron-specific protein localized to the nucleus and presynaptic nerve terminal. *J Neurosci* 8: 2804-2815

Martin EW, Holehouse AS, Peran I, Farag M, Incicco JJ, Bremer A, Grace CR, Soranno A, Pappu RV, Mittag T (2020) Valence and patterning of aromatic residues determine the phase behavior of prion-like domains. *Science* 367: 694-699

Matveeva A, Watters O, Rukhadze A, Khemka N, Gentile D, Perez IF, Llorente-Folch I, Farrell C, Lo Cacciato E, Jackson J *et al* (2024) Integrated analysis of transcriptomic and proteomic alterations in mouse models of ALS/FTD identify early metabolic adaptions with similarities to mitochondrial dysfunction disorders. *Amyotroph Lateral Scler Frontotemporal Degener* 25: 135-149

Mazat JP, Letellier T, Bedes F, Malgat M, Korzeniewski B, Jouaville LS, Morkuniene R (1997) Metabolic control analysis and threshold effect in oxidative phosphorylation: implications for mitochondrial pathologies. *Mol Cell Biochem* 174: 143-148

McDonald NA, Fetter RD, Shen K (2020) Assembly of synaptic active zones requires phase separation of scaffold molecules. *Nature* 588: 454-458

McNaught KS, Belizaire R, Isacson O, Jenner P, Olanow CW (2003) Altered proteasomal function in sporadic Parkinson's disease. *Exp Neurol* 179: 38-46

Merkwirth C, Jovaisaite V, Durieux J, Matilainen O, Jordan SD, Quiros PM, Steffen KK, Williams EG, Mouchiroud L, Tronnes SU *et al* (2016) Two Conserved Histone Demethylases Regulate Mitochondrial Stress-Induced Longevity. *Cell* 165: 1209-1223

Middleton ER, Rhoades E (2010) Effects of curvature and composition on alpha-synuclein binding to lipid vesicles. *Biophys J* 99: 2279-2288

Milovanovic D, Wu Y, Bian X, De Camilli P (2018) A liquid phase of synapsin and lipid vesicles. *Science* 361: 604-607

Min CK, Yeom DR, Lee KE, Kwon HK, Kang M, Kim YS, Park ZY, Jeon H, Kim DH (2012) Coupling of ryanodine receptor 2 and voltage-dependent anion channel 2 is essential for Ca(2)+ transfer from the sarcoplasmic reticulum to the mitochondria in the heart. *Biochem J* 447: 371-379

Mink JW, Blumenschine RJ, Adams DB (1981) Ratio of central nervous system to body metabolism in vertebrates: its constancy and functional basis. *Am J Physiol* 241: R203-212

Mitroi DN, Karunakaran I, Graler M, Saba JD, Ehninger D, Ledesma MD, van Echten-Deckert G (2017) SGPL1 (sphingosine phosphate lyase 1) modulates neuronal autophagy via phosphatidylethanolamine production. *Autophagy* 13: 885-899

Mohapatra S, Wegmann S (2023) Biomolecular condensation involving the cytoskeleton. *Brain Res Bull* 194: 105-117

Molliex A, Temirov J, Lee J, Coughlin M, Kanagaraj AP, Kim HJ, Mittag T, Taylor JP (2015) Phase separation by low complexity domains promotes stress granule assembly and drives pathological fibrillization. *Cell* 163: 123-133

Monzel AS, Enriquez JA, Picard M (2023) Multifaceted mitochondria: moving mitochondrial science beyond function and dysfunction. *Nat Metab* 5: 546-562

Monzio Compagnoni G, Di Fonzo A, Corti S, Comi GP, Bresolin N, Masliah E (2020) The Role of Mitochondria in Neurodegenerative Diseases: the Lesson from Alzheimer's Disease and Parkinson's Disease. *Mol Neurobiol* 57: 2959-2980

Murakami T, Qamar S, Lin JQ, Schierle GS, Rees E, Miyashita A, Costa AR, Dodd RB, Chan FT, Michel CH *et al* (2015) ALS/FTD Mutation-Induced Phase Transition of FUS Liquid Droplets and Reversible Hydrogels into Irreversible Hydrogels Impairs RNP Granule Function. *Neuron* 88: 678-690

Murphy DD, Rueter SM, Trojanowski JQ, Lee VM (2000) Synucleins are developmentally expressed, and alpha-synuclein regulates the size of the presynaptic vesicular pool in primary hippocampal neurons. *J Neurosci* 20: 3214-3220

Musa S, Eyaid W, Kamer K, Ali R, Al-Mureikhi M, Shahbeck N, Al Mesaifri F, Makhseed N, Mohamed Z, AlShehhi WA *et al* (2019) A Middle Eastern Founder Mutation Expands the Genotypic and Phenotypic Spectrum of Mitochondrial MICU1 Deficiency: A Report of 13 Patients. *JIMD Rep* 43: 79-83

Nakamura K, Nemani VM, Azarbal F, Skibinski G, Levy JM, Egami K, Munishkina L, Zhang J, Gardner B, Wakabayashi J *et al* (2011) Direct membrane association drives mitochondrial fission by the Parkinson disease-associated protein alpha-synuclein. *J Biol Chem* 286: 20710-20726

Nakano T, Imanaka K, Uchida H, Isaka N, Takezawa H (1987) Myocardial ultrastructure in Kearns-Sayre syndrome. *Angiology* 38: 28-35

Nargund AM, Fiorese CJ, Pellegrino MW, Deng P, Haynes CM (2015) Mitochondrial and nuclear accumulation of the transcription factor ATFS-1 promotes OXPHOS recovery during the UPR(mt). *Mol Cell* 58: 123-133

Nargund AM, Pellegrino MW, Fiorese CJ, Baker BM, Haynes CM (2012) Mitochondrial import efficiency of ATFS-1 regulates mitochondrial UPR activation. *Science* 337: 587-590

Nemani VM, Lu W, Berge V, Nakamura K, Onoa B, Lee MK, Chaudhry FA, Nicoll RA, Edwards RH (2010) Increased Expression of α-Synuclein Reduces Neurotransmitter Release by Inhibiting Synaptic Vesicle Reclustering after Endocytosis. *Neuron* 65: 66-79

Ng YS, Bindoff LA, Gorman GS, Klopstock T, Kornblum C, Mancuso M, McFarland R, Sue CM, Suomalainen A, Taylor RW *et al* (2021a) Mitochondrial disease in adults: recent advances and future promise. *The Lancet Neurology* 20: 573-584

Ng YS, Lax NZ, Blain AP, Erskine D, Baker MR, Polvikoski T, Thomas RH, Morris CM, Lai M, Whittaker RG *et al* (2021b) Forecasting stroke-like episodes and outcomes in mitochondrial disease. *Brain* 145: 542-554

Ng YS, McFarland R (2023) Mitochondrial encephalomyopathy. *Handb Clin Neurol* 195: 563-585

Nieto M, Gil-Bea FJ, Dalfo E, Cuadrado M, Cabodevilla F, Sanchez B, Catena S, Sesma T, Ribe E, Ferrer I *et al* (2006) Increased sensitivity to MPTP in human alpha-synuclein A30P transgenic mice. *Neurobiol Aging* 27: 848-856

Nott TJ, Petsalaki E, Farber P, Jervis D, Fussner E, Plochowietz A, Craggs TD, Bazett-Jones DP, Pawson T, Forman-Kay JD *et al* (2015) Phase transition of a disordered nuage protein generates environmentally responsive membraneless organelles. *Mol Cell* 57: 936-947

Ordonez DG, Lee MK, Feany MB (2018) alpha-synuclein Induces Mitochondrial Dysfunction through Spectrin and the Actin Cytoskeleton. *Neuron* 97: 108-124 e106

Outeiro TF, Lindquist S (2003) Yeast cells provide insight into alpha-synuclein biology and pathobiology. *Science* 302: 1772-1775

Owusu-Ansah E, Song W, Perrimon N (2013) Muscle mitohormesis promotes longevity via systemic repression of insulin signaling. *Cell* 155: 699-712

Pagliarini DJ, Calvo SE, Chang B, Sheth SA, Vafai SB, Ong SE, Walford GA, Sugiana C, Boneh A, Chen WK *et al* (2008) A mitochondrial protein compendium elucidates complex I disease biology. *Cell* 134: 112-123

Palikaras K, Lionaki E, Tavernarakis N (2015) Coordination of mitophagy and mitochondrial biogenesis during ageing in C. elegans. *Nature* 521: 525-528

Palty R, Silverman WF, Hershfinkel M, Caporale T, Sensi SL, Parnis J, Nolte C, Fishman D, Shoshan-Barmatz V, Herrmann S *et al* (2010) NCLX is an essential component of mitochondrial Na+/Ca2+ exchange. *Proc Natl Acad Sci U S A* 107: 436-441

Pan X, Liu J, Nguyen T, Liu C, Sun J, Teng Y, Fergusson MM, Rovira, II, Allen M, Springer DA *et al* (2013) The physiological role of mitochondrial calcium revealed by mice lacking the mitochondrial calcium uniporter. *Nat Cell Biol* 15: 1464-1472

Panowski SH, Wolff S, Aguilaniu H, Durieux J, Dillin A (2007) PHA-4/Foxa mediates diet-restriction-induced longevity of C. elegans. *Nature* 447: 550-555

Parihar MS, Parihar A, Fujita M, Hashimoto M, Ghafourifar P (2008) Mitochondrial association of alpha-synuclein causes oxidative stress. *Cell Mol Life Sci* 65: 1272-1284

Parikh S, Goldstein A, Karaa A, Koenig MK, Anselm I, Brunel-Guitton C, Christodoulou J, Cohen BH, Dimmock D, Enns GM *et al* (2017) Patient care standards for primary mitochondrial disease: a consensus statement from the Mitochondrial Medicine Society. *Genet Med* 19

Park D, Wu Y, Lee SE, Kim G, Jeong S, Milovanovic D, De Camilli P, Chang S (2021) Cooperative function of synaptophysin and synapsin in the generation of synaptic vesicle-like clusters in non-neuronal cells. *Nat Commun* 12: 263

Park SK, Link CD, Johnson TE (2010) Life-span extension by dietary restriction is mediated by NLP-7 signaling and coelomocyte endocytosis in C. elegans. *FASEB J* 24: 383-392

Parker WD, Jr., Parks J, Filley CM, Kleinschmidt-DeMasters BK (1994) Electron transport chain defects in Alzheimer's disease brain. *Neurology* 44: 1090-1096

Patel A, Lee HO, Jawerth L, Maharana S, Jahnel M, Hein MY, Stoynov S, Mahamid J, Saha S, Franzmann TM *et al* (2015) A Liquid-to-Solid Phase Transition of the ALS Protein FUS Accelerated by Disease Mutation. *Cell* 162: 1066-1077

Patel A, Malinovska L, Saha S, Wang J, Alberti S, Krishnan Y, Hyman AA (2017) ATP as a biological hydrotrope. *Science* 356: 753-756

Patron M, Checchetto V, Raffaello A, Teardo E, Vecellio Reane D, Mantoan M, Granatiero V, Szabo I, De Stefani D, Rizzuto R (2014) MICU1 and MICU2 finely tune the mitochondrial Ca2+ uniporter by exerting opposite effects on MCU activity. *Mol Cell* 53: 726-737

Patron M, Tarasenko D, Nolte H, Kroczek L, Ghosh M, Ohba Y, Lasarzewski Y, Ahmadi ZA, Cabrera-Orefice A, Eyiama A *et al* (2022) Regulation of mitochondrial proteostasis by the proton gradient. *EMBO J* 41: e110476

Paupe V, Prudent J, Dassa EP, Rendon OZ, Shoubridge EA (2015) CCDC90A (MCUR1) is a cytochrome c oxidase assembly factor and not a regulator of the mitochondrial calcium uniporter. *Cell Metab* 21: 109-116

Pavlakis SG, Phillips PC, DiMauro S, De Vivo DC, Rowland LP (1984) Mitochondrial myopathy, encephalopathy, lactic acidosis, and strokelike episodes: a distinctive clinical syndrome. *Ann Neurol* 16: 481-488

Peng W, Wong YC, Krainc D (2020) Mitochondria-lysosome contacts regulate mitochondrial Ca(2+) dynamics via lysosomal TRPML1. *Proc Natl Acad Sci U S A* 117: 19266-19275

Perocchi F, Gohil VM, Girgis HS, Bao XR, McCombs JE, Palmer AE, Mootha VK (2010) MICU1 encodes a mitochondrial EF hand protein required for Ca(2+) uptake. *Nature* 467: 291-296

Petrungaro C, Zimmermann KM, Kuttner V, Fischer M, Dengjel J, Bogeski I, Riemer J (2015) The Ca(2+)-Dependent Release of the Mia40-Induced MICU1-MICU2 Dimer from MCU Regulates Mitochondrial Ca(2+) Uptake. *Cell Metab* 22: 721-733

Phair RD, Misteli T (2000) High mobility of proteins in the mammalian cell nucleus. *Nature* 404: 604-609

Piazzesi A, Wang Y, Jackson J, Wischhof L, Zeisler-Diehl V, Scifo E, Oganezova I, Hoffmann T, Gomez Martin P, Bertan F *et al* (2022) CEST-2.2 overexpression alters lipid metabolism and extends longevity of mitochondrial mutants. *EMBO Rep*: e52606

Pickett SJ, Grady JP, Ng YS, Gorman GS, Schaefer AM, Wilson IJ, Cordell HJ, Turnbull DM, Taylor RW, McFarland R (2018) Phenotypic heterogeneity in m.3243A>G mitochondrial disease: The role of nuclear factors. *Ann Clin Transl Neurol* 5: 333-345

Piroska L, Fenyi A, Thomas S, Plamont MA, Redeker V, Melki R, Gueroui Z (2023) alpha-Synuclein liquid condensates fuel fibrillar alpha-synuclein growth. *Sci Adv* 9: eadg5663

Plovanich M, Bogorad RL, Sancak Y, Kamer KJ, Strittmatter L, Li AA, Girgis HS, Kuchimanchi S, De Groot J, Speciner L *et al* (2013) MICU2, a paralog of MICU1, resides within the mitochondrial uniporter complex to regulate calcium handling. *PLoS One* 8: e55785

Polymeropoulos MH, Lavedan C, Leroy E, Ide SE, Dehejia A, Dutra A, Pike B, Root H, Rubenstein J, Boyer R *et al* (1997) Mutation in the alpha-synuclein gene identified in families with Parkinson's disease. *Science* 276: 2045-2047

Protasoni M, Zeviani M (2021) Mitochondrial Structure and Bioenergetics in Normal and Disease Conditions. *Int J Mol Sci* 22

Quintana A, Kruse SE, Kapur RP, Sanz E, Palmiter RD (2010) Complex I deficiency due to loss of Ndufs4 in the brain results in progressive encephalopathy resembling Leigh syndrome. *Proc Natl Acad Sci U S A* 107: 10996-11001

Raffaello A, De Stefani D, Sabbadin D, Teardo E, Merli G, Picard A, Checchetto V, Moro S, Szabo I, Rizzuto R (2013) The mitochondrial calcium uniporter is a multimer that can include a dominant-negative pore-forming subunit. *EMBO J* 32: 2362-2376

Rahman S, Blok RB, Dahl HH, Danks DM, Kirby DM, Chow CW, Christodoulou J, Thorburn DR (1996) Leigh syndrome: clinical features and biochemical and DNA abnormalities. *Ann Neurol* 39: 343-351

Rath S, Sharma R, Gupta R, Ast T, Chan C, Durham TJ, Goodman RP, Grabarek Z, Haas ME, Hung WHW *et al* (2021) MitoCarta3.0: an updated mitochondrial proteome now with sub-organelle localization and pathway annotations. *Nucleic Acids Res* 49: D1541-D1547

Ray S, Singh N, Kumar R, Patel K, Pandey S, Datta D, Mahato J, Panigrahi R, Navalkar A, Mehra S *et al* (2020) alpha-Synuclein aggregation nucleates through liquid-liquid phase separation. *Nat Chem* 12: 705-716

Rea SL, Ventura N, Johnson TE (2007) Relationship between mitochondrial electron transport chain dysfunction, development, and life extension in Caenorhabditis elegans. *PLoS Biol* 5: e259

Reijns MA, Alexander RD, Spiller MP, Beggs JD (2008) A role for Q/N-rich aggregation-prone regions in P-body localization. *J Cell Sci* 121: 2463-2472

Riback JA, Katanski CD, Kear-Scott JL, Pilipenko EV, Rojek AE, Sosnick TR, Drummond DA (2017) Stress-Triggered Phase Separation Is an Adaptive, Evolutionarily Tuned Response. *Cell* 168: 1028-1040 e1019

Roczniak-Ferguson A, Petit CS, Froehlich F, Qian S, Ky J, Angarola B, Walther TC, Ferguson SM (2012) The transcription factor TFEB links mTORC1 signaling to transcriptional control of lysosome homeostasis. *Sci Signal* 5: ra42

Rolland SG, Schneid S, Schwarz M, Rackles E, Fischer C, Haeussler S, Regmi SG, Yeroslaviz A, Habermann B, Mokranjac D *et al* (2019) Compromised Mitochondrial Protein Import Acts as a Signal for UPR(mt). *Cell Rep* 28: 1659-1669 e1655

Rosen DR, Siddique T, Patterson D, Figlewicz DA, Sapp P, Hentati A, Donaldson D, Goto J, O'Regan JP, Deng HX *et al* (1993) Mutations in Cu/Zn superoxide dismutase gene are associated with familial amyotrophic lateral sclerosis. *Nature* 362: 59-62

Rossignol R, Faustin B, Rocher C, Malgat M, Mazat JP, Letellier T (2003) Mitochondrial threshold effects. *Biochem J* 370: 751-762

Rostovtseva TK, Gurnev PA, Protchenko O, Hoogerheide DP, Yap TL, Philpott CC, Lee JC, Bezrukov SM (2015) alpha-Synuclein Shows High Affinity Interaction with Voltage-dependent Anion Channel, Suggesting Mechanisms of Mitochondrial Regulation and Toxicity in Parkinson Disease. *J Biol Chem* 290: 18467-18477

Ruff KM, Dar F, Pappu RV (2021) Ligand effects on phase separation of multivalent macromolecules. *Proc Natl Acad Sci U S A* 118

Ryu EJ, Harding HP, Angelastro JM, Vitolo OV, Ron D, Greene LA (2002) Endoplasmic reticulum stress and the unfolded protein response in cellular models of Parkinson's disease. *J Neurosci* 22: 10690-10698

Sampson MJ, Lovell RS, Davison DB, Craigen WJ (1996) A novel mouse mitochondrial voltage-dependent anion channel gene localizes to chromosome 8. *Genomics* 36: 192-196

Sancak Y, Markhard AL, Kitami T, Kovacs-Bogdan E, Kamer KJ, Udeshi ND, Carr SA, Chaudhuri D, Clapham DE, Li AA *et al* (2013) EMRE is an essential component of the mitochondrial calcium uniporter complex. *Science* 342: 1379-1382

Schapira AH, Cooper JM, Dexter D, Jenner P, Clark JB, Marsden CD (1989) Mitochondrial complex I deficiency in Parkinson's disease. *Lancet* 1: 1269

Schapira AH, Mann VM, Cooper JM, Dexter D, Daniel SE, Jenner P, Clark JB, Marsden CD (1990) Anatomic and disease specificity of NADH CoQ1 reductase (complex I) deficiency in Parkinson's disease. *J Neurochem* 55: 2142-2145

Schulz-Schaeffer WJ (2015) Is Cell Death Primary or Secondary in the Pathophysiology of Idiopathic Parkinson's Disease? *Biomolecules* 5: 1467-1479

Selvaraj S, Sun Y, Watt JA, Wang S, Lei S, Birnbaumer L, Singh BB (2012) Neurotoxin-induced ER stress in mouse dopaminergic neurons involves downregulation of TRPC1 and inhibition of AKT/mTOR signaling. *J Clin Invest* 122: 1354-1367

Semenov AN, Rubinstein M (1998) Thermoreversible Gelation in Solutions of Associative Polymers. 1. Statics. *Macromolecules* 31: 1373-1385

Senchuk MM, Dues DJ, Schaar CE, Johnson BK, Madaj ZB, Bowman MJ, Winn ME, Van Raamsdonk JM (2018) Activation of DAF-16/FOXO by reactive oxygen species contributes to longevity in long-lived mitochondrial mutants in Caenorhabditis elegans. *PLoS Genet* 14: e1007268

Settembre C, Di Malta C, Polito VA, Garcia Arencibia M, Vetrini F, Erdin S, Erdin SU, Huynh T, Medina D, Colella P *et al* (2011) TFEB links autophagy to lysosomal biogenesis. *Science* 332: 1429-1433

Shahmoradian SH, Lewis AJ, Genoud C, Hench J, Moors TE, Navarro PP, Castano-Diez D, Schweighauser G, Graff-Meyer A, Goldie KN *et al* (2019) Lewy pathology in Parkinson's disease consists of crowded organelles and lipid membranes. *Nat Neurosci* 22: 1099-1109

Shamseldin HE, Alasmari A, Salih MA, Samman MM, Mian SA, Alshidi T, Ibrahim N, Hashem M, Faqeih E, Al-Mohanna F *et al* (2017) A null mutation in MICU2 causes abnormal mitochondrial calcium homeostasis and a severe neurodevelopmental disorder. *Brain* 140: 2806-2813

Shao LW, Peng Q, Dong M, Gao K, Li Y, Li Y, Li CY, Liu Y (2020) Histone deacetylase HDA-1 modulates mitochondrial stress response and longevity. *Nat Commun* 11: 4639

Sharova M, Skoblov M, Dadali E, Demina N, Shchagina O, Konovalov F, Ampleeva M, Sharkova I, Kutsev S (2022) Case report: Unusual episodic myopathy in a patient with novel homozygous deletion of first coding exon of MICU1 gene. *Front Neurol* 13: 1008937

Sherer TB, Richardson JR, Testa CM, Seo BB, Panov AV, Yagi T, Matsuno-Yagi A, Miller GW, Greenamyre JT (2007) Mechanism of toxicity of pesticides acting at complex I: relevance to environmental etiologies of Parkinson's disease. *J Neurochem* 100: 1469-1479

Shimobayashi SF, Ronceray P, Sanders DW, Haataja MP, Brangwynne CP (2021) Nucleation landscape of biomolecular condensates. *Nature* 599: 503-506

Shin Y, Chang YC, Lee DSW, Berry J, Sanders DW, Ronceray P, Wingreen NS, Haataja M, Brangwynne CP (2018) Liquid Nuclear Condensates Mechanically Sense and Restructure the Genome. *Cell* 175: 1481-1491 e1413

Singleton AB, Farrer M, Johnson J, Singleton A, Hague S, Kachergus J, Hulihan M, Peuralinna T, Dutra A, Nussbaum R *et al* (2003) alpha-Synuclein locus triplication causes Parkinson's disease. *Science* 302: 841

Sofou K, de Coo IFM, Ostergaard E, Isohanni P, Naess K, De Meirleir L, Tzoulis C, Uusimaa J, Lonnqvist T, Bindoff LA *et al* (2018) Phenotype-genotype correlations in Leigh syndrome: new insights from a multicentre study of 96 patients. *J Med Genet* 55: 21-27

Sommerville EW, Ng YS, Alston CL, Dallabona C, Gilberti M, He L, Knowles C, Chin SL, Schaefer AM, Falkous G *et al* (2017) Clinical Features, Molecular Heterogeneity, and Prognostic Implications in YARS2-Related Mitochondrial Myopathy. *JAMA Neurol* 74: 686-694

Song DD, Shults CW, Sisk A, Rockenstein E, Masliah E (2004) Enhanced substantia nigra mitochondrial pathology in human alpha-synuclein transgenic mice after treatment with MPTP. *Exp Neurol* 186: 158-172

Song LK, Ma KL, Yuan YH, Mu Z, Song XY, Niu F, Han N, Chen NH (2015) Targeted Overexpression of alpha-Synuclein by rAAV2/1 Vectors Induces Progressive Nigrostriatal Degeneration and Increases Vulnerability to MPTP in Mouse. *PLoS One* 10: e0131281

Spiegel S, Milstien S (2003) Sphingosine-1-phosphate: an enigmatic signalling lipid. *Nat Rev Mol Cell Biol* 4: 397-407

Spillantini MG, Schmidt ML, Lee VM, Trojanowski JQ, Jakes R, Goedert M (1997) Alpha-synuclein in Lewy bodies. *Nature* 388: 839-840

Spinelli JB, Haigis MC (2018) The multifaceted contributions of mitochondria to cellular metabolism. *Nat Cell Biol* 20: 745-754

St-Pierre J, Drori S, Uldry M, Silvaggi JM, Rhee J, Jager S, Handschin C, Zheng K, Lin J, Yang W *et al* (2006) Suppression of reactive oxygen species and neurodegeneration by the PGC-1 transcriptional coactivators. *Cell* 127: 397-408

Strzelecka M, Trowitzsch S, Weber G, Luhrmann R, Oates AC, Neugebauer KM (2010) Coilin-dependent snRNP assembly is essential for zebrafish embryogenesis. *Nat Struct Mol Biol* 17: 403-409

Su X, Ditlev JA, Hui E, Xing W, Banjade S, Okrut J, King DS, Taunton J, Rosen MK, Vale RD (2016) Phase separation of signaling molecules promotes T cell receptor signal transduction. *Science* 352: 595-599

Subramaniam SR, Vergnes L, Franich NR, Reue K, Chesselet MF (2014) Region specific mitochondrial impairment in mice with widespread overexpression of alpha-synuclein. *Neurobiol Dis* 70: 204-213

Sun J, Wang L, Bao H, Premi S, Das U, Chapman ER, Roy S (2019) Functional cooperation of alpha-synuclein and VAMP2 in synaptic vesicle recycling. *Proc Natl Acad Sci U S A* 116: 11113-11115

Suomalainen A, Nunnari J (2024) Mitochondria at the crossroads of health and disease. *Cell* 187: 2601-2627

Szabadkai G, Bianchi K, Varnai P, De Stefani D, Wieckowski MR, Cavagna D, Nagy AI, Balla T, Rizzuto R (2006) Chaperone-mediated coupling of endoplasmic reticulum and mitochondrial Ca2+ channels. *J Cell Biol* 175: 901-911

Takahashi Y, Daitoku H, Hirota K, Tamiya H, Yokoyama A, Kako K, Nagashima Y, Nakamura A, Shimada T, Watanabe S *et al* (2011) Asymmetric arginine dimethylation determines life span in C. elegans by regulating forkhead transcription factor DAF-16. *Cell Metab* 13: 505-516

Tapias V, Hu X, Luk KC, Sanders LH, Lee VM, Greenamyre JT (2017) Synthetic alpha-synuclein fibrils cause mitochondrial impairment and selective dopamine neurodegeneration in part via iNOS-mediated nitric oxide production. *Cell Mol Life Sci* 74: 2851-2874

Tatomer DC, Terzo E, Curry KP, Salzler H, Sabath I, Zapotoczny G, McKay DJ, Dominski Z, Marzluff WF, Duronio RJ (2016) Concentrating pre-mRNA processing factors in the histone locus body facilitates efficient histone mRNA biogenesis. *J Cell Biol* 213: 557-570

Territo PR, Mootha VK, French SA, Balaban RS (2000) Ca(2+) activation of heart mitochondrial oxidative phosphorylation: role of the F(0)/F(1)-ATPase. *Am J Physiol Cell Physiol* 278: C423-435

Thomas KJ, McCoy MK, Blackinton J, Beilina A, van der Brug M, Sandebring A, Miller D, Maric D, Cedazo-Minguez A, Cookson MR (2011) DJ-1 acts in parallel to the PINK1/parkin pathway to control mitochondrial function and autophagy. *Hum Mol Genet* 20: 40-50

Tian Y, Garcia G, Bian Q, Steffen KK, Joe L, Wolff S, Meyer BJ, Dillin A (2016) Mitochondrial Stress Induces Chromatin Reorganization to Promote Longevity and UPR(mt). *Cell* 165: 1197-1208

Tomar D, Thomas M, Garbincius JF, Kolmetzky DW, Salik O, Jadiya P, Joseph SK, Carpenter AC, Hajnoczky G, Elrod JW (2023) MICU1 regulates mitochondrial cristae structure and function independently of the mitochondrial Ca(2+) uniporter channel. *Sci Signal* 16: eabi8948

Toth ML, Sigmond T, Borsos E, Barna J, Erdelyi P, Takacs-Vellai K, Orosz L, Kovacs AL, Csikos G, Sass M *et al* (2008) Longevity pathways converge on autophagy genes to regulate life span in Caenorhabditis elegans. *Autophagy* 4: 330-338

Tufi R, Gleeson TP, von Stockum S, Hewitt VL, Lee JJ, Terriente-Felix A, Sanchez-Martinez A, Ziviani E, Whitworth AJ (2019) Comprehensive Genetic Characterization of Mitochondrial Ca(2+) Uniporter Components Reveals Their Different Physiological Requirements In Vivo. *Cell Rep* 27: 1541-1550 e1545

Tyynismaa H, Carroll CJ, Raimundo N, Ahola-Erkkila S, Wenz T, Ruhanen H, Guse K, Hemminki A, Peltola-Mjosund KE, Tulkki V *et al* (2010) Mitochondrial myopathy induces a starvation-like response. *Hum Mol Genet* 19: 3948-3958

Tyynismaa H, Mjosund KP, Wanrooij S, Lappalainen I, Ylikallio E, Jalanko A, Spelbrink JN, Paetau A, Suomalainen A (2005) Mutant mitochondrial helicase Twinkle causes multiple mtDNA deletions and a late-onset mitochondrial disease in mice. *Proc Natl Acad Sci U S A* 102: 17687-17692

Vais H, Mallilankaraman K, Mak DD, Hoff H, Payne R, Tanis JE, Foskett JK (2016) EMRE Is a Matrix Ca(2+) Sensor that Governs Gatekeeping of the Mitochondrial Ca(2+) Uniporter. *Cell Rep* 14: 403-410

Valente EM, Abou-Sleiman PM, Caputo V, Muqit MM, Harvey K, Gispert S, Ali Z, Del Turco D, Bentivoglio AR, Healy DG *et al* (2004) Hereditary early-onset Parkinson's disease caused by mutations in PINK1. *Science* 304: 1158-1160

van der Beek J, Jonker C, van der Welle R, Liv N, Klumperman J (2019) CORVET, CHEVI and HOPS - multisubunit tethers of the endo-lysosomal system in health and disease. *J Cell Sci* 132

van der Laan M, Meinecke M, Dudek J, Hutu DP, Lind M, Perschil I, Guiard B, Wagner R, Pfanner N, Rehling P (2007) Motor-free mitochondrial presequence translocase drives membrane integration of preproteins. *Nat Cell Biol* 9: 1152-1159

van Ham TJ, Thijssen KL, Breitling R, Hofstra RM, Plasterk RH, Nollen EA (2008) C. elegans model identifies genetic modifiers of alpha-synuclein inclusion formation during aging. *PLoS Genet* 4: e1000027

Varhaug KN, Hikmat O, Nakkestad HL, Vedeler CA, Bindoff LA (2021) Serum biomarkers in primary mitochondrial disorders. *Brain Commun* 3: fcaa222

Vercellino I, Sazanov LA (2022) The assembly, regulation and function of the mitochondrial respiratory chain. *Nat Rev Mol Cell Biol* 23: 141-161

Verstreken P, Ly CV, Venken KJ, Koh TW, Zhou Y, Bellen HJ (2005) Synaptic mitochondria are critical for mobilization of reserve pool vesicles at Drosophila neuromuscular junctions. *Neuron* 47: 365-378

Vetralla M, Wischhof L, Cadenelli V, Scifo E, Ehninger D, Rizzuto R, Bano D, De Stefani D (2023) TMEM65-dependent Ca²⁺ extrusion safeguards mitochondrial homeostasis. *bioRxiv*: 2023.2010.2010.561661

Volpicelli-Daley LA, Luk KC, Patel TP, Tanik SA, Riddle DM, Stieber A, Meaney DF, Trojanowski JQ, Lee VM (2011) Exogenous alpha-synuclein fibrils induce Lewy body pathology leading to synaptic dysfunction and neuron death. *Neuron* 72: 57-71

Waldeck-Weiermair M, Malli R, Parichatikanond W, Gottschalk B, Madreiter-Sokolowski CT, Klec C, Rost R, Graier WF (2015) Rearrangement of MICU1 multimers for activation of MCU is solely controlled by cytosolic Ca(2.). *Sci Rep* 5: 15602

Wang J, Choi JM, Holehouse AS, Lee HO, Zhang X, Jahnel M, Maharana S, Lemaitre R, Pozniakovsky A, Drechsel D *et al* (2018) A Molecular Grammar Governing the Driving Forces for Phase Separation of Prion-like RNA Binding Proteins. *Cell* 174: 688-699 e616

Wang J, Wilhelmsson H, Graff C, Li H, Oldfors A, Rustin P, Bruning JC, Kahn CR, Clayton DA, Barsh GS *et al* (1999) Dilated cardiomyopathy and atrioventricular conduction blocks induced by heart-specific inactivation of mitochondrial DNA gene expression. *Nat Genet* 21: 133-137

Wang L, Das U, Scott DA, Tang Y, McLean PJ, Roy S (2014) alpha-synuclein multimers cluster synaptic vesicles and attenuate recycling. *Curr Biol* 24: 2319-2326

Wang W, Zhao F, Ma X, Perry G, Zhu X (2020) Mitochondria dysfunction in the pathogenesis of Alzheimer's disease: recent advances. *Mol Neurodegener* 15: 30

Wang X, Su B, Liu W, He X, Gao Y, Castellani RJ, Perry G, Smith MA, Zhu X (2011) DLP1-dependent mitochondrial fragmentation mediates 1-methyl-4-phenylpyridinium toxicity in neurons: implications for Parkinson's disease. *Aging Cell* 10: 807-823

Wang Y, Nguyen NX, She J, Zeng W, Yang Y, Bai XC, Jiang Y (2019) Structural Mechanism of EMRE-Dependent Gating of the Human Mitochondrial Calcium Uniporter. *Cell* 177: 1252-1261 e1213

Weber SC, Brangwynne CP (2015) Inverse size scaling of the nucleolus by a concentration-dependent phase transition. *Curr Biol* 25: 641-646

Wei Y, Kenyon C (2016) Roles for ROS and hydrogen sulfide in the longevity response to germline loss in Caenorhabditis elegans. *Proc Natl Acad Sci U S A* 113: E2832-2841

Welander H, Bontha SV, Nasstrom T, Karlsson M, Nikolajeff F, Danzer K, Kostka M, Kalimo H, Lannfelt L, Ingelsson M *et al* (2011) Gelsolin co-occurs with Lewy bodies in vivo and accelerates alpha-synuclein aggregation in vitro. *Biochem Biophys Res Commun* 412: 32-38

Williams R, Laskovs M, Williams RI, Mahadevan A, Labbadia J (2020) A Mitochondrial Stress-Specific Form of HSF1 Protects against Age-Related Proteostasis Collapse. *Dev Cell* 54: 758-772 e755

Wilton KM, Morales-Rosado JA, Selcen D, Muthusamy K, Ewing S, Agre K, Nickels K, Klee EW, Ho ML, Morava E (2020) Developmental brain abnormalities and acute encephalopathy in a patient with myopathy with extrapyramidal signs secondary to pathogenic variants in MICU1. *JIMD Rep* 53: 22-28

Wischhof L, Gioran A, Sonntag-Bensch D, Piazzesi A, Stork M, Nicotera P, Bano D (2018) A disease-associated Aifm1 variant induces severe myopathy in knockin mice. *Mol Metab* 13: 10-23

Wischhof L, Scifo E, Ehninger D, Bano D (2022) AIFM1 beyond cell death: An overview of this OXPHOS-inducing factor in mitochondrial diseases. *EBioMedicine* 83: 104231

Wrobel L, Topf U, Bragoszewski P, Wiese S, Sztolsztener ME, Oeljeklaus S, Varabyova A, Lirski M, Chroscicki P, Mroczek S *et al* (2015) Mistargeted mitochondrial proteins activate a proteostatic response in the cytosol. *Nature* 524: 485-488

Wu X, Cai Q, Shen Z, Chen X, Zeng M, Du S, Zhang M (2019) RIM and RIM-BP Form Presynaptic Active-Zone-like Condensates via Phase Separation. *Mol Cell* 73: 971-984 e975

Wu Z, Senchuk MM, Dues DJ, Johnson BK, Cooper JF, Lew L, Machiela E, Schaar CE, DeJonge H, Blackwell TK *et al* (2018) Mitochondrial unfolded protein response transcription factor ATFS-1 promotes longevity in a long-lived mitochondrial mutant through activation of stress response pathways. *BMC Biol* 16: 147

Xiang S, Kato M, Wu LC, Lin Y, Ding M, Zhang Y, Yu Y, McKnight SL (2015) The LC Domain of hnRNPA2 Adopts Similar Conformations in Hydrogel Polymers, Liquid-like Droplets, and Nuclei. *Cell* 163: 829-839

Xu H, Guan N, Ren YL, Wei QJ, Tao YH, Yang GS, Liu XY, Bu DF, Zhang Y, Zhu SN (2018) IP(3)R-Grp75-VDAC1-MCU calcium regulation axis antagonists protect podocytes from apoptosis and decrease proteinuria in an Adriamycin nephropathy rat model. *BMC Nephrol* 19: 140

Yang P, Mathieu C, Kolaitis RM, Zhang P, Messing J, Yurtsever U, Yang Z, Wu J, Li Y, Pan Q *et al* (2020) G3BP1 Is a Tunable Switch that Triggers Phase Separation to Assemble Stress Granules. *Cell* 181: 325-345 e328

Yang W, Hekimi S (2010) Two modes of mitochondrial dysfunction lead independently to lifespan extension in Caenorhabditis elegans. *Aging Cell* 9: 433-447

Zarranz JJ, Alegre J, Gomez-Esteban JC, Lezcano E, Ros R, Ampuero I, Vidal L, Hoenicka J, Rodriguez O, Atares B *et al* (2004) The new mutation, E46K, of alpha-synuclein causes Parkinson and Lewy body dementia. *Ann Neurol* 55: 164-173

Zhao Q, Wang J, Levichkin IV, Stasinopoulos S, Ryan MT, Hoogenraad NJ (2002) A mitochondrial specific stress response in mammalian cells. *EMBO J* 21: 4411-4419

Zheng B, Liao Z, Locascio JJ, Lesniak KA, Roderick SS, Watt ML, Eklund AC, Zhang-James Y, Kim PD, Hauser MA *et al* (2010) PGC-1alpha, a potential therapeutic target for early intervention in Parkinson's disease. *Sci Transl Med* 2: 52ra73

Zimprich A, Biskup S, Leitner P, Lichtner P, Farrer M, Lincoln S, Kachergus J, Hulihan M, Uitti RJ, Calne DB *et al* (2004) Mutations in LRRK2 cause autosomal-dominant parkinsonism with pleomorphic pathology. *Neuron* 44: 601-607

Zuchner S, Mersiyanova IV, Muglia M, Bissar-Tadmouri N, Rochelle J, Dadali EL, Zappia M, Nelis E, Patitucci A, Senderek J *et al* (2004) Mutations in the mitochondrial GTPase mitofusin 2 cause Charcot-Marie-Tooth neuropathy type 2A. *Nat Genet* 36: 449-451